Antarctic Division
Department of the Arts, Sport, the Environment, Tourism and Territories

AUSTRALIAN NATIONAL ANTARCTIC RESEARCH EXPEDITIONS

# ANARE REPORTS

135

F.R. Bond

## Background to the Aurora Australis

ISBN 0 642 15417 1

This book is dedicated to Dr P.G. Law and Dr F. Jacka who, in December 1957, as the then director and senior physicist respectively, of the Antarctic Division, gave the author the opportunity to study the Aurora Australis.

# The author

Major F.R. Bond (AMF Ret'd), B.Sc (Special), FAIP

The author was educated at the King's School, Grantham, and became Head of Newton House, named after Sir Isaac Newton, a former pupil. Gaining a "Revis" Scholarship for the University College, Nottingham, and a School Governor's Grant, he studied at University College, Leicester, and was awarded a B.Sc (Special) External Degree of London University in 1940.

Called up for military service in July 1940, in July 1944 he was appointed Staff Captain (Scientific Research) to the Army Operational Research Group (AORG), and was promoted to Major in 1945 while serving with No. 10 Indian Army Operational Research Section in Burma. After further service in AORG, he was commissioned into the Australian Army, retiring from the Australian Army Operational Research Group in 1956.

Major Bond joined the Australian Public Service in 1956. Two years later he was appointed as a physicist in the Upper Atmosphere Physics Section of the Antarctic Division. In 1964 he was a member of the summer party of the Australian National Antarctic Research Expedition (ANARE) to Wilkes, and on the return journey had the good fortune to be *directly beneath* part of a quiet rayed–band aurora.

In 1966, he was again a member of a summer party of an ANARE, this time to test a lens he had designed for the all–sky camera, which later formed part of an unmanned automatic geophysical observatory.

In 1968 he became Head of the Upper Atmosphere Physics Section, which had observatories at Macquarie Island, Mawson, Davis and Casey. He was appointed a Fellow of the Australian Institute of Physics and remained Head of Section until his retirement in January 1983.

# Contents

**Plates**



**Tables**

# Preface

This book is intended as an introduction for students beginning a study of the aurorae as part of the study of upper atmosphere physics. In the hope that the book will also interest the general reader, it is written in a less formal style than that of most text books, with a minimum of mathematics.

Descriptions are kept short, so it is important to read the captions under the numerous figures.

The book is restricted in three senses. Firstly, because of the large volume of material available, I have been selective in the material presented, and I apologise in advance to the many authors whose work has not been cited. Secondly, I have dealt with only those parts of the general subject of upper atmosphere physics that are directly necessary to present an outline of present knowledge of the aurora. Thirdly, the book presents only the descriptive phase of physics.

The student is reminded that, although the book provides a broad general outline, there is no substitute for reading the original papers and keeping up with current literature.

# 1. Introduction

Forecasting the weather and timing the seasons and changes in climate is as important to us as to the first people on Earth. The rare visits of the aurora to the middle latitudes were one of the ill omens thought to presage bad weather. Even in the last century reporters would comment on the weather for some days before and after this visitation of the polar lights.

Meteorologists classify the sighting of an aurora as a "meteor", from the Greek, "phenomenon in the heavens". The study of the aurora has frequently been the forerunner of diverging studies in Upper Atmosphere Physics or Solar Terrestrial Physics. Over the past two decades, Solar Terrestial Physics has led to a better understanding of the factors affecting weather problems and to a search for explanations that, hopefully, will lead to better solutions.

With the arrival of the Industrial Age pollution became a problem, and we have sought, for instance, for non-polluting methods of generating electricity, or new methods of waste disposal to defend the very air we breathe. The theoretical studies of Upper Atmosphere Physics that led to the explanation of the aurora have been applied in the Union of Socialist Soviet Republics to a non-polluting and economic method of generating electricity fed into the Moscow distribution grid. A similar method, which involves the break-up of material into charged particles, has been proposed for the destruction of garbage in New York.

Since the Nuclear Age began, our concern has been the prevention of a nuclear World War III. In the early 1960's scientists convinced governments that megatonne atmospheric nuclear explosions were releasing quantities of Strontium 90 into the atmosphere. The long-life isotope of strontium can replace calcium and was reaching dangerous levels in grass and other plant foodstuffs, and unacceptable levels in cow's milk fed to babies.

The demonstration of these facts led to the 1963 Treaty that banned the atmospheric testing of nuclear weapons, signed by the United States of America and the USSR, and acceded to by a number of other countries.

Since 1974, world meteorologists and upper atmosphere physicists have demonstrated that, on present evidence and assuming a conservative number of nuclear explosions, a nuclear war would produce thick dust particle clouds in both the lower and the upper atmosphere. These dust particles would reflect sunlight upwards and lead to a world-wide nuclear winter with temperatures as low as -15°C to -25°C. The nuclear winter could last for up to about two years. This, combined with a wide distribution of nuclear fallout, could lead to the extinction of much of the animal and vegetable life on Earth. The realisation of these consequences at government levels internationally, on both sides of the Iron Curtain, has led inexorably to a renewal of necessary, albeit cautious, diplomatic discussions between the USA and the USSR, which may be one small step towards the survival of *Homo sapiens*. The three preoccupations outlined above, emphasising the need for accurate weather forecasting, control of pollution, and prevention of a nuclear World War III, show clearly that the studies of Upper Atmosphere and Solar Terrestrial Physics are now more than ever necessary for our well-being on our Earth.

The study of the aurora has played and will continue to play a major role in our understanding of solar–terrestrial relationships. The aurora is the only long–term visible marker in an important region of Earth's environment.

As we shall see later (Chapter 4), the aurora is closely associated with the Earth's magnetic field. In the Northern Hemisphere the Earth's magnetic field is complicated by the Siberian Magnetic Anomaly, which is almost as strong as the North Magnetic Pole itself and is, in effect, a second pole.

In the Southen Hemisphere the Earth's magnetic field is simple, having only a single magnetic pole; hence the study of the *Aurora Australis*, or Southern Lights, and its association with other phenomena is *less complicated* than similar studies in the Northern Hemisphere.

Auroral behaviour is closely associated with other phenomena that can affect our practical life on Earth. For example, charged particle precipitation, which causes the aurora, also interrupts the radio communications that are the most simple and economic to use.

Also, when the aurora is active, the charged particles interact with Earth's external magnetic field to form electric currents in the upper atmosphere. These currents in their turn cause induced electric currents in and near the ground, which can interrupt electricity supply and affect telephone connections.

Indeed, since Cavendish, in 1790, estimated the height of the aurora above the Earth as between 52 and 71 miles (84 and 114 km), people must have wondered what lay between Earth and the aurora.

To better understand our environment, consider a set of spherical envelopes surrounding a globe. These envelopes are characterised either by the way temperature changes with distance from the surface of the globe, or height above Earth, or by their electrical properties.

There are two aspects in the concept of temperature. We all understand temperature as varying degrees of hot and cold. However, to understand our environment we must sometimes think of temperature as a state of energetic excitement of particles. A high degree of excitement is hot, while a low degree of excitement is cold. Near the ground the concept of hot and cold applies, but above about 80 km, due to the rarified nature of the atmosphere, the concept of energy excitement is applicable. The envelopes in order of distance from Earth are:

- The *troposphere* (up to about 11 km; the temperature falls to -60°C at the *tropopause*, the upper boundary.)
- The *stratosphere* (11-50 km; the temperature rises from -60°C at the tropopause to 0°C at the stratopause. The heating is due to absorption of ultra-violet light by the *ozone layer* at 20-40 km. A window in the ozone layer lets through a small portion of this dangerous light, excessive doses of which cause cancer, burn the skin and affect the eyes.)
- The *mesosphere* (50-80 km; the temperature falls from 0°C at the stratopause to about -100°C at the *mesopause*. Above the mesopause, the gases and charged particles are so rarified that only the energy excitement concept of temperature applies.)
- The *thermosphere* (80-400 km; the temperature rises from -100°C at the mesopause to 650°C at the *thermopause*).
- The *exosphere* (400-700 km; above 700 km particles that carry no electrical charge can escape from the pull of Earth's gravitational field. We see later how most charged particles are retained.)
- The *ionosphere* (50-500 km; with increase in height the proportion of ions or charged particles to neutral particles increases. For practical purposes at 500 km only neutrons, protons and electrons exist.)
- The *magnetosphere* (50-70 000 km; marks the limit of the Earth's magnetic field, called the magnetopause.)

As we have implied, the studies of meteorologists and upper atmosphere physicists overlap. Meteorologists are mainly interested in the region up to the stratopause, below which most of our weather originates. However, meteorology regards the aurora as a meteor, in the sense that it is an atmospheric phenomenon. Upper atmosphere physicists are principally interested in charged particles, magnetic fields, electric fields and the currents they

produce. The bounds of upper atmospheric physics lie from the lower edge of the ozone layer at 20 km to the Sun.

Many co-relationships, or correlations between conditions on the Sun and weather on Earth have been reported. To date, only two have stood the test of time. The first is the occurrence of drought in the western prairie region of the United States at intervals of 22 years, which corresponds with the 22 year sunspot cycle. The second confirmed case is the eleven–year cyclic change in latitude of the tracks of high and low atmospheric pressure regions across southern Australia with the eleven–year cycle change in sunspot activity but recent evidence suggests even this may be in doubt.

A more recent correlation, which has not yet stood the test of time, relates the changes in direction of the magnetic field emanating from the Sun to the vorticity of wind circulation around "highs" and "lows" in the lower meteorological atmosphere.

The Sun revolves in 27 days. Earth takes 365.25 days to go round it . The magnetic field from the Sun, reaching far beyond Earth, usually has four sectors, each separated by a sector boundary (Figure 100). When the sector boundary overtakes the slower Earth moving in its orbit, weather forecasts for the next two days may be less accurate than on the 27 days. Therefore, for up to eight days in each 27 days there may be less accurate weather forecasts than if we could take into account the effect of the sector boundary crossing the Earth. This phenomenon was first reported for the winter period in the United States (Larsen and Kelly 1977) based on earlier work by Wilcox and Ness 1965.

No direct comparison has yet been made in the Southern Hemisphere. However, closely related work by Burns *et al.* suggests that a similar relationship may apply to the Australian summer, so there may be a global rather than a seasonal effect. The cause of this association between boundary crossing and vorticity is not yet known.

We shall be concerned in later chapters with the detailed effects of the aurora in the ionosphere and the magnetosphere, and now give a broad picture of these processes.

Heat and light from the Sun are accompanied by the emission of charged particles, mainly protons, electrons and $\alpha$– particles. Such a mixture of particles is called a "plasma". A plasma has the capability of carrying with it a "frozen-in" magnetic field. Hot solar plasma around the Sun can be photographed during a total eclipse. It is referred to as the *solar corona* or, further from the Sun, after the particles have cooled, the *solar wind*. The continuously expanding solar corona reaches out into space far beyond the orbit of Earth, carrying with it part of the Sun's magnetic field. This magnetic plasma interacts with Earth's magnetic field which is a complicated one; however, if there were no solar wind, its magnetic field at great distances from Earth would be only slightly different from that of a small bar magnet at the centre of Earth.

In fact, Earth's magnetic field forms a comet-shaped cavity in the solar wind. It is compressed on the Sunward, or day side and extends into a long tail on the night side. The cavity is called the "magnetosphere". It is the behaviour and interactions of particles, electric fields and currents, magnetic fields and wave phenomena in the near-vacuum region of the magnetosphere that is the subject material of upper atmosphere physics. The near-Earth region below about 20 km, in which Earth's weather is found, is generally excluded, although the interactions of the magnetosphere and the meteorological region are also studied.

On the Sunward side, the magnetosphere extends to a distance of about 63 700 km or ten times the radius of Earth, but on the night side the magnetosphere reaches far beyond the orbit of the Moon (about 370 000 km). In this vast region, the only visible markers of the interactions taking place are the aurorae: the Northern Lights (aurora borealis), and the Southern Lights (aurora australis).

Some of the solar particles that form the solar wind enter the magnetosphere and are guided down the magnetic field lines towards Earth. Those particles, which cause the aurorae, form a belt in each of the two polar regions.

The light of the aurorae is formed in the same way as the light from any other vapour. When vapour of any element is bombarded by electrons having the right energy, the atoms of that element take on a higher energy state. After a short interval, the atoms fall to a lower energy state by emitting a photon of light of a particular colour. For sodium vapour street lights, the colour is that of a particular "line" in the yellow part of the visible spectrum. For the oxygen atoms that give rise to part of the light of the aurora, the colours are green and two shades of red. Molecules bombarded by electrons act in a more complicated way, and give out light in a set of "bands" of the visible spectrum. Nitrogen molecules are responsible for both blue and red colours in the aurora. More than 160 different shades of colour have been identified in auroral forms.

Auroral forms are discussed in the next chapter, and subsequent chapters amplify the brief description given in this introduction.

## 2. Description of auroral forms

Mysterious, beautiful, wonderful . . . coloured profusion in visual chaos . . . ribbons of light snake across the night sky . . . batteries of celestial searchlights zero in on the magnetic zenith, waltzing to the music of the celestial spheres, forming an ever-changing crown in the heavens. Successive bands of increased light intensity move upwards, highlighting the display and flaming heavenwards . . . patches of light pulsate rhythmically; in another region of the night sky, other patches of light pulsate, out of phase . . .

The aurora australis, or the Southern Lights, at the height of a display.

The early peoples of Africa may well have seen parts of the display of the aurora australis before people in the Northern Hemisphere saw the display of the Northern Lights, the aurora borealis.

Out of the visual chaos of the auroral display, we have come gradually to recognise patterns. The components of the auroral display are usually described in terms of *form, structure, condition, brightness* and *colour(s).*

Each hemisphere can be divided into three regions: the *auroral, cis-auroral,* and *trans-auroral* regions. The *auroral regions* are a belt in each hemisphere that is defined by lines placed 7.5 degrees distant from, and on each side of, the line of maximum overhead auroral frequency. We shall see later how this line was determined. The regions in the lower latitudes are called the *cis-auroral regions*, and those in the higher latitudes are called *trans-auroral regions.* The adjacent maps (Figures 1 and 2) illustrate these divisions in terms of the parameter $\Theta_3$ (see later) introduced by Bond and Jacka (1962).

We now turn to a description of auroral form. The simplest form of the aurora is the *homogeneous arc.* The arc appears as a thin ribbon or sheet of luminosity in the shape of a simple, slightly curving bow or arch (Plate 1).

The lower border of the arc is usually between about 90 km and 120 km above the Earth's surface, with an average height of about 105 km. The heights of the lower border in the Northern Hemisphere were first determined by Størmer (1913), and later confirmed by Vegard and Krogness (1920) in Norway. Dr Gleb Simonov, of the Australian Antarctic Division, confirmed the average height of 105 km for auroral forms in the Southern Hemisphere, using an improvement of Størmer's method; unfortunately this meticulous work was not published, due to Simonov's premature death in 1966.

The thickness of an auroral arc in the Northern Hemisphere has been estimated at 250 m (Elvey 1957), and of two active auroral curtains (see later) at 336 m and 144 m (Akasofu 1961), from photographs of aurora in the magnetic zenith.

Auroral arcs are usually from about a hundred to several thousand kilometres in length. In the Northern Hemisphere, where continuous all-sky camera photographs were available from Central Siberia to Canada, Akasofu (1965) reported that arcs extended over at least 5000 km. Bands (see later) on 11 February 1968 seemed to extend for a distance of 10 000 km.

With the introduction of satellites, pictures taken over the Southern polar cap show that auroral arcs extend almost continuously around the greater part of the auroral region (Snyder and Akasofu 1976). The montage of photographs in Figure 3, taken during the Defence Meteorological Satellite Program of the United States of America and presented by Akasofu (1976) shows the aurora in plan, and indicates that the arcs and bands are virtually continuous, at least in the quiet-arc stage of the auroral display over polar regions. For comparison, a montage of the corresponding two sectors of the auroral oval (see later) is given in Figure 4 (Bond and Paine 1971).

The vertical extent of arcs above the lower border varies from a few kilometres to several tens of kilometres. When an arc is low on the polewards horizon, the segment below the arc often looks black.

Arcs are generally whitish-green in colour. Where a red colour appears at heights greater than the height of the green colour, Størmer (1955) referred to the colour as red Type A. Arcs are usually of low intensity, but brighten considerably before a change takes place in the pattern or behaviour of the aurora. Størmer also distinguished an arc with a red lower border (Type B).

The height of the lower border of this arc is usually about 60 — 80 km, in general lower than the more usual green, or whitish-green, arc.

In the cis-auroral and auroral regions, arcs extend in a roughly East-West direction, but this is not the case in the trans-auroral region. Mawson and Chree reported in 1925 that, over Cape Denison, arcs rotate slowly in the zenith. Weill (1958), from observations at Dumont d'Urville, noted that the azimuth of arcs in the trans-auroral region points generally in the direction of the Sun. Since both Dumont d'Urville and Cape Denison were very close to the South Magnetic Pole (Dip Pole) when these observations were made, Denholm and Bond (1961) investigated the behaviour of the aurora reported from stations that were more distant from the Dip Pole, to see whether the phenomenon was general to the trans-auroral region. Their analysis indicated that the phenomenon of the Sun-oriented arc was not just a local effect in the region of the Dip Pole, but was a common phenomenon of the trans-auroral region (Figure 5).

The quiet auroral arc can either exist for a short period or can persist under certain conditions, for several hours, often isolated in the sky. The first sign of activity in a quiet homogeneous arc is often an increase in brightness, the lower border becoming more sharply defined, and soon afterwards the formation of rays begins along the arc.

Størmer's, report on the aurora borealis drew attention to what he termed *false rays*. Two examples are shown in Figures 6 and 7.

While returning from Wilkes in 1964, the writer was fortunate to see into the structure of a quiet rayed band because a portion of the band was overhead in the magnetic zenith. A map of the rayed band and a sketch of the aurora in the zenith are shown (Figures 8 and 9).

Again, in the Northern Hemisphere, Akasofu (1963), presented an all-sky camera photograph together with an explanatory diagram (Figures 10 and 11). He drew attention to the similarity of the large-scale auroral pattern to the small-scale pattern produced by Webster's (1957) demonstration that a thin electron sheet-beam often breaks up into an array of vortex-like filaments (see Figures 12a and b). Webster indicated that the instability is produced by a space charge within the sheet-beam. He suggested that auroral rays could be produced by such a sheet-beam instability, a suggestion that had been made previously by Alfvén and Fälthammar (1950).

In our discussion of auroral forms, the next degree of complication is the *homogeneous band*. This is also a ribbon-like form that displays folds and curves. Long bands may move quite rapidly across the sky, while short lengths of homogeneous and rayed bands often hang like draperies in the sky, and move as if blown by an invisible wind. Coloured photographs of bands are shown in Plates 2 and 3. When two or more rayed bands form on either side of the magnetic zenith, the rays appear to converge and form an auroral corona, or crown (see Plate 4). Arcs are the simplest band-like forms of the aurora.

Aurorae may also appear as other discrete forms, usually in conjunction with, or following, a display with band-like forms.

The most striking of these is the *ray*, a shaft of luminosity aligned along the direction of the vector[1] representing the Earth's total magnetic field. Rays may exist as a single ray, a small bundle of rays, or many scattered rays (Figure 13). They are distinguishable from *rayed bands* by the lack of continuity of illuminations between them, particularly by the lack of continuity of the lower border.

Very tall rays that display a rather uniform brightness have been described. They may appear with a green colour from the base upwards, merging into yellow-orange near the middle, changing to red, or, when the ray passes out of the Earth's shadow, even purple, at the top.

The aurora also appears in diffuse forms. The *patch* is an example of a diffuse auroral form. More or less isolated, patches of luminosity have no discernible continuous lower border. The angle that a typical patch subtends at the eye is about 10°. Patches are often rather diffuse, like patches of cloud. In the later stages of a display in the auroral regions it is common for patches to pulsate in brightness.

The *veil* is a somewhat extensive uniform luminosity that frequently covers a large portion of the sky. It may occur along with, or as a background for, other forms. In auroral regions it is usually greenish white, but in both auroral and cis-auroral regions it can frequently be red.

Each of the auroral forms described –– the discrete forms, (arcs, bands) and rays and the diffuse forms, patches and veil each needs to be qualified in terms of its **structure**.

Arcs and bands may be homogeneous or rayed. At high elevations they may appear striated. *Striations* are fine filaments lying parallel and very close to the main form. Striations should be distinguished from multiple forms, which are often nearly parallel throughout much of their length. Of course striations may occur in one or more of a set of multiple forms.

Any system of description requires an indication of brightness. The usual intensity index for the green atomic oxygen emission at 557.7 nm is adopted from Seaton (1954) and Hunten *et al.* (1956).
(nm = nanometre = $10^{-9}$m = 0.000000001 m)

| Intensity (557.7 nm) Kilo-Rayleigh (kR) | Intensity Index | Remarks on visual appearance of typical aurora |
|---|---|---|
| <0.1 | 0 | sub-visual |
| 1 | 1 | comparable with Milky Way; green colour not perceived |
| 10 | 2 | comparable with moonlit cirrus cloud; green colour sometimes perceived |
| $10^2$ | 3 | comparable with brightly moonlit cirrus cloud or moonlit cumulus cloud |
| $10^3$ | 4 | much brighter than 3; sometimes casts easily discernible shadows |

Finally, to complete the description of an auroral form, we must specify the **colour** or colours present.

The most frequently occurring colour is green, due to a line in the visual spectrum at wave length 557.7 nm caused by an emission from atomic oxygen. At low levels of luminance this colour may appear white, and unless viewed through a spectrometer or a green filter very close to 557.7 nm, high cirrus cloud may easily be mistaken for an auroral arc or band, especially when near the zenith.

At higher levels of luminance, a bright white or yellow aurora may be seen. This relatively rare event is due to the presence in the correct proportions of green (557.7 nm) from atomic oxygen and red (Type A — 630.0 nm and 734.4. nm) also from atomic oxygen, together with

[1] A vector is a quantity having both magnitude and direction. It may be represented by a straight line of a length corresponding to the magnitude of the vector on a convenient scale, marked with an arrow in the sense or direction of the vector.

blue (391.4 nm, 427.8 nm) from ionised molecular nitrogen. Naturally these colours also occur separately and mixed in different proportions. The arcs that are formed low in the upper atmosphere show the red (Type B) colour due to the first positive bands in the spectrum being of molecular nitrogen. This is a conspicuous feature of low auroral arcs and bands in the auroral regions.

For a systematic number — letter code description of auroral forms, the reader is referred to the *International Auroral Atlas* (1963).

This chapter discussed the basic forms of the aurora: arcs, bands, rays, patches, and veil. The next chapter shall examine the patterns of the auroral display as seen from individual stations throughout the auroral regions.

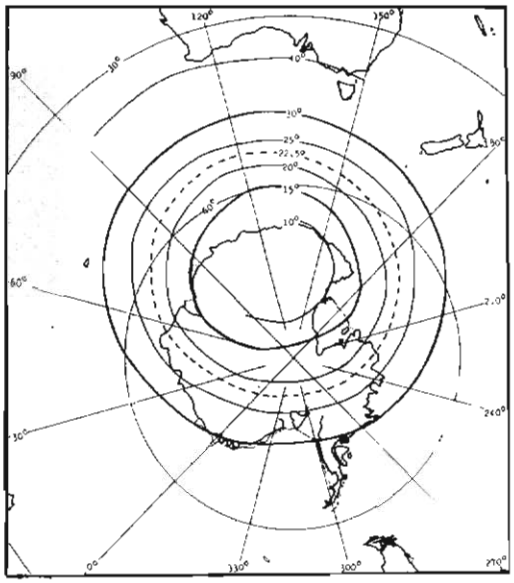

Figure 1. The Southern Hemisphere auroral region. $\Theta$ is the co-latitude measured from the Auroral Pole. The auroral zone is shown as the dashed line co-latitude $\Theta_3 = 22.5°$. The inner limit of the auroral region is the solid line co-latitude $\Theta_3 = 15°$. The outer limit of the auroral region is the solid line $\Theta_3 = 30°$. (*Published in the International Auroral Atlas, Edinburgh 1963, from a drawing by Bond.*)

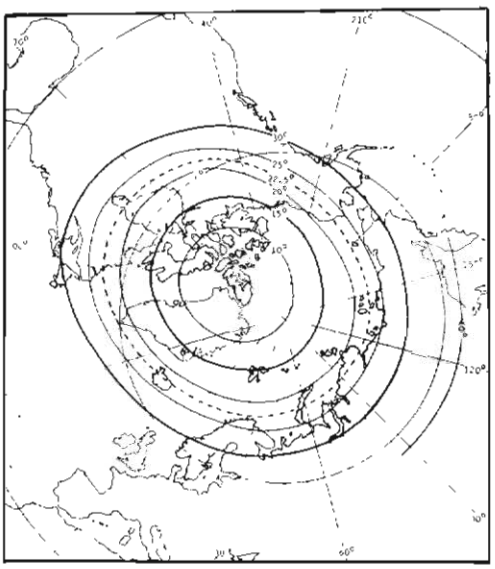

Figure 2. The Northern Hemisphere auroral region. The auroral zone is shown as the dashed line $\Theta_3 = 22.5°$. The inner limit of the auroral region is the solid line co-latitude $\Theta_3 = 15°$. The outer limit is the solid line co-latitude $\Theta_3 = 30°$. (*Published in the International Auroral Atlas, Edinburgh 1963, from a drawing by Bond.*)

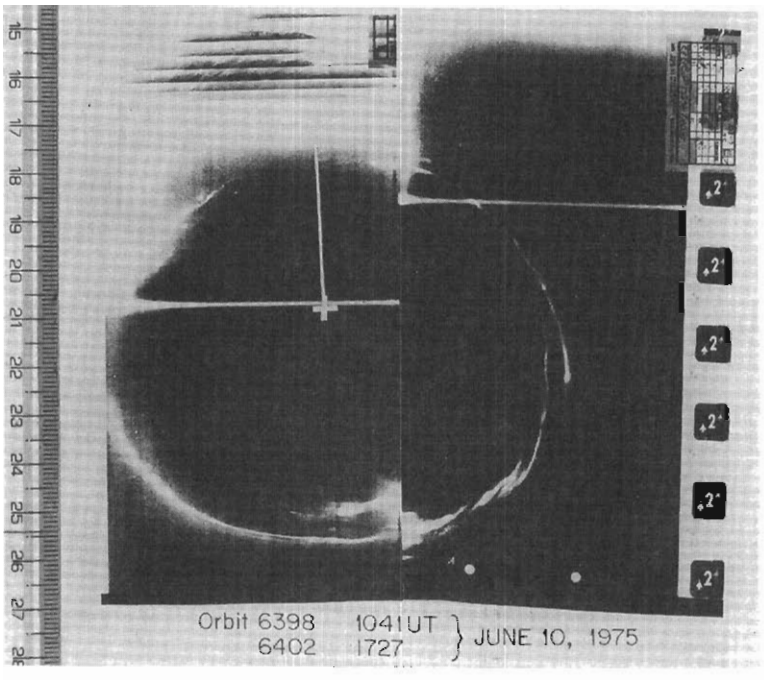


Figure 3. A montage of two satellite photographs showing the quiet-arc auroral oval. (*Akasofu 1976*)

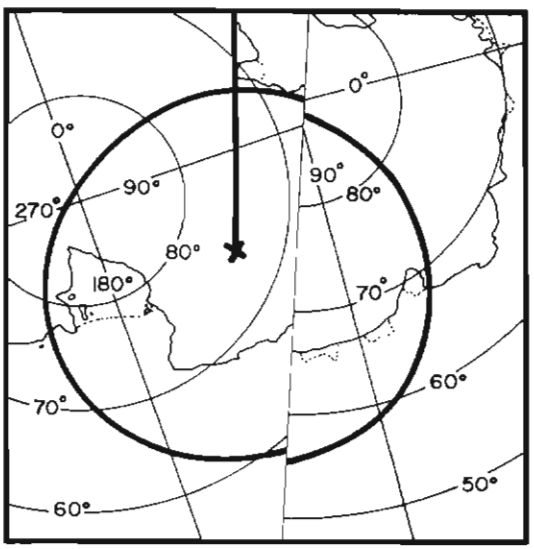


Figure 4. A montage of the two quiet-arc auroral ovals corresponding to the satellite photographs in Figure 3, with auroral pole and Sun-longitude superimposed. (*Bond and Paine 1971*)

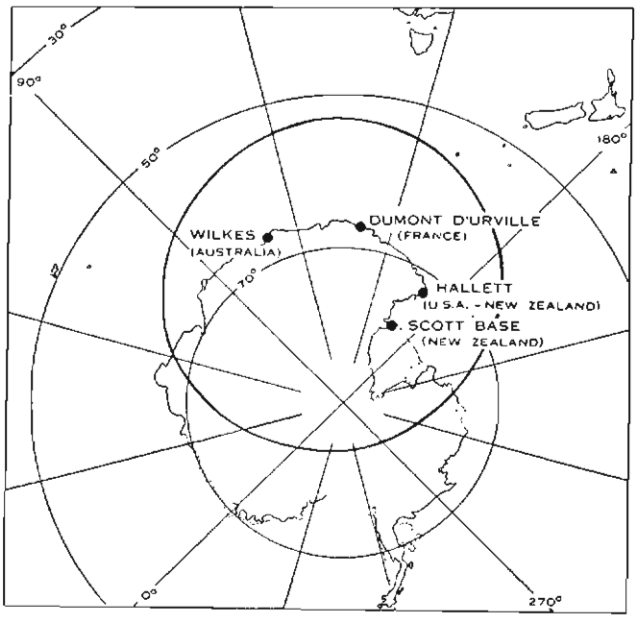


Figure 5. Station locations in relation to southern isoaurore of maximum frequency. (*Bond and Jacka 1960*)

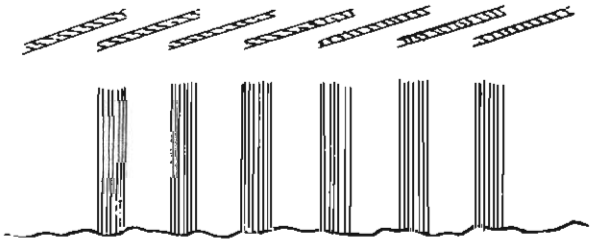

Figure 6. Rays produced by accumulated light effect of sheets behind each other. Upper sketch as seen in magnetic zenith; lower one, from a great distance equatorwards of the sheet. (*Størmer 1955, p. 326*)

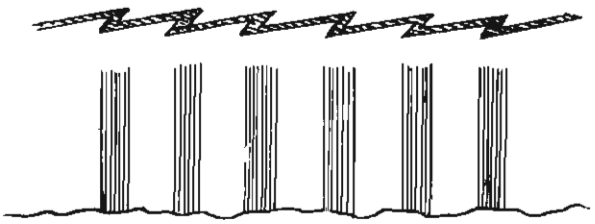

Figure 7. Rays produced by a folded sheet. (*Størmer 1955*)

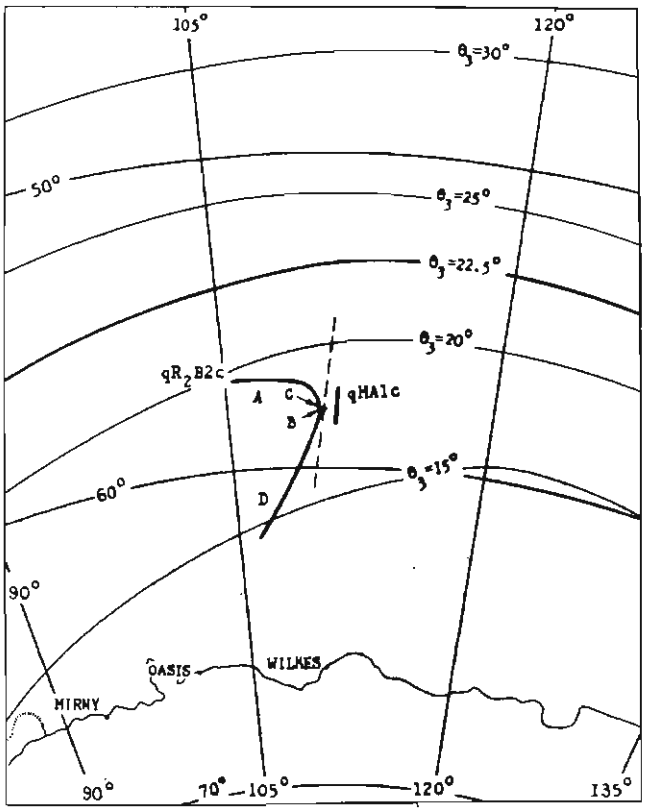


Figure 8. Auroral display at 0030 hours, 30 January 1964. Solid line: auroral forms; dashed line: ship's position and route.

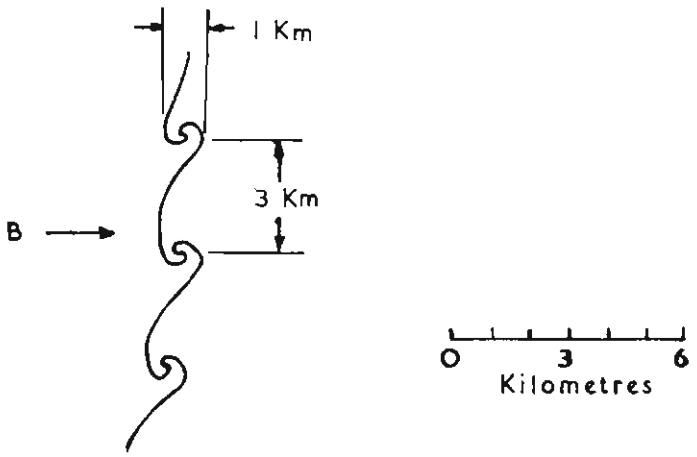


Figure 9. Enlargement of region B in Figure 8.


Figure 10. Photograph of the bottom edge of a band taken at College (Alaska) between 2300 and 2400 hours on 24 March 1961. Five stars of Ursa Major appear in the photograph. (*Akasofu 1963*)

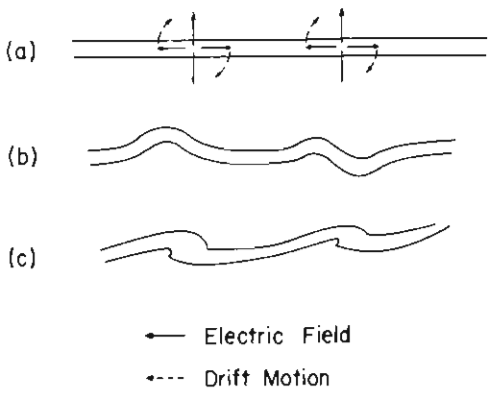


Figure 11. Schematic diagram to show the growth of an instability of auroral electron sheet-beam due to a positive space charge in it (looking up the bottom edge of the beam in the northern auroral zone). (*Akasofu 1963*)

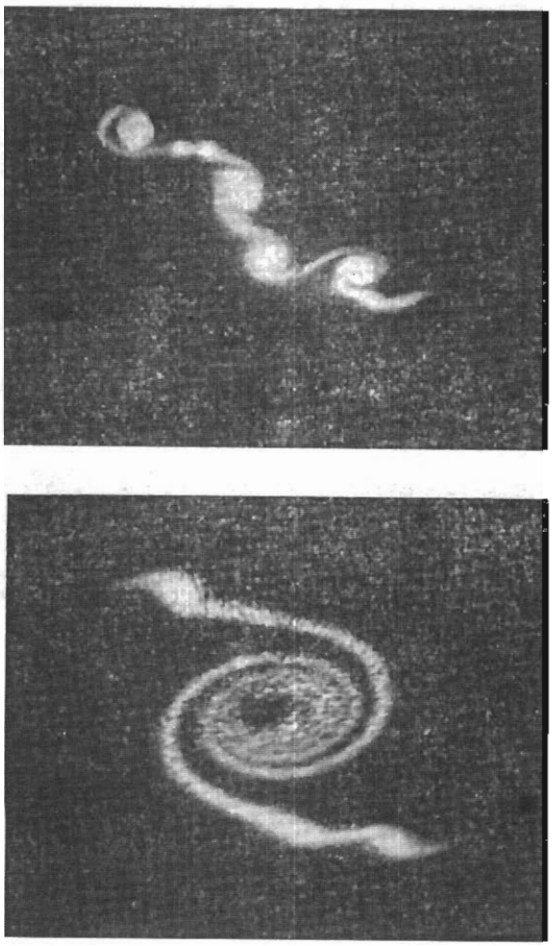


Figure 12. Electron sheet-beams after vortex breakup has taken place.
Beam voltage: (a) 37 v, (b) 38 v
Beam current: (a) 0.63 ma, (b) 0.35 ma
Magnetic field: (a) 155 gauss, (b) 135 gauss (*Webster 1957*)

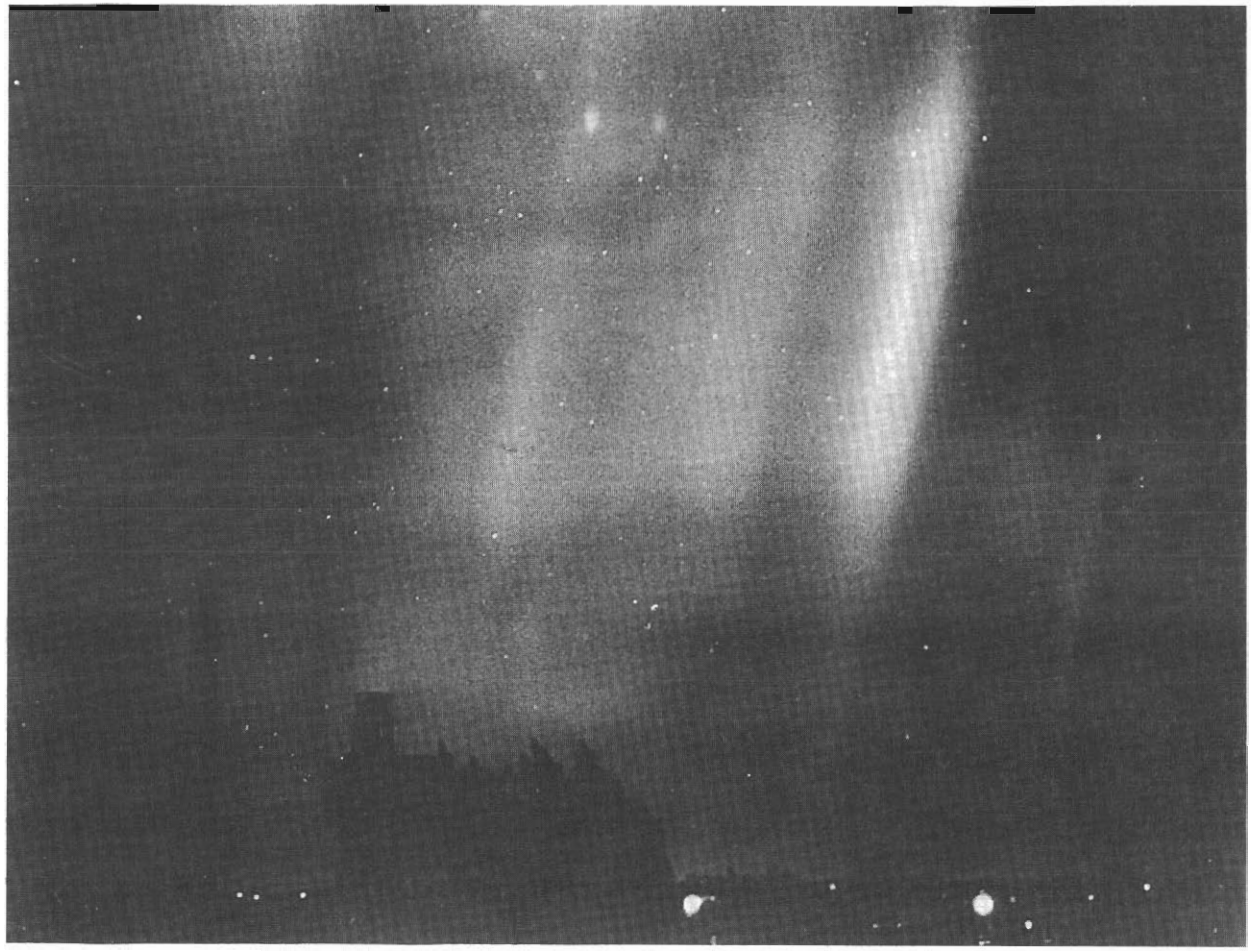

Figure 13. Auroral rays. (*Photograph by A. Campbell-Drury, Antarctic Division, taken from Hawthorn, Melbourne, 11 February 1959.*)

# 3. The pattern of auroral displays

In the middle latitudes, the periodic visitation of "lights in the night sky", are a reminder of the nightly displays of the aurorae in polar regions. The night-long display over the northern polar cap was first given the name aurora borealis in 1621 by Pierre Gassendi[2], later Professor of Mathematics at the College Royal de France in Paris. The first European to report on the aurora australis was probably de Mairan, in 1712.

In modern writings, an auroral form, which is only a part of an auroral display, is often referred to as an aurora. Again the words "an aurora" are sometimes used to describe the whole auroral display, or alternatively, the auroral display may be said to be made up of a number of auroras, little distinction being made between auroral forms existing at a given time, and auroral forms following in succession. In most older works and in some modern writings the Latin plural *aurorae* is used in a similar way.

Many fine examples of descriptive writing are to be found among the earlier word pictures of auroral displays. Perhaps an example from *Meteorological Observations, Hobart Town* by Francis Abbott, Observer, will suffice as illustration (Abbott 1859). He is describing a display in the cis-auroral region.

On the 29th August 1859, from 6h.55m. to 7h.25m. p.m., there appeared a most brilliant Aurora Australis extending from W. through the S. to the Eastern part of the horizon in one continued arc of about 190° and shooting up to the zenith. The Eastern and Western extremities of the conoid were of pale ruby, and deep red colour, intermixed through the whole vault with bands of pale yellow and shades of deep and light green, with here and there a dark cloud jutting in; elsewhere the circumpolar stars glittered like diamonds set in an emerald and ruby ground. The phenomenon had for thirty minutes a most magnificent appearance, the bands [i.e. rays] being in complete repose formed a truncated cone of glory, the apex of which, if projected, would have terminated in the zenith. This brilliant and beautiful magneto-electric storm appeared again about 9.30 p.m., flickering in brisk corruscations of most beautiful colour, from the horizon to the zenith, and, when reaching the converging point, it produced at one time a beautiful halo, and at another period it had the effect of falling from the apex in a shower of nebulous matter, like star dust . . .

A second display of the Aurora appeared on the night of 2nd September following, equally brilliant and extensive, but less transitory, and with this difference, that from Sunset the whole of the Southern sky was of deep ruby colour . . .

From 12 to 1 o'clock on the morning of the 3rd the Aurora broke out into flickering streamers and corruscations, as brilliant, and with as much diversity of colour as on the 29th August, forming in the zenith a well defined corona, which shortly after became diffused and then dispersed. On both occasions a line drawn from the centre of the arc in Azimuth through the corona in the zenith was parallel to the magnetic meridian . . . Sun-spots were at a maximum, a diagram of three groups containing 70 spots of various sizes, was made on the same day with the Sun on the meridian.

With these descriptions of displays in the cis-auroral region we return to the more modern terminology given earlier. The following description of the auroral display seen from Macquarie Island is taken from Bond (1960a).

Climatic conditions at Macquarie Island are extremely unfavourable for auroral observing; the sky is very rarely clear for more than a few hours at a time. However, an examination of the Macquarie Island observations over the period 1951 — 1959 indicates that the main pattern of auroral behaviour may be described in terms of two phases.

The first phase commences as a succession of one or more arcs or bands appearing above the southern horizon. Aligned roughly along parallels of geomagnetic latitude, these arcs or bands may show rayed structure of intensity 1 or 2 and very rarely intensity 3 (on the usual 0 – 4 scale). There is then a general northwards progression of the display. This may be a continuous drift, sometimes with a succession of advances or retreats; or it may be a

[2] Dr George I. Siscoe argues in *EOS* 59:994 (1978) that the origin of the term goes back to correspondence between Galileo and Guiducci, 1619.

discontinuous progression involving fading of the aurora at one position and a new appearance at another. A new arc or band may form in advance of an existing display. An arc or band may disappear only to be replaced by another further to the south and the advance be repeated. When this phase has a duration exceeding 30 minutes it is almost invariably associated with a positive bay in the H magnetogram.

In general, the northward drift continues until the beginning of the second phase, which is characterised by a quite sudden increase in intensity and development of bright rayed structure. This may be followed by flaming[1]. The discrete structure is replaced by moving, diffuse-rayed forms and pulsating and diffuse surfaces which latter slowly drift or progress to the South. This second phase is always associated with a negative bay in the H magnetogram. This main sequenee may be halted at any stage and one or more stages may be absent. Occasionally after the second phase has begun, arcs reappear for a short time interval and the whole or part of a seqnence may be repeated one or more times.

Again referring to the auroral region, the pattern of the auroral display at Mawson has been described by Eather (1964).

A typical auroral event at Mawson proceeds as follows:

A quiet homogeneous arc or band will appear in the south early in the night. This band is not very bright and invariably white or green in eolour. Even though the light level is low, long exposure photographs may be taken as the aurora remains fixed in position for considerable periods of time.

The aurora gradually moves northwards and after about two or three hours appears as a quiet band or arc in the northern sky. Then the band will suddenly become active — its brightness increases and the homogeneous structure breaks up into a rayed structure. These rays may travel along the length of the band with high veloeities. Pulses of intense brightness appear and move rapidly along the band. It is at this stage that colours begin to appear — yellow, red, blue and purple, only lasting seconds at a time.

The display spreads and moves towards the zenith where a brilliant corona may develop. A corona consists of long auroral rays converging up to one point (the magnetic zenith). The type, shape and colour of the aurora change rapidly, and the active bands tend to move southward again, their intensity decreasing. Patches of auroral light usually remain over the sky for half an hour or so. Single rays of light often oceur. The brightness of the patches gradually decreases, leaving a dark sky or perhaps some bands in the south which may remain until dawn.

The aurora in the trans-auroral region, is described by Denholm (1961).

Most auroras observed from Wilkes were arcs, bands, or rays. There was a complete absence of pulsating auroras, frequently observed near the maximum frequency isoaurore (ANARE logs, Macquarie Island) and of flaming aurora. To one who has observed auroras near the auroral zone there is a strong subjective impression that, in general, auroras near Wilkes were much less bright, but of more stable form, than those farther north.

Auroras may appear in some part of the sky during any of the dark hours between 1600 and 0700 hours LT. A regular feature is that near midnight relatively bright green rays or rayed bands, sometimes accompanied by glow, appear near the horizon about azimuth 340° which is the direction of the portion of the auroral zone closest to Wilkes[4]. The display then moves above the horizon and is seen as multiple rayed bands subject to frequent changes of shape, and sometimes accompanied by homogeneous bands. Parts of the display may enter the station's zenithal region. The display becomes weaker in intensity, and after about an hour it may disappear completely.

In 1959 auroras were rarely observed farther than 2° from Wilkes in the region of the sky from south-west through south to south-east. Aurora that did occur in the southern sky was usually part of a form that also extended into the northern sky. When colour was discernible it was usually the normal auroral green; weaker auroras appeared in the usual grayish-white. Red aurora Type A was observed on two occasions. On July 15, 1959, between 1005 and 1100 UT, a bright red 'diffuse surface' was present in the north-western sky, and on May 8, 1959, between 1100 and 1115 UT, a faint red glow was observed near the NW horizon. At these times Kp was 9 and 5, respectively, and the local K indices 7 and 4, respectively.

At 1630 UT on August 7, 1959, a homogeneous band of unusual colouring was observed at about 5° elevation between azimuths 290° and 340°. This aurora was a brilliant white, with a red lower border (Type B) and

[3] A succession of bright bands moving upwards through the existing forms highlighting the display and giving the impression of flames.

[4] See Figure 5.

of visual intensity comparable with that of the moon . . . A possible explanation for the bright white portion without visual trace of green or other coloration above the lower border is that the oxygen red doublet 6300/6364 Å, the violet nitrogen bands at 3914 and 4278 Å, and the green oxygen line at 5577 Å were present in such relative intensities as to appear white to the eye. The white appearance lasted only about 1 minute, then deteriorated into the usual auroral green. This bright green homogeneous band, without red lower border persisted in the low NW sky until about 1745 UT.

The orientations of all simply shaped homogeneous auroras observed from Wilkes in 1959 are plotted against local apparent time in the adjacent figure [Figure 14]. The orientations of auroras within 3° of Wilkes are distinguished from those of auroras further away. The auroras have been plotted on synoptic maps, and orientation was measured as the angle from geographic north to the tangent to the plan position of the aurora, clockwise being taken as positive. It can be seen that most of the orientations are grouped about the Sun—Earth line, but near midnight there are a few points well off this line. Inspection of data shows that all except two of the points in this midnight group are about 5° from Wilkes and between Wilkes and the auroral zone. If the orientation variation phenomenon is a consequence of an auroral pattern fixed in orientation relative to the Sun, then the anomalous orientation of these northerly auroras may be interpreted as being due to auroras lying along portions of pattern lines that are inclined at about 60° to the pattern lines over Wilkes[5].

After these descriptions of the aurora in the cis-auroral, auroral and trans-auroral regions, a subsequent chapter will turn to the story of how these regions of the aurora came to be located. However, the nature of the Earth's magnetic field must first be considered.

[5] The references to 3° and 5° are measures of Great Circle Distances.

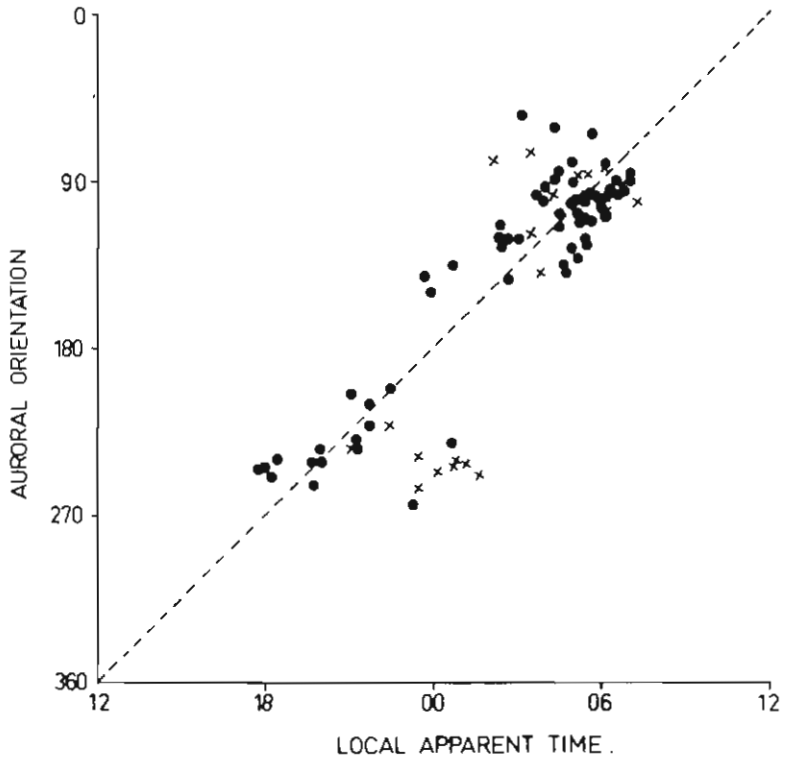


Figure 14. Azimuths of Sun-oriented auroral arcs recorded at Wilkes. *(Denholm 1961)*

# 4. The magnetic field of the Earth

The *attractive* power of lodestone, magnetite ($Fe_3O_4$) or iron ore with magnetic properties, was observed by Thales during the sixth century BC and reported by Aristotle in his *De Anima*. In China, the attractive power of lodestone is mentioned in the *Lii Shih Chhun Chhiu*, written in the third century BC (Needham 1962), and the earliest known text to clearly describe the magnetic needle compass was, according to Needham (1962), *Mêng Chhi Pi Than*, which was written by Shen Kua about 1080 AD. There are earlier possible references to the south-pointing needle, but apparently these cannot be accepted without qualification.

The *directive* property of lodestone appears to have been known in China as early as 83 AD. A reference appears in the *Lun Hêng* by Wang Chhung. Wang Chen-To translated it as: "But when the south-controlling spoon is thrown upon the ground, it comes to rest pointing at the south", but Needham suggested that a better translation would be, "its handle points to the south".

The first undeniable mention of magnetic declination again appears in Chinese literature. In *Pên Tshao Yen I*, dated 1116 AD, Khou Tsung-Shih says:

> Again, if one pierces a small piece of wick transversely with this (magnetised) needle, and floats it on water, it will also point to the south, but will always incline (to the East) towards the compass point Ping (i.e. S 15°E).

A. Crichton Mitchell (quoted in Chapman and Bartels 1940) considered that the earliest mention in European literature of the *polarity* and *directional* properties of a magnet was by a monk of St Albans called Alexander Neckam (1157 — 1217). Neckam wrote two treatises, *De Utensilibus* and *De Rerum Naturis*. In the first he noted that mariners used a magnetised needle to indicate north. In the second he describes a magnetised needle placed on a pivot, probably a primitive European forerunner of the modern mariner's compass.

The fact that a magnetic compass does not usually point to geographic north was known to manufacturers of portable sundials made at Nuremberg as early as 1451 AD, more than 300 years after declination was known to the Chinese. The compasses attached to the sundials made at Nuremberg at about this time have a line marked on them showing that the direction of Compass North was about 10°E of True (Geographic) North. About 1491, Erhard Etzlaub of Nuremberg produced maps with a diagram of a compass dial showing an eastwards deviation or magnetic declination of $11\frac{1}{4}°$. For the term magnetic declination mariners use the term magnetic variation of the compass.

Magnetic inclination or dip seems to have been discovered by Georg Hartmann, Vicar of St Sebald's at Nuremberg. On 4 March 1544 he wrote in a letter to the Duke of Albrect, "A non-magnetic needle, which is balanced horizontally on a pivot, becomes inclined when magnetised." However, it was an Englishman, Robert Norman, who in 1576 made a dip-circle and published a work on "the Declining of the Needle", now called magnetic inclination.

The first publication to pull together these ideas was the famous treatise *De Magnete* by William Gilbert, published in 1600 AD. Gilbert's concept of a uniformly magnetised sphere or *terrella* to represent the Earth was the basic starting point of our present concepts of the magnetic field of the Earth.

The relevant part of Gilbert's work reads:

> The declination[6] of a magnetic needle above a terrella is shown by means of several equal iron wires, of the length of a barley-corn, arranged along a meridian. The wires on the equator are directed by the virtue of the stone toward

[6] The modern term for declination is inclination.

the poles, and lie down upon its body along the plane of its horizon. The nearer they are brought to the poles, the more they are raised up by their versatory nature. At the poles themselves they point perpendicularly toward the very centre. But iron spikes, if they are of more than a due length, are not raised straight up except on a vigorous stone. [see Figure 15]

Gilbert appears to have held the view that the variation of compass (declination) remained constant at a particular location, and he may well have thought that the perfect compass on a perfect Earth would point to Geographic North.

It was not until 1622 that Edmund Gunter found that the magnetic declination at London was then 5° less than the value for 1580, which had been determined by William Borough, a navigator and cartographer. Henry Gellibrand confirmed the fact of continuing change by continuing the observations until 1634 (Gellibrand 1635). The rate of change is now recorded on world magnetic charts published at frequent intervals.

By 1634, serviceable mariners' compasses were in use, and the need to show magnetic information on maps had become important. Many charts covering small areas gradually became available.

The first world magnetic chart showing "variations of the compass" was prepared by Edmund Halley, and published in London in 1702. Halley later became Professor of Geometry at Oxford, and in 1720, Astronomer Royal, but he is, perhaps best remembered for the comet that bears his name. A man of wide interests, he also wrote on the association between the aurora borealis and magnetic disturbance.

The first world chart of magnetic inclination was published by Johan Carl Wilcke (1768). However, progress was not rapid, and it was not until 1837 that Edward Sabine produced a world map of total magnetic intensity, which Carl Gauss used to test his theory of geomagnetism. Sabine was then the Superintendent of the (British) Colonial Magnetic Observatories at Toronto, St Helena (in the South Atlantic Ocean), the Cape of Good Hope (South Africa) and Hobarton (Hobart, Tasmania).

Today, measurements of the Earth's magnetic field are taken at intervals at about 10 000 locations on the surface of the Earth. These data are periodically supplemented by measurements taken on board ships, aircraft and satellites, whose position in space is accurately known.

The magnitude and direction of the total magnetic field at a point (Figure 16) is represented by a vector **F** (or **B**) that can be specified by its rectangular elements or components **X**, **Y**, **Z**, or by the magnetic elements **H**, D, and I, where **H** is the horizontal component of the magnetic field. Its direction is specified by D, the declination (or in mariner's terms, magnetic variation), and I, the inclination (or dip). Observations of any three *independent* magnetic elements from **H**, D, I, **X**, **Y**, **Z**, are sufficient to enable the calculation for the remainder.

There is a world network of over 150 magnetic observatories, where the magnetic elements are continuously registered. Some of these observatories are quite old; even the *New Observatory* at Göttingen in Germany, constructed of non-magnetic materials, appears to have been completed in 1833. Consequently, the records from a number of locations around the world cover a longish period and from these the rate of change of the magnetic elements can be deduced. Thus world maps of the magnetic elements need only be updated with recent observations. Such maps are usually produced every five or ten years by the responsible authorities in Britain, the United States of America and the Union of Soviet Socialist Republics.

World maps are produced in Mercator's Projection, together with maps in azimuthal equidistant projection, for the two polar regions. For non-navigational work, world maps on a simple rectangular grid more readily permit interpolation; for examples see Figures 17, 18, 19 and 20. It should be noted that the *direction* of the magnetic element **H** can be shown either as an isogonic chart of lines of equal declination or as lines of horizontal force called *magnetic*

*meridians*. The magnetic meridians are defined by the property that the tangent at any point is along the direction of **H.**

Maps showing the Earth's magnetic field, or the Geomagnetic Field, probably provide the most accurate representation of the surface magnetic field of the Earth. However, for computational purposes it is desirable to have a mathematical model of the geomagnetic field, and this is the subject of the next chapter.

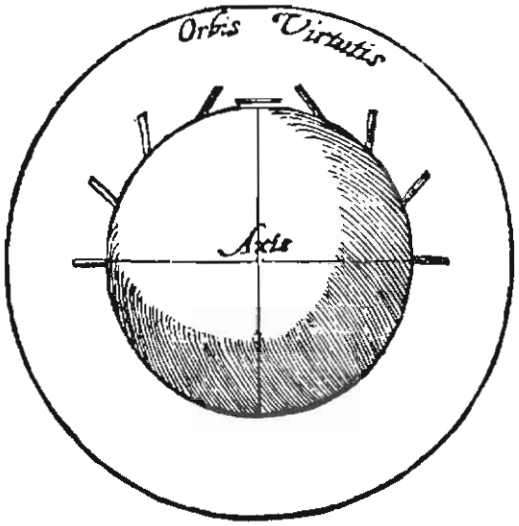


Figure 15. Variety in the declinations of iron spikes at various latitudes of a terrella. (*Gilbert 1600*)

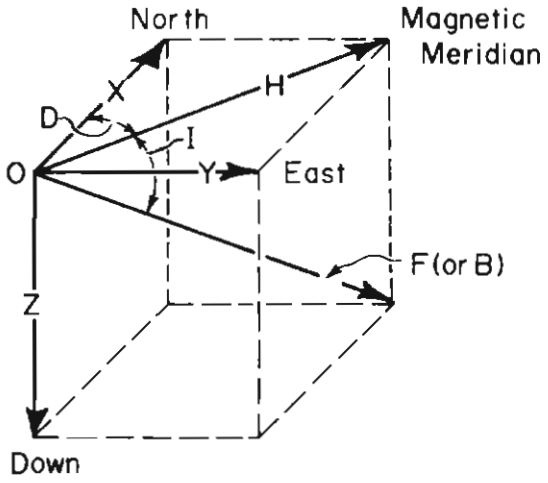


Figure 16. The magnetic elements at the point 0. In the Southern Hemisphere **Z** is negative (up). (after *Chapman and Bartels 1940, vol. 1, p. 2*)

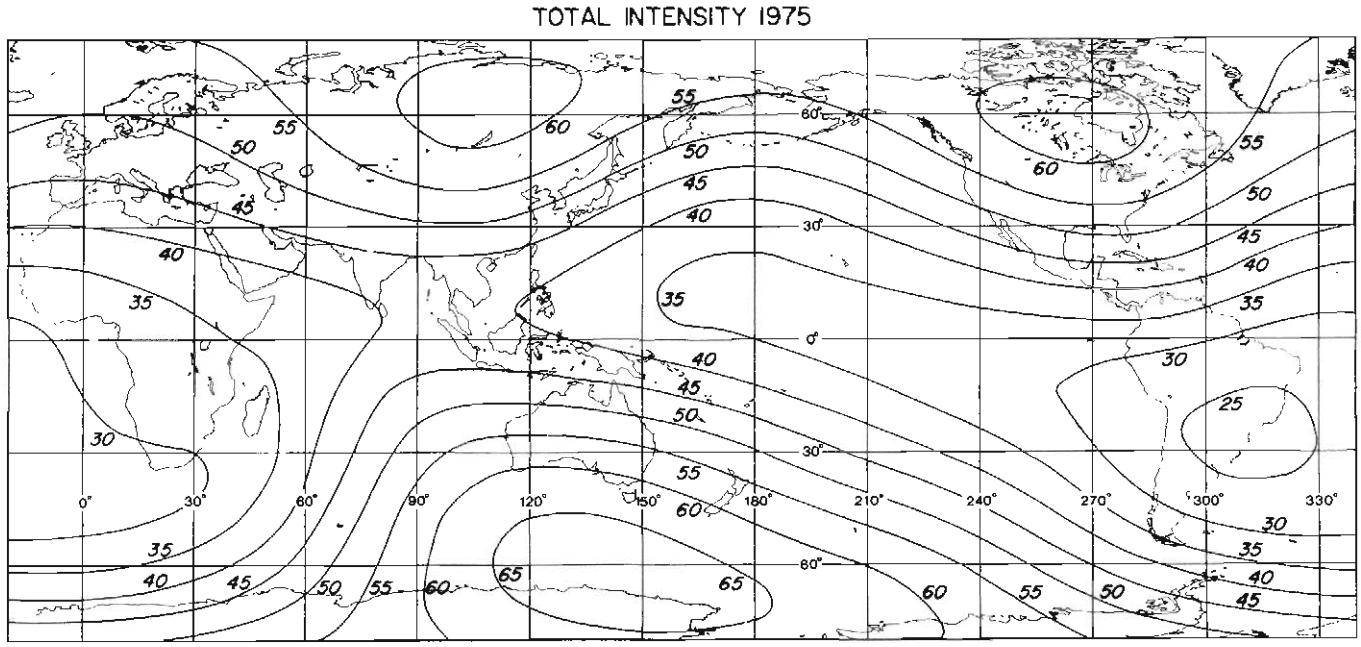


Figure 17. Map in simple rectangular coordinates showing total magnetic intensity in 1975 in microtesla (mT). (*Redrawn from the corresponding British Admiralty Charts, 1975*)

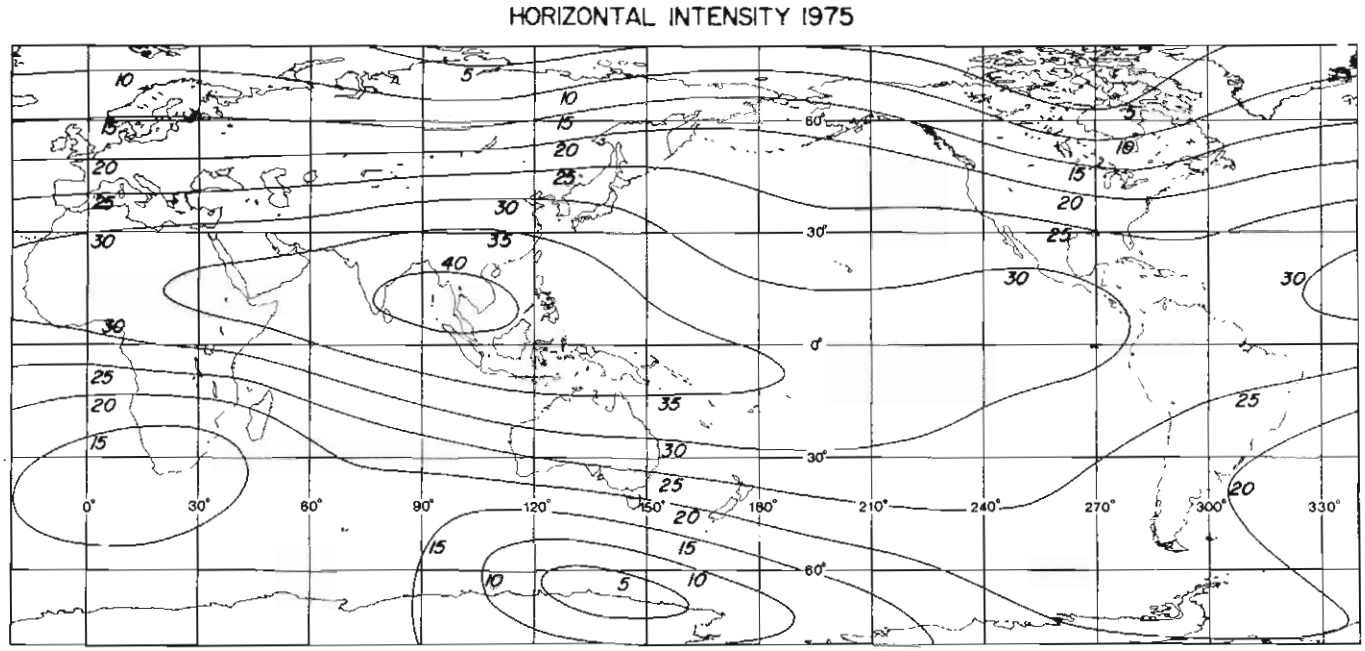


Figure 18. Map in simple rectangular coordinates showing horizontal magnetic intensity in 1975 in microtesla (mT). (*Redrawn from the corresponding British Admiralty Charts, 1975*)

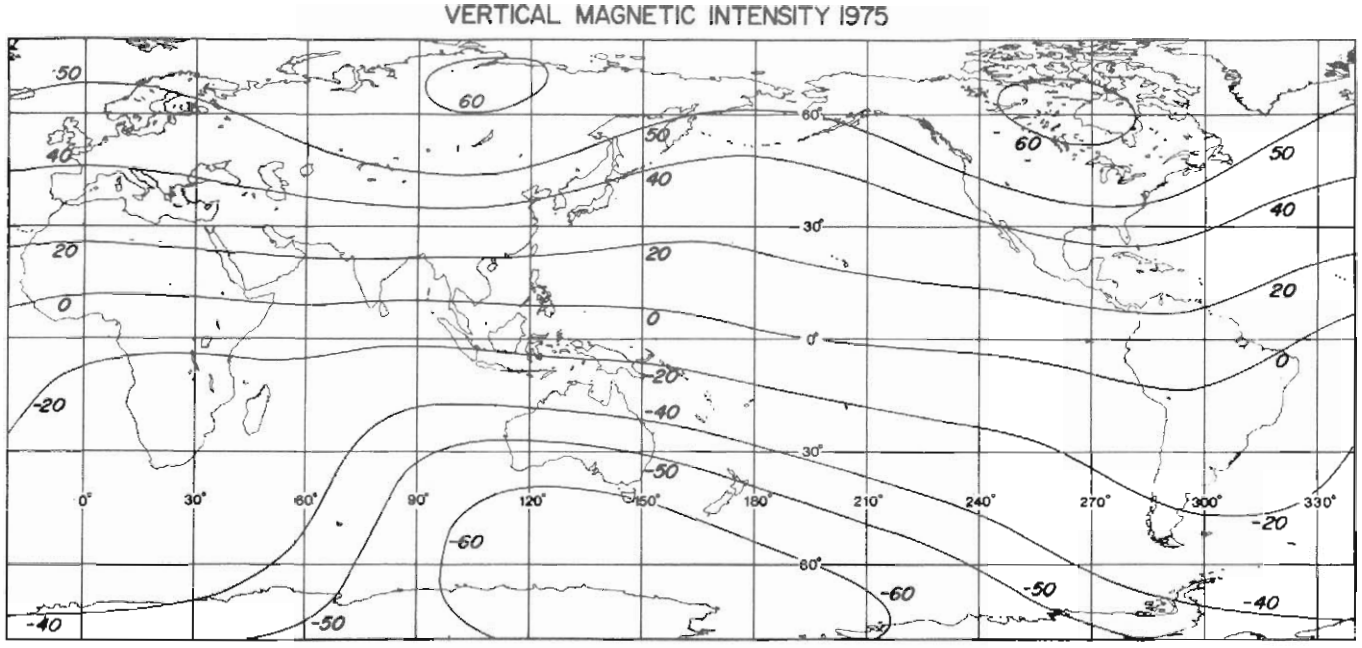


Figure 19. Map in simple rectangular coordinates showing vertical magnetic intensity in 1975 in microtesla (mT). (*Redrawn from the corresponding British Admiralty Charts, 1975*)

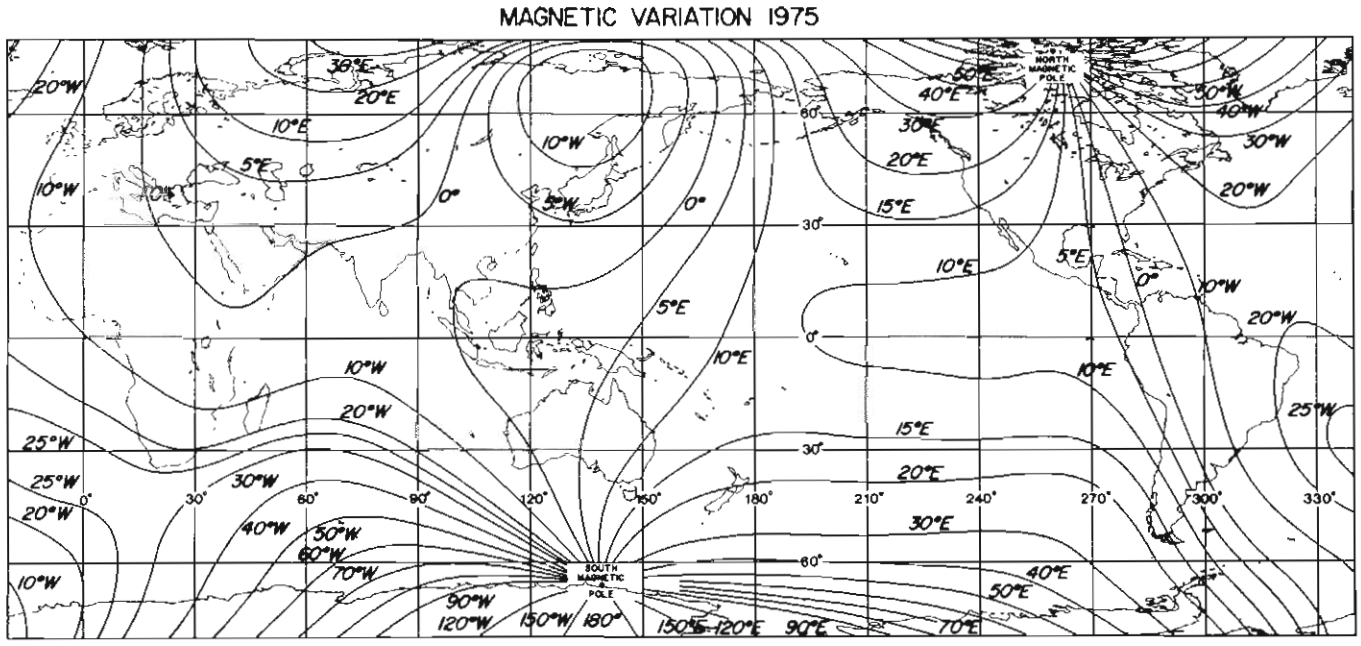


Figure 20. Map in simple rectangular coordinates showing magnetic declination (magnetic variation) in 1975 in degrees. (*Redrawn from the corresponding British Admiralty Charts, 1975*)

# 5. Mathematical approximations of the geomagnetic field

The simplest model of the geomagnetic field is that proposed by Gilbert in 1600. In Gilbert's *terrella* the magnetic field of the Earth was represented by a spherical lodestone oran ir on sphere, uniformly magnetised along the geographic axis, so that the South Geographic Pole had north magnetic polarity.

For any uniformly magnetised sphere, there can be found the parameters of a small magnet, or dipole, which, if placed at the centre of a hollow non-magnetic sphere of the same size, will produce the same surface field and the same external magnetic field as the uniformly magnetised sphere.

After Gilbert's work some progress was made, but the next major step was taken by Professor Carl Frederick Gauss, the director of the observatory of Göttingen. Gauss published a fundamental paper on the theory of the Earth's magnetic field in 1838. He used Sabine's total intensity chart (1837), Barlow's isogones (1833)[7] and Horner's isoclines (1836)[8] to test a mathematical representation of the Earth's magnetic field.

The mathematical representation used the technique of Spherical Harmonic Analysis, which is, in a more developed form, still in use today. (The general reader may wish to omit the side-lined sections.)

A point inside the Earth or in space can be specified in relation to the centre, O, of a spherical Earth, by the Spherical Polar Coordinates (r, $\theta$, $\lambda$,) where:
r is the radial distance from O
$\theta$ is the co-latitude measured from the Geographic North Pole, and
$\lambda$ is the geographic longitude measured eastward from the Greenwich meridian (see Figure 21).
The geomagnetic potential, V, at a point defined by the spherical coordinates (r, $\theta$, $\lambda$,), can be written in the form:

$$V = a \sum_{n=1}^{\infty} \left\{ \left(\frac{r}{a}\right) T_n^e + \left(\frac{a}{r}\right)^{n+1} T_n^i \right\} = V^e + V^i,$$

where *a* denotes the radius of the Earth, the affix *e* denotes the contribution to the potential of fields having external origin, *i* denotes the contribution to the potential of fields having internal origins, and T is defined later.

The magnetic measurements taken around the world are made under magnetically quiet conditions. In these circumstances the contribution of external fields, to the geomagnetic potential is at a minimum, and can for most purposes be ignored, without introducing any great error.

We therefore write the term $T_n$ as

$$T_n = T_n^i = \sum_{m=o}^{n} \left( g_n^m \cos m\lambda + h_n^m \sin m\lambda \right) P_{nm}(\cos\theta)$$

[7], [8] Taken from Chapman and Bartels (1940) - no references found.

where $g_n^m$ and $h_n^m$ are the Gauss coefficients, and $P_{nm}(\cos\theta)$ are functions introduced by Schmidt (1935) and related to the associated Legendre functions (Jackson 1962) $p_n^m(\cos\theta)$ by

$$P_{nm}(\cos\theta) = \left\{\frac{2(n-m)!}{(n+m)!}\right\}^{\frac{1}{2}} P_n^m(\cos\theta).$$

We will now examine the various mathematical approximations to the Earth's true Geomagnetic Field.

The simplest approximation is Gilbert's (1600), which represents the Earth's magnetic field by a small magnet (or dipole) at the centre of the Earth, with its axis coincident with the Geographic Axis, and the magnetic north pole of the magnet pointing to the Geographic South Pole.

The approximation to the geomagnetic field that consists of that field of a dipole at the centre 0 of the Earth that is the best fit to the real geomagnetic field is called the *centred dipole field*. In early work, this approximation was often called the *geomagnetic field*, and this designation still lingers in the literature.

The two points at which the axis of the centred dipole cuts the sphere representing the Earth are called the *Centred Dipole North* (or *Boral*) *Pole* and *Centred Dipole South* (or *Austral*) *Pole*. In older work these poles are known as the *Geomagnetic Poles*. They should not be confused with the *Dip Poles* (magnetic poles), which vary quite rapidly.

The poles of the centred dipole move only very slowly. Great efforts have been made to increase the accuracy of the individual magnetic measurements from which the mathematical models are made, and to increase the number of locations at which the magnetic field is measured, particularly in areas of low population, and on and over the seas.

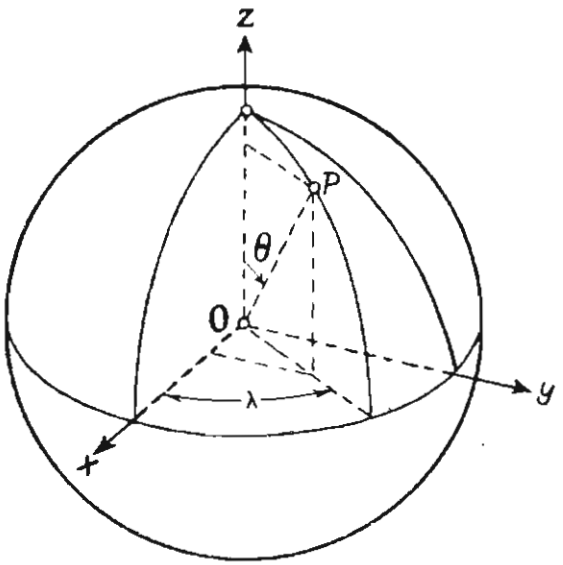


Figure 21. Diagram of the Spherical Polar Coordinates. The point P is shown on the surface of the sphere. (after *Chapman and Bartels 1940, vol. 2, p. 607*)

It would therefore be helpful if authors specified the literature source of the Poles of the Centred Dipole Field used in their publications.

To demonstrate that the Centred Dipole Field is a useful approximation to the true Geomagnetic field, take the three first-order terms of the Spherical Harmonic Expansion of V. Thus

$$V_1 = \frac{a^3}{r^2}\left[g_1^0 P_{10}(\cos\theta) + \left(g_1^1\cos\lambda + h_1^1\sin\lambda\right)P_{11}(\cos\theta)\right]$$

$$= \frac{a^3}{r^2}\left[g_1^0\cos\theta + g_1^1\sin\theta\cos\lambda + h_1^1\sin\theta\sin\lambda\right]$$

Defining a specialised direction $\theta_0, \lambda_0$ such that

$$g_1^0 = H_o\cos\theta_o,$$

$$g_1^1 = H_o\sin\theta_o\cos\lambda_o,$$

$$h_1^1 = H_o\sin\theta_o\sin\lambda_o,$$

it follows that

$$V_1 = \frac{a^3}{r^2}H_o\cos\Theta.$$

where $\Theta$ is the angle between the direction $(\theta,\lambda)$ and the specialised direction $(\theta_o,\lambda_o)$, given by $\cos\Theta = \cos\theta\cos\theta_o + \sin\theta\sin\theta_o\cos(\lambda-\lambda_o)$.
Thus $V_1$ represents the potential of a centred dipole magnetised in the direction $(-\theta_o,-\lambda_o)$, having an axis through $(\theta_o,\lambda_o)$ in the Northern Hemisphere and through $(180+\theta_o,180+\lambda_o)$ in the Southern Hemisphere.

When the specialised direction is $\theta_o = \lambda_o = 0°$, that is, the direction of the North Geographic Pole, then $\Theta = \theta$ and

$$V_1 = \frac{a^3}{r^2}H_o\cos\theta.$$

This is the same as the magnetic potential of a sphere of radius "a" uniformly magnetised along the direction $(-\theta_o,-\lambda_o)$. It then follows that

$$Z_1 = \left(\frac{\partial V_1}{\partial r}\right)_{r=a} = -2H_o\cos\theta$$

and

$$H_1 = -\left(\frac{1}{r}\frac{\partial V}{\partial\theta}\right)_{r=a} = H_o\sin\theta.$$

This is the same magnetic field as that of a uniformly magnetised sphere, or that of an axial dipole at the centre of a sphere having a magnetic moment M given by $M = H_o a^3$, which was the case postulated by Gilbert.

For the International Geomagnetic Reference Field (IGRF) for 1975.0, we have (in units of $1\gamma = 10^{-5}$ Gauss) the following values for the first three Gauss coefficients, $g_1^0, g_1^1$ and $h_1^1$.

$$g_1^0 = -30186$$
$$g_1^1 = -2036$$
$$h_1^1 = 5735$$

Hence the Centred Dipole Northern Hemisphere Pole was located at approximately 78.6°N, 70.45°W (geographic) and the pole in the Southern Hemisphere was located at approximately 78.6°S, 109.55°E on 1 January 1975.

For comparison, Schmidt (1898) for the epoch 1885.0 found the location of the Northern Hemisphere Pole, which he called the North Geomagnetic Pole, at approximately geographic latitude 78.5°N and geographic longitude 68.5°W. It must be remembered that Schmidt's data did not have as complete a world coverage, and may not have been as accurate as the IGRF 1975.0 data; however, part of the difference may be due to the slow secular change of the Earth's magnetic field.

The equation of the external lines of force of the Earth's magnetic field in the centred dipole approximation is simply determined.

Let $(r, \Theta, \Lambda)$ be the coordinates of a spherical coordinate system centred in the dipole and having its axis parallel to the magnetic moment $a$, (Figure 22). We also introduce the latitude $\Phi = \frac{1}{2}\pi - \Theta$.

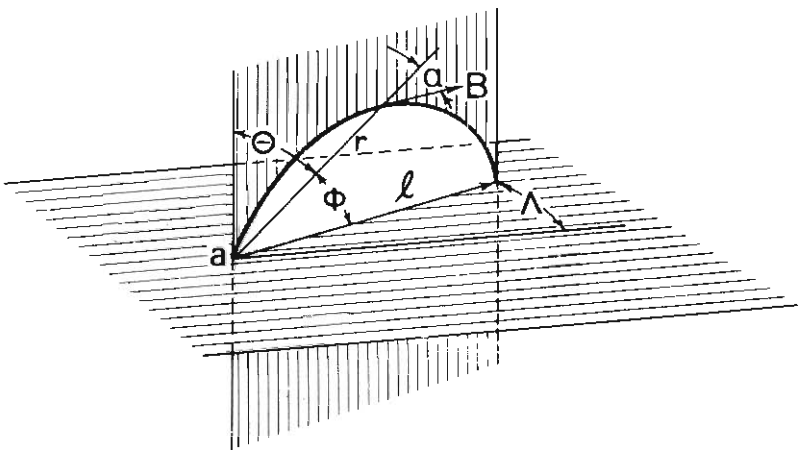


Figure 22. Diagram of a line of force of a dipole having magnetic moment *a*. (*after Alfven and Fälthammar 1950, p. 4*)

The magnetic field is then given by

$$B = -\text{grad } \psi$$

where $\psi = \psi = \frac{ar}{r^3} = a\frac{\sin\Phi}{r^2}$

The components are:

$$B_r = B_p \sin\Phi$$

$$B_\Phi = -\tfrac{1}{2} B_p \cos\Phi$$

$$B_\Lambda = 0,$$

and the total field strength:

$$B = \sqrt{B_r^2 + B_\Phi^2 + B_\Lambda^2} = \tfrac{1}{2} B_p \Lambda = \frac{a\Lambda}{r^3}$$

where $B_p = 2a / r^3$

and $\Lambda = \sqrt{\left(1 + 3\sin^2\Phi\right)}$

$B_r$ represents the "vertical" and $B_\Phi$ the "horizontal" component of the field. A magnetic line of force is given by the equations

$$r = \ell \cos^2\Phi,$$

$$\Lambda = \text{const},$$

where $\ell$ is the distance from the origin to the point of intersection with the equatorial plane ($\Phi = 0$). The angle $\alpha$ between the line of force and the radius vector is given by

$$\tan\alpha = \tfrac{1}{2}\cot\Phi$$

$$\sin\alpha = \frac{\cos\Phi}{\Lambda}$$

$$\cos\alpha = \frac{2\sin\Phi}{\Lambda}$$

The 'inclination' of the field is $\frac{1}{2}\pi - \alpha$.
The total strength of the field along a given line of force can also be written

$$B = \frac{a}{r^3}\Lambda = \frac{a}{\ell^3}(\cos\Phi)^{-6}\Lambda = \frac{a}{\ell^3}\eta,$$

where $\eta = \dfrac{\sqrt{\left(1 + 3\sin^2\Phi\right)}}{\cos^6\Phi}$

In a Cartesian coordinate system $(x, y, z)$ we have

$$B_x = 3xz\frac{a}{r^5},$$

$$B_x = 3yz\frac{a}{r^5}$$

$$B_z = (3z^2 - r^2)\frac{a}{r^5},$$

where $r^2 = x^2 + y^2 + z^2$.

As already noted, the *geomagnetic field* is, in approximation, a centred dipole field. If a dipole situated at the centre of the Earth is fitted to the geomagnetic data, the dipole moment becomes $a \simeq 8.1 \times 10^{25}$ gauss cm$^3$, which corresponds to a polar field strength of about 0.62 gauss.

Another dipole concept provides an even better approximation to the geomagnetic field. In the previous case, we constrained the dipole to lie at the centre 0. Now we discuss the best-fit dipole, which is not constrained to lie at 0. This is called the *Eccentric Dipole Field*.

Schmidt (1934) found that the magnetic centre $C(x_o, y_o z_o)$ for the best-fit dipole approximation of the geomagnetic field is given by the equations:

$$x_o = \frac{a\left(L_1 - g_1^1 E\right)}{3H_0^2},$$

$$y_o = \frac{a\left(L_2 - h_1^1 E\right)}{3H_0^2}, \quad z_o = \frac{a\left(L_o - g_1^o E\right)}{3H_0^2}$$

where $H_o^2 = g_1^o g_1^o + g_1^1 g_1^1 + h_1^1 h_1^1$,

$$L_o = 2g_1^o g_2^o + \left(g_1^1 g_2^1 + h_1^1 h_2^1\right)\sqrt{3},$$

$$L_1 = -g_1^1 g_2^o + \left(g_1^o g_2^1 + g_1^1 g_2^2 + h_1^1 h_2^2\right)\sqrt{3},$$

$$L_2 = -h_1^1 g_2^o + \left(g_1^o h_2^1 + h_1^1 g_2^2 + g_1^1 h_2^2\right)\sqrt{3},$$

and $$E = \frac{L_o g_1^o + L_1 g_1^1 + L_2 h_1^1}{4H_o^2},$$

The $g_n^m$, $h_n^m$ in the equations above differ from those given in Chapman and Bartels (1940). The Chapman and Bartels version is a direct copy from Schmidt (1935), but Schmidt's axes are different from those used by Chapman and Bartels earlier in their chapter. For consistency, the $g_n^m$ and $h_n^m$ coefficients are corrected above.

For the IGRF 1975.0 data, the magnetic centre C, was at

$x_o = -374.54$ km
$y_o = 244.14$ km
$z_o = 150.04$ km

or at a point along a line from the centre of the Earth, 0, to the point on the surface at 19°28'N, 147°54'E, i.e. about 579.6 km (360 miles) north and 193.2 km (120 miles) east of Guam, at a distance of about 471.6 km (293 miles) from the centre.

These systems of approximations to geomagnetic latitude and longitude form the subject of the next chapter.

# 6. Geomagnetic latitude and longitude systems

The "natural" system of geomagnetic latitudes is provided by the lines of constant inclination or dip (Figures 23 and 24). Unfortunately, this "natural" system does not generally conform to the pattern of the auroral zone as determined by the lines of constant overhead frequency called *isoaurores*.

The "natural"system of geomagnetic longitudes is provided by the magnetic meridians, or lines showing the direction of horizontal magnetic force (Figures 25 and 26). At any point along the magnetic meridian, the tangent to the meridian indicates the direction of the horizontal component of the Earth's magnetic field.

The magnetic latitude and longitude system that corresponds to the approximation of the Earth's magnetic field by a dipole at the centre of the Earth, aligned along the spin axis, is, obviously, the geographic system. Although this is the least accurate approximation, it is sometimes found in the context of archeomagnetism and paleomagnetism, and was also used in early determinations of the shape of the magnetosphere.

Schmidt (1918) introduced a set of geomagnetic coordinates, now called *centred dipole coordinates*. The latitudes of this system are determined by the intersections of a set of planes, perpendicular to the centred dipole axis, with a sphere representing the Earth. Longitudes are defined by a set of planes, which includes the centred dipole axis. Schmidt chose to define the zero of centred dipole longitude as that great circle that includes the poles of the centred dipole axis and the geographic South Pole (Figures 27 and 28).

This system is mathematically simple but, as we shall see, gives a poor approximation to the true geomagnetic coordinates in the polar regions, particularly in the Northern Hemisphere.

Corresponding to the eccentric dipole approximation of the geomagnetic field, a set of eccentric dipole latitudes and longitudes was presented by Cole (1963) (Figures 29 and 30). Starting with poles of the eccentric dipole determined by Parkinson and Cleary (1958), who used the data of the Gaussian coefficients for the geomagnetic field of 1955 as presented by Finch and Leaton (1957), Cole presented equations for eccentric dipole latitude and longitude in terms of three sets of direction cosines ($\ell_i$, $m_i$, $n_i$) of the eccentric poles and the magnetic centre, together with the coordinates (X, Y, Z) of the magnetic centre.

The curves of eccentric dipole co-latitude are the intersections of a set of cones of semi-angle $(\Theta_1)$, with a unit sphere representing the Earth.
The co-latitudes $(\Theta_1)$ are determined by the equation

$$\ell_3(\sin\theta\cos\lambda - X) + m_3(\sin\theta\sin\lambda - Y) + n_3(\cos\Theta - Z)$$
$$= \cos\Theta_1\{[\ell_1(\sin\theta\cos\lambda - X) + m_1(\sin\theta\sin\lambda - Y) + n_1(\cos\theta - Z)]^2$$
$$+[\ell_2(\sin\theta\cos\lambda - X) + m_2(\sin\theta\sin\lambda - Y) + n_2(\cos\theta - Z)]^2\}^{\frac{1}{2}}$$

The longitudes $\Lambda_1'$ are determined by the intersections of planes containing the axis of the eccentric dipole with a unit sphere. The longitudes are given by the equation

$$\ell_2(\sin\theta\cos\lambda - X) + m_2(\sin\theta\sin\lambda - Y) + n_2(\cos\theta - Z)$$
$$= \tan\Lambda_1'\{\ell_1(\sin\theta\cos\lambda - X) + m_1(\sin\theta\sin\lambda - Y) + n_1(\cos\theta - Z)\}.$$

The values of the direction cosines and coordinates of the magnetic centre for 1955 were:

| | | |
|---|---|---|
| $\ell_1 = -0.5146$ | $m_1 = -0.8481$ | $n_1 = -0.1262$ |
| $\ell_2 = 0.8543$ | $m_2 = -0.4947$ | $n_2 = -0.1596$ |
| $\ell_3 = 0.0728$ | $m_3 = -0.1894$ | $n_3 = 0.9791$ |
| $X = -0.0577$ | $Y = 0.0320$ | $Z = 0.0184$ |

Following Schmidt (1918) for centred dipole longitude, Cole defined the zero as that longitude that passed through the poles of the eccentric dipole and the South Geographic Pole.

In the $(\Theta_1, \Lambda_1')$ system, the South Geographic Pole lies at 61.02°E. Hence the dipole longitude $\Lambda_1$ is given by

$$\Lambda_1 = \Lambda_1' - 61.02$$

for the data presented (Figures 29 and 30).

Realising that, for studies of cosmic rays and the propagation of whistlers[9] the centred dipole approximation to the Earth's magnetic field was not sufficiently accurate, Hultqvist (1958) used a perturbation method to devise a way of representing the geomagnetic field lines in higher approximation. The deviation from the centred dipole field at the surface of the Earth, of the feet of field lines, with starting points in the plane of the centred dipole Equator, was calculated from the five first terms of the spherical harmonic analysis due to Vestine *et al.* (1947) of the geomagnetic field for epoch 1945.

If the starting point of field-line tracing is a circle in the equatorial plane of the centred dipole, given by field lines at centred dipole latitude $\Phi = 60°$, then the end points of the field lines resulting from the perturbation calculation essentially behave as a corrected latitude $\Phi_2 = 60°$ with corresponding co-latitude $\Theta_2 = 30°$.

Mayaud (1960) introduced a new concept of a system of magnetic coordinates, based on the work of Hultqvist, which he called *Equatorial Ring Coordinates*. Tables and maps of this system of geomagnetic coordinates were published by Hakura (1965) (see Figures 31 and 32). These longitudes can be labelled in terms of $\Lambda_2$.

Hakura's paper also deals with the question of geomagnetic time; however, Cole's (1963) concept of geomagnetic time in the paper on eccentric dipole coordinates adapted, where necessary, to the system of geomagnetic coordinates being used, seems preferable since it does not involve graphical interpolation.

Essentially, geomagnetic time at a station is the difference between the geomagnetic longitude of the Sun and the geomagnetic longitude of the station, measured eastwards from the Sun, i.e. from 1200 hours.

Geomagnetic coordinate systems were developed further by Northrop and Teller (1960) in a paper on the stability of the adiabatic motion of charged particles in the Earth's magnetic field. They discuss three mathematical invariants that describe the movement of charged particles.

Studies of the motion of charged particles in the Earth's magnetic field showed that many particles will spiral round a field line, and will be reflected at a "magnetic mirror" formed by the stronger magnetic fields in high latitudes, so oscillating from polar region to polar region. This movement is described in Størmer (1955) and Alfvén and Fälthammar (1963).

[9] *Whistlers* are wave phenomena, originated by lightning, that propagate along the field lines of the Earth's magnetic field. As recorded, and when the magnetic tape records are replayed, the phenomena is heard as a whistling sound. When they were first heard on telephones, picked up by the overhead wires acting as an aerial, it was conjectured that they were signals from the Martians.

The reflection of particles at magnetic mirror points depends upon the invariance of the magnetic moment of the particle. The condition of reflection is given approximately by the Alfvén equation

$$\frac{F}{\sin^2\alpha} = \text{constant},$$

where F is the strength of the magnetic field and $\alpha$ is the angle between the velocity vector direction of the particle and the direction of the magnetic field.

When $\alpha = 90°$, reflection occurs, and $F = F_m$, the magnetic field at the mirror point. However, if the initial value of $\alpha$ is small enough, $\alpha$ never reaches the value $\alpha = 90°$ and so the particle is precipitated. The critical value of $\alpha$ defines a "loss cone".

Besides oscillating between the two polar regions, the electrons that do not enter the loss cone drift from west to east, while protons drift from east to west, giving rise at certain latitudes to the corpuscular radiation belt discovered independently by Van Allen of the USA and Vernov of the USSR (Van Allen 1968).

In a static or slowly varying geomagnetic field the particle will encircle the Earth and return to the initial field line and then, of course, continue to circle the Earth, provided that the longitudinal invariant, I, is conserved.

The longitudinal invariant, I, is given by

$$I = \int (1 - F / F_m)^{\frac{1}{2}} ds$$

The integration is carried out from the mirror point $F_m$ in the Southern Hemisphere along the field line *s* to the corresponding mirror point in the Northern Hemisphere.

The third invariant requires that the total flux in a magnetic tube of force shall remain constant.

For the second invariant, Vestine and Sibley (1960) prepared maps of both hemispheres in corrected centred dipole coordinates (48 gauss coefficients) showing contour lines corresponding to equal values of the integral I. They also indicated the similarity between the distribution of the aurora and the general shape of the I curves.

In a paper on the distribution of auroras, Bond and Jacka (1962) argued that for each value of I determined from a set of Gaussian coefficients of the geomagnetic field, there exists an equal value I' determined from the corresponding centred dipole field. Since there is a centred dipole latitude $\Lambda$, which corresponds to I', we can define an equal-valued 'invariant' latitude $\Lambda_3$ that corresponds to I.

To achieve this situation, Bond prepared maps in geographic coordinates on which the I curves for $F_m = 0.45$ gauss presented by Vestine and Sibley (1960) were projected along the field lines to the mean auroral lower border height of 105 km and labelled with the relevant co-latitude $\Theta_3$ (Figures 33 and 34).

In a prior publication of this concept, McIlwain (1961) gave a more elegant mathematical presentation, and also separately produced a computer program by which field lines could be traced, given a set of gaussian coefficients. O'Brien (1962) independently published this latitude concept, giving the equation

$$L \cos^2 \Lambda_4 = I,$$

where L is the McIlwain parameter – the distance from the centre of the Earth to the minimum value of **F** (or **B**) on the field line – is conceptually similar to $\ell$ for the centred dipole field.

The time-longitude concept $\Lambda_4'$ Bond (1968) developed is conceptually similar to the eccentric dipole longitude $\Lambda_1$ due to Cole (1963). Maps of this longitude concept are presented in Figures 35 and 36. In the same paper, the author developed a more accurate longitude concept, $\Lambda_4$, for the determination of magnetic conjugacy.

A radial line was taken from the centre of the Earth through the intersection of a designated $\Lambda_4'$ longitude and the estimated $\Theta_4$ geomagnetic equator. Starting points from which magnetic field lines can be traced were located on this radial line. Suitable heights for these starting points were chosen as the equatorial distances in the dipole approximation for values $\Theta = 5°$ to $\Theta = 85°$ at 5° intervals.

From a given starting point the field line was traced with a modified McIlwain program to give the two ends of the field line at the average auroral lower border height of 105 km. This set of starting points gave pairs of end points all originating at time-longitude $\Lambda_4'$. Thus the line, from the Northern Auroral Pole, through the northern and southern sets of end points, to the Southern Auroral Pole, defines the $\Lambda_4$ longitude corresponding to the value of $\Lambda_4'$ chosen. Maps of these conjugate longitudes are presented in Figures 37 and 38.

Kilfoyle and Jacka (1968) suggested that the zero of geomagnetic longitudes should coincide at the geographical equator with the Greenwich longitude. This concept has the advantage that geographic longitudes and geomagnetic longitudes have similar numerical values, rather than the considerable differences that follow from continuing the precedent set by Schmidt (1918) for centred dipole longitude.

In an attempt to devise a longitude zero, Evans *et al.* (1969) chose a plane that would approximately bisect the angle between that geomagnetic meridian plane containing the South Geographic Pole and the corresponding plane containing the North Geographic Pole. For the sets of coordinates for the six altitudes 0, 100, 300, 600, 1000 and 3000 km, the meridian plane chosen crossed the geographic equator at 284.0°E geographic longitude.

It is not certain whether the advantages in relation to L-geomagnetic time, which the proponents assert will accrue, improve on the system proposed by Cole (1963) as adapted to L-geomagnetic coordinates.

For completeness, a map produced by Campbell and Matsushita (1967) to determine geomagnetic conjugacy should be mentioned. On this map L-geomagnetic latitudes at 100 km are presented (see Figure 39), but the nature of the other latitude lines and the longitude lines is not indicated. The poles appear to be the magnetic dip poles, and since the longitude lines pass from dip pole to dip pole, the "longitudes" appear to be similar to the magnetic meridians and the "latitudes" appear to be similar to the lines of constant dip.

The concept of conjugacy is that two points on the Earth's surface are linked by a geomagnetic field line. The conjugate points given by Campbell's and Matsushita's map are somewhat different from the conjugate points given by field-line tracings using McIlwain's program.

A determination of L-latitudes and longitudes was carried out by Boyd (1977). Besides providing maps of L-coordinates (see Figures 40, 41 and 42), he also provided two computer programs in terms of a set of spherical harmonic coefficients from which the L-coordinates of a point given in geographic coordinates can be determined more quickly.

Against the various models of geomagnetic latitude and longitude that we have presented, in the next chapter we shall examine the distribution of the frequency of occurrence of the aurora and the determination of the auroral zone.

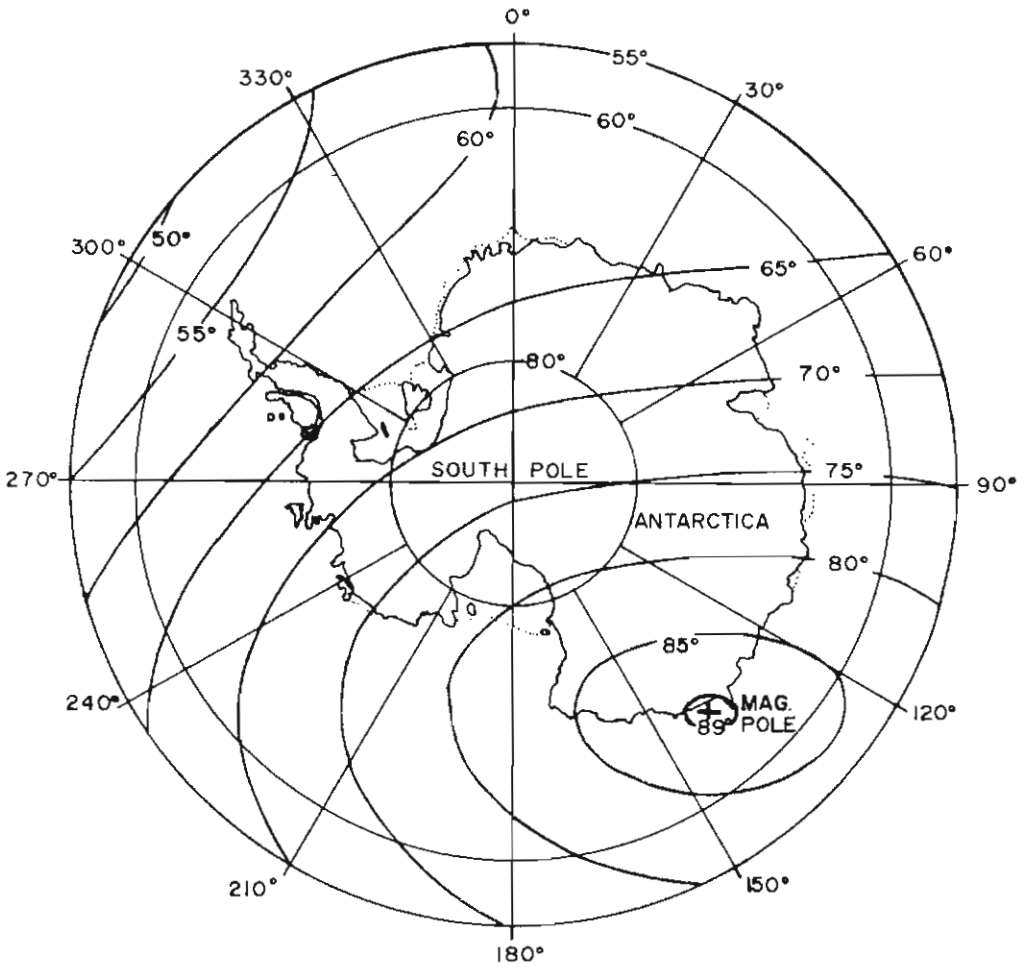


Figure 23. Lines of constant magnetic dip for the Southern Hemisphere for 1975.

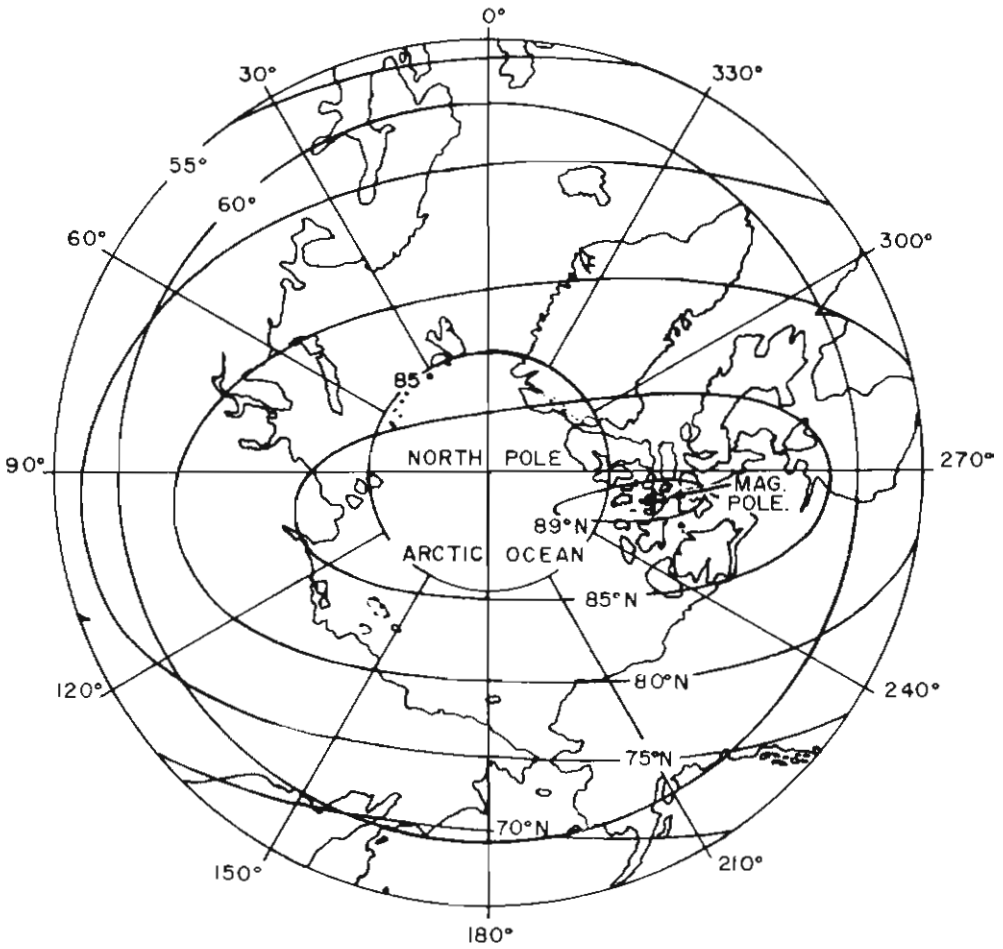


Figure 24. Lines of constant magnetic dip for the Northern Hemisphere for 1975.

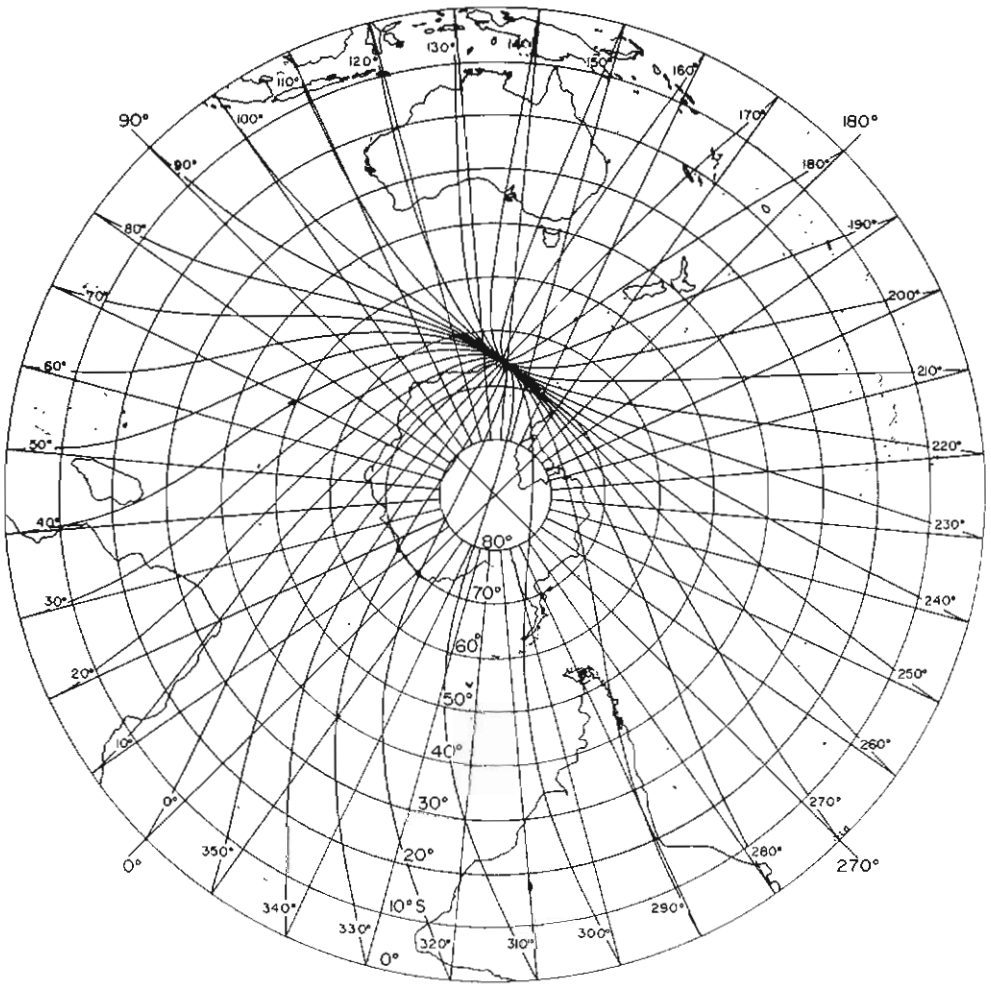


Figure 25. Magnetic meridians for the Southern Hemisphere for 1975. (*Program by H. Burton, Antarctic Division, 1980*)

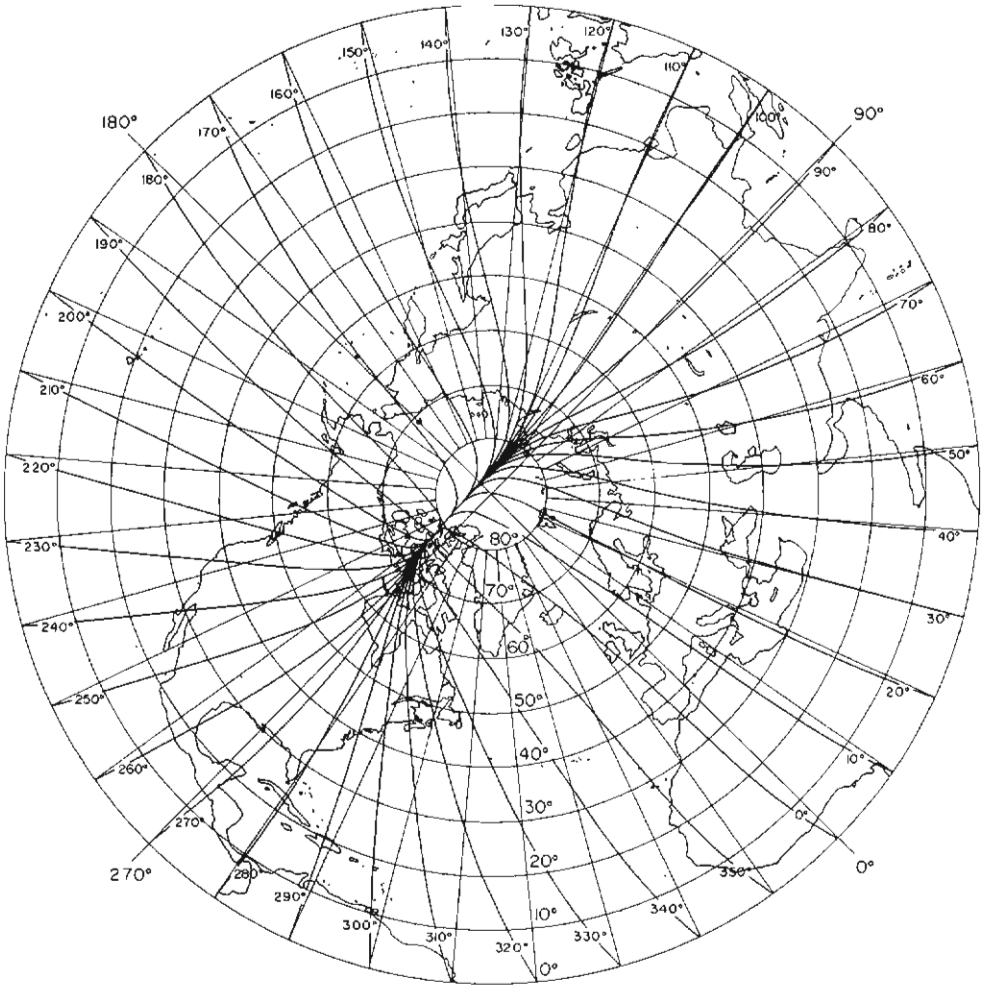


Figure 26. Magnetic meridians for the Northern Hemisphere for 1975. (*Program by H. Burton, Antarctic Division, 1980*)

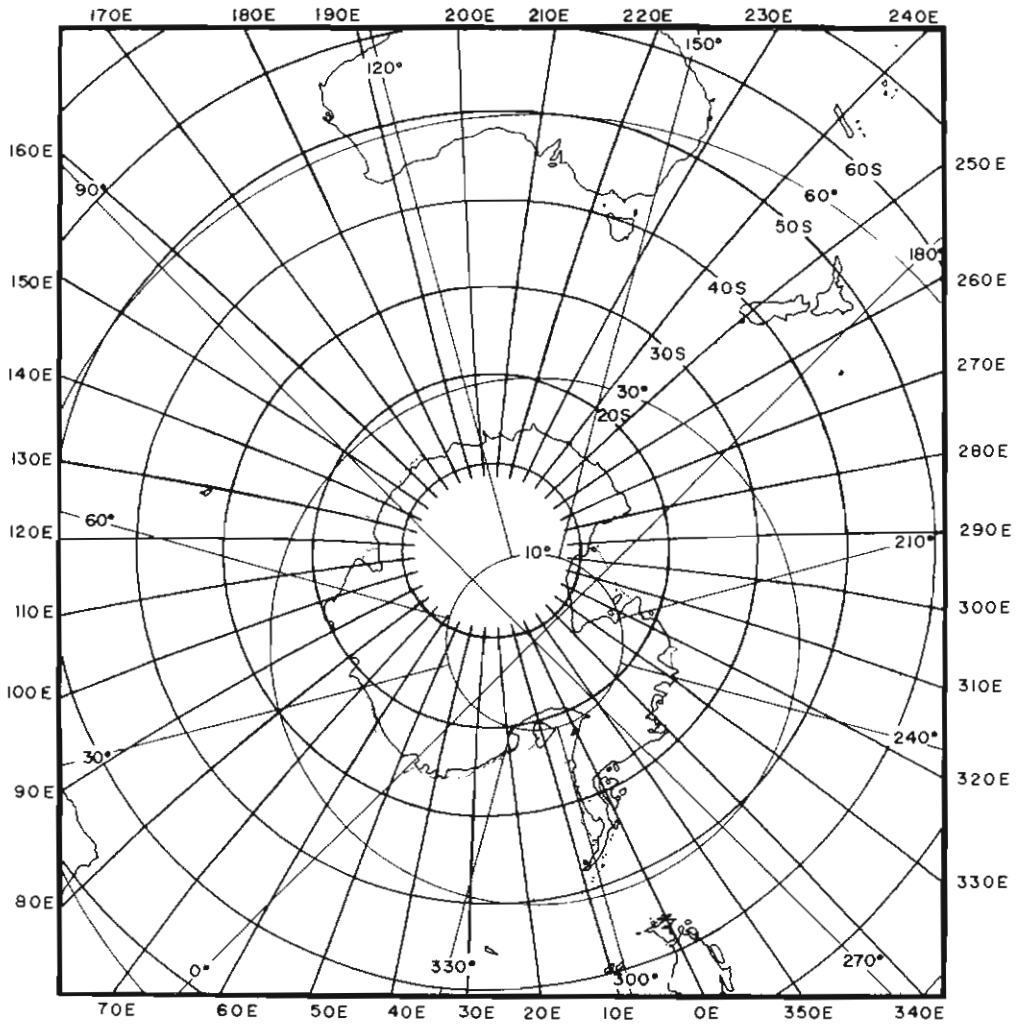


Figure 27. Centred dipole latitudes and longitudes for 1975 based on the International Geomagnetic Reference Field 1975.

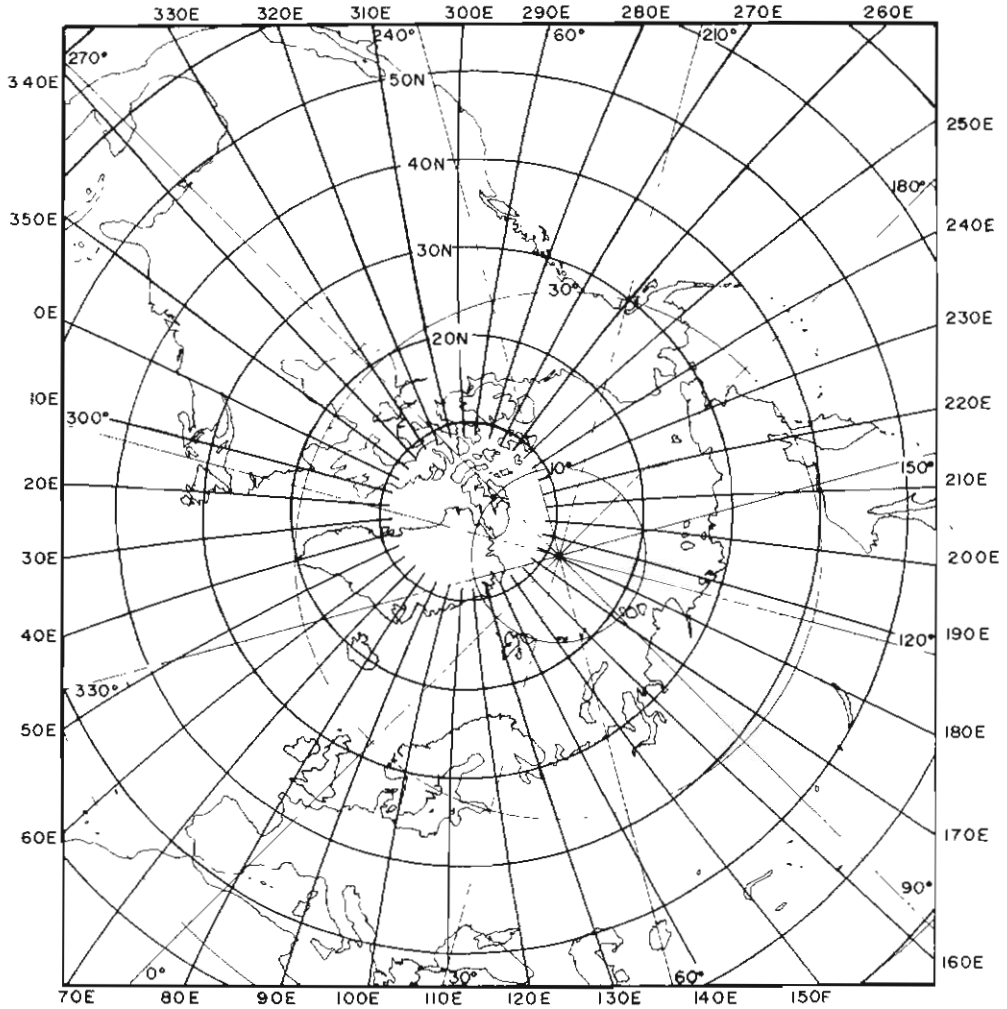


Figure 28. Centred dipole latitudes and longitudes for the Northern Hemisphere based on the International Geomagnetic Reference Field 1975.

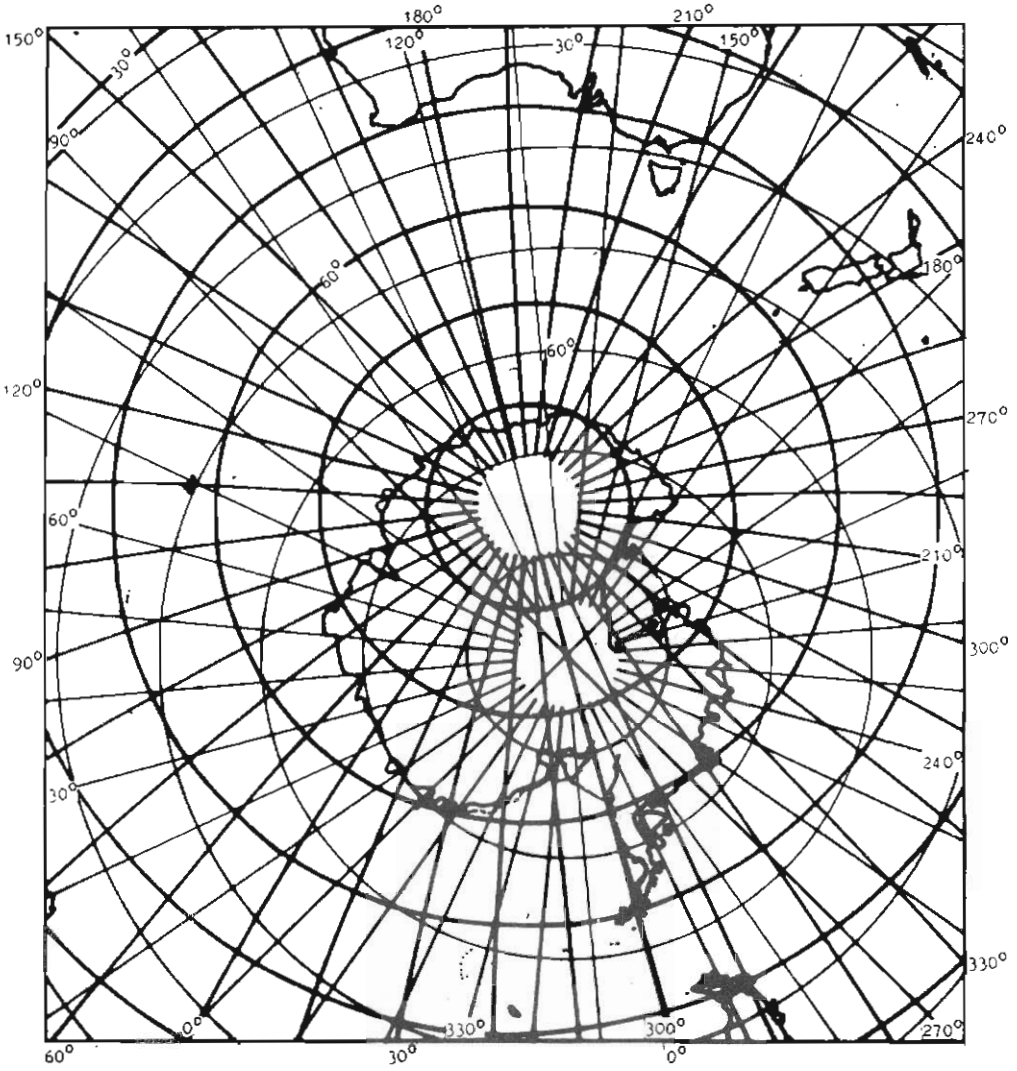


Figure 29. Eccentric dipole latitudes $\Phi_1$ and longitude $\Lambda_1$ superimposed upon an outline azimuthal equidistant projection map of the Southern Hemisphere. (*Base map by Department of National Mapping, Australia*)

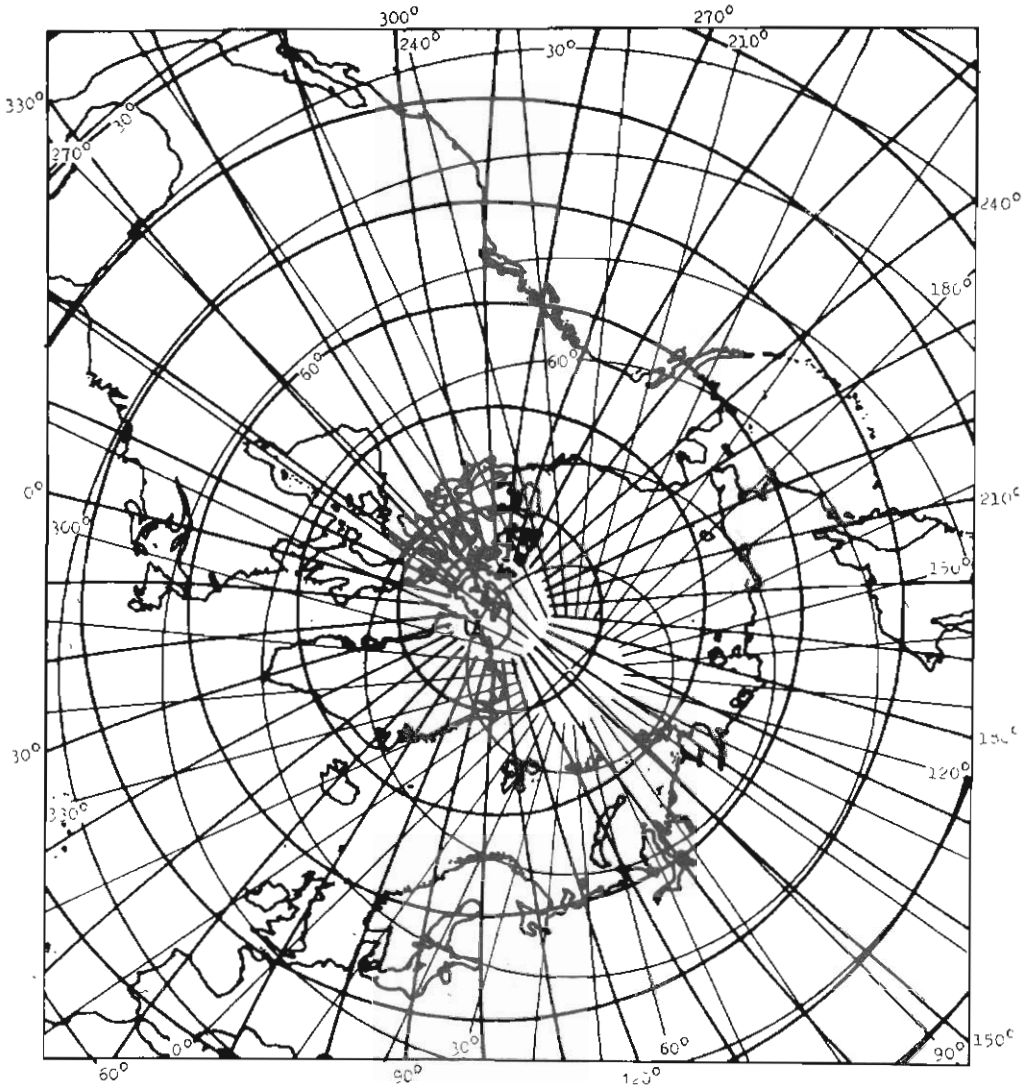


Figure 30. Eccentric dipole latitude $\Phi_1$ and longitude $\Lambda_1$ superimposed upon an approximate hand-drawn outline azimuthal equidistant projection map of the Northern Hemisphere. (*Base map by Department of National Mapping, Australia*)

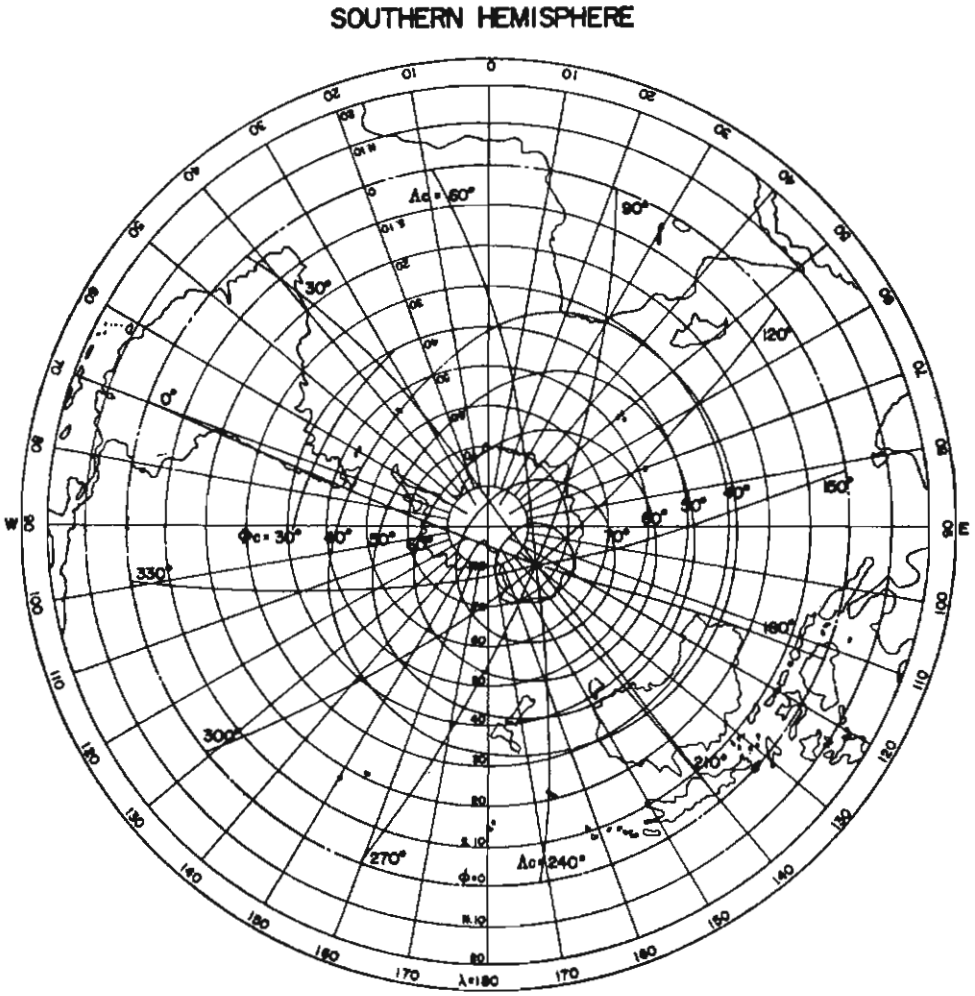


Figure 31. A southern polar map in the geographic coordinates, on which the corrected geomagnetic latitude $(\Phi_2)$ and the longitude $(\Lambda_2)$ are drawn in 10° and 30° intervals respectively. The estimated corrected Geomagnetic Pole is at (75°S,129°E). (*Hakura 1965*)

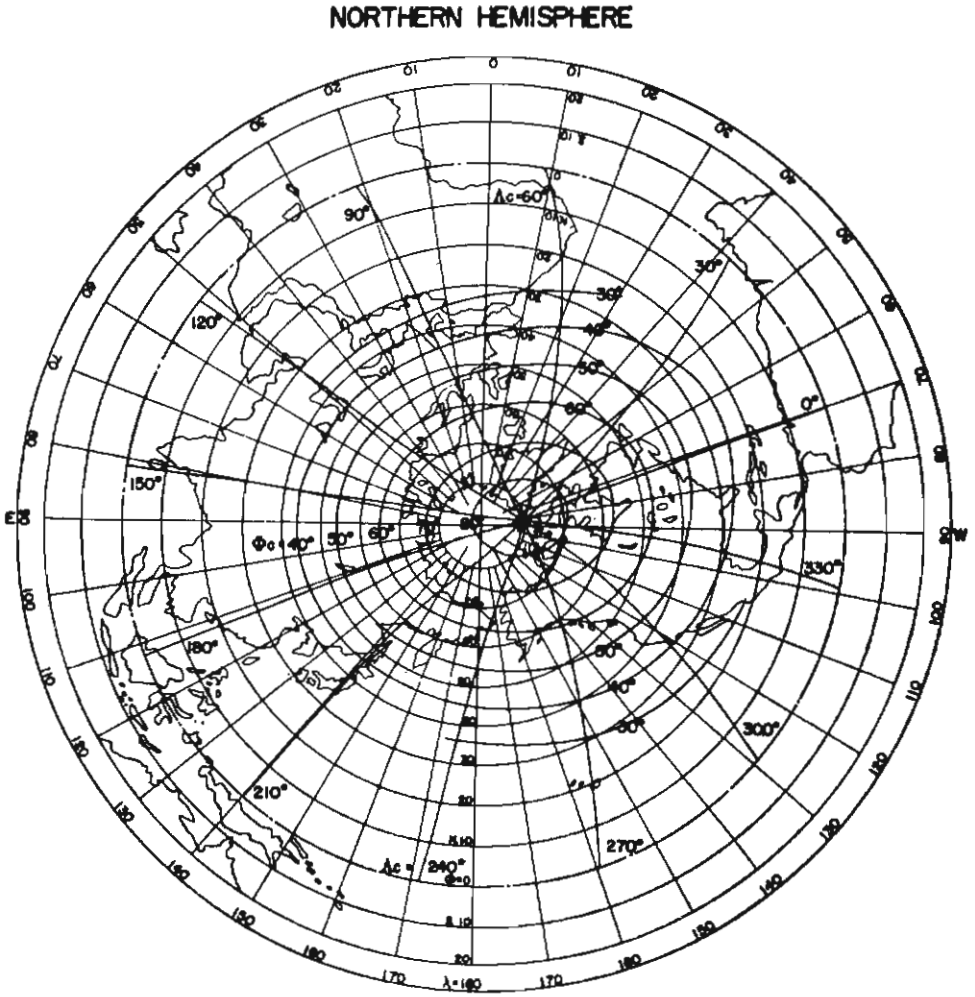


Figure 32. A northern polar map in the geographic coordinates, on which the corrected geomagnetic latitude $(\Phi_2)$ and the longitude $(\Lambda_2)$ are drawn in 10° and 30° intervals respectively. The estimated corrected Geomagnetic Pole is at (80°N,180°W). (*Hakura 1965*)

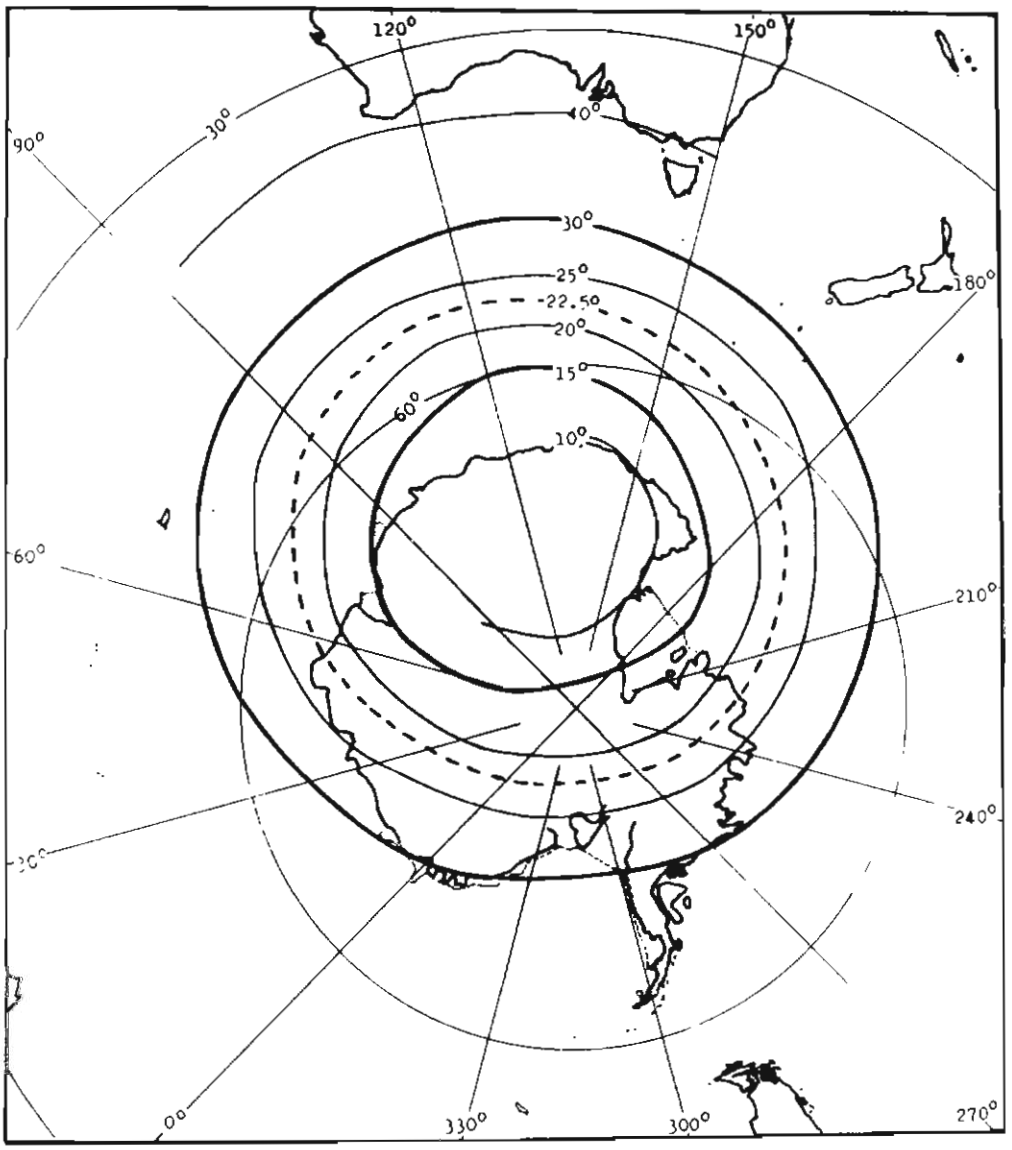


Figure 33. Invariant co-latitude coordinates $\Theta_3$ (90° – $\Lambda_3$) superimposed on an outline azimuthal equidistant projection map of the Southern Hemisphere. The dashed line $\Theta_3$ = 22.5° represents the Auroral Zone (see Chapter 7). (*Base map by Department of National Mapping, Australia*)

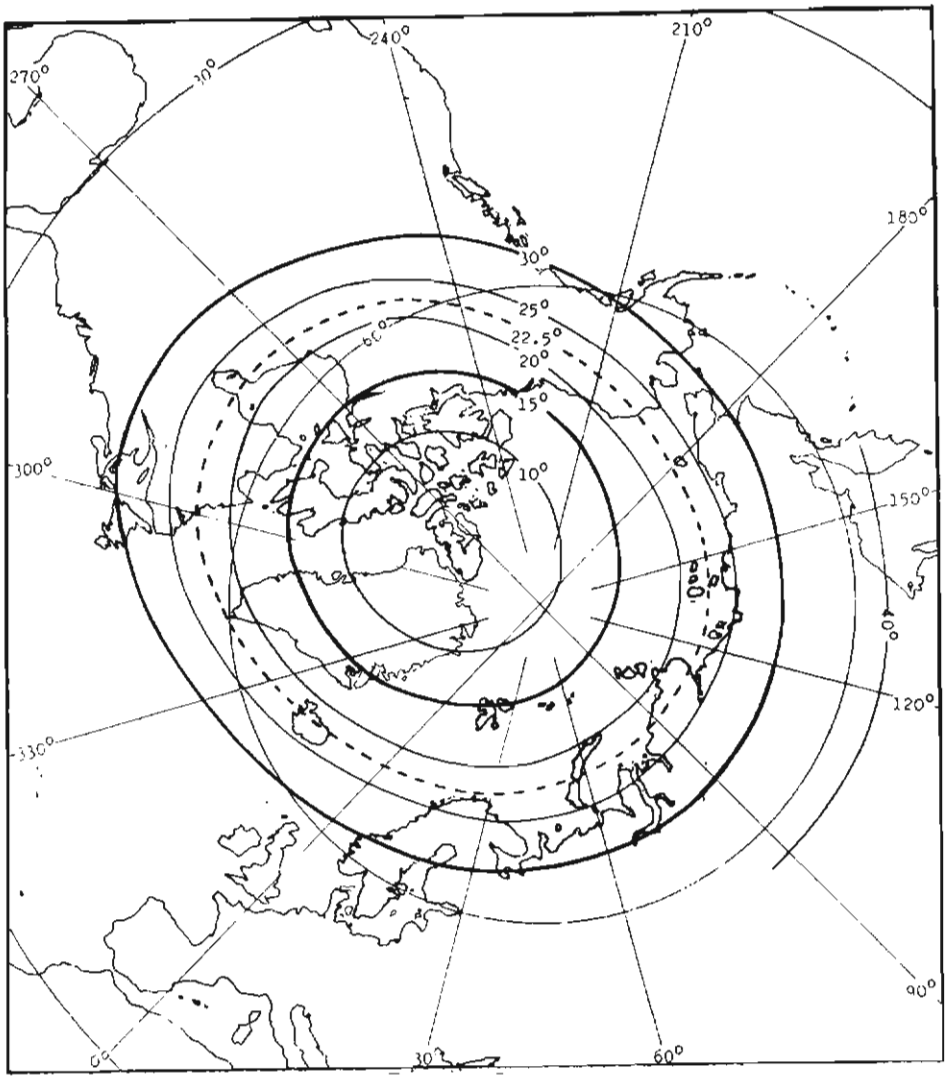


Figure 34. Invariant co-latitude coordinates $\Theta_3$ (90° – $\Lambda_3$) superimposed on an outline azimuthal equidistant projection map of the Northern Hemisphere. The dashed line $\Theta_3$ = 22.5° represents the Auroral Zone (see Chapter 7). (*Base map by Department of National Mapping, Australia*)

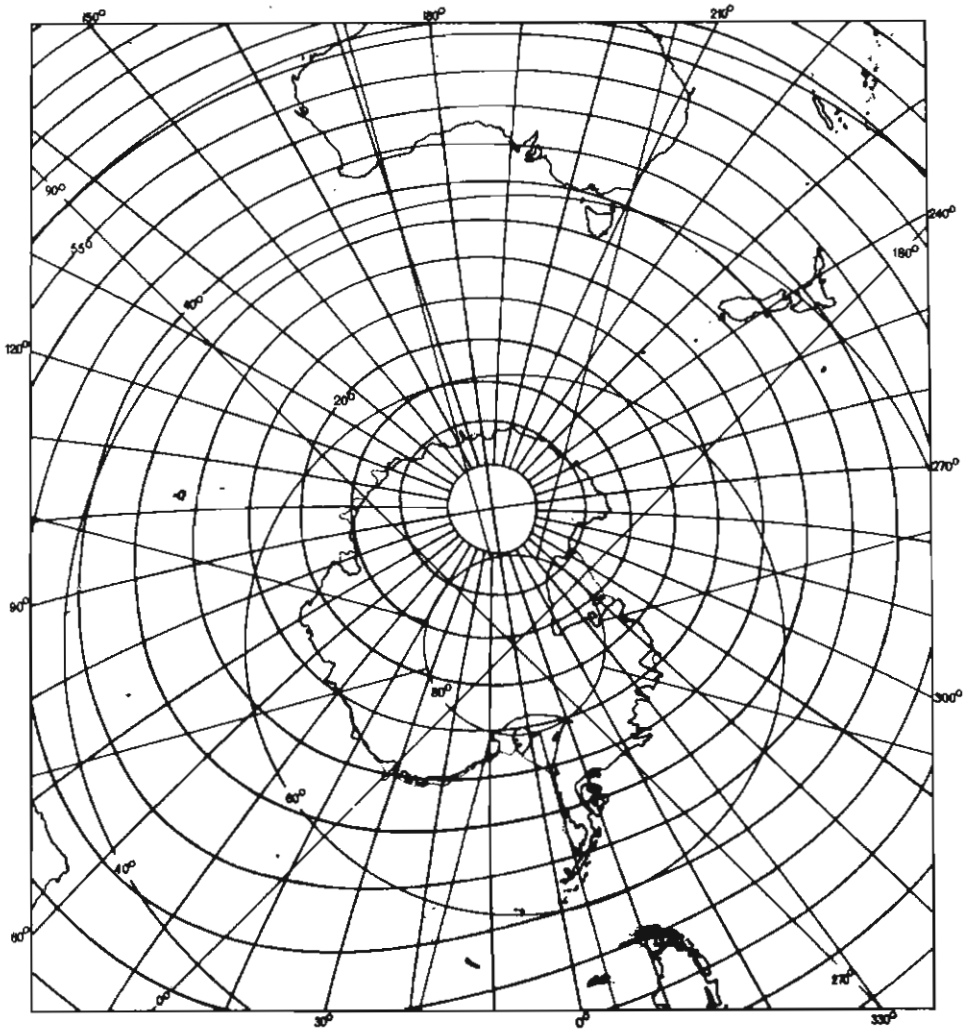

Figure 35. The Southern "Auroral" Pole, gg 74.5°S and 126.0°E with the grid of $\Theta_4$ co-latitudes and $\Phi_4$ time-longitudes on a map in azimuthal equidistant projection, south geographic polar case. (*Bond 1968*)

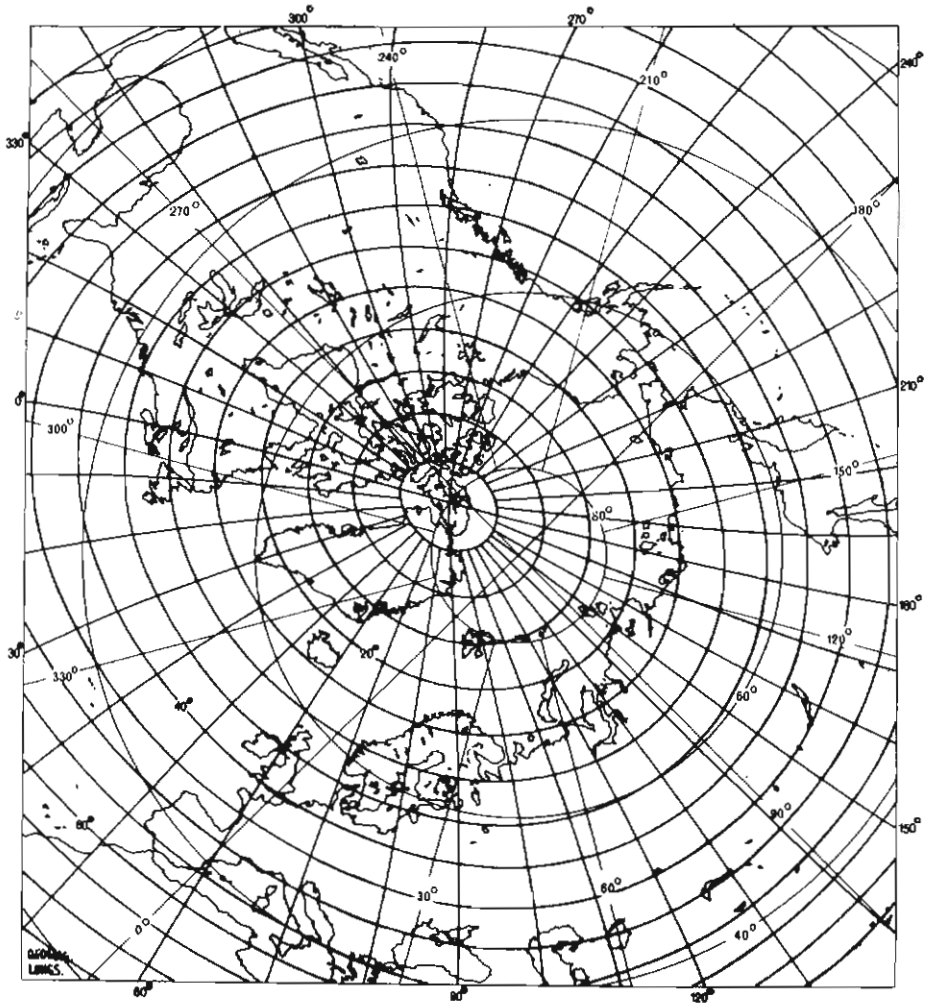

Figure 36. The Northern "Auroral" Pole gg 80.0°N and 79.6°W with the grid of $\Theta_4$ co-latitudes and $\Phi_4$ time-longitudes on a map in azimuthal equidistant projection, north geographic polar case. (*Bond 1968*)

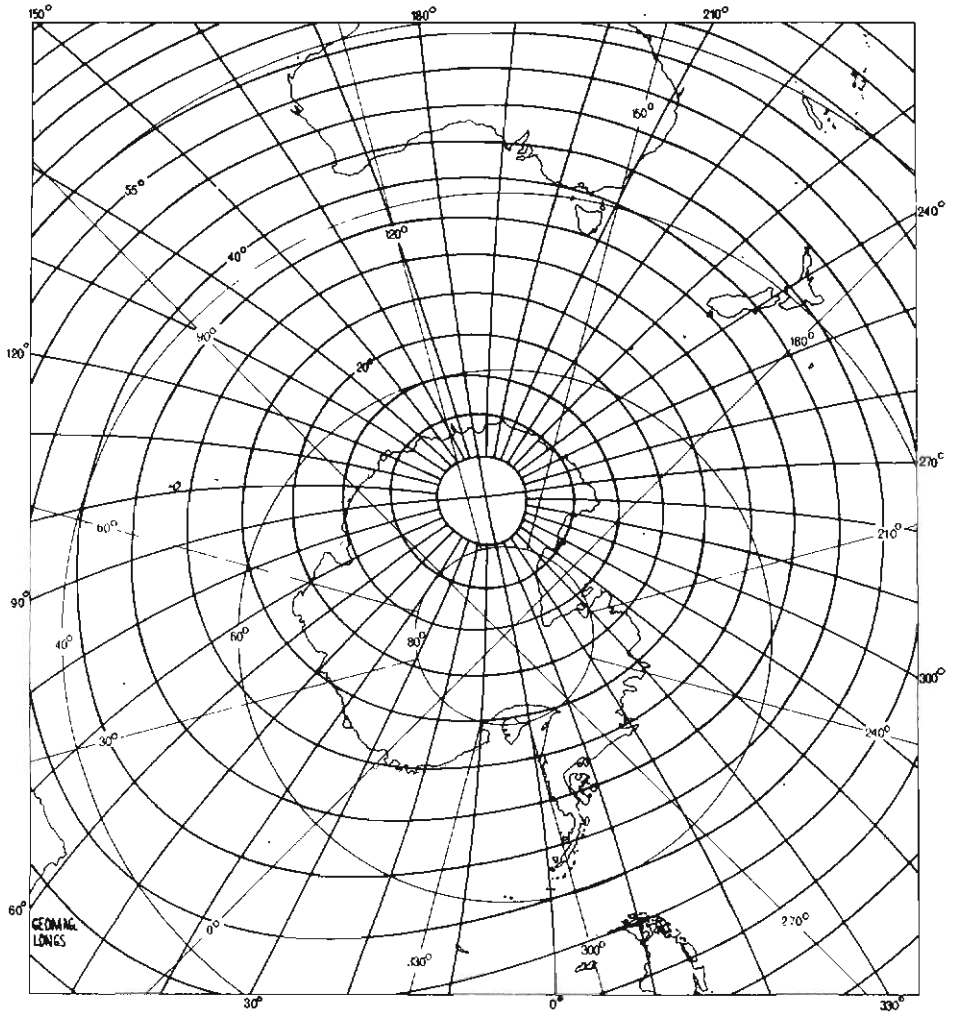


Figure 37. The Southern "Auroral" Pole with the grid of $\Phi_4$ co-latitudes and $\Phi_4$ magnetic longitudes on a map in azimuthal equidistant projection, south geographic polar case.

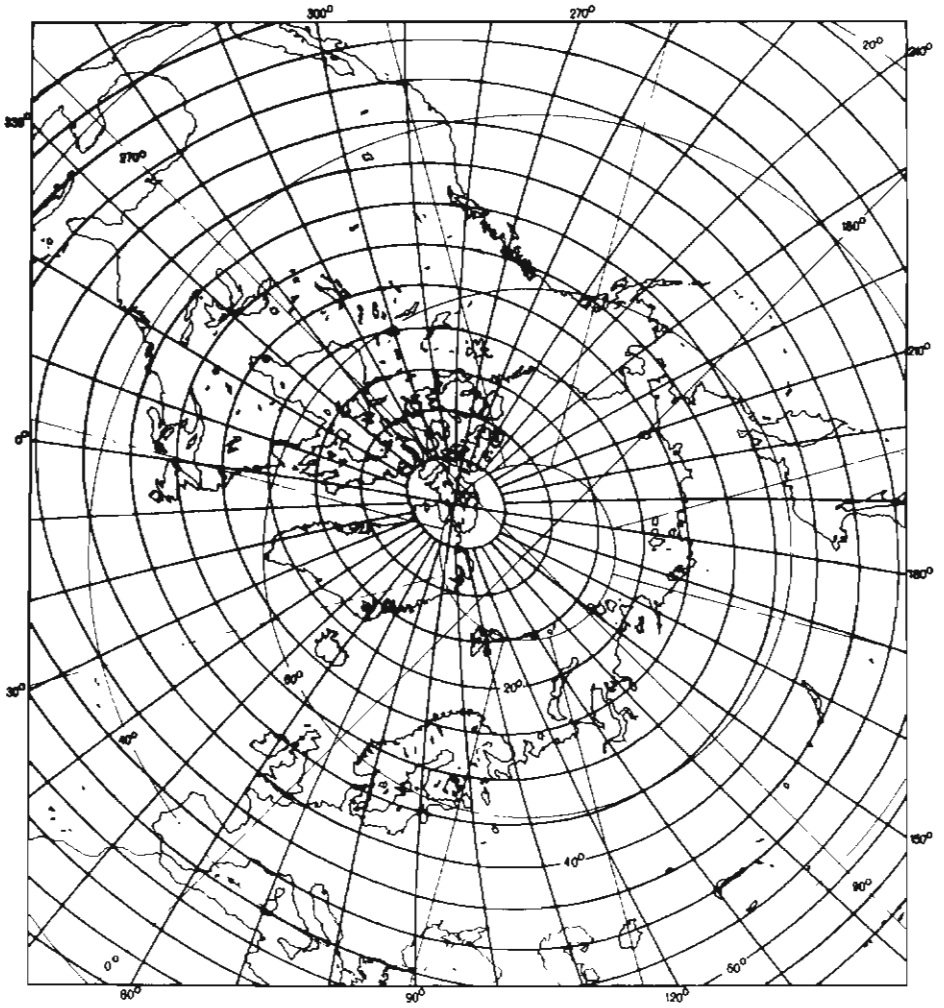


Figure 38. The Northern "Auroral" Pole with the grid of $\Phi_4$ co-latitudes and $\Phi_4$ magnetic longitudes on a map in azimuthal equidistant projection, north polar case.

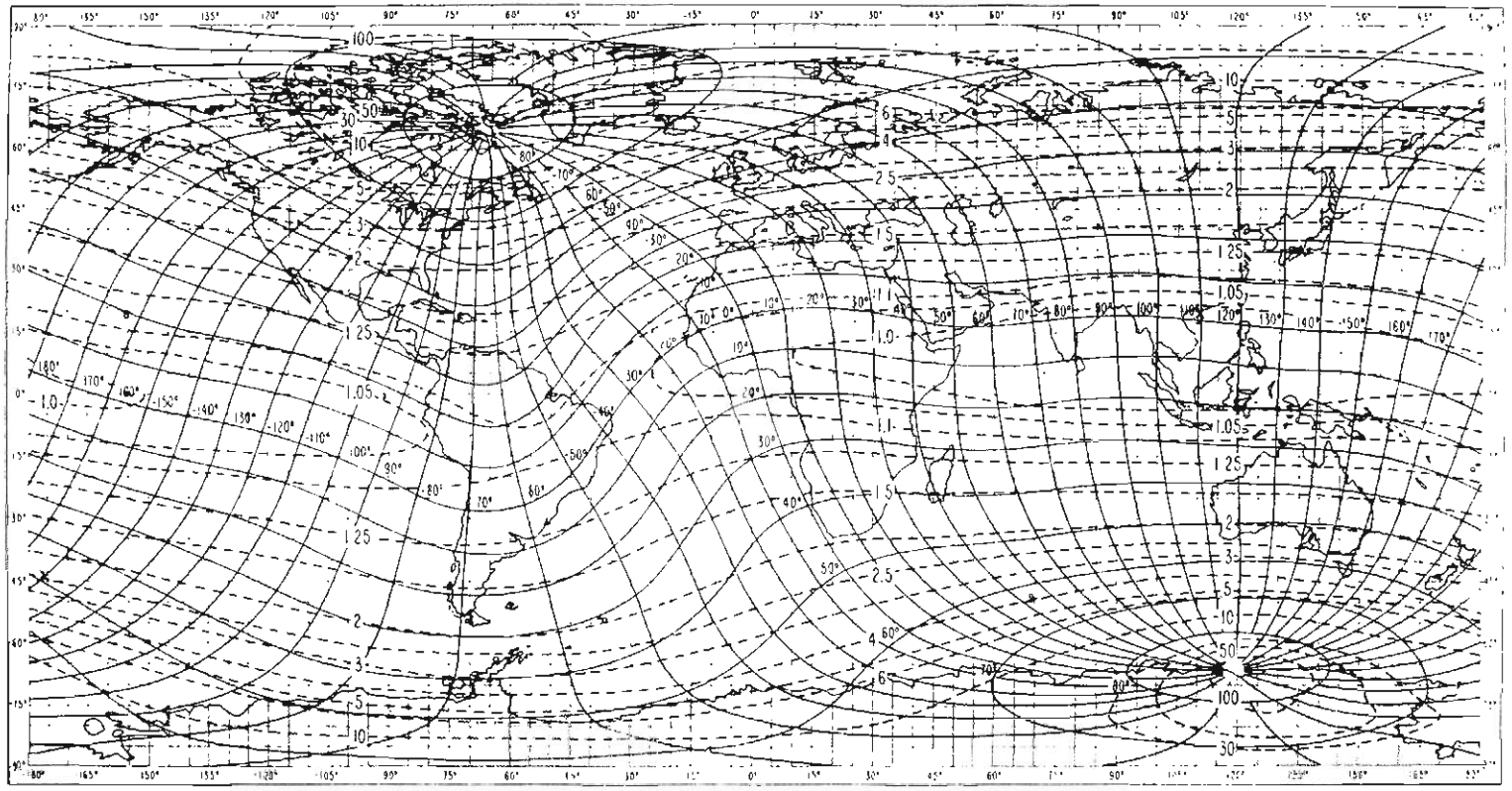

Figure 39. Grid for determining magnetic conjugate points. McIlwain's L values are shown as dashed lines. (*Campbell and Matsushita 1967*).

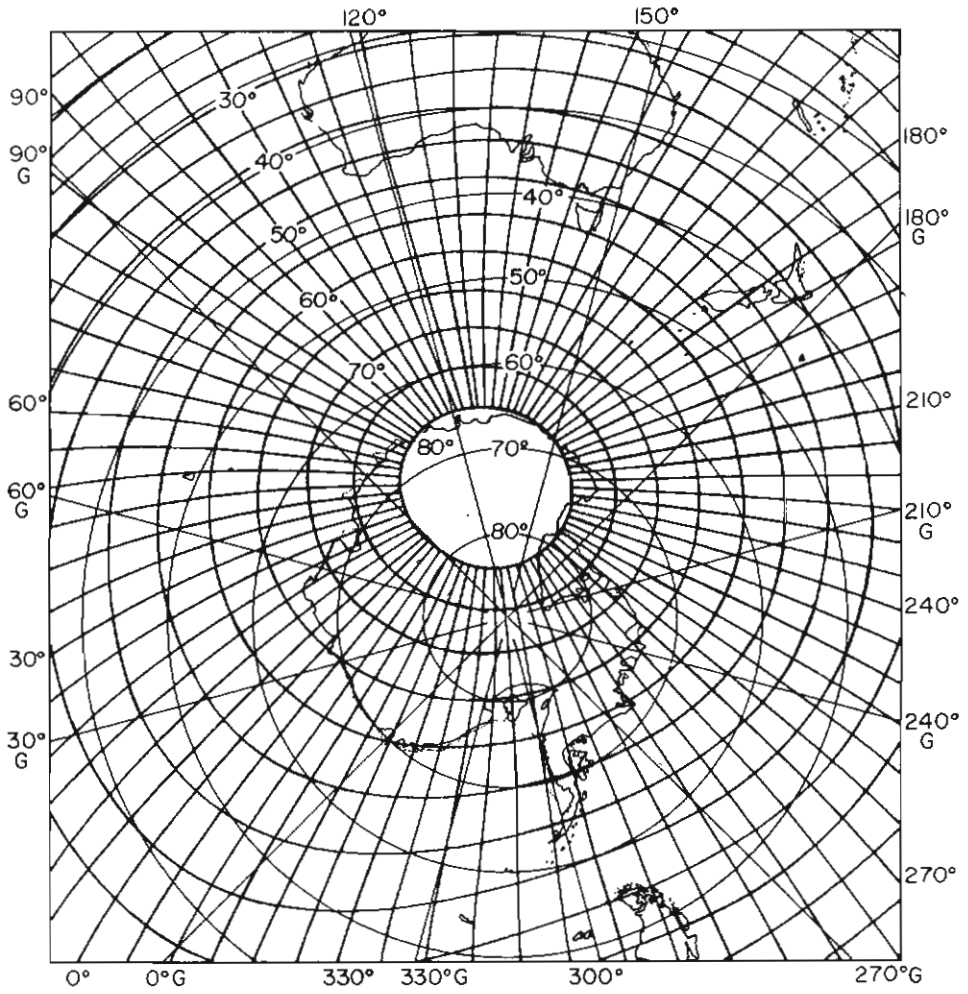


Figure 40. Invariant geomagnetic coordinates superimposed on an azimuthal equidistant geographic grid for the Southern Hemisphere. The letter G indicates lines of geographic longitude. (*Boyd 1977*)

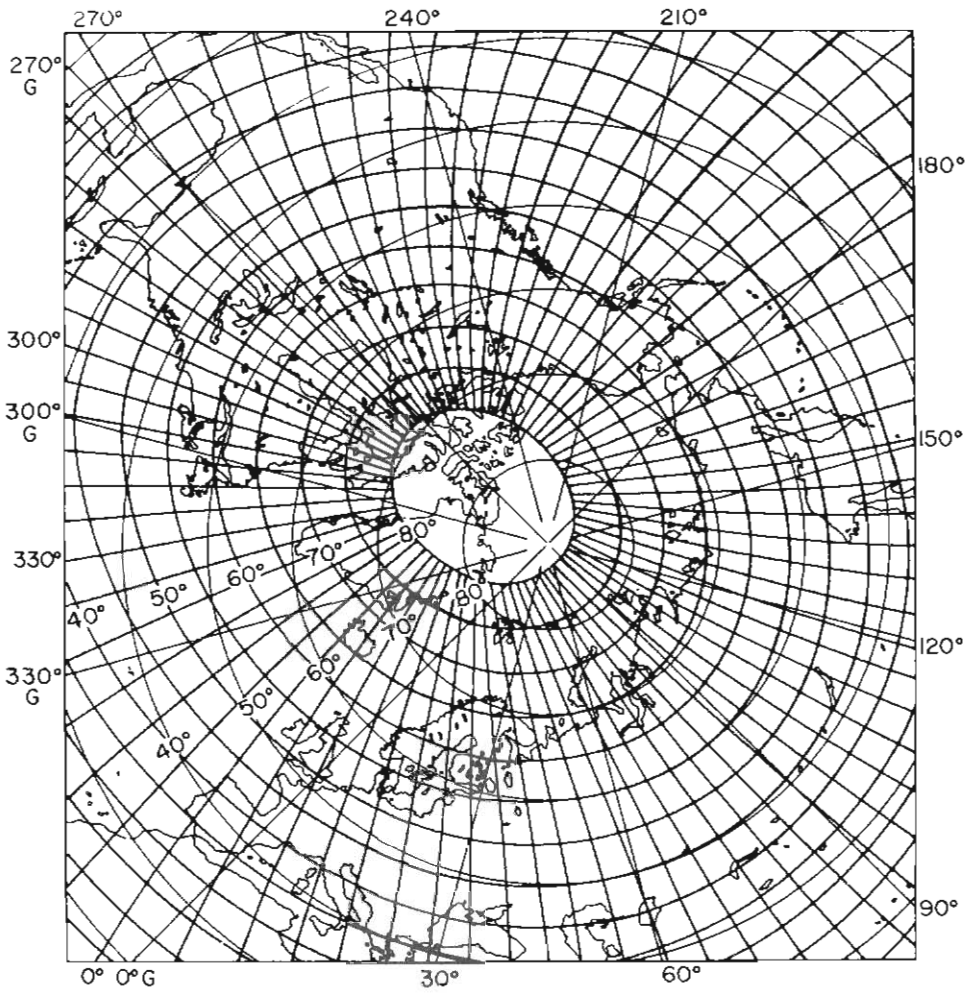


Figure 41. Invariant geomagnetic coordinates superimposed on an azimuthal equidistant geographic grid for the Northern Hemisphere. (*Boyd 1977*)

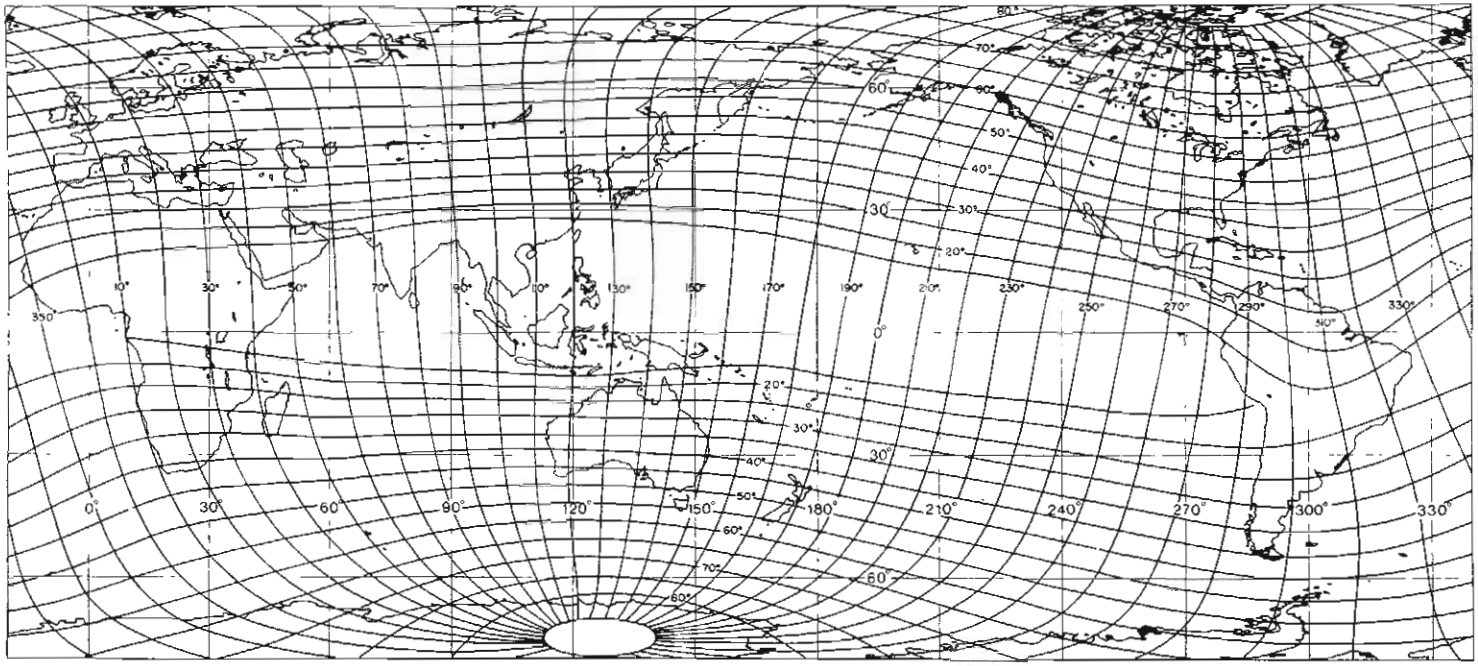

Figure 42. Invariant coordinates superimposed on a simple rectangular grid of geographic coordinates. (*Boyd 1977*)

# 7. The auroral zone

The geographical distribution of the aurora in the Northern Hemisphere was reported by Fritz (1881). He introduced the term *isochasm*, lines indicating the frequency of nights on which the aurora could be seen in any direction from a given location. Figure 43 shows the isochasms for the Northern Hemisphere.

An early paper based on the isochasms of the Southern Hemisphere was produced by Boller (1898), whose map, redrawn, is presented in Figure 44. Boller's data consisted of 791 nights during which the aurora had been reported. He drew two rather conjectural zones of maximum frequency for the Antarctic. The inner zone, in the shape of a crescent, partly girdles the Antarctic continent, which was centred on the 150° meridian of geographic longitude and located south of Macquarie Island. The outer zone was a circle of about 35° co-latitude about the pole of the centred dipole (CDP). Finally he considered that the majority of observations lay within a circle of about 38° around the magnetic dip pole (MP).

In 1930, Davies positioned the auroral zone of maximum frequency in relation to the southern pole of the centred dipole. He considered that the zone lay in an annulus with a mean radius of about 20° around the pole (Figure 45).

The next step was taken by White and Geddes (1939), who found the auroral data then available did not permit an accurate estimate of the position of the zone of maximum auroral frequency. However, from a general discussion of the data, they were able to suggest an approximate position for part of the zone, as shown in Figure 46.

Magnetic fields external to the Earth were first considered in this context when Vestine (1938) related the location of the auroral zone in the Northern Hemisphere to the magnetic daily disturbance variation $S_D$. Sensitive magnetometers show a daily variation even under quiet magnetic conditions; this variation, termed *solar daily variation*, is denoted by $S_q$. On days when there is magnetic disturbance, there is a variation over and above the $S_q$ variation; this is the *disturbance daily variation*, $S_D$.

Vestine used magnetic data from stations near the northern auroral zone, so instead of working with the geomagnetic components **X** and **Z** of the Earth's magnetic field **F**, he used the component **X'** in the direction of centred dipole longitude and **Z'** (=**Z**). In local time, using the yearly average of the morning maximum values of **X'** and **Z'** components of the $S_D$ field, Vestine first found the direction of the vector sum of **X'** and **Z'** and then the intersection of this direction with the height of 300 km. The point on the Earth vertically below this intersection gave the location of the auroral zone for the Northern Hemisphere.

Vestine (1944) compared his magnetically derived auroral zone with the isochasms of Fritz and also against a collection of later data. He found that the magnetically derived auroral zone agreed closely with the Fritz 100% isochasm and with the 100% isochasm of the more recent data.

In 1945, Vestine and Snyder investigated the patterns of change of each of the components **X'** and **Z'** with centred dipole latitude, again using the morning and evening maxima of the $S_D$ field for stations in middle and high latitudes and relating these patterns to the isochasms of auroral frequency. From corresponding patterns of magnetic data from stations in the Southern Hemisphere they adduced the location of the auroral zone together with the lower-frequency isochasms, and presented auroral data to support the auroral distribution (see Figure 47).

The North American auroral isochasms were found to closely fit the isolines of constant dip (Gartlein and Sprague 1959). Using an empirical formula, the authors asserted that the auroral zone in the Southern Hemisphere coincides with the isoline for a magnetic inclination of 76°. Bond and Jacka (1962) pointed out that the isoline for a magnetic inclination of 72° Gartlein's and

Sprague's outer limit of the overhead frequency of aurora–passes close to both Melbourne, Australia, and Mawson, Antarctica (Figure 48). The overhead frequency of aurora during 1957–58, the period of the International Geophysical Year, was 0.75% for Melbourne and 97.4% for Mawson. Hultqvist (1959) pointed out that Gartlein's isochasms for North America were a close fit to the Hultqvist curves ($\Theta_2$, in the previous chapter). We emphasise that it is purely a coincidence that, for North America, the dip isolines and the geomagnetic co-latitudes $\Theta_2$, $\Theta_3$ and $\Theta_4$ are closely parallel.

The concept of an *isoaurore,* a line indicating the frequency of nights on which the aurora is seen overhead, was suggested as a replacement for the concept of an isochasm (Chapman 1953). In a paper on the southern auroral zone, Bond and Jacka (1960) pointed out that a zone based on the Hultqvist curves would lie about 1° of latitude south of Macquarie Island. They also presented a tentative location of the auroral zone based on the overhead aurora, isoaurore, concept.

To derive the tentative zone, synoptic maps were prepared showing the occurrence of auroral arcs with discernible lower borders recorded by all-sky cameras at Mawson and Macquarie Island. From these maps, frequency of occurrence versus centred dipole latitude was determined on a number of centred dipole meridians. The frequency distributions all had a mode within a few degrees of the observer's meridian. Because some faint auroral forms observable overhead may not be observable at lower elevations, an estimate of the latitude of the mode was taken at the midpoint of the range in which the frequency exceeded two-thirds of the maximum observed frequency. Since these data were very meagre, the authors tentatively introduced the hypothesis that the isoaurores were symmetrical about the centred dipole longitude through the southern magnetic dip pole. The resulting auroral zone was a reasonable fit with the previously published data (Figure 49).

A better estimate of the southern auroral zone was made by Fel'dstein (1960), using the by-then analysed data from the International Geophysical Year (IGY). This zone is shown in Figure 50.

When more data obtained during the IGY became available, Bond and Jacka (1962) assessed all the approximations of geomagnetic latitude to see which gave the best fit to the auroral data.

Considerable care was taken in the analysis of auroral overhead frequency. The definition of *overhead aurora* in general use during the IGY was that proposed by W. Stoffregen of the Uppsala Ionospheric Observatory. He suggested all-sky camera plots (ASCA PLOTS) be used and that overhead aurora be defined as those forms appearing within a circle of zenith distance 60°, which corresponds to a circle on the Earth's surface with radius 1.5° of great-circle distance.

The observing periods of 24 hours were divided into periods of three hours (or parts thereof) Universal Time (UT-formerly Greenwich Mean Time). For each period with one or more clear (non-cloudy) hours, the presence or absence of overhead aurora was noted from the basic data. These clear-hour data were then divided into classes according to the value of the planetary geomagnetic disturbance index, Kp, and the three–hour period in which the clear hour(s) occurred. The relative frequency of occurrence of auroras f(Kp,t) was then determined for each Kp–time class. It was now assumed that these frequencies f(Kp,t) were representative of the whole population of three-hour periods.

For each night during which at least one clear hour occurred, the presence or absence of overhead aurora during any one of the hours of that night was noted from the basic data. These nights were then grouped according to the dominant (maximum f(Kp,t)) Kp–time class. Since the Kp index is known for every night the relative nightly frequency of occurrence of auroras F (Kp,t) was determined from the dominant hourly function f(Kp,t). The remaining cloudy nights and the cloudy periods of those (few) nights during which clear hours occurred without

overhead aurora were now similarly grouped according to the dominant Kp–time class represented, and the relative frequencies F(Kp,t) ascribed to each group of nights.

Denoting by N(Kp,t) the total number (clear and cloudy) of nights in a group characterised by the same dominant Kp–time class, the estimate

$$P = \Sigma N(Kp,t).\, F(Kp,t) \,/\, \Sigma N(Kp,t)$$

of the probability of occurrence of overhead aurora during a night was then evaluated.

The estimate P made full use of the information contained in the list of basic data; it was an unbiased estimate and the values obtained from the several stations could be meaningfully compared.

Table 1. Nightly probability of overhead aurora (%)

| Station | Symbol | P(%) |
|---|---|---|
| Awarua | Aw | 9.5 |
| Byrd | By | 94.1 |
| Camden | Ca | 0.2 |
| Campbell Island | CI | 25.7 |
| Cape Hallett | Ht | 80.1 |
| Davis | Da | 87.5 |
| Dumont d'Urville | DU | 67.5 |
| Ellsworth | El | 54.9 |
| Halley Bay | HB | 28.1 |
| Hobart | Ho | 5.1 |
| Kerguelen Island | Kg | 14.6 |
| Macquarie Island | MI | 86.0 |
| Mawson | Mw | 97.4 |
| Melbourne | Me | 0.75 |
| Roi Baudouin | RB | 60.1 |
| Scott Base | SB | 63.4 |
| Shackleton | Sh | 55.2 |
| South Pole | SP | 89.7 |
| Syowa | Sy | 94.5 |
| Wilkes | Wi | 67.8 |

A plot of the probability of overhead aurora against the magnetic inclination of the several stations gave no indication of any simple relationship. The same was true for inclination at 100 km. Similarly, a plot of probability of overhead aurora against centred dipole latitude showed no sign of a simple relationship.

However, with the co-latitudes, which in the last chapter we designated as $\Theta_1, \Theta_2, \Theta_3$, a simple curve did result. The probability of occurrence of overhead aurora decreases rapidly as one moves from the auroral zone towards the equator. In the region of this rapid decrease, the estimate P in fact represents the actual overhead frequency at a point nearly 1.5° zonewards of the observing station. A similar effect is expected to a lesser extent on the polewards side of the auroral zone. For these reasons, the smooth curve was drawn somewhat inside the plotted points to represent truly the probability of overhead occurrence of auroral forms (Figure 51). The maximum probability isoaurore on this representation was read from the probability curve as situated at $\Theta_3$= 22.5°. This value is shown in Figure 52, together with other representative values.

The spiralling of charged particles along magnetic field lines at an angle $\alpha$ to the magnetic field, and progressing in longitude were discussed in Chapter 8. Here it is emphasised that if the

angle $\alpha$ be small, then there exists a "loss cone" within which particles will not mirror, but will be precipitated into the upper atmosphere. The $\Theta_3$ curve (or the $\Theta_4$ curve – the two curves are virtually identical), therefore best represents the auroral zone in the Southern Hemisphere.

To test the accuracy of this determination of the zone, Bond and Jacka (1963) transferred the southern auroral zone, along the field lines, to the Northern Hemisphere and compared the equivalent northern auroral zone with that derived by Fel'dstein. This comparison is shown in Figure 53. The comparison is good for Europe and the northern region of Asia, where Fel'dstein had the most data. For Alaska and northern Canada, the Bond and Jacka curve agrees more closely with the shape reported by Gartlein and Sprague (1960), who had more data for this region than Fel'dstein had.

Akasofu (1968) pointed out later that the auroral zone is the locus of the midnight position of the auroral oval. However, before addressing the question of the auroral oval, let us examine the movement of auroral forms in latitude.

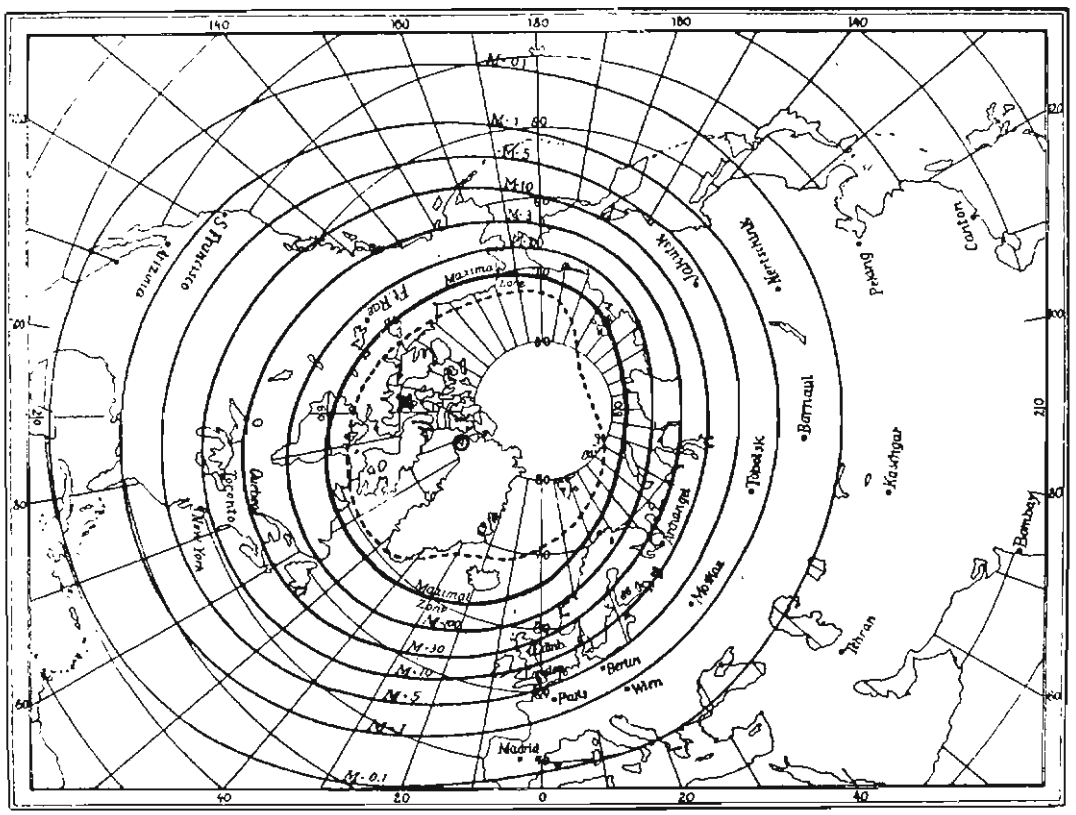


Figure 43. The distribution of isochasms, or lines of equal auroral frequency, in the Northern Hemisphere. (*Fritz 1881*)

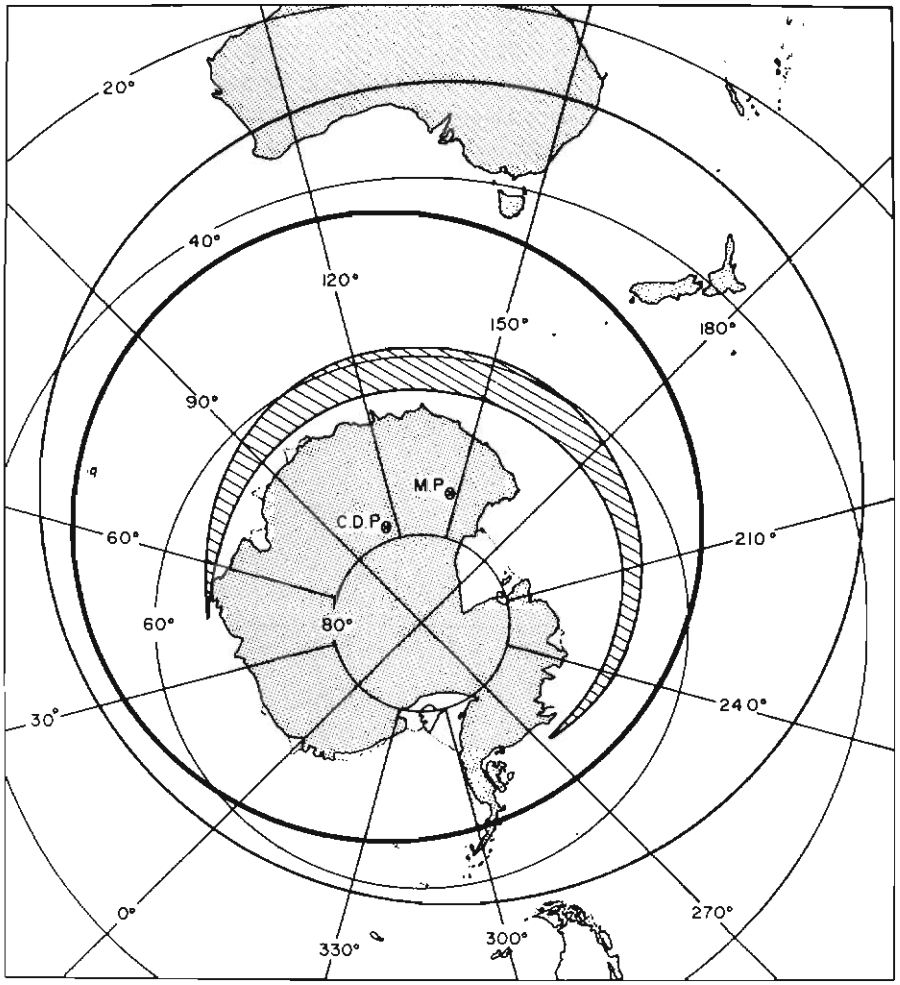


Figure 44. The southern auroral zone after Boller (1898), re-drawn. See text for explanation.

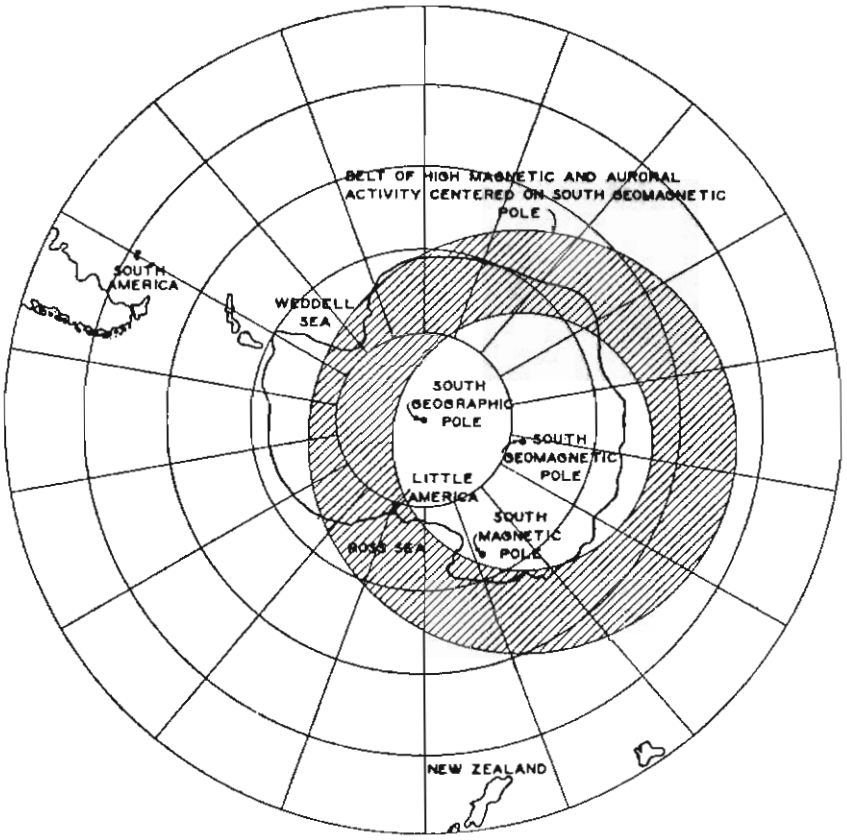


Figure 45. The southern auroral zone. (*Davies 1930*)

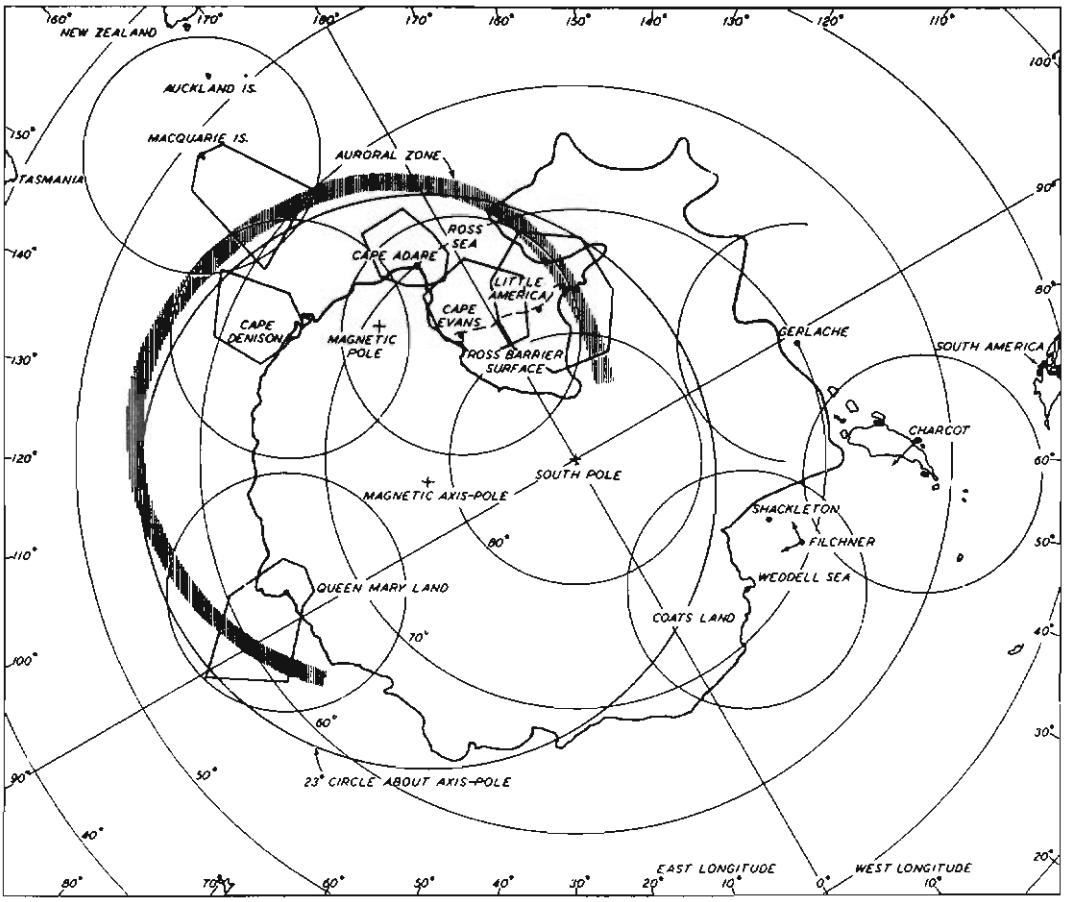


Figure 46. The partial auroral zone suggested by White and Geddes (1939). The circles represent the field of view from the observation points. The polygons, compiled from azimuthal distributions, represent the areas over which auroras had been recorded. Where few auroras had been seen, azimuthal directions are indicated by arrows.

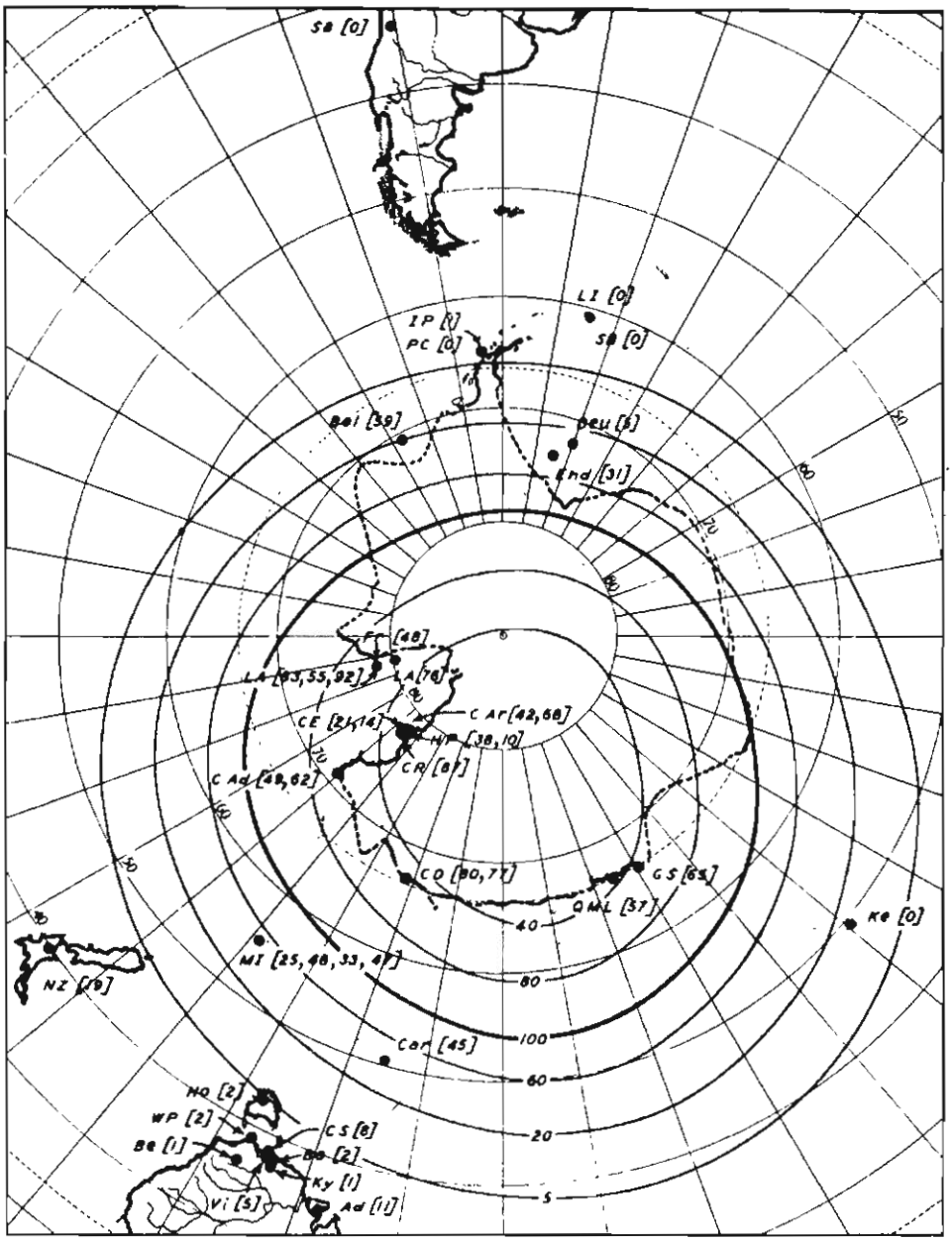


Figure 47. Estimated percentage-frequency of days with occurrence of aurora, clear, dark nights, high latitudes, Southern Hemisphere. (Stations shown by letters; after Vestine and Snyder 1939).

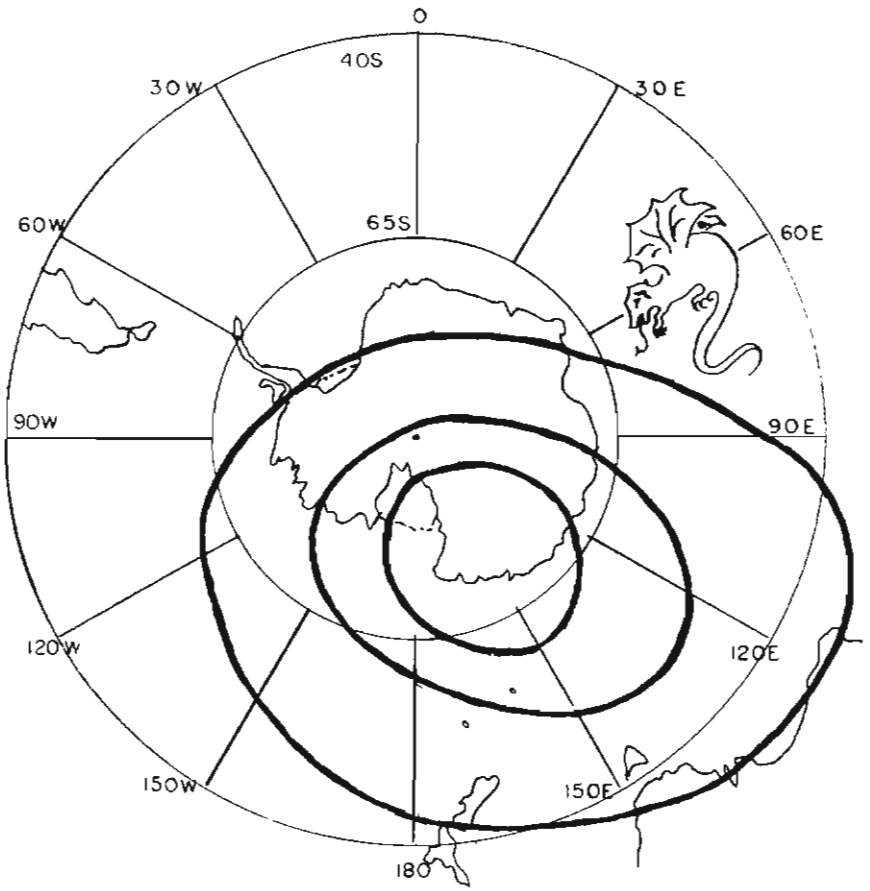


Figure 48. Diagram of the southern auroral zone and its inner and outer limits. (*Gartlein and Sprague 1959*)

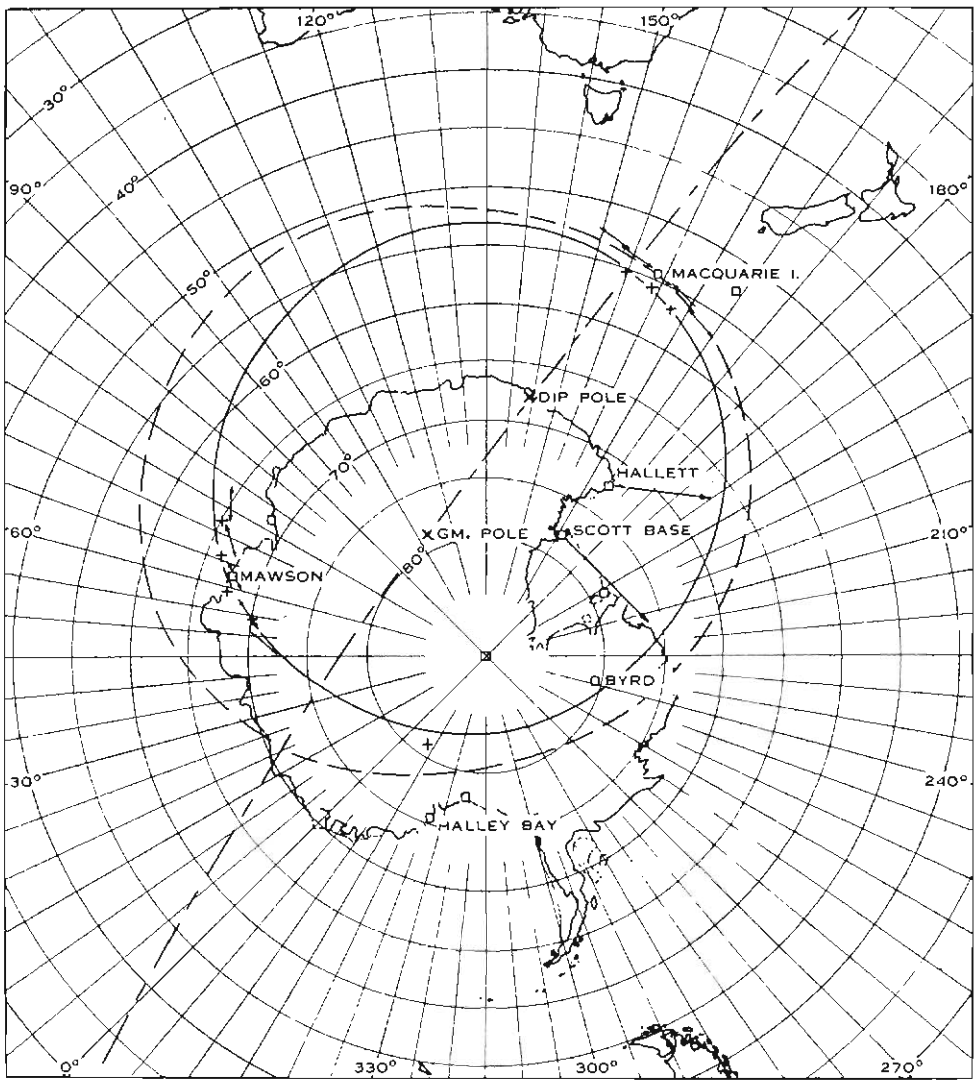


Figure 49. The estimated position of the southern auroral zone, based on observed positions shown by crosses near Macquarie Island and Mawson and assuming symmetry about the geomagnetic (centred dipole) meridian through the dip pole. The dashed curve shows Hultqvist's (1958) projection from 5.6 Earth radii in the geomagnetic (centred dipole) equatorial plane.

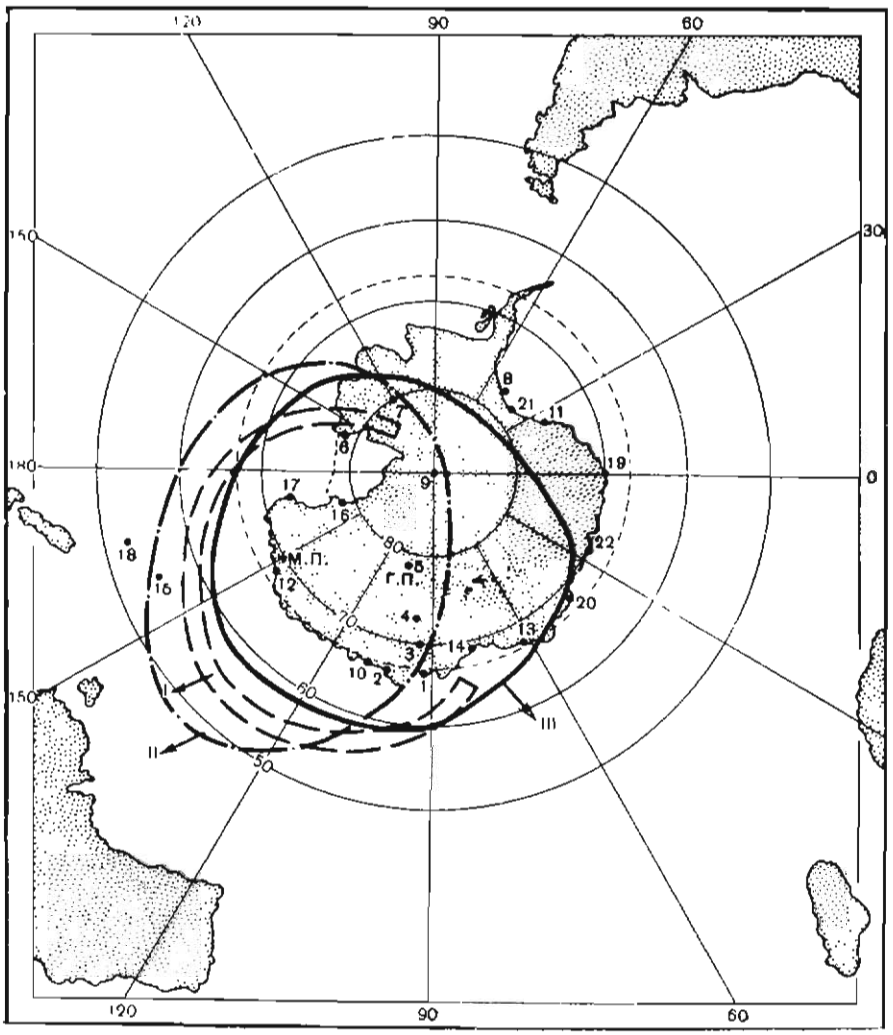


Figure 50. The southern auroral zone according to Fel'dstein (1960) at III, together with the versions of White and Geddes (1939) at I and Gartlein and Sprague (1960) at II. The numbers 1-22 refer to the stations from which overhead aurora were observed. (*Fel'dstein 1960*)

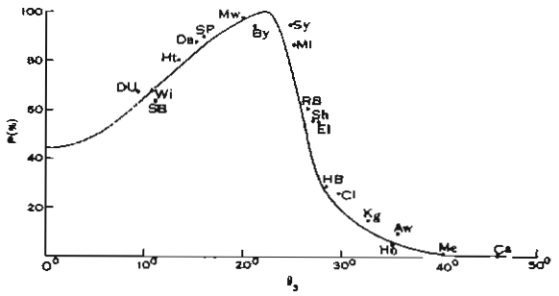


Figure 51. Probability of overhead aurora during a night *versus* co-latitude $\Theta_4$. (*Bond and Jacka 1962*)

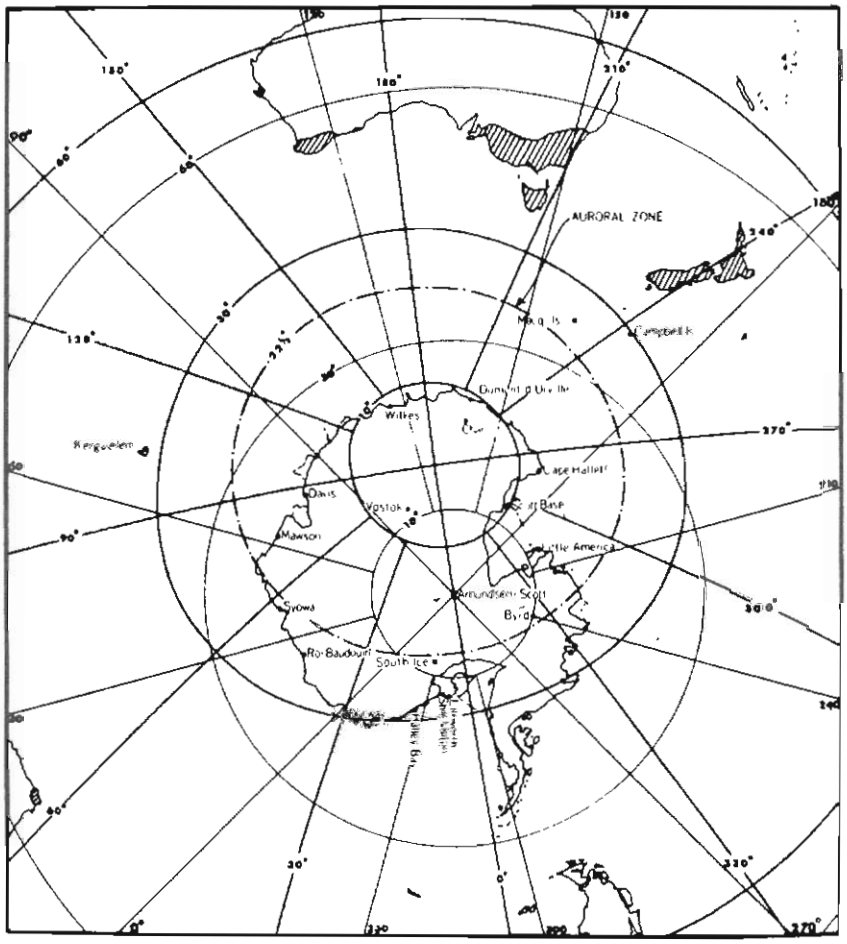


Figure 52. The Southern Auroral Zone at $\Theta_3 \simeq \Theta_4 = 22.5°$ together with all-sky camera stations and areas from which visual observations were used. (*Bond and Jacka 1962*)

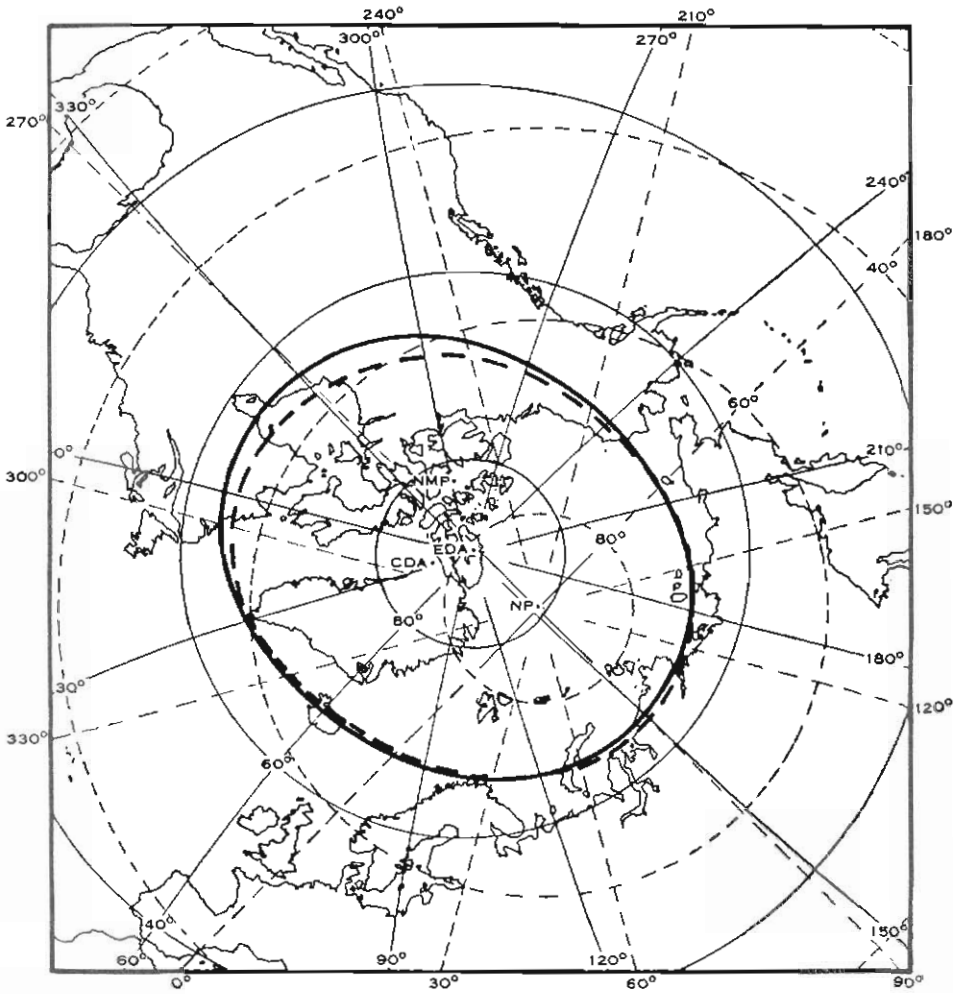


Figure 53. The conjugate to the Southern Hemisphere auroral zone, together with Fel'dstein's (1960) estimate of the Northern Hemisphere auroral zone shown by the heavy dashed line. (*Bond and Jacka 1963*)

# 8. Movement of auroral forms in latitude and longitude

The auroral display moves furthest towards the equator when the external magnetic field of the Earth is most disturbed. A typical magnetic disturbance recorded by a magnetometer at Macquarie Island for the components Horizontal **H**, declination D, and vertical **Z** is illustrated in Figure 54. The deviation of the magnetometer over and above the quiet-day $S_q$ curve (Figure 55) gives a measure of the disturbance field $S_D$. The $S_q$ curves in **H** and **Z** show a slight positive movement before magnetic midnight (1205 hours UT) and a slight negative movement after midnight.

The magnetograms for moderately disturbed days show, in general, a more marked positive bay[10] in **H** and **Z** before magnetic midnight and a negative bay after midnight, but the change can occur before magnetic midnight.

In a survey of reports of auroral movement and magnetic bays by several authors, as well as observations from Macquarie Island, Bond (1960a) found evidence that, in the evening sector, the movement of auroras was slowly equatorwards during the period of the positive bay, and then rapidly westwards, followed by polewards and easterly, during the period of the negative bay. We shall see later (Chapter 9) that it is the passage of the westerly surge of the aurora over the magnetometer's geomagnetic longitude that brings the changeover from a positive bay to a negative bay.

At Macquarie Island the positive bay in **H** of the type depicted can be regarded as being produced by an easterly linear conventional current and the negative bay can be regarded as being produced by an equivalent linear westerly conventional current. As discussed later, the particle precipitation that causes the aurora also causes active currents in the upper atmosphere.

One measure of magnetic disturbance at a magnetometer station is the three-hour K-index, (Bartels 1938). The purpose of the K-index is to assign a single digit in such a way that the whole range of geomagnetic activities is covered, from the quietest conditions, K=0, to the conditions of the most intense storm, K=9. The day in Universal Time is divided up into three-hour periods 0-3, 3-6, 6-9, ...., 21-24 hours UT. For each three-hour period, the maximum deviations of two components, **H** and D, of the magnetic field are recorded in nT (nano Tesla) units (although most geomagneticians still use $\gamma$ units ($1\ \gamma = r.10^{-5}$, $1\ nT = r.10^{-4}$)). The **Z** component is not used. The greater of the two deviations is assigned to the three-hour period, the D component being measured in equivalent nT ($\gamma$) units.

The K-index is determined from a table showing the minimum values of the deviation for the index units 0 to 9. The standard table is shown below.

Table 2. Standard table of the minimum values of the deviation for the index units 0 to 9.

| K-index | 0 | 1 | 2 | 3 | 4 | 5 | 6 | 7 | 8 | 9 |
|---|---|---|---|---|---|---|---|---|---|---|
| Minimum value of deviation ($\gamma$) | 0 | 2.5 | 5 | 10 | 20 | 35 | 60 | 100 | 150 | 250 |

This table, with the minimum values multiplied by 2, applies to observations at about centred dipole latitude 50°.

[10]The word bay is used because of the similarity of the shape to that of a bay in a map of a coastline.

The same basic scale is applied to other latitudes by determining which of a set of lower limits for K=9 applies at the station in question. The lower-limit values are 300, 350, 500, 600, 750, 1000, 1200 and 2500 $\gamma$. The first applies to near-equatorial latitudes, and the last to some auroral zone stations where the most disturbed magnetic conditions occur. The factor to be applied to determine the lower bound for each index number is found by dividing the assigned lower bound for K=9 at the station by 250. Tables of the three-hourly K-index value and the minimum deviation or lower limit for K=9 have been published for most permanent magnetometer stations.

Where the K value for a station is known for a given three-hour period, and an estimate of the likely deviation is required, the table below is used.

For each K-index there is a local equivalent amplitude, AK. As before, the factor to be applied is found by dividing the lower limit for K=9 for the station by the number 250. Thus for a station at middle latitudes where the minimum value for Kp = 9 is 500 the factor by which the amplitude AK is to be multiplied is 2 and for a magnetic disturbance for which the station value is K = 3 the minimum value of the amplitude AK from Table 3 is 2.15 $\gamma$ = 30 $\gamma$.

Table 3. Local equivalent amplitudes for the K-index.

| K = | 0 | 1 | 2 | 3 | 4 | 5 | 6 | 7 | 8 | 9 |
|---|---|---|---|---|---|---|---|---|---|---|
| ak($\gamma$) | 0 | 3 | 7 | 15 | 27 | 48 | 80 | 140 | 240 | 400 |

There are several indices by which the *world–wide* degree of magnetic disturbance can be quantified. The one used here is the Planetary Geomagnetic Index, Kp (Bartels 1949) which measures magnetic disturbance for three-hour periods. The Kp-index, designed as a measure of particle precipitation causing magnetic disturbance, is a quasi-logarithmic scale obtained from the K indices from specified mid-latitude magnetic observatories.

The three-hourly equivalent planetary amplitude, ap (the corresponding linear scale in $\gamma$ units), is related to the Kp index in Table 4. The values 0o, 1o, ...., 9o correspond to the values in the ak scale. The values 1-, 2-, refer to one-third of a unit *below* the unit scale. The values 0+, 1+, 2+ refer to one-third of a unit *above* the unit scale. When Kp is used as a ten unit scale, the unit values refer to 0o, 1o, ...., 9o.

Table 4. The three-hourly equivalent planetary amplitude, ap, related to the Kp-index.

| Kp = | 0o | 0+ | 1– | 1o | 1+ | 2– | 2o | 2+ | 3– | 3o | 3+ | 4– |
|---|---|---|---|---|---|---|---|---|---|---|---|---|
| ap = | 0 | 2 | 3 | 4 | 5 | 6 | 7 | 9 | 12 | 15 | 18 | 22 |
| Kp | 4o | 4+ | 5– | 5o | 5+ | 6– | 6o | 6+ | 7– | 7o | 7+ | 8– |
| ap = | 27 | 32 | 39 | 48 | 56 | 67 | 80 | 94 | 111 | 132 | 154 | 179 |
| Kp = | 8o | 8+ | 9– | 9o | | | | | | | | |
| ap = | 207 | 236 | 300 | 400 | | | | | | | | |

From data obtained during the IGY, Bond (1960a) prepared synoptic maps showing the distribution of simple arc auroral forms in the region of Macquarie Island and Eastern Australia at 15 minute intervals. Auroral positions were computed from recorded elevations and azimuths of

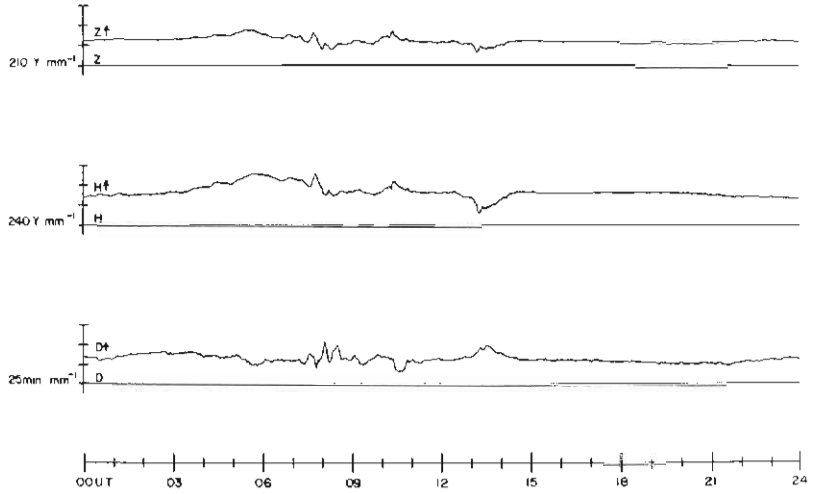


Figure 54. Reduced-scale diagrammatic copy of a typical magnetic record from the magnetometer at Macquarie Island. (*Original magnetogram supplied by Bureau of Mineral Resources, Geology and Geophysics, Canberra*)

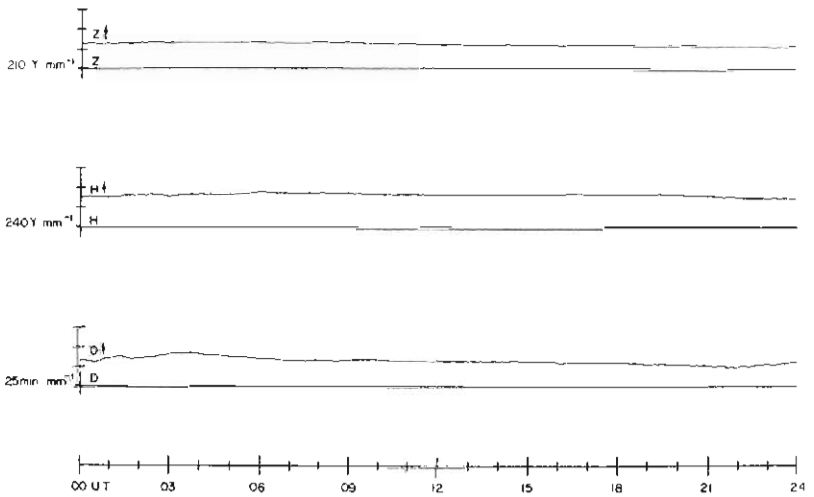


Figure 55. A quiet-day curve for the same month as the typical disturbed-day curve shown in Figure 54. (*Original magnetogram supplied by Bureau of Mineral Resources, Geology and Geophysics, Canberra*)

points on the lower border, assumed to be at a constant height of 105 km. From the maps, the co-latitude of the lower border nearest the equator that crossed geographic longitude 152°E was extracted for each quarter hour and tabulated against the prevailing value of the Kp index. These data are presented in Figure 56 which clearly shows the equatorwards appearance of the northern-most auroral form with increasing magnetic disturbance. Over the range of Kp values 1-7, the mean co-latitudes are comparable with those reported for homogeneous arcs at Macquarie Island by Jacka (1953). A similar relationship with the K-index for Macquarie Island is to be found in the radio-echo observations tabulated by Gadsden (1959).

With this pattern of movement of the aurora in mind, we shall later consider the instantaneous pattern of the quiet-arc aurora, the auroral oval. However, in order to present the steps that led to the concept of the auroral oval, it will first be necessary to discuss ionospheric equivalent current systems, at least as far as they were known before 1960. This forms the subject of the next chapter.

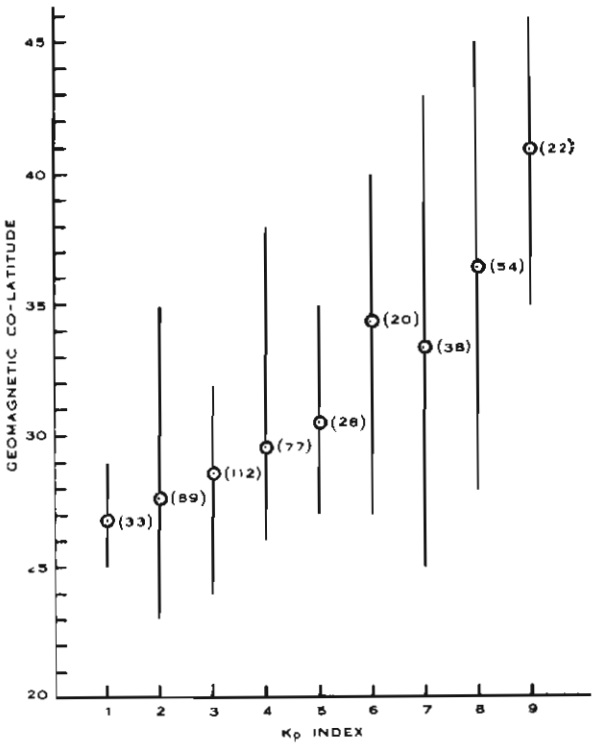


Figure 56. The mean and limits of the equator-most auroral form against centred dipole co-latitude (previously known as geomagnetic latitude) for various levels of geomagnetic disturbance (Kp). (*Bond 1960a*)

# 9. Ionospheric current systems

The concept of ionospheric current systems resulted from Birkeland's (1901) analysis of the auroral and magnetic data collected during the Norwegian Arctic Expeditions of 1899–1900 and 1902–1903 and during the International Polar Year 1882–1883.

Birkeland found it convenient to relate the magnetic variations at two auroral zone stations to a supposed linear current passing near the two stations. In Figure 57, (A) represents a linear current flowing into the paper, above and parallel to the ground, (B) represents a similar linear current flowing below the ground. The continuous line arrows represent the magnetic vectors at (C) and (D) due to the current (A), while dashed line arrows represent the magnetic vectors at (C) and (D) due to the current (B).

Birkeland found that the pattern due to the current (A) was representative of the type of magnetic variations due to a current flowing along the auroral zone at heights estimated to be between 100 and 300 km, with the mean height near 100 km.

The situation at 0140 UT on 2 January 1883 is shown in Figure 58. In this case, Birkeland estimated that a linear current of 317 000 amperes would have been required to produce the vertical-force perturbation of 150 $\gamma$. As a check on the assumed height of the current, he considered two cases at Bossekop: one where the vertical magnetic component was negligible, and one where there was an exceptionally large horizontal component. From these two cases he deduced that the currents were somewhat lower than 200 km. However, Birkeland did not consider the effect of the induced current in the ground caused by a current in the ionosphere. When the effect on the magnetometer of the induced Earth current is taken into account, the height of the ionospheric current is found to be lower.

An example given by Birkeland of the current system for a magnetic storm is shown in Figure 59. It should be noted that Birkeland considered the current flowed downwards into the ionosphere, along the auroral zone, and upwards from the ionosphere.

From a detailed analysis of many examples of magnetic disturbance and magnetic storms, Chapman (1935) proposed a set of ideal equivalent electric current systems. He considered the disturbance field, D, to be composed of a daily part, $S_D$, a storm field $D_{st}$ and an irregular part $D_i$ such that

$$D = S_D + D_{st} + D_i.$$

The $D_i$ field is usually quite small.

The current systems Chapman proposed were those that could explain the magnetic changes that take place; he did not suggest they actually existed. These current systems were related to an "ideal" Earth with coincident magnetic and geographic axes. When making comparisons with the actual Earth, an investigator would have to consider the relationship of a station to the actual auroral zone to locate the corresponding station in relation to the "ideal" auroral zone, or zone of maximum current.

The current-system diagrams gave the simplest method of illustrating the main features of the ionospheric magnetic field related to the aurora. There was no indication that such currents were actually flowing; however, the variations in the magnetic-field components could not be produced by currents flowing within the Earth, because the Earth-currents are responsible for only a small part of the variation field.

By applying the "right-hand rule" to the current system, an indication of the size and magnitude of the horizontal component of magnetic disturbance can be obtained. In the diagrams

that follow, the total current flowing between adjacent lines is 10 000 amperes. In the auroral zones the flow is too intense for individual current lines to be shown.

In order to visualise the behaviour of the vertical component, the auroral zone (or now more correctly the instantaneous auroral oval) separates the stations inside the zone that have a maximum vertical force in the forenoon from those outside the zone that have a maximum vertical force in the afternoon. The vertical force is downwards in the Northern Hemisphere and upwards in the Southern Hemisphere.

Three figures illustrate the theoretical current systems: the daily disturbance, $S_D$, current system is shown in Figure 60; the storm-time, $D_{st}$, current system (Figure 61) consists everywhere of a Westwards current, with a concentration of current in the auroral region; Figure 62 shows the combination of the $S_D$ and $D_{st}$ current systems. These theoretical current systems have been confirmed to some extent by current systems derived by spherical harmonic analysis of magnetic data.

Examples of current systems based on actual magnetic data, are the two-cell model such as that proposed by Silsbee and Vestine (1942) (Figure 63) and Vestine *et al.* (1947), and the one-cell model (Figure 64) proposed by Akasofu *et al.* (1965). Fukushima (1953) suggested that both systems exist during substorms, with the growth of the eastward electrojet being unrelated to changes in the westward electrojet. Sugiura and Heppner (1965) further suggested that the eastward electrojet would be very intense during magnetic bay activity in the late-evening sector (Figure 65). The effect on the development of knowledge of the aurora of these early discussion of current system patterns will be considered in a later chapter.

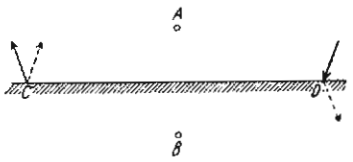


Figure 57. The magnetic force at C and D due to a horizontal electric current (directed into the page) overhead at A (force shown by full lines) or underground at B (force shown by broken lines). (*Chapman and Bartels 1940*)

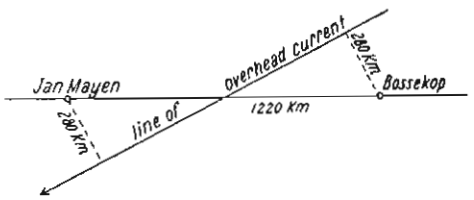


Figure 58. The situation, in plan, of an overhead horizontal electric current, inferred from the vectors of the disturbing magnetic force at Jan Mayen and Bossekop at 0140 UT on 2 January 1883. (*Chapman and Bartels 1940*)

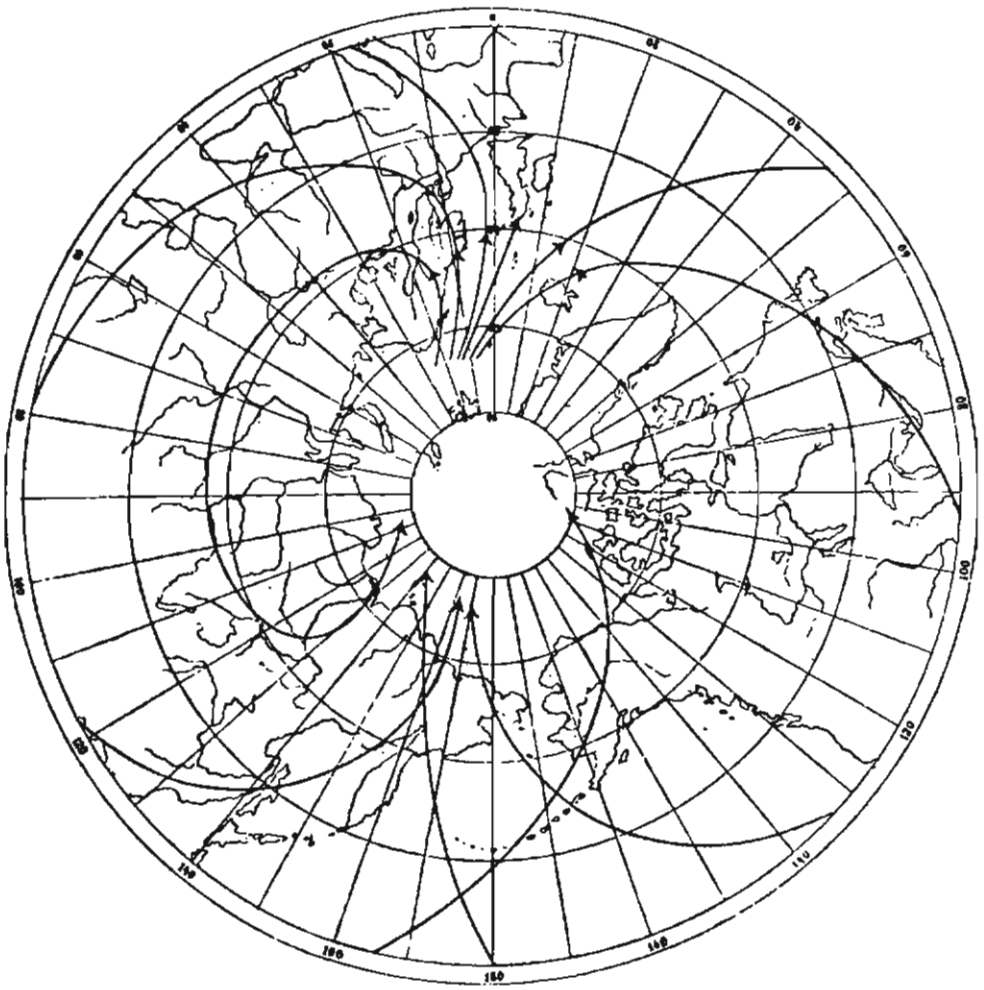

Figure 59. Birkeland's diagram of the overhead current system at Greenwich midnight during a typical magnetic storm. (*Chapman and Bartels 1940*)

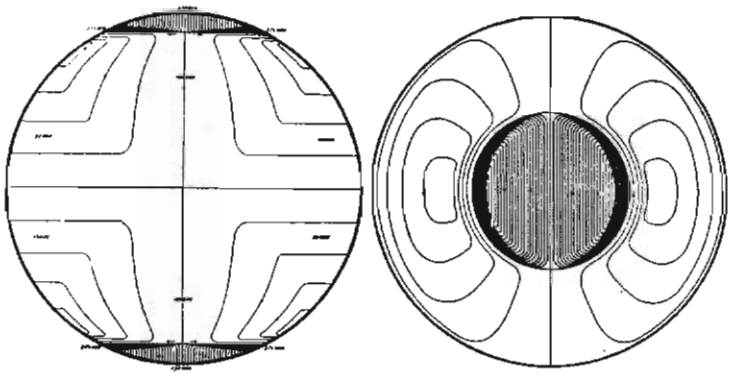

Figure 60. View of the idealised overhead electric current system that could produce the $S_D$ field. (*Chapman and Bartels 1940*)

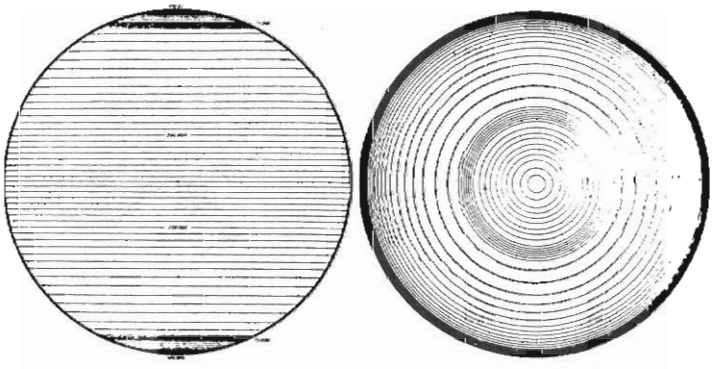

Figure 61. Views of the idealised overhead electric current system that could produce the field of the average storm-time ($D_{st}$) disturbance. (*Chapman and Bartels 1940*)

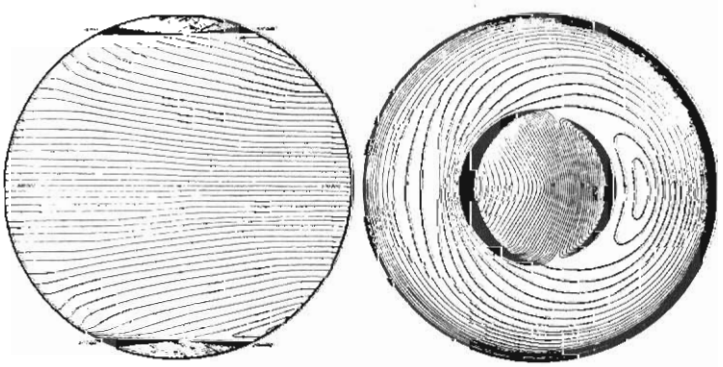

Figure 62. View of the idealised overhead electric current system that could produce the 'regular' field of a geomagnetic storm; this system is a combination of the two illustrated in Figures 60 and 61. (*Chapman and Bartels 1940*)

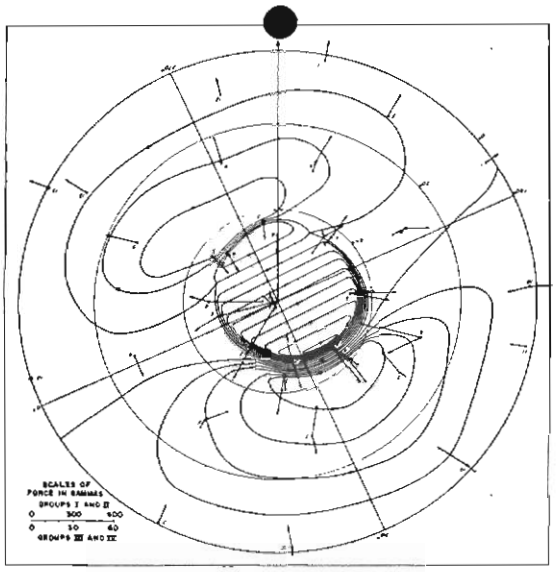

Figure 63. Equivalent current system for an average polar magnetic substorm (*Silsbee and Vestine 1942*)

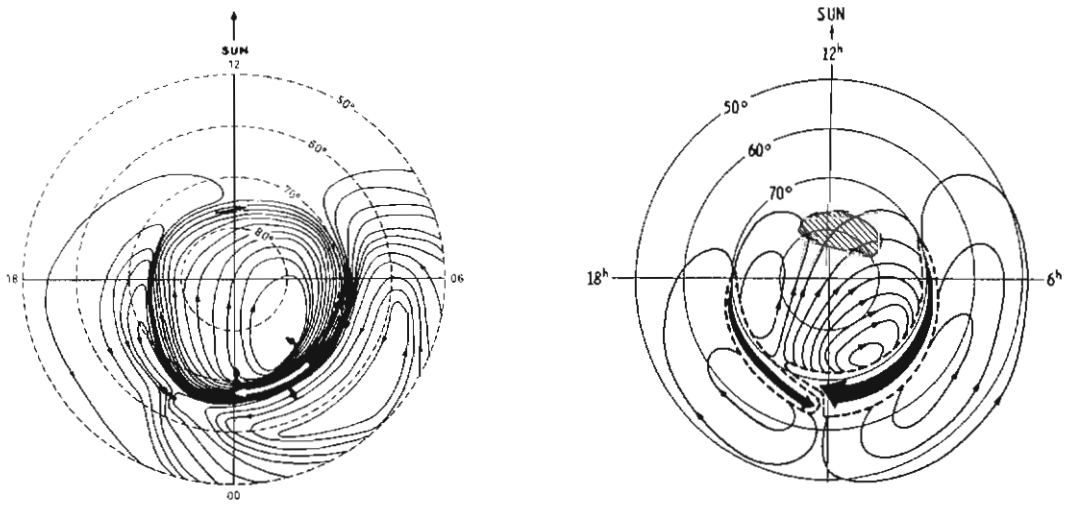


(*left*)

Figure 64. Equivalent current system for an intense polar magnetic substorm (*Akasofu et al. 1965*)

(*right*)

Figure 65. Equivalent current system for geomagnetic bays proposed by Sugiura and Heppner (1965). It involves a strong eastward electrojet in the pre-midnight sector.

# 10. The auroral oval; the instantaneous position of the auroral display

In 1959, although results from the early satellites Sputnik II and Explorers I and III had been analysed and published, the Van Allen-Vernov radiation belts and the aurora did not appear to be related in space when the locations of the belts were compared with the centred dipole field lines that link the auroral regions (see Figure 110 in Chapter 14). The electron precipitation causing the auroras was considered to be a separate phenomenon. The auroral precipitation provided a belt of high electron density compared with the low electron density of particles in the same energy range both polewards and equatorwards of the auroral forms.

The motion of the aurora and magnetic bays was the subject of a paper by Bond and Cole in 1959. In the first part, Bond reviewed the existing literature and reported recent observations by scientists at the Australian National Antarctic Research Expeditions' station on Macquarie Island. From these data it was deduced that the simplest hypothesis that fitted the observations was that the observed movements were in fact mass movements of electrons within the narrow confines of the aurora. (It is now known that a belt of particles with a wider energy range carry the currents in the ionosphere.) The second part of the paper (by Cole) was based on dynamo theory. When a conductor moves through a magnetic field, a current will pass along the conductor, provided the current circuit can be completed. Cole assumed a wind that blows the conductor, consisting of the region of auroral electron precipitation, across the Earth's (vertical) magnetic field, so producing a current. Weill (1958) had pointed out that aurora over the polar cap are Sun-aligned, while at stations at and near the auroral zone the average alignment is parallel to the auroral zone. These directions are the same as the average directions of the current vectors found for the $S_D$ magnetic disturbance current system presented by Vestine *et al.* (1947). Thus, Bond and Cole suggested, auroras seem to be visible markers of the $S_D$ current system. (The general $S_D$ current system pattern is regarded as fixed in the ionosphere in relation to the Sun and under which the Earth rotates.)

Although superseded by subsequent research, this work may have influenced developments. The theory seemed to be supported by Denholm's (1961) paper, which gave a plot (Figure 66) of hourly mean orientations fixed relative to the Sun, using eccentric dipole time. The maximum isoaurore was that from Bond and Jacka (1960).

Davis (1963), who refers to Bond and Cole (1959), presented the hypothesis that the major characteristics of the aurora can be represented by patterns fixed in geomagnetic latitude and "approximate" geomagnetic time. Thus there is a picture of a basic auroral pattern beneath which the Earth rotates. Davis based this pattern on auroral observations from stations in the polar regions of North America and on synoptic maps of the aurora photographed by all-sky cameras in Alaska and Canada. For his hypothesis to be supported, he considered that the conditions outlined in the following paragraphs would be necessary. These conditions were virtually the findings from his auroral analysis. The resulting pattern is presented in Figure 67.

The average orientation of auroral forms varies daily at all stations. The pattern indicating the alignment of forms must agree with the observations from every station at all times of the day.

Near the average time of reversal from westwards to eastwards motion, at approximately magnetic midnight, the alignment of auroral forms undergoes large change (Figure 68). This is the auroral breakup or substorm (discussed later).

Auroral arcs at the auroral zone may have an unbroken length of several thousand kilometres. Moreover, as evidenced by synoptic maps of the aurora, some forms have such variation in intensity along their length as to be readily visible along some portions, while being barely visible, or invisible, along other portions (Figure 68).

Auroral arcs in the late evening hours bend polewards to form a concentric array of extended loops opening westwards (Figure 68). The average rate of westwards drift of the evening loop array is that to be expected if the array were fixed in space and the Earth were rotating beneath it. At a time near geomagnetic midnight, the direction of motion of the auroral forms reverses abruptly. Auroral forms are generally discontinuous and diffuse after the motion reversal. However, loops similar to those of the evening hours are occasionally seen, but now opening to the east.

To illustrate the pattern of the aurora to be expected at any station in the Northern Hemisphere, Davis (1962a) presented diagrams of the situation at twelve Universal Times (Figure 69). He also pointed out that no evidence had been found of the inner auroral zone predicted theoretically by Alfvén (1955) and supported by evidence from Lassen (1959).

Lassen (1959) considered that the auroral forms that appeared near the zenith in the morning hours at Godhaven were of the same type that appeared at other stations during the morning and day-time hours. He cited this as evidence for an inner auroral zone (Figure 70).

Fel'dstein (1963) faced the problem of reconciling two concepts: that of the Earth rotating under a fixed pattern, and the fact that during daylight hours the aurora was closer to the centre of the auroral zone than the night-time aurora. He had previously noted (1960) that the times of the night-time and morning maximum occurrences are displaced regularly with latitude. In his 1963 paper, Fel'dstein reproduced the curves of morning and night-time maxima, using dashed lines to indicate those parts of the curves that fall outside an oval (Figure 71). These spiral curves are fixed relative to the Sun. The figure also shows (in dot-dashed lines) the positions of the auroral zone at 1500–1600 UT and 2000 UT on 13 February 1958, taken from a paper by Khorosheva (1961).

To confirm the auroral oval concept, Fel'dstein presented a polar diagram of overhead aurora in geomagnetic latitude and geomagnetic time as corrected by Hultqvist (Figure 72). The overhead aurora were obtained from 24 Northern Hemisphere stations expressed as a percentage frequency of occurrence. This figure shows the data in regions < 20%, 20–50%, 50–75%, 75–90% and > 90% frequency of overhead aurora at the relevant times. The oval for > 75% frequency can readily be distinguished.

The next important development was Fel'dstein's and Starkov's (1967) attempt to define accurately the limits of the auroral oval, the boundaries of the region in which the aurora was overhead. For this purpose they used not only the three-hour index, Kp, but also the quarter-hour index, Q, and an hourly index, Qp.

The latitude values (using Hultqvist's geomagnetic latitude) for the edges of the auroral belt were obtained by averaging all the values of the edge location, obtained from the contributing stations for each level of activity. The results for near-midnight local corrected geomagnetic time for the three indices Q, Qp and Kp are shown in Figure 73. They show that in the L co-ordinate system (for Kp values Kp = 1 to Kp = 6) the main locations of the auroral oval, in the northern hemisphere, lies sensibly at the same numerical latitude. The results for four levels of the Q index for the whole day are shown in Figure 74.

Fel'dstein and Starkov also considered the definition of the auroral oval using the azimuth of auroral arcs from six auroral zone stations. The sectors of the auroral oval for Q = 3 contributed by each station are numbered on Figure 75.

The mean auroral arc alignment plotted in corrected geomagnetic latitude and local geomagnetic time was also presented; it is shown in Figure 76.

To determine the quiet arc auroral oval for the Southern Hemisphere, Thomas and Bond began to analyse the mass of data collected during the International Geophysical Year (over 10 000 synoptic maps). Their evidence for the existence of the southern auroral oval was presented at the Birkeland Symposium at Oslo in 1967 (Jacka and Bond 1968).

It was illustrated for a given Kp value in the form of a mass plot on a polar diagram in geomagnetic co-ordinates $\Phi_4, \lambda_4$ for auroral forms seen from 23 stations during July 1958, for intervals of Kp = 3 (Figure 77).

The auroral oval expands with increase in Kp (as discussed in Chapter 8). This is illustrated in Figure 78 on one of the over ten thousand synoptic maps showing the location of overhead aurora during the International Geophysical Year.

Figure 78 represents the situation at 1100 hours UT on 13 September 1957 when Kp had the value Kp = 9–, after a westerly surge from a midnight position East of 180°E had passed through the area. During the display, a broad red arc was reported for over two hours over Sydney, New South Wales. This was probably the visible form of a subvisual Red Arc (SAR Arc) (see Chapter 19). These SAR arcs are usually subvisual, but due to the intensity and duration of the magnetic storm this arc was readily visible.

The mean position of the auroral oval and the inner and outer limits of each of the ten levels of the Kp Index were given in Bond and Thomas (1971). The ovals were determined from the quiet arcs and bands only. The stations and areas from which the data were obtained are shown in Figure 52 (Chapter 7).

The findings are given as a set of polar diagrams in Figure 79.

A method of drawing geographical maps of the auroral oval, provided that the Kp value, date and time are known, was published in Bond and Paine (1972). They also presented a set of maps of the auroral oval at 2-hour intervals for Kp = 3 for both the Southern and the Northern Hemisphere. A selection of similar maps is shown in Figure 80.

For those who still intuitively prefer the Ptolemaean concept that the Sun moves round the Earth, the corresponding maps from Figure 80 are presented in Figure 81.

Both in the display of 13 September 1967 and one on 15 July 1959 as seen from the southern regions of Western Australia, the red tops of tall rays persisted after the lower portions of the rays had disappeared (Bond 1960b). The heads of these rays expanded into a red, diffuse surface. Perhaps the red top of such a ray could have accounted for Moses' report of a burning bush that was not consumed. When seen from equatorwards of a display, the aurora is in the form of a red glow on the horizon. In Australia, this glow has sometimes been mistaken for distant bush fires.

The early studies we have considered form the background against which Professor Akasofu put forward his concept of the auroral substorm in 1964; this is the subject of the next chapter.

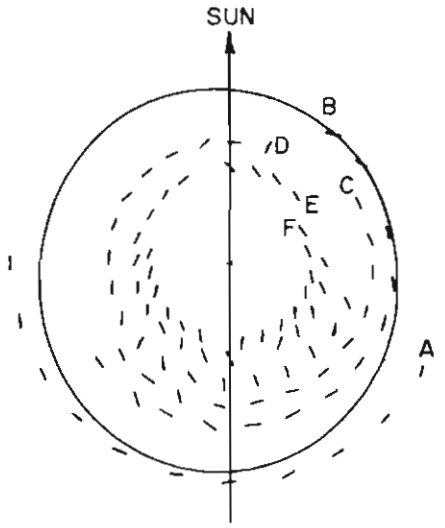


Figure 66. Hourly mean orientations at Antarctic stations in a system centred on the eccentric dipole axis and orientation fixed relative to the Sun. Stations: A, Macquarie Island; B, Mawson; C, a point 3° east of Mawson; D, Hallett; E, Scott Base; F, Wilkes. The closed curve is the maximum isoaurore.

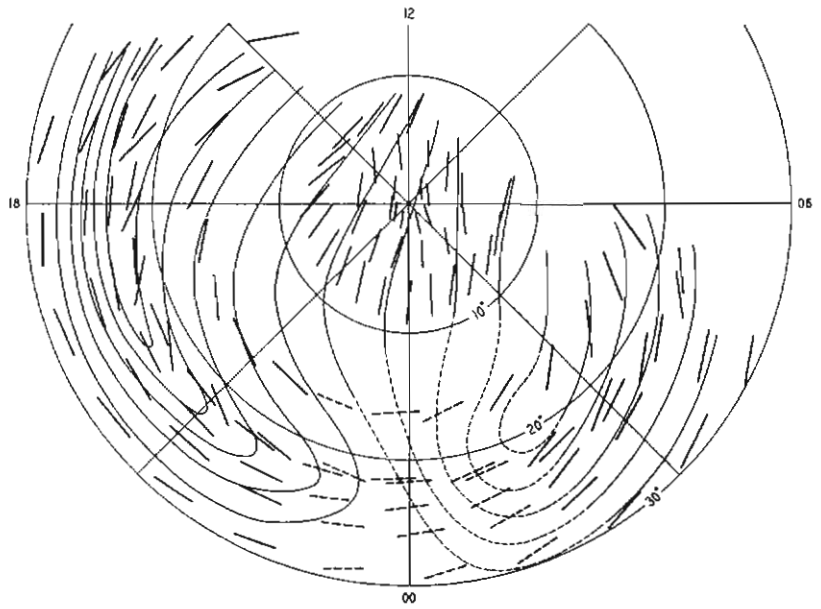


Figure 67. Hourly median alignments of auroral arcs in the Northern Hemisphere on a polar coordinate system in geomagnetic (centred dipole) co-latitude and local time. A diagrammatic pattern of auroral forms is superimposed. The dashed portions of the lines representing auroral forms refers to the period of auroral break-up. (*Davis 1962a*)

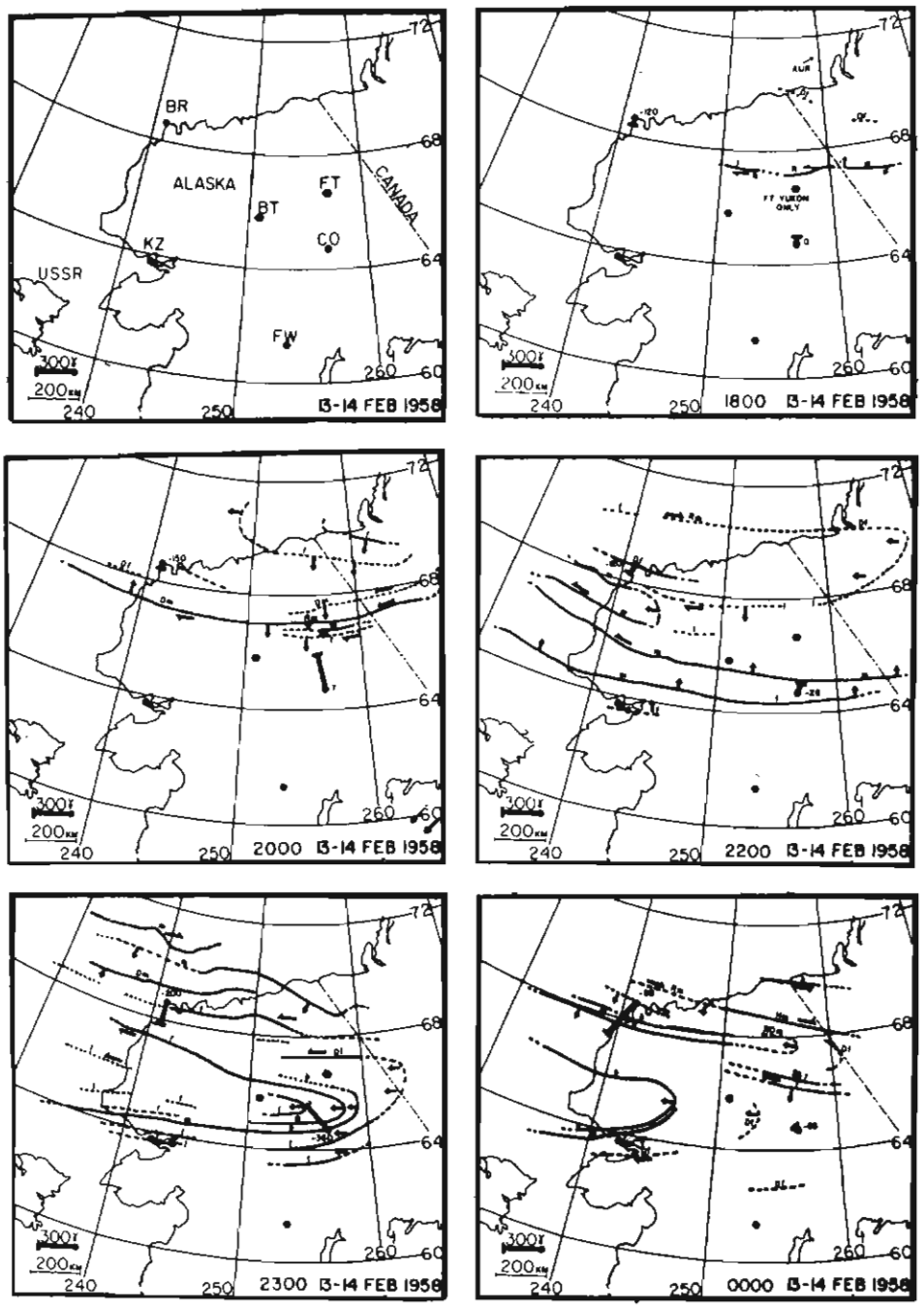


Figure 68. Synoptic maps of the display over Alaska 13–14 February 1958. The heavy bar represents magnetic disturbance in magnitude and action of the horizontal component, the number beside it gives the strength of the vertical component. Top left, location map. BR, Barrow; BT, Bettles; FT, Fort Yukon; CO, College; KZ, Kotzebue; FW, Farewell. (*Davis 1962a*)

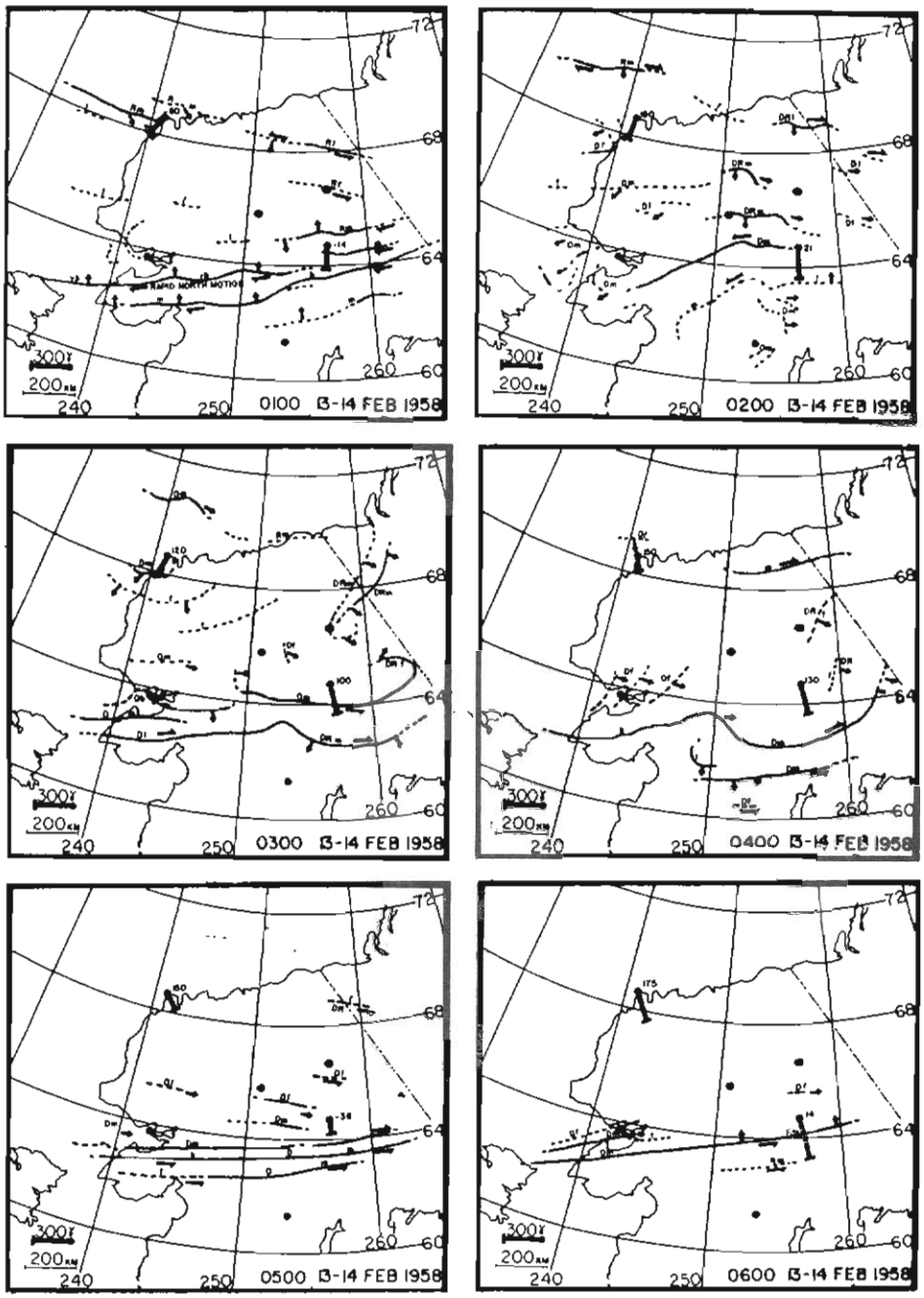
0100 13-14 FEB 1958
0200 13-14 FEB 1958
0300 13-14 FEB 1958
0400 13-14 FEB 1958
0500 13-14 FEB 1958
0600 13-14 FEB 1958
300Y
200KM
240
250
260
64
68
72
60

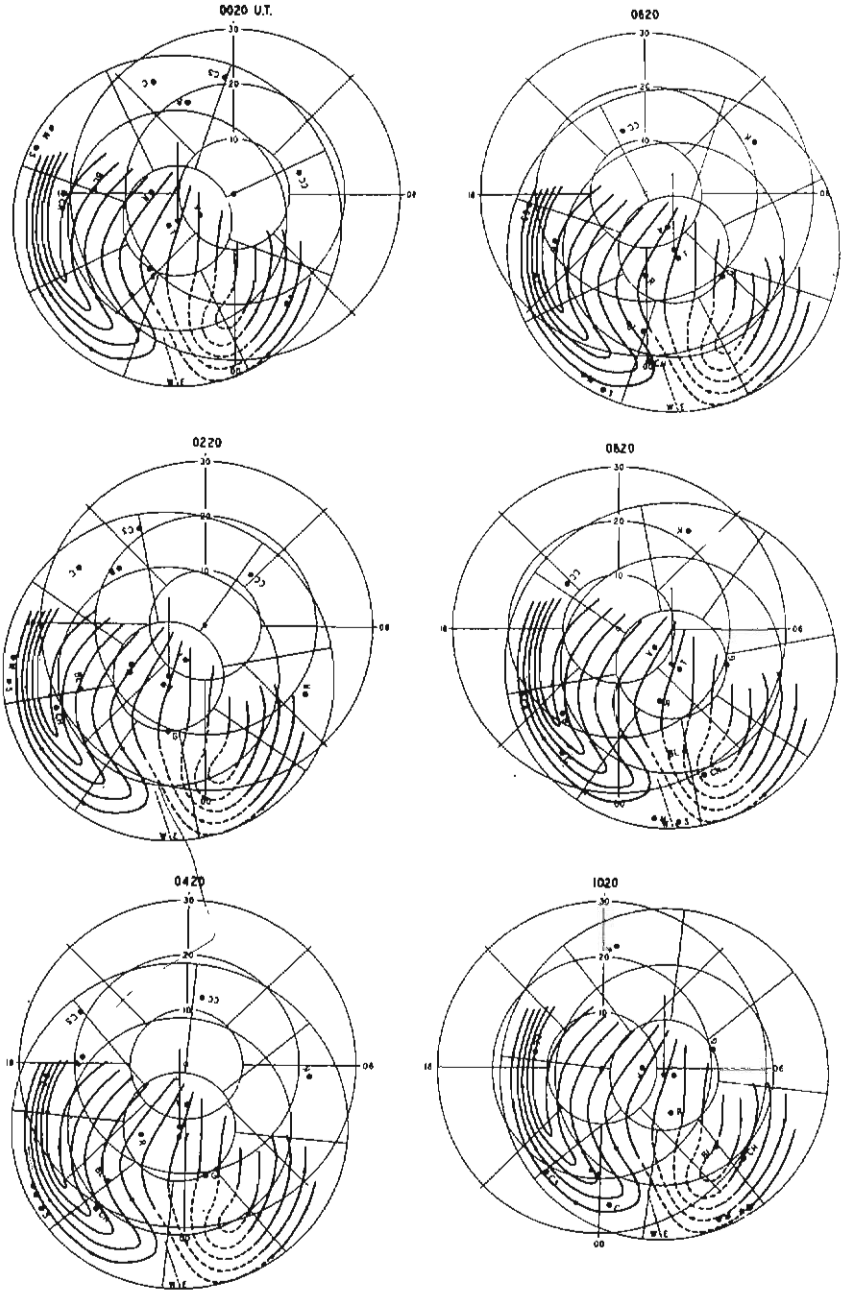


Figure 69. The auroral pattern at twelve Universal Times (UT) according to Davis. The fixed coordinate system represents geographic co-latitude local time. The movable coordinate system shows centred dipole co-latitude and longitude. The aurora is represented by heavy lines and the direction of motion of irregularities along auroral forms is shown by arrowheads. The straight dashed line near midnight separates the region in which movement of auroral forms is principally westerly. (*Davis 1962a*)

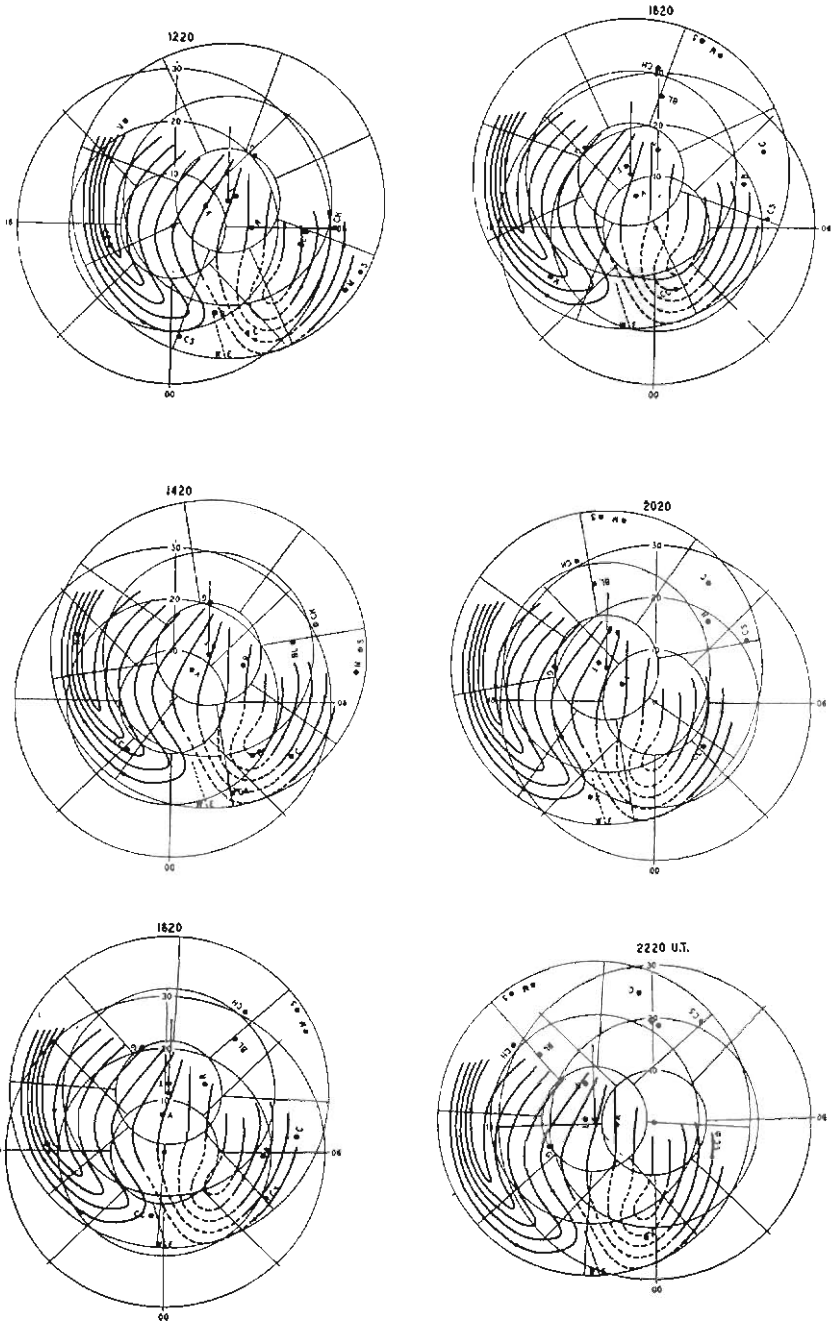
1220
1820
1420
2020
1820
2220 U.T.

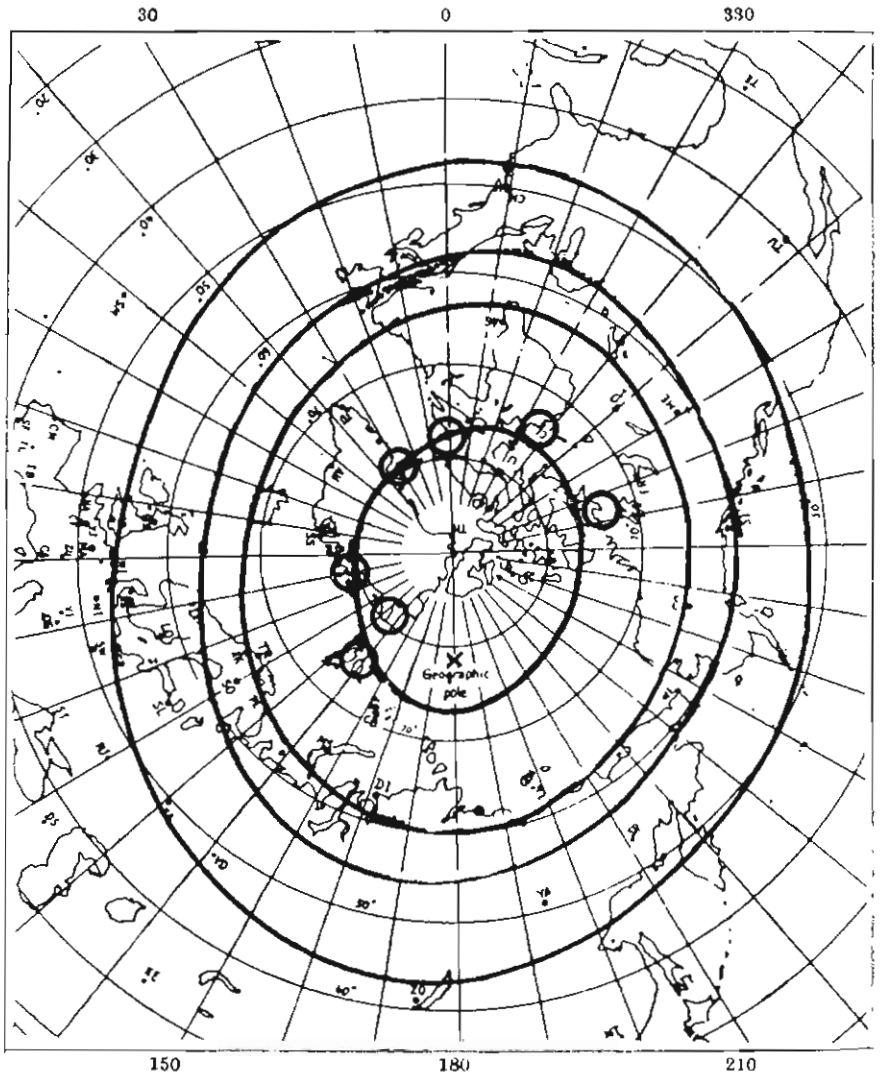


Figure 70. Auroral isoaurores (after Hultqvist 1959) stations with morning aurora near zenith. (*Lassen 1959*)

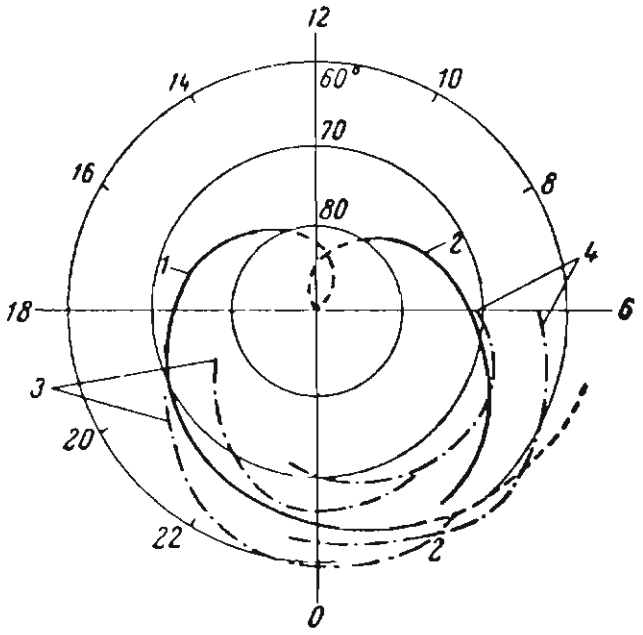


Figure 71. Fel'dstein's auroral oval. (1) The diurnal change in the onset of the night-time maxima of frequency of overhead aurora. (2) The diurnal change in the onset of the morning maxima of frequency of overhead aurora. (3) The auroral zone 1500–1600 hours UT on 13 February 1958. (4) The auroral zone 2000 hours UT on 13 February 1958. (*Fel'dstein 1963*)

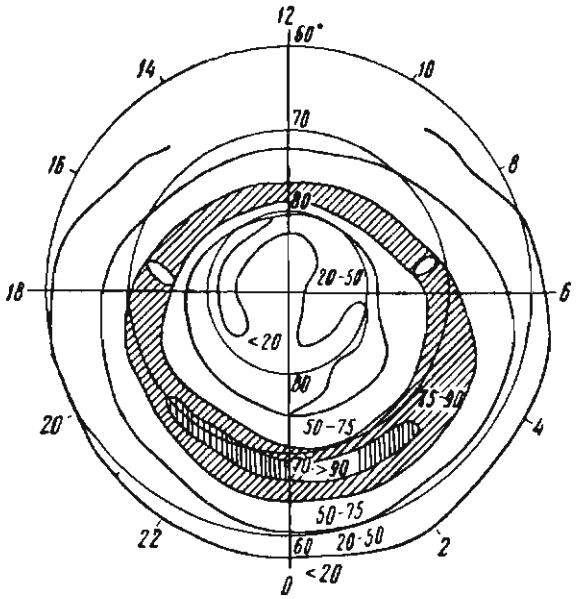


Figure 72. The percentage frequency of overhead aurora on a Corrected Geomagnetic Latitude and Geomagnetic Time polar grid, Northern Hemisphere. (*Fel'dstein 1963*)

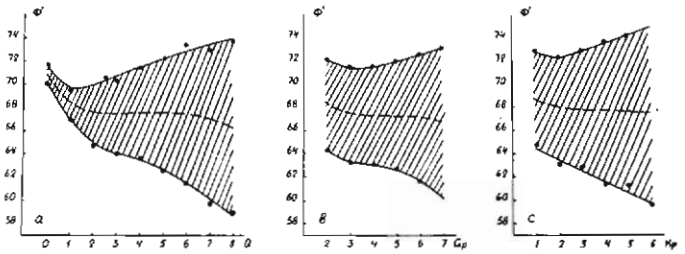

Figure 73. The dependence of the location of the northern and southern edges of the auroral belt on the indices Q(a), Qp(b) and Kp(c) of magnetic activity around midnight (2200-0200 hours) in local geomagnetic time. $\Phi'$ is the corrected geomagnetic latitude. The dashed line represents the centre of the auroral belt. *(Fel'dstein and Starkov 1967)*

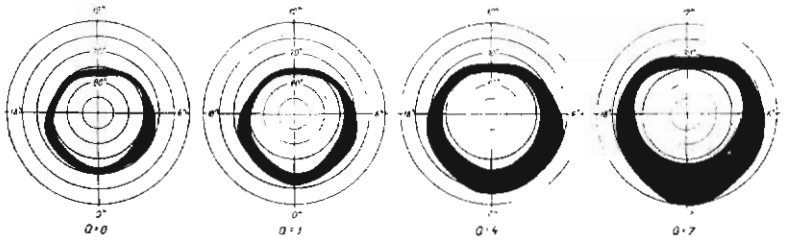

Figure 74. An auroral belt at different degrees of geomagnetic activity. *(Fel'dstein and Starkov 1967)*

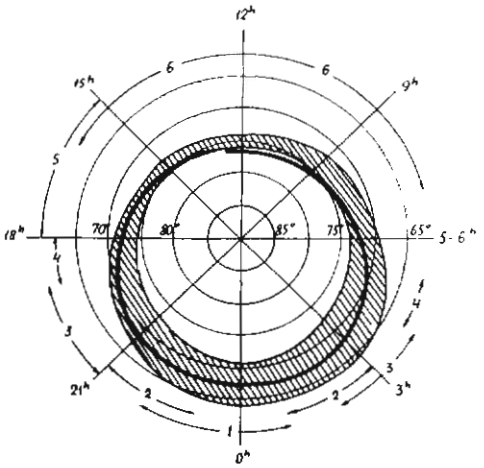

Figure 75. The full line represents the auroral oval, constructed from data on the orientation of arcs and bands. The auroral belt for Q = 3 is shown hatched. 1, Dixon; 2, Barrow; 3, Churchill; 4, Chelyskin; 5, Weise; 6, Pyramida. *(Fel'dstein and Starkov 1967)*

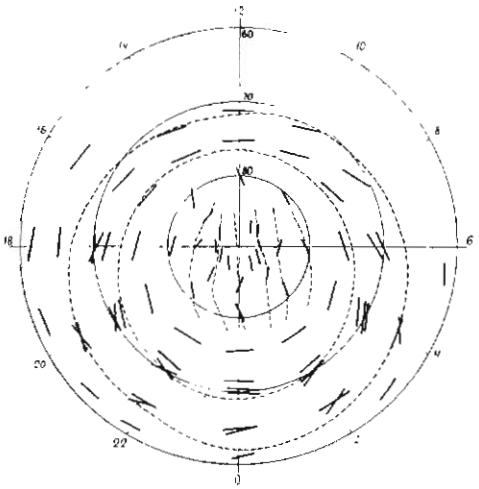

Figure 76. Hourly mean values of arc and band alignments plotted on a corrected geomagnetic latitude and geomagnetic time polar coordinate grid. The dashed lines represent smoothed alignments of aurora. (*Fel'dstein and Starkov 1967*)

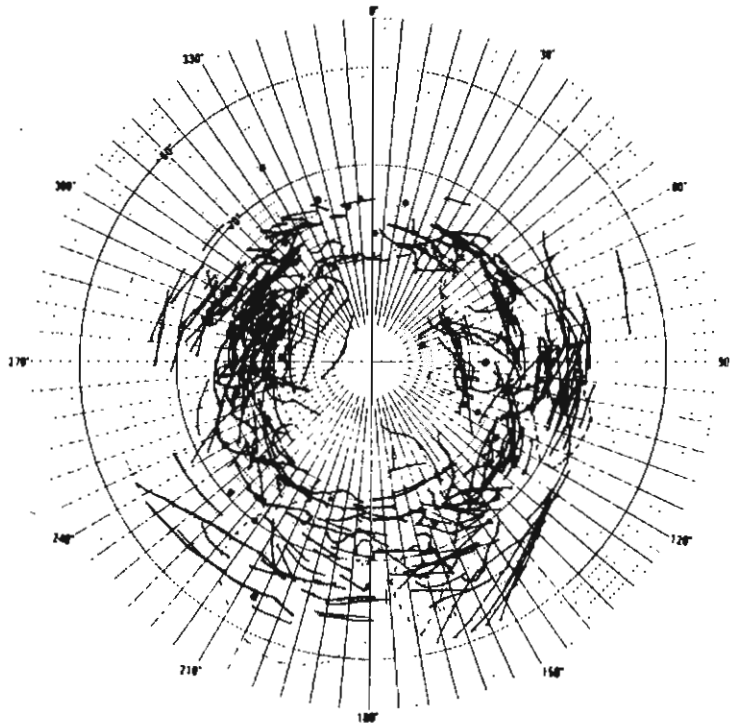

Figure 77. A polar plot of overhead aurora seen from 23 Southern Hemisphere Stations during July 1958 at times when the Planetary Geomagnetic Index Kp had the value Kp = 3. The plots are in the form of geomagnetic latitude and geomagnetic time-longitude $\Phi_4, \lambda_4$ with 0° longitude (1200 hours) always pointing to the Sun. Arc and band forms are shown as continuous lines, rays by dots, and diffuse aurora as areas enclosed by dashed lines. (*Jacka and Bond 1968*)

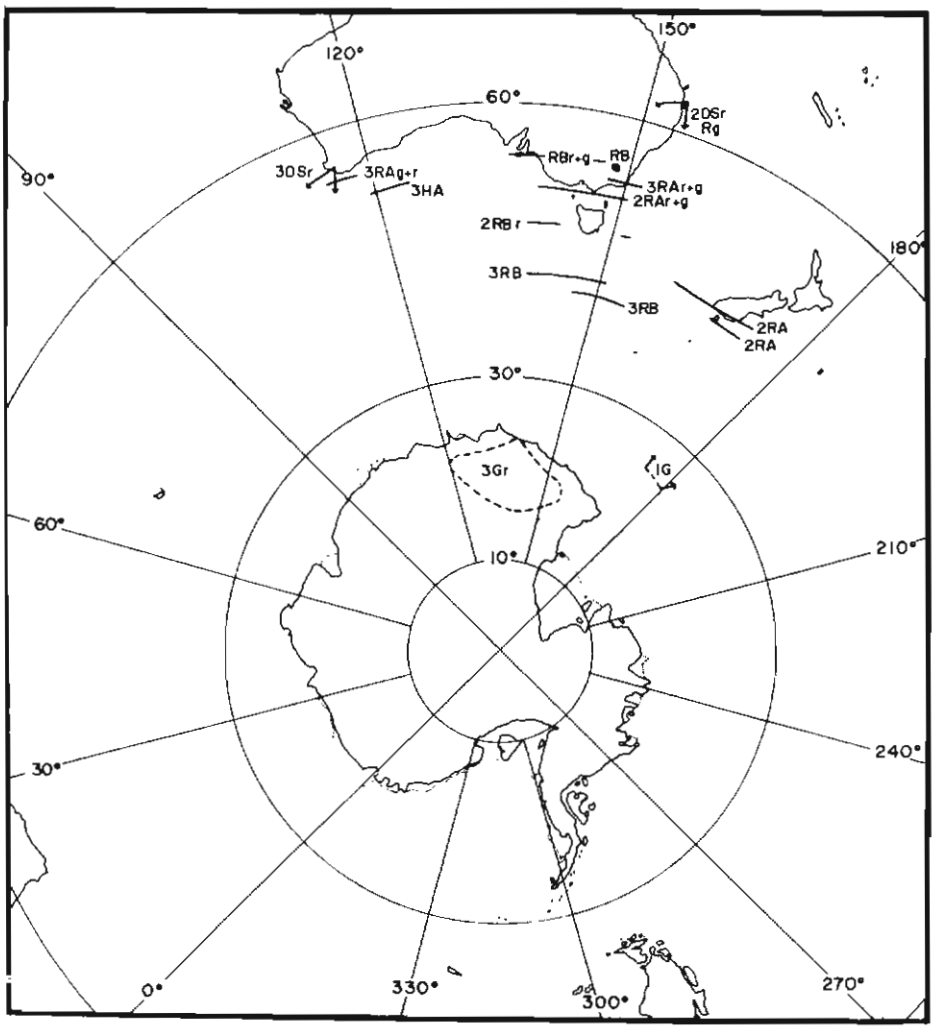


Figure 78. Synoptic map of reported aurora at 1100 hours UT on 13 September 1957 with Kp = 9–. Auroral forms are described in the sequence, International Brightness Coefficient, type of form (DS, diffuse surface (between directions indicated by arrows); G, glow; HA, homogeneous arc; RA, rayed arc; RB, rayed band; • coronal form), colour from lower border upwards (r, red; g, green).

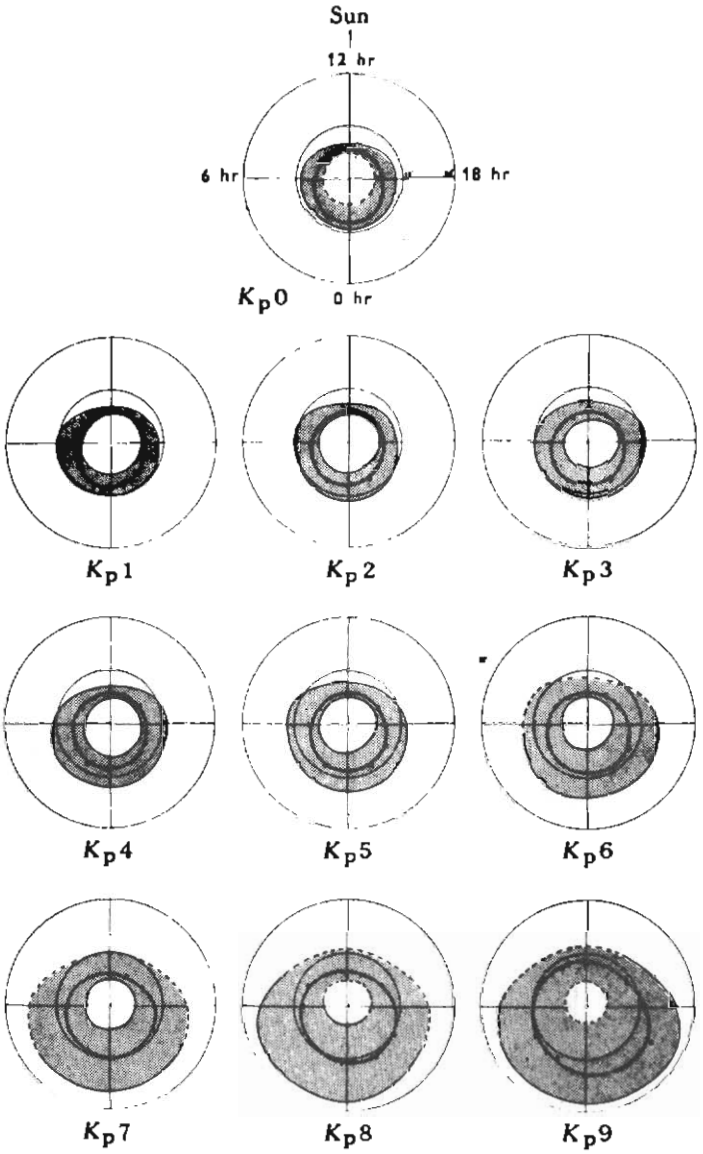


Figure 79. Smoothed mean locations of the auroral ovals (heavy lines) shown together with the inner and outer envelopes (shaded areas) of the ovals for Kp = 0 – 9. Where the data are few, the probable envelopes are shown by dashed lines. The dots represent the mean for each sector, illustrating the close fit obtained. (*Bond and Thomas 1971*)

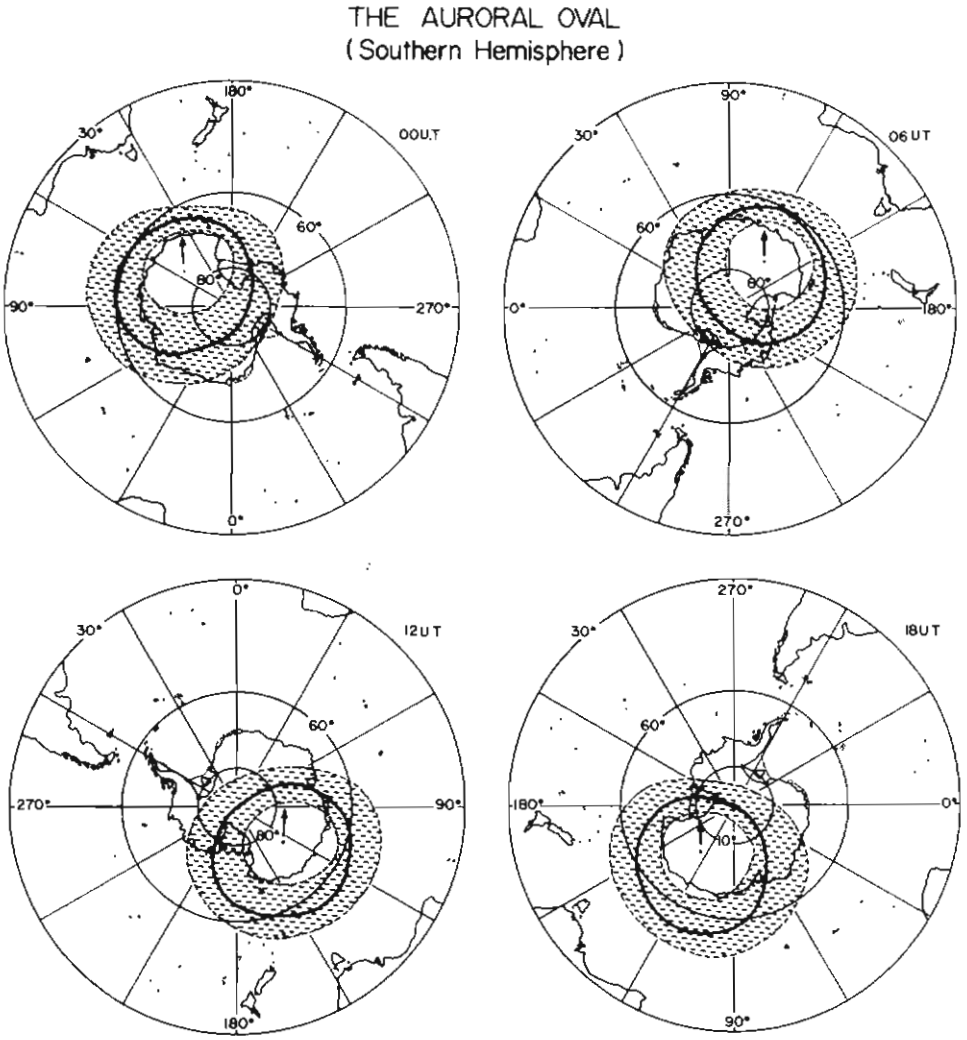


Figure 80. The auroral oval fixed in relation to the Sun, which is in the direction of the top of the page (as shown by the arrows pointing away from the Auroral Pole). Six-hourly intervals are shown in Universal Time for Planetary Geomagnetic Disturbance Index Kp = 3.

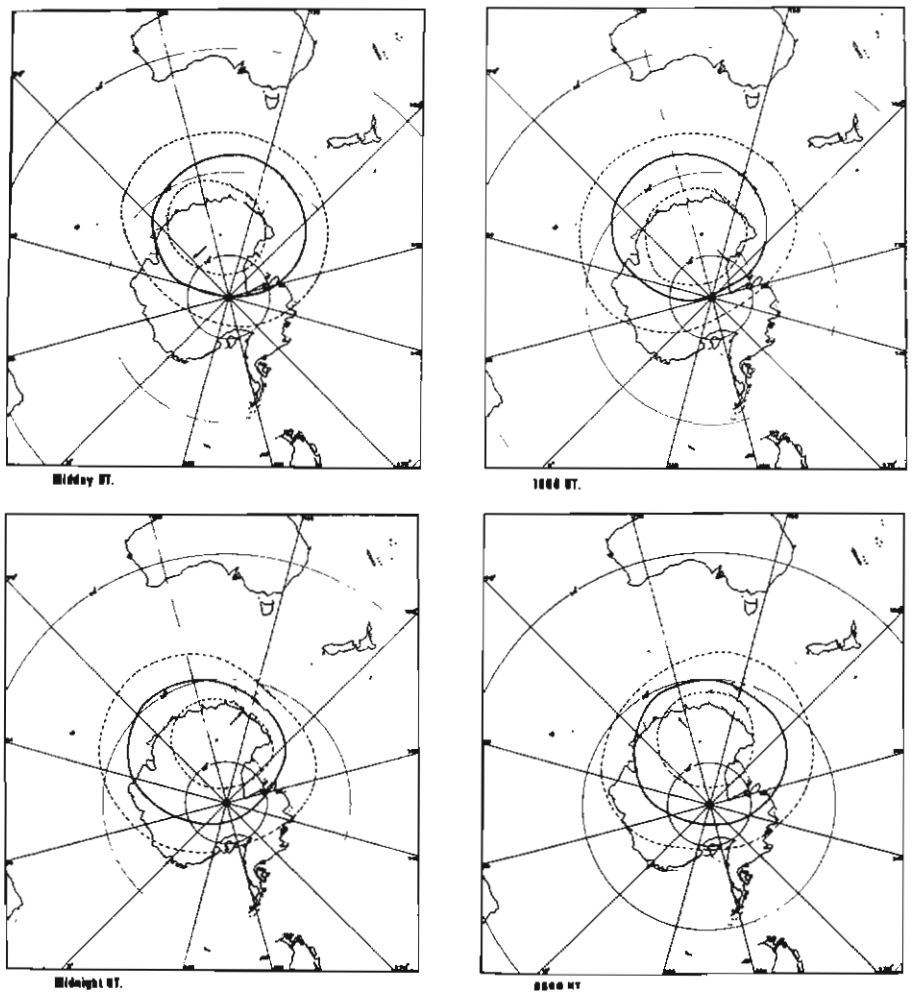

Figure 81. The auroral oval in relation to Australia. The Sun is in the direction of the arrow from the Auroral Pole. Six-hourly intervals are shown in Universal Time for Planetary Geomagnetic Disturbance Index Kp = 3. Australian Eastern Standard Time is 10 hours ahead of UT. (*Bond and Paine 1971*)

# 11. The auroral substorm

The germ of the idea of the *auroral substorm*; a term coined by S. Chapman, was probably contained in the concept of the *polar elementary storm* introduced by Birkeland in 1908, although he was describing a specific type of magnetic substorm. The modern concept deals essentially with the change from a positive magnetic bay to a negative bay, and the change in the direction of movement of auroral forms near magnetic midnight. The magnetic change has already been discussed in Chapter 7.

Akasofu and Chapman (1961) considered the phenomenon of currents flowing in the ionsophere, which they called the *Disturbance Polar Field*, and in particular they dealt with the Disturbance Polar substorm. However, it was Akasofu (1964) who first developed the concept of the auroral substorm. It explained all the then-known observations, and with additions by Fel'dstein and Starkov (1967), is still largely applicable.

The auroral substorm can be explained with the aid of a set of polar diagrams (Figure 82) in centred dipole coordinates.

Firstly, in Figure 82a, we deal with the quiet arc auroral oval, which exists between intervals of disturbance. Sun-oriented auroras may appear in the trans-auroral region. Whether Sun-oriented aurora are present or not, one or more quiet arcs exist in the region of the magnetic midnight meridian. This situation may last for minutes or hours.

The first indication of the expansive phase of the substorm is the brightening of one of the arcs near the magnetic meridian (Figure 82b). Quite suddenly (Figure 82c), the bright arc begins rapidly to move polewards at speeds of 20-100 km $min^{-1}$, and at the western end a loop forms and moves westwards towards the evening side of the Earth. (This westwards surge of aurora has previously been discussed as a westwards movement of aurora during the evening hours.) At the same time there is an eastwards movement of the aurora at the eastern end of the break-up bulge. The region traversed by the polewards moving arc contains the short broken bands, previously known as "draperies", which are gradually replaced by patches and rays (Figure 82d).

After 30 minutes to an hour the recovery phase begins (Figure 82e). As soon as the more polewards active auroral band reaches its highest latitude, it may start to return. Often, however, it stays at the most polewards position for as long as 10–30 minutes, and then starts to return. The westerly surge also slows down, and the surge may degenerate into small, irregular folds.

One to two hours later the auroral oval arcs re-form, and tend to move equatorwards. The auroral patches slowly fade to an auroral veil.

Finally two to three hours after the substorm the quiet arc situation again prevails.

The pattern of the associated magnetic disturbances depends upon the position of the magnetometer station in relation to the auroral surge (Akasofu 1968). In Figure 83, the magnetometer H trace at A, a station about 2° (or more) of latitude equatorwards of the surge shows a simple positive bay. At station B, somewhat nearer the surge, the H trace shows a positive bay followed by a negative bay. About 1° equatorwards of the surge a station at C would record a negative bay followed by positive and negative fluctuations. In the region of the surge itself, as recorded by a magnetometer at D, the trace shows the onset of a deep negative bay with the passage of the surge. Polewards of the surge at stations E and F, the magnetometer H traces are similar to those at stations B and A respectively.

Akasofu's 1964 presentation, supplemented by morning observations from Pyramida and Chelyskin (northern Russia), is shown in Figure 84.

Before the substorm begins (Figure 84a), the day-side picture around midday is that of rays and bands. At the start of the substorm, both before and after midday, thin, rayed arcs, aligned

along the auroral oval appear and auroral brightness increases. Later the arcs move equatorwards, and aurorae on the day and night side form the general pattern of an oval.

The recovery phase shows a general movement of the aurorae towards the equator and then the quiet arc oval, the auroral display typical of magnetically quiet conditions, gradually returns.

During prolonged magnetic storms, new substorms begin before the existing substorm has run its course; the new substorm starts at any phase of the display during the existing substorm. In average magnetic conditions there may be 3–4 substorms at different locations of local magnetic midnight during the 24 hour period.

With this generalised description of the auroral substorm, and noting that mention was made earlier of the terms *auroral* and *magnetic conjugacy*, the next chapter will turn to those topics.

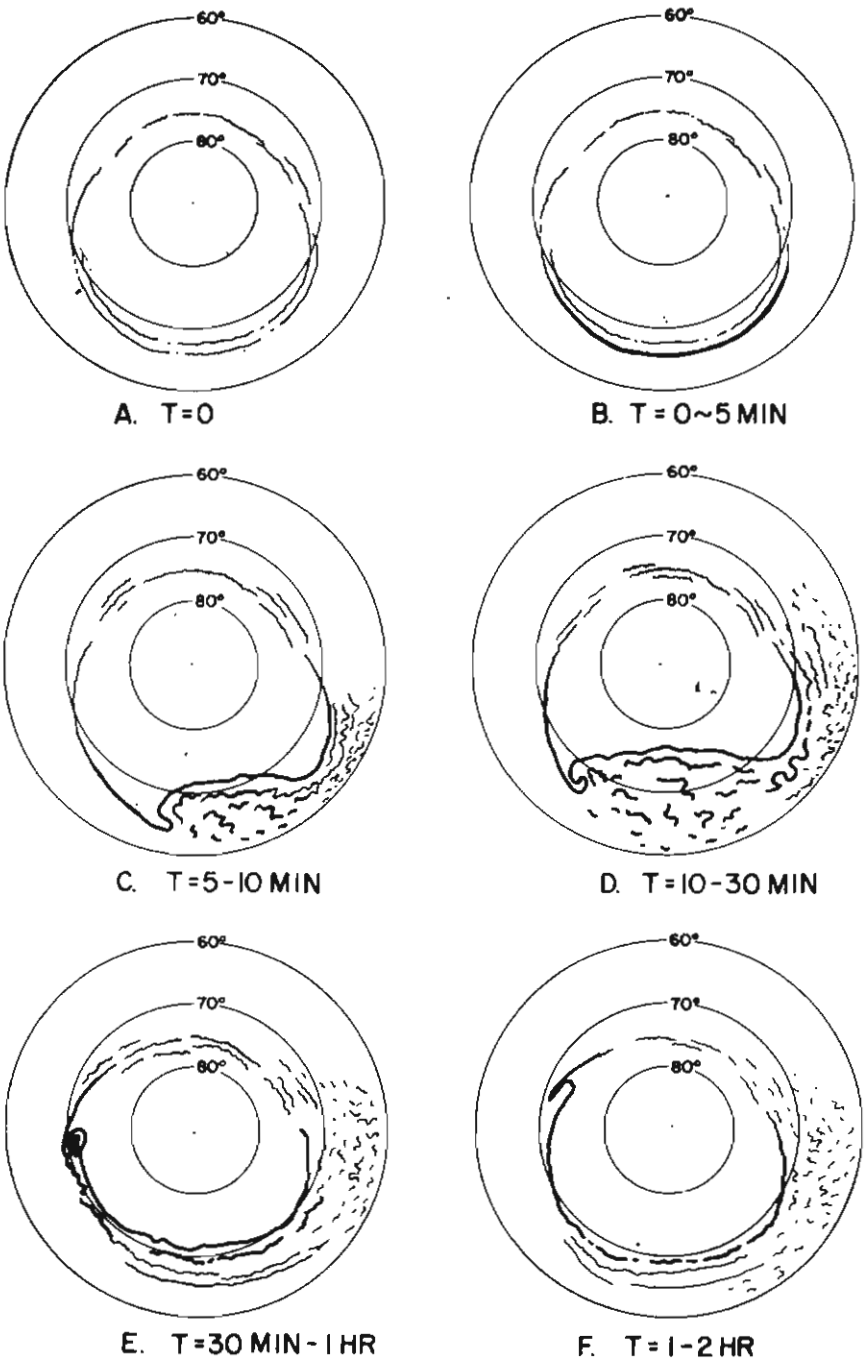


Figure 82. Schematic diagram to illustrate the development of the auroral substorm. The North Geomagnetic Pole is at the centre of each set of concentric circles. The Sun is towards the top of the diagram. (*Akasofu 1964*)

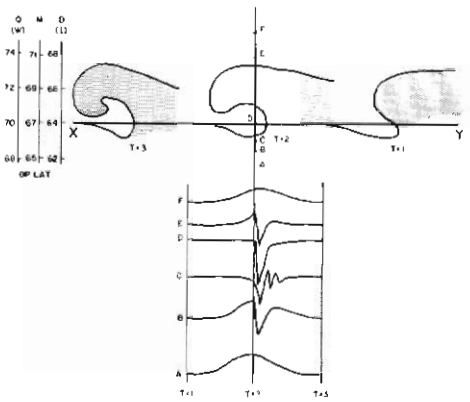

Figure 83. Magnetic variations (the H component) in the vicinity of a westward travelling surge. (*Akasofu 1968*)

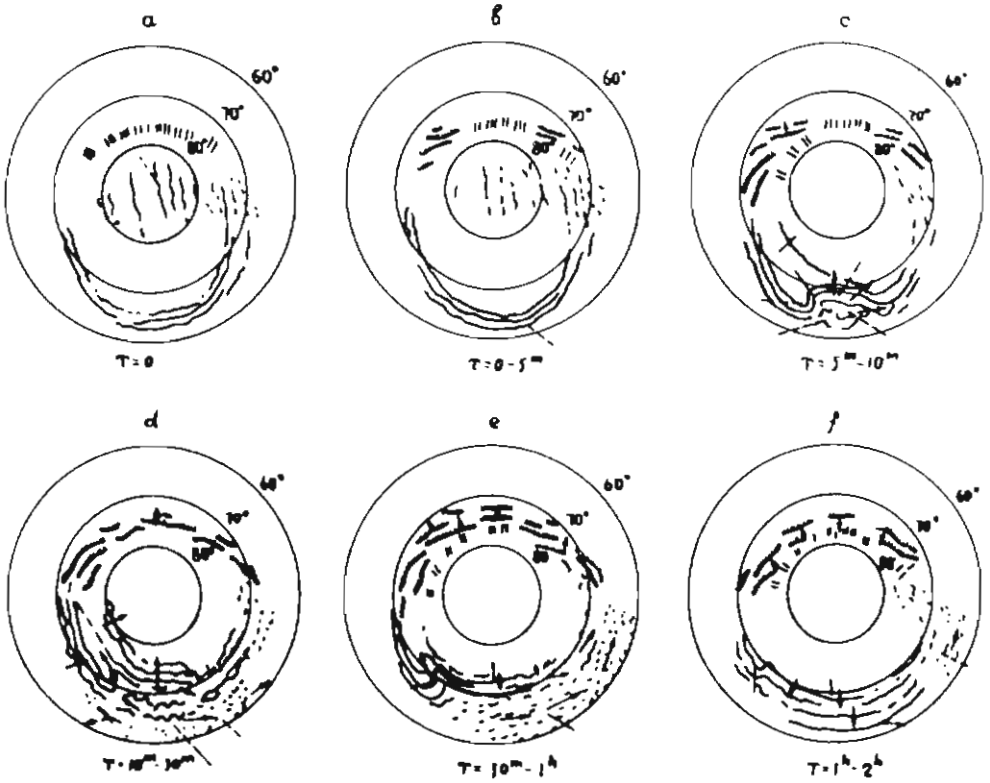

Figure 84. Diagram illustrating the development of an auroral substorm on the day side. The night side and trans-auroral Sun-oriented arcs are according to Akasofu (1964). (*Fel'dstein and Starkov 1967*)

# 12. Auroral and magnetic conjugacy

When a point in the Southern Hemisphere is linked by means of a magnetic field line with a point in the Northern Hemisphere, the two points are said to be *magnetically conjugate*. Magnetic conjugacy, in the absence of the solar wind, is established by McIlwain's L–geomagnetic coordinate system. This chapter deals with magnetic and auroral conjugacy at latitudes where the effect of the solar wind is small; the effect of the solar wind will be considered in a later chapter.

Using all-sky camera data obtained on four clear nights at Campbell Island and Farewell, Alaska, De Witt (1962) found considerable similarity in auroral forms at the same times above each station. He compared their conjugacy in the centred dipole system, but even in this system Farewell and Campbell Island are only approximately magnetically conjugate.

De Witt also analysed data from Macquarie Island and Kotzebue, Alaska, but found that the data for only one night were satisfactory for processing. Even for this night there were only a few hours of simultaneous observations under partially cloudy conditions. Throughout this short period, the aurora in the two areas were both in the form of arcs.

Bond and Jacka (1963), as noted earlier, transferred the Southern Auroral Zone along the magnetic field lines and compared the resulting zone with that determined by Fel'dstein. The good agreement achieved demonstrated the conjugacy of the two zones.

Conjugacy was confirmed in the following year. Fel'dstein (1964), using the all-sky camera plots published in *Annals of the International Geophysical Year* (Stoffregen 1962), presented the locus of the midnight positions of the auroral oval, and also the locus of the midday positions of the auroral oval for both hemispheres. He compared these plots with the Hultqvist curves for corrected geomagnetic latitude (Figure 85), and found the corresponding set of parallel curves in each hemisphere.

An analysis of the all-sky camera data from Buckles Bay (Macquarie Island) and Kotzebue (Alaska) for the period November 1962 to March 1963 showed the point near Kotzebue that is conjugate to Buckles Bay lies at geographical latitude 67.32°N and geographical longitude 196.16°E, or 0.4°N and 1.3°W of Kotzebue (Bond 1969). It was found that the location and shape of clearly discernible simple auroral forms (Figures 86a, 86b) during the initial quiet phase of the display were consistent with magnetic conjugacy in terms of co-latitude $\Theta_3$ (latitude $\Phi_3$). Increases and decreases in the brightness of corresponding auroral forms occurred simultaneously at both stations, to within one minute, and were assessed to be of the same order of magnitude. During the later stages of a display, the auroral features were slightly displaced in latitude and longitude in a manner possibly related to the angle of attack of the solar wind on the magnetosphere.

An experiment that would avoid cloud cover and give closely accurate conjugate camera positions was devised by Belon *et al.* (1967). Two NC-135 jet aircraft equipped with all-sky cameras and photometers were flown on three flights across the northern and southern auroral zones. In Figure 87 the two sets of ten solid circles on the figure represent successive pairs of conjugate points calculated from the Hendricks and Cain (1966) model of the Earth's magnetic field, which were to be reached by the aircraft at intervals of 15 minutes. The dashed lines enclosing the flight paths show centred dipole latitudes and longitudes. Figure 88 shows an example of the all-sky camera results for 1047 h 40 s UT on 14 March 1967.

This experiment provided some unique examples of surprisingly detailed cases of auroral conjugacy. However, during magnetically disturbed periods, the similarity of the auroral features deteriorates rapidly with increasing latitude.

The question of conjugacy of the auroral ovals was answered by Fel'dstein *et al.* (1974). They compared the auroral ovals (Fel'dstein and Starkov 1967; Bond and Thomas 1971) using redetermined Northern Hemisphere boundaries for the midnight position of the auroral envelopes and found good agreement with both the Southern Hemisphere data for mean positions, and for the boundaries (Figure 89).

It seems, therefore, that for the equatorwards low-latitude auroral forms, good conjugacy is reasonably well established, which implies that magnetic field lines are closed at these latitudes under quiet conditions.

The association between the aurora and the short-duration small changes in the Earth's magnetic field have been discussed briefly in several chapters. The origins of this association, and the association with magnetic disturbance of the Sun, are addressed in the next chapter.

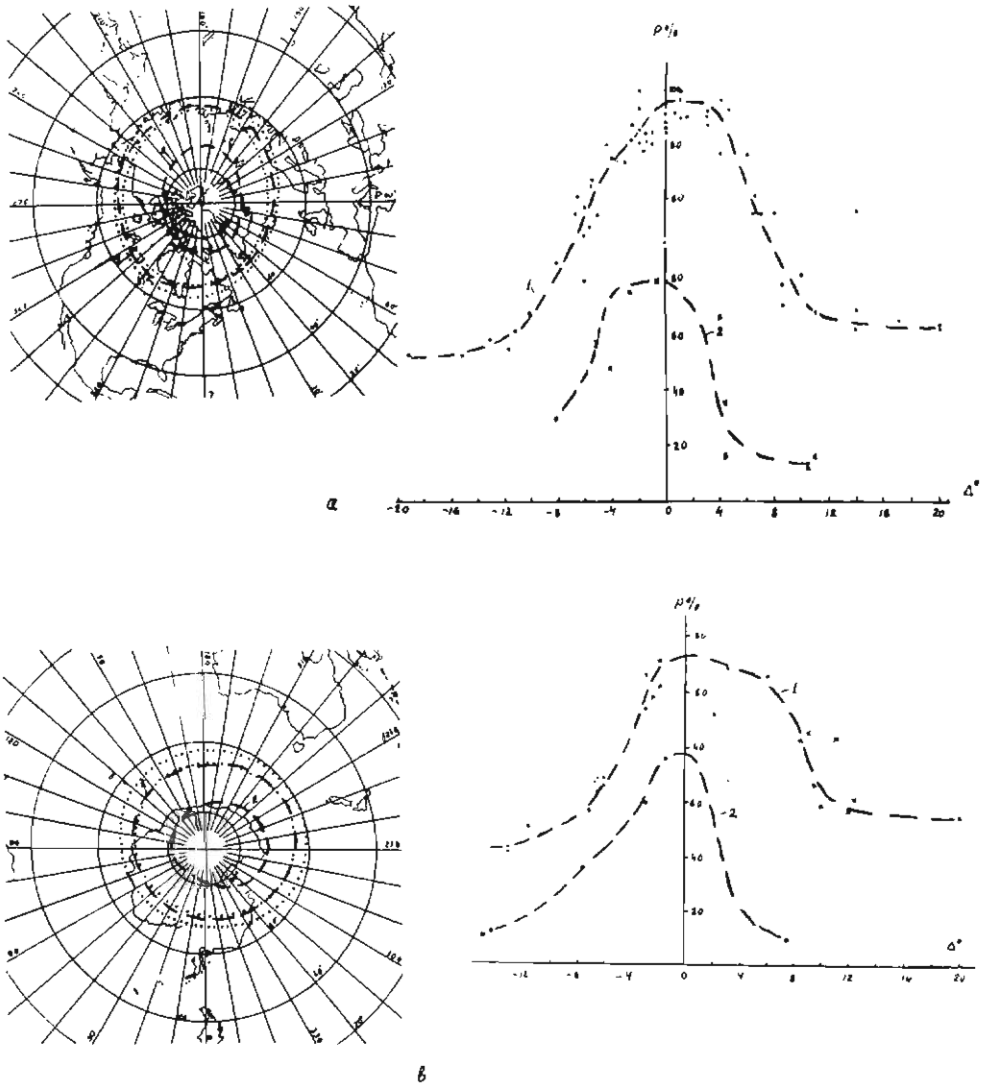

Figure 85. The zones (dashed lines) for night (1) and day (2) in the Northern (a) and Southern (b) Hemispheres. The projection of circles by Hultqvist are represented by dots. The latitudinal distribution of the frequency of auroral appearance in percent for night (1) and day (2) hours depends on the distance to the corresponding auroral zones ($\Delta$ (in degrees): positive – ° the pole; negative – to the equator). (*Fel'dstein 1964*)

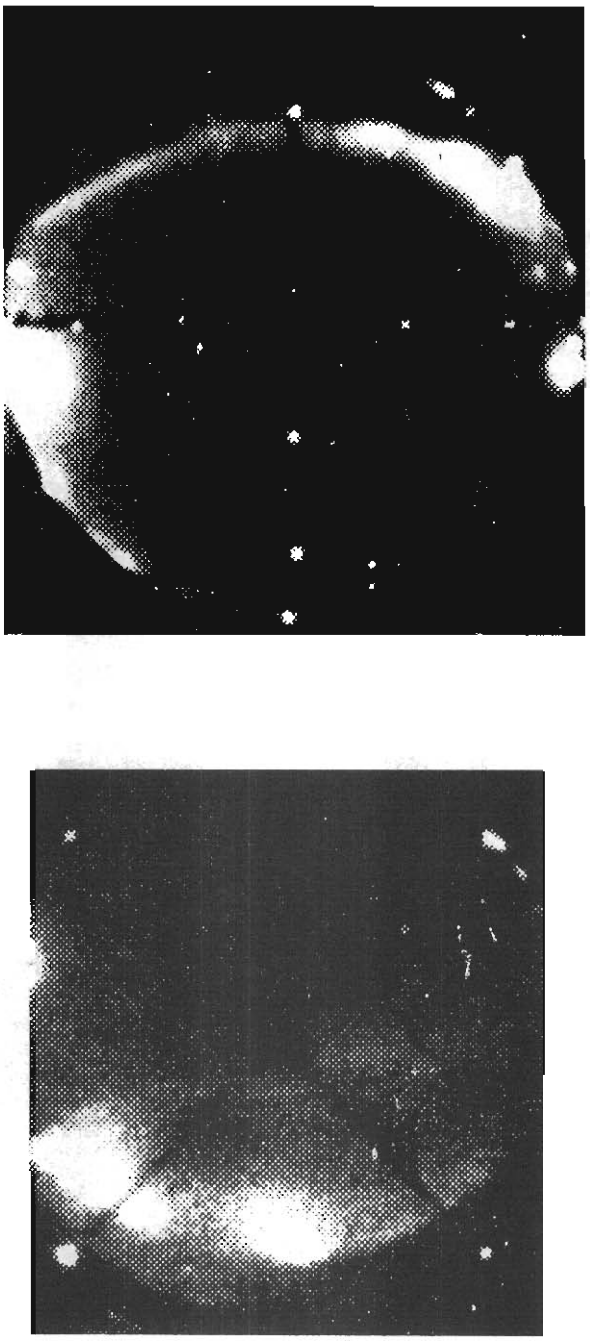

Figure 86a. Simultaneous photographs of the aurora above the approximately magnetically conjugate locations of Kotzebue (upper) and Macquarie Island (lower) showing an auroral arc with minor intensity increases at 1011 h UT on 1 March 1963. The moon was setting in the north west as seen from Macquarie Island. Extraneous lights on the upper photograph are from Kotzebue township.

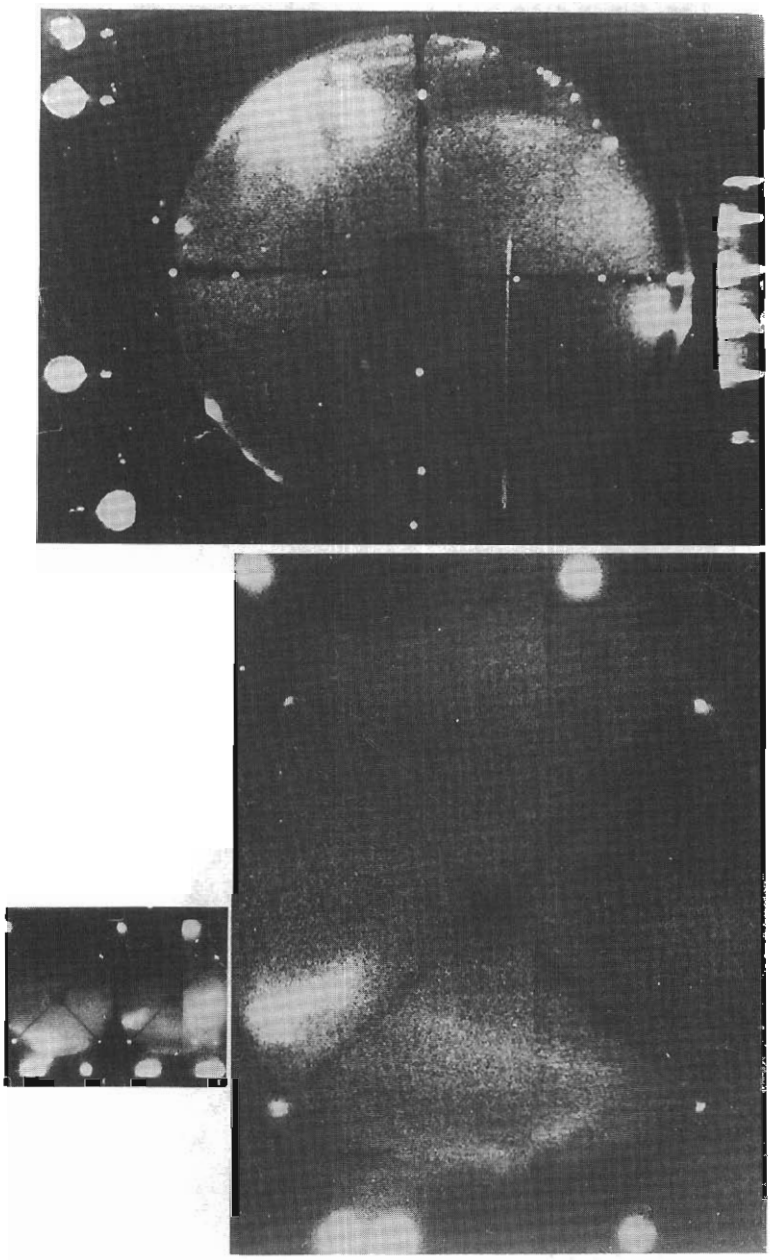

Figure 86b. The first recording of conjugate rays in conjunction with a homogeneous band. The camera had a "half frame" fault (lower left), so the enlargement is a composite of the half frame and the next frame one minute later (10 second exposure). Photographs taken at 1211 h UT on 3 January 1963.

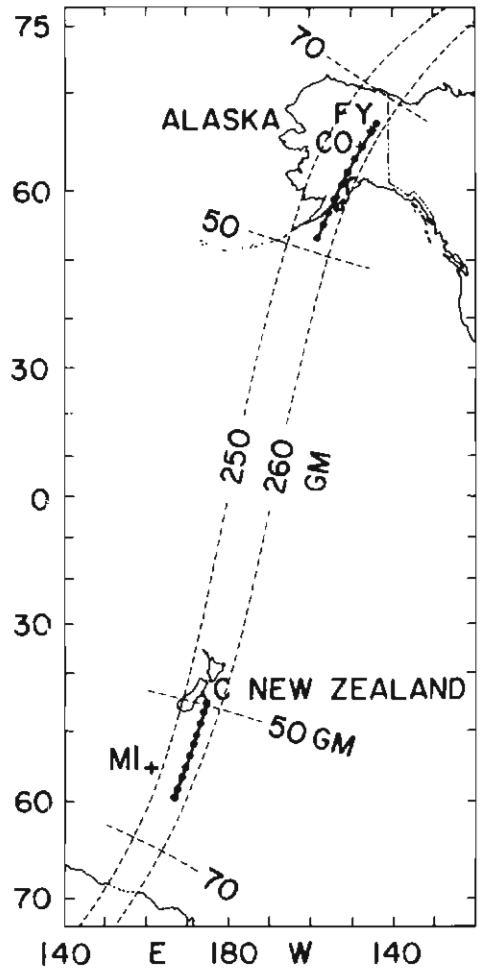


Figure 87. Aircraft flight paths in the Northern and Southern Hemispheres. Solid circles indicate conjugate locations reached simultaneously. (*Belon et al. 1967*)

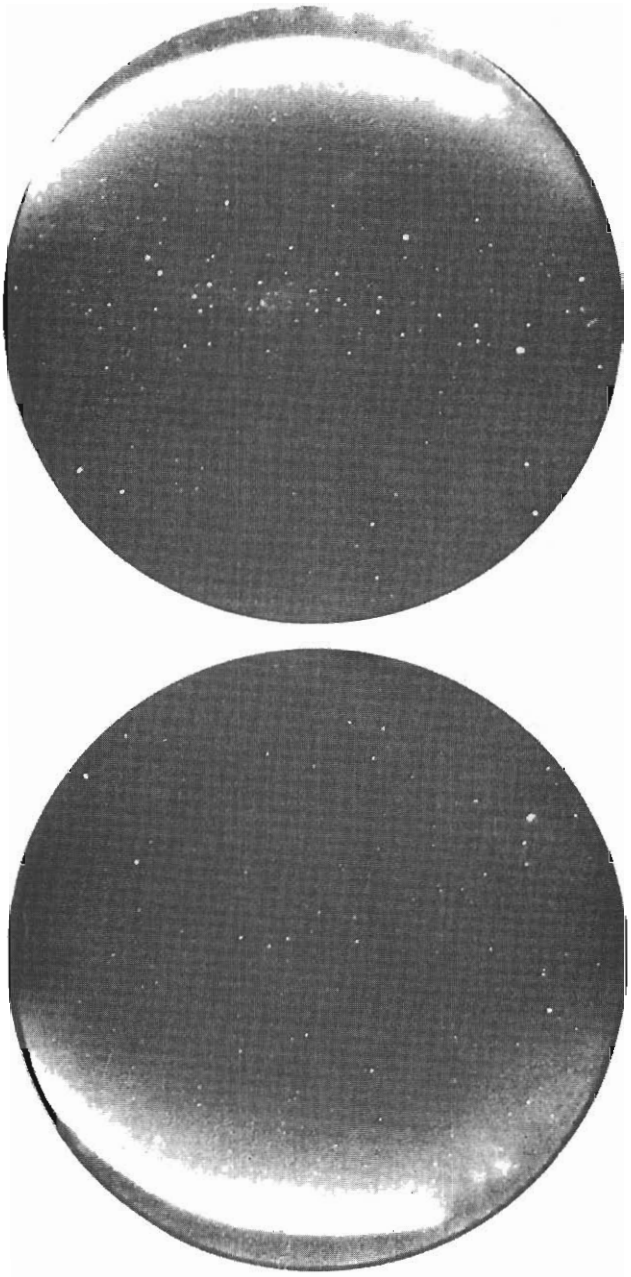

Figure 88. Simultaneous photographs by airborne all-sky cameras at magnetically conjugate points for 1047 h 40 s UT on 14 March 1967. (*Belon et al. 1967*)

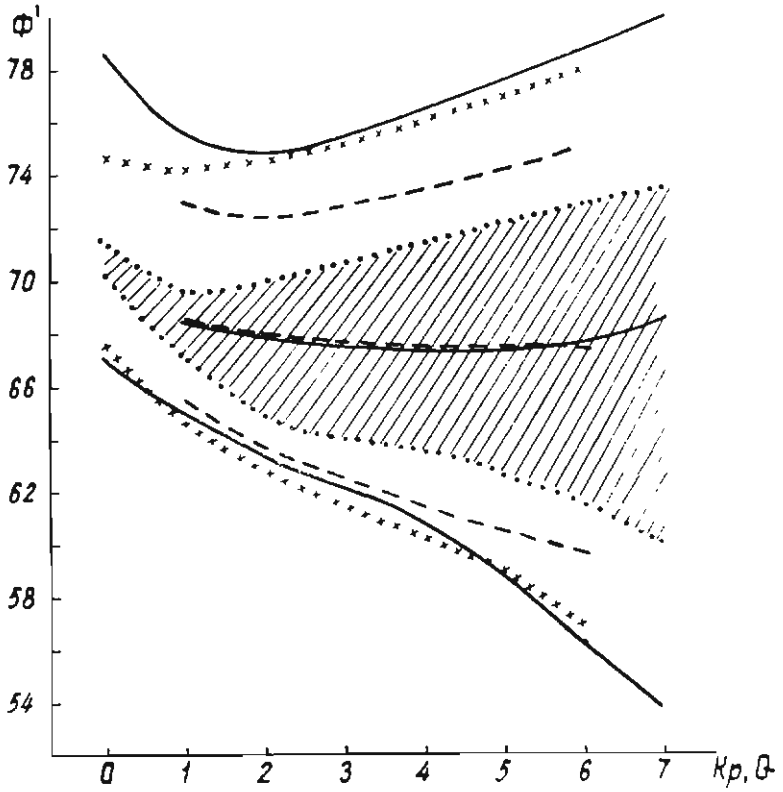


Figure 89. The dynamics of the luminescence band in the midnight sector with the Planetary Geomagnetic Index (Kp). The boundary for the Southern Hemisphere is shown by a solid line, for the Northern Hemisphere, dashed line. The corresponding lines in the middle of the diagram show the positions of the mean lines of luminescence bands. Crosses show the envelope of all auroral forms in the Northern Hemisphere. Dotted lines show the boundary variations dependent upon the quarter hour Q index of magnetic activity. (*Fel'dstein et al. 1974*)

# 13. The Sun, magnetic disturbance and aurora

Before the nature of the aurora was understood, it was known that when the aurora was present over middle latitudes, sensitive magnetic compasses observed an effect. In 1716, Edmund Halley on many occasions noted marked oscillations about the mean quiet position of a compass when an aurora was present.

The association of magnetic disturbance with the Sun was discovered as a result of the study of sunspot behaviour. Sunspots – small single black spots or groups of black spots on the face of the Sun (Figure 93) – were first noted in Europe by Theophrastus of Athens, 372–287 BC who also left a record of an auroral display (aurora borealis). Schwabe, an apothecary of Dessau in Germany, carefully observed the behaviour of sunspots from 1826 to 1843, and it was said that "the Sun never rose unclouded above the horizon of Dessau without being encountered by Schwabe's imperturbable telescope". He noticed that the number of sunspots rose and fell over a period of about 10 years. This cyclic change in the number of sunspots is now considered to have an average period of about 11.2 years.

In 1851–52, by averaging the daily range of magnetic disturbance over the whole year, but excluding the effects due to large flares on the Sun, the scientists Wolf, Sabine, Gautier and Lamont discovered the general connection between the sunspot cycle and the degree of magnetic disturbance. An example of this association, using more recent data, is shown in Figure 91.

Thus the degree of disturbance of the Earth's magnetic field is related to the number of sunspots. As the aurora is related to the disturbance of the Earth's magnetic field, it is logical to look for a relationship between the activity of the Sun and the aurora.

An early attempt was made by Schuster (1911). He suggested that magnetic storms were due to an increase of ultraviolet light in flares from the Sun resulting in an increase of ionisation of the upper atmosphere. These flares are accompanied by radio fade-outs, but they usually cause only a small, temporary augmentation of the Sq component of the Earth's magnetic field, which is much smaller in its effect than the disturbance field observed in association with the aurora.

A more fruitful approach was taken by Birkeland who pointed out in 1896 that electrons travelling towards the Earth would be deflected to the night side and could thus give rise to the aurorae (Chapman and Bartels 1940, p. 831). He experimented with projecting electrons towards a small magnetised sphere and found that many of the electrons were deflected to the polar regions. Størmer (1955) developed a mathematical theory to explain these observations. He showed that an electron, travelling into a simple dipole model of the Earth's field, can reach the Earth only within two narrow zones centred on the poles of the magnetic axis. If an equatorial ring current were established, the zones would be moved towards the Equator, as Bruche (1931) had previously demonstrated (Figure 92).

Schuster argued that, unless very high velocities were invoked, there would be serious electrostatic dispersion of an electron stream. However, the interval between a major flare on the Sun and the subsequent major magnetic storm is about 14–36 h, which eliminates the possibility of a fast stream. Lindemann (1919) suggested that the problem of dispersion could be overcome if a charged particle stream concept were replaced by the concept of a neutral ionised stream.

The concept of a neutral ionised stream was taken up by Chapman and Ferraro (1932). Consider particles that have been previously emitted from the surface of the Sun at any point in time, say t, then the particles will lie on a curve. Each point on the curve will relate back to the time $t_0$, when the particle at the point was emitted from the Sun. Since the transverse velocity at emission is only about 2 $km^{-1}$, if the radial velocity is about 1000 km $s^{-1}$, then the path of the particles will be along the extension of radius through the point of emission S (Figure 93). The

stream will thus bend backwards, lagging behind the Sun's rotation (the rotating water hose-pipe effect). With a velocity of 100 km $s^{-1}$ the elapsed time between an event on the Sun and the arrival of particles generated by the event will be about 1.7 days.

As the stream of particles approaches and sweeps past the Earth, a cavity will be formed and the magnetic field of the Earth will be compressed (Figure 94). The approach of the ionised gas towards the Earth's magnetic field will induce currents at the boundary of the ionised gas, which can be represented by an image dipole field (Figure 95). As the magnetic field of the Earth makes a deeper hollow in the neutral ionised plasma (Figure 96), protons will bridge the gap in the hollow behind the Earth. A distorted particle ring, around which electrons can flow, will be formed and this current will generate the main phase of the magnetic storm. No quantitative explanation of the main phase of the magnetic storm was presented. However, the possibility of the drift of electrons under the crossed electric and magnetic fields was postulated.

An alternative theory was presented by Alfvén (1958). He proposed that ionised gas contains its own "frozen in" magnetic field. It can be shown that, due to the electric field E, tangential to the Earth's orbit, the motion of electrons will be a drift in the anti-solar direction. Near a dipole field there is superimposed an anti-clockwise drift, due to the inhomogeneity produced by the interaction of the magnetic field in the beam of ionised gas. Figure 97 shows the motion of electrons in the equatorial plane and the "forbidden region" around the dipole that electrons cannot reach. The electron density will be greatest near the boundary of the forbidden region. Electrons may oscillate perpendicular to the equatorial plane and may reach the upper atmosphere. The curve at the polar regions found by tracing the path of the electrons from the boundary line down the magnetic field lines is shown in Figure 98, and identified as the auroral zone.

The electric field theory was tested by Malfors (1946) and Block (1955), using a beam of ionised gas passing through an electric field to a small magnetised sphere in a near-vacuum. As shown in Figure 99, eccentric luminous rings were produced around the terrella, as predicted by the theory.

In 1958, E.N. Parker published the first of a series of papers that led to a change of ideas. The concept of a beam of ionised gas changed to that of a solar wind of plasma, which carries its own built-in magnetic field, streaming outwards into space beyond the orbit of the Earth.

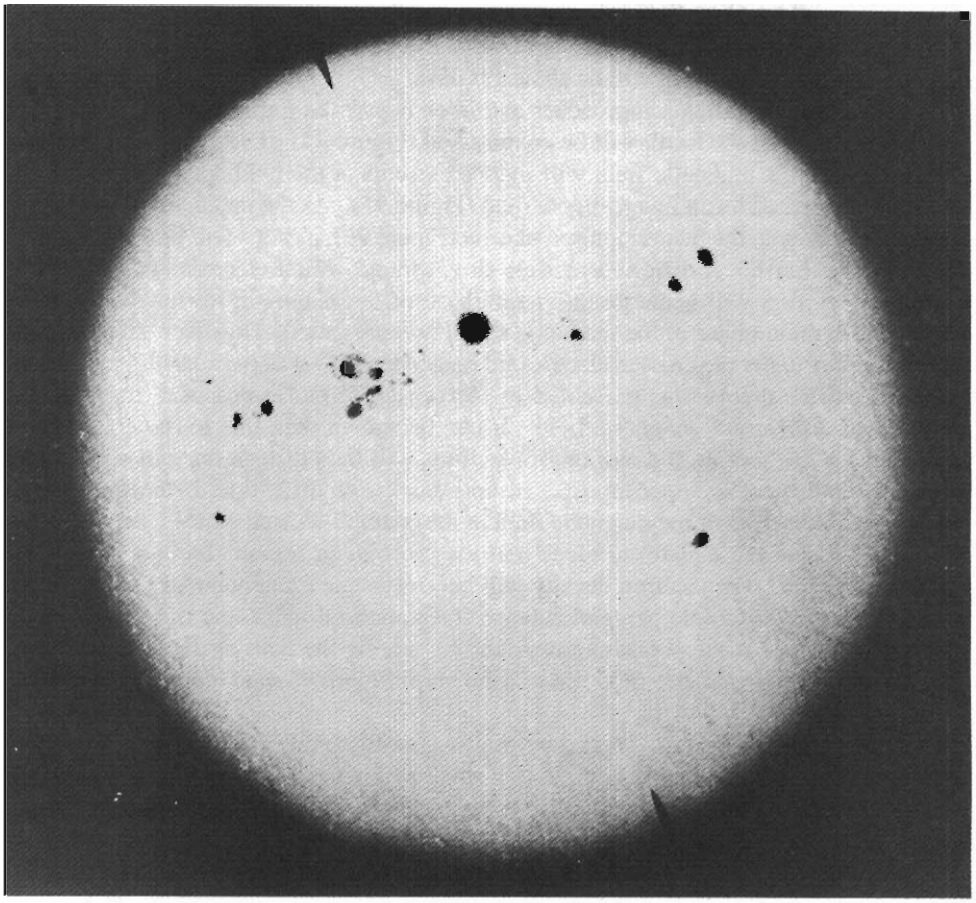

Figure 90. Photograph of the Sun, taken on 30 November 1929 (Mount Wilson Observatory), showing sunspots.

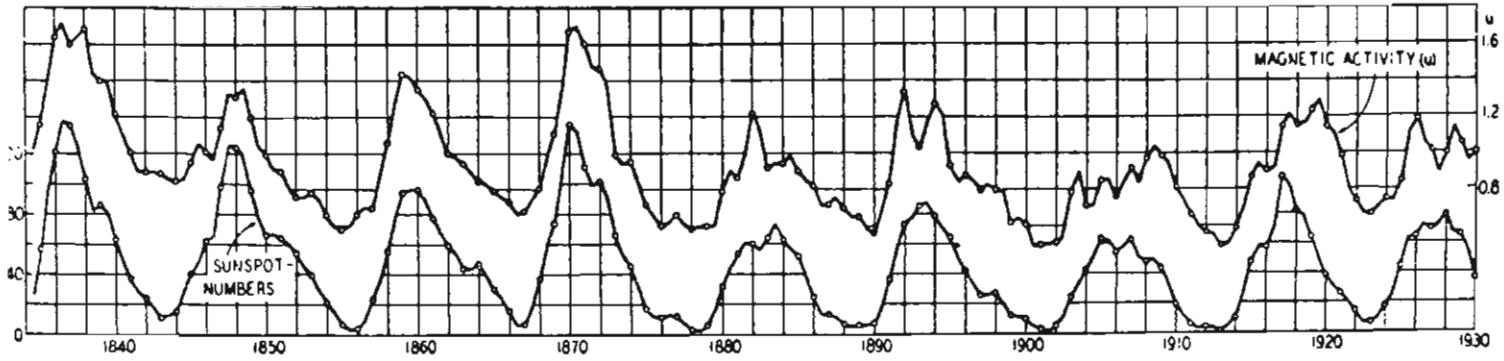


Figure 91. The lower graph shows mean yearly sunspot numbers. The upper graph shows the mean yearly value of magnetic activity (u). The daily value of u is given by the difference between the mean value of the horizontal component of the Earth's magnetic field at a particular location on the day in question and the value on the previous day, without regard to sign. (*Chapman and Bartels 1940*)

(a)

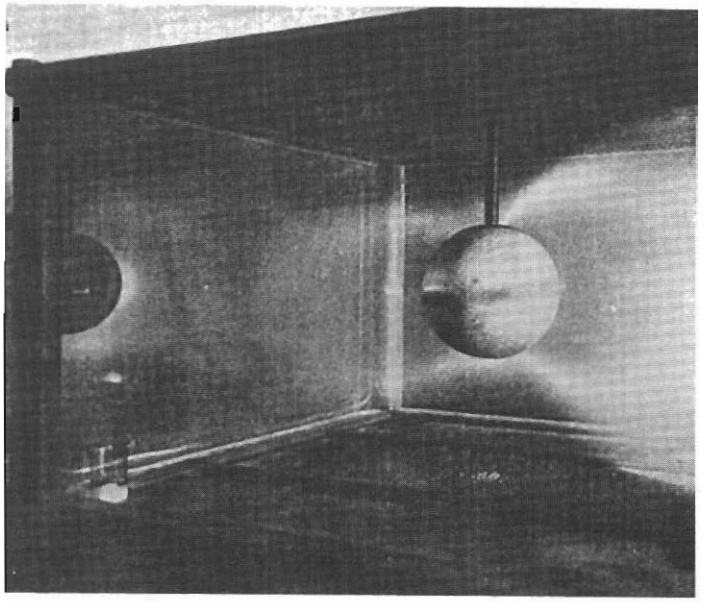

(b)

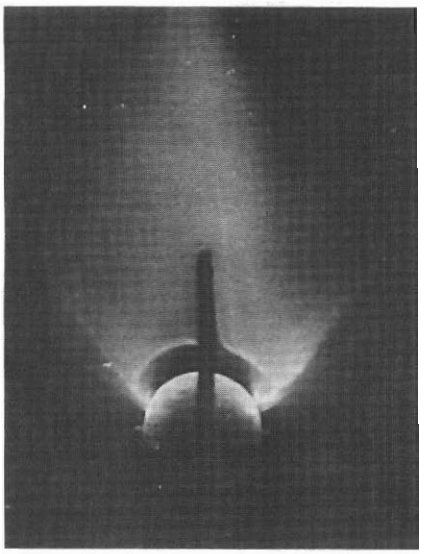

(c)

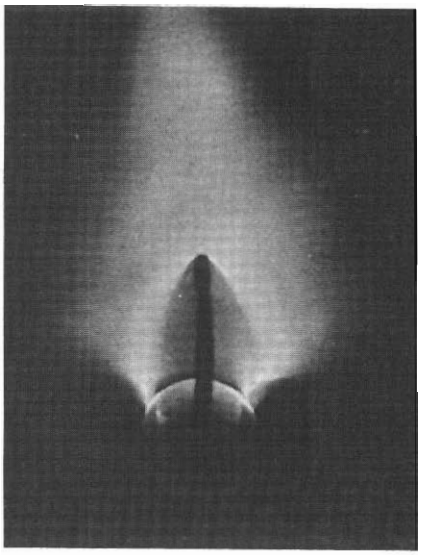

Figure 92. (a) Birkeland's (1896) terrella experiment, showing the terroidal space around the Earth. The magnetic equator is horizontal.
Lower Figures. Bruche's (1931) experimental verification of the effect of a ring current on the location of the polar-light zone (b) without and (c) with the ring current. The magnetic equator and the ring are shown vertical. (*Chapman and Bartels 1940*)

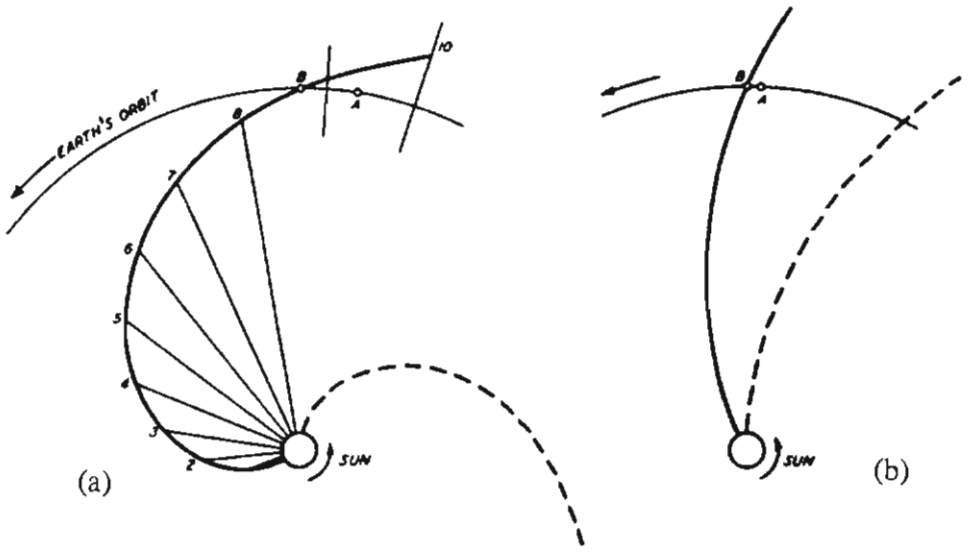


Figure 93. Diagram illustrating the hose-pipe effect at a particle velocity of (a) 2000 km $s^{-1}$ and (b) 1000 km $s^{-1}$. A and B are successive positions of the Earth in its orbit. The bold line indicates the positions of particles emitted at equal successive intervals from a point on the Sun. For example the number 8 indicates the position of a particle emitted 8 intervals ago. (*Chapman and Bartels 1940*)

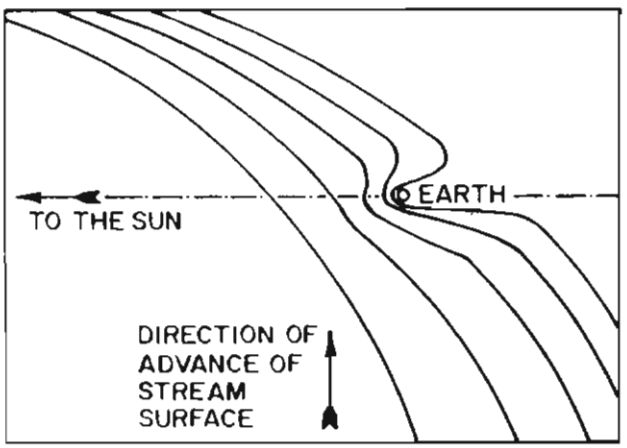


Figure 94. An illustration of how the magnetic field of the Earth would form a cavity in a stream of particles from the Sun. (*Chapman and Bartels 1940*)

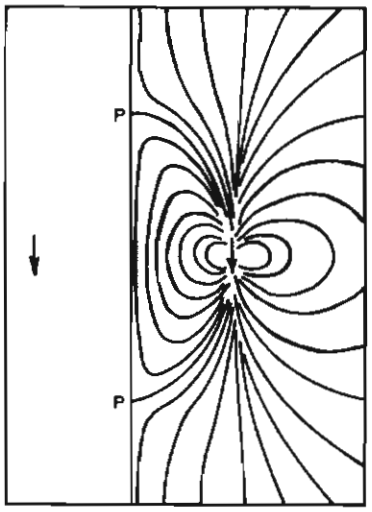


Figure 95. An illustration of the magnetic field of the Earth in the presence of an image dipole. The foci of the induced currents are shown as the points P. (*Chapman and Bartels 1940*)

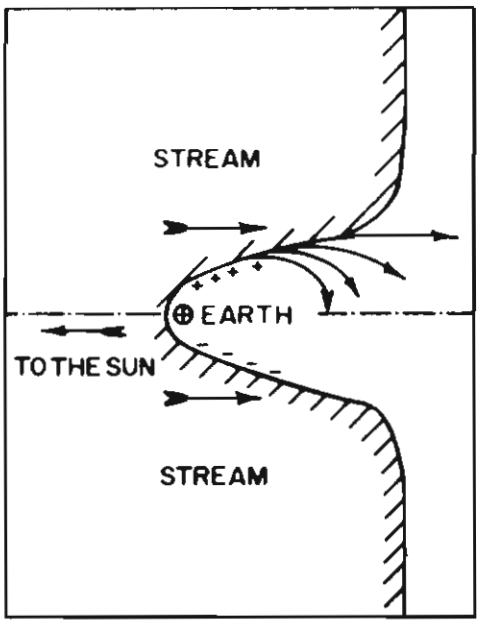


Figure 96. Protons bridging the gap of the cavity behind the Earth. (*Chapman and Bartels 1940*)

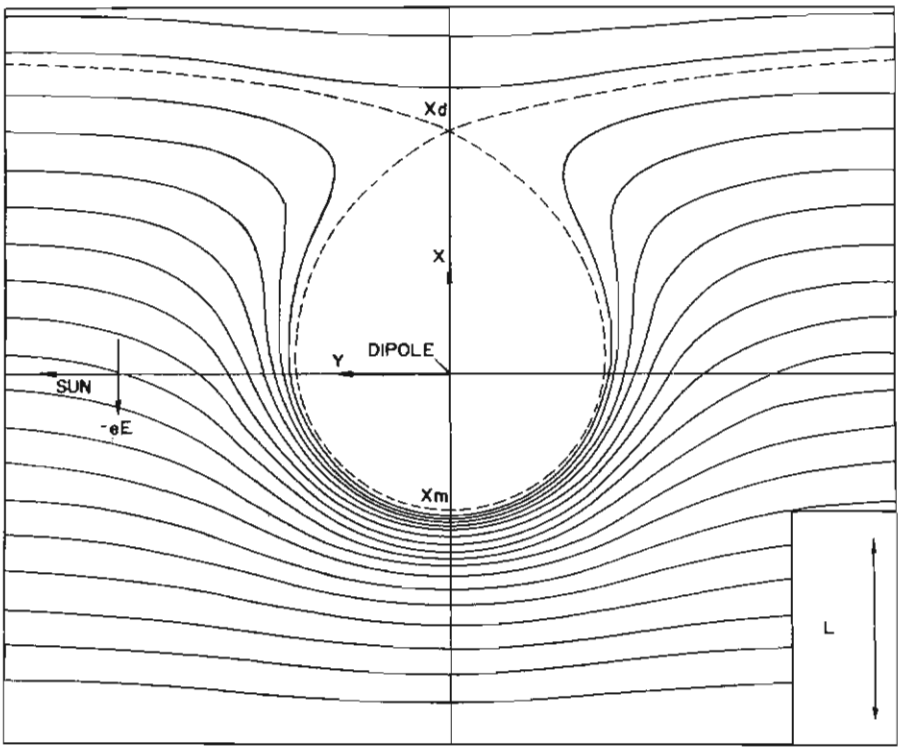


Figure 97. Movement of electrons about a dipole under the influence of an electric field E. (*Alfvén 1958*)

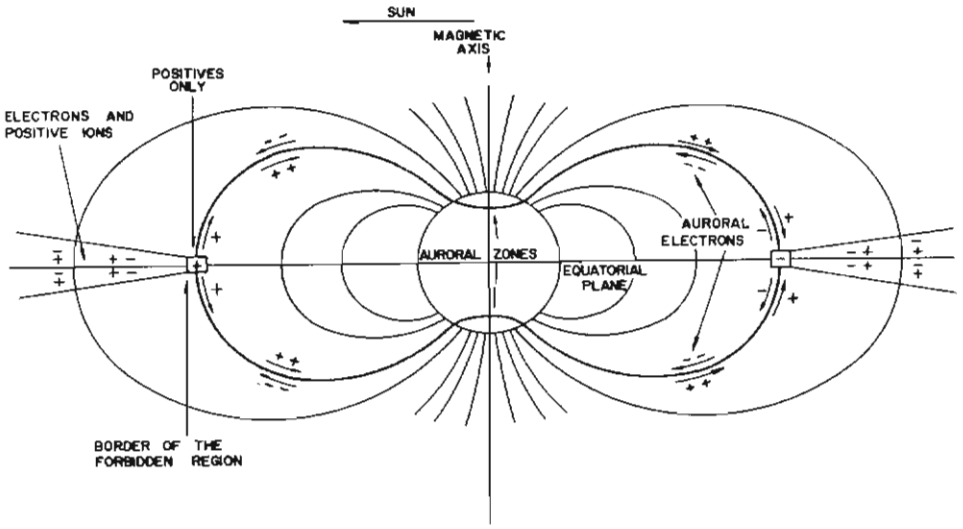


Figure 98. The system of tracing the paths of particles from the boundary of the "forbidden region" down the dipole field lines to the Auroral Zone. (*Alfvén 1958*)

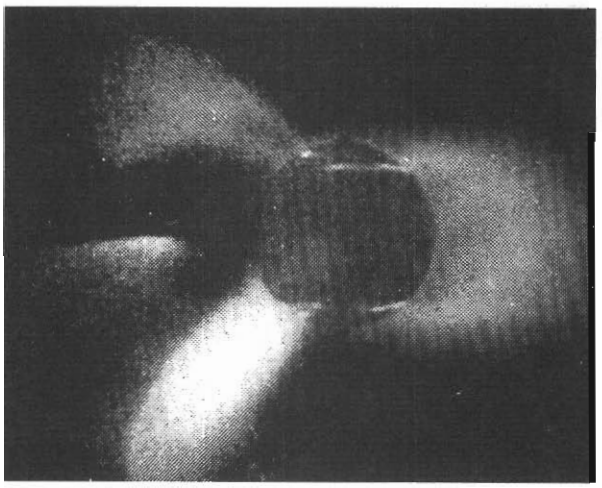

$V_p$ = - 2 kV

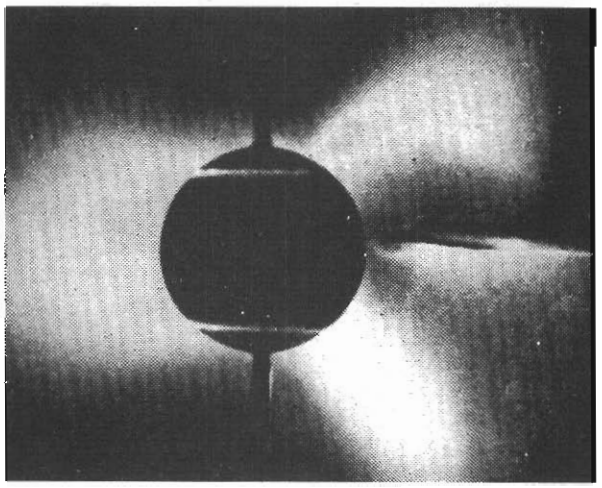

$V_p$ = - 2 kV

Figure 99. Visible discharge. Vp = potential with respect to the terrella of the horizontal plate inserted on the cathode side. Vc = –2kV, Va = +3OV, B = 1090 gauss, pressure 2.5 x $10^{-3}$ mm. Details of one of a group of experiments by Block that, he considered, gave support to Alfvén's electric field theory. (*Block 1955*)

# 14. The solar wind and the magnetosphere

Empedocles, in the Sixth Century BC, assumed matter is composed of four primary substances: earth, water, air and fire. In the twentieth century we now classify matter in terms of the degree of compactness; solids, liquids, gases and plasma. Such is the advance of science! However, we now know of two even less compact conditions of matter, which are found in cosmic rays, so in fact we do make some progress.

The term *plasma* was coined by I. Langmuir. In 1923, he developed the theory of an ionised gas, a mixture of particles with equal numbers of positive and negative charges; he called the medium *plasma*. The continuous streaming of gas (or plasma) out from the Sun would, Biermann (1951, 1952, 1957) pointed out, explain why tails of comets always point away from the Sun. The nearly radial direction of the comet tail indicated corpuscular velocities of at least several hundred km $s^{-1}$.

The effect of a steady-state solar corona would, Chapman (1954) suggested, be felt beyond the Earth. The concept of a continuously expanding solar corona was proposed by Parker (1958). The outward-streaming gas draws out the lines of force of the solar magnetic field. He inferred that in the equatorial plane the general pattern of the magnetic field from the Sun would be similar to the curve produced by a rotating water hose-pipe, as previously found for a particle stream.

By 1969, the Parker concept had been strongly supported by measurements made by instruments carried by satellites. The bulk velocity of the solar wind had been observed to vary between about 275 and 850 km $s^{-1}$, with some high and lower values generally associated with disturbed and quiet geomagnetic conditions. The number of protons in each cubic centimetre varied between 1 and 10, and even up to 100 during disturbed conditions. The magnetic intensity of the solar wind varied from $3\gamma$ to $7\gamma$, but higher values occur. The temperature of the protons lay between about 300 and 800°K, with higher temperatures recorded.

The presence of sectors in the direction of the magnetic field – a sector with the field directed away from the Sun followed by a sector with the field directed towards the Sun – was observed by use of the IMP 1 satellite and reported by Wilcox and Ness (1965). This is illustrated in Figure 100.

Recent space measurements analysed by Smith *et al.* (1976) indicate that the equatorial current sheet of the Sun is rather like the wavy skirt of a spinning ballerina. When the Earth is below the current sheet, the magnetic field points towards the Sun; when the Earth is above the current sheet the magnetic field points away from the Sun. This concept is shown diagrammatically in Figure 101.

Next, consider the interaction of the Earth's magnetic field and the solar wind. This interaction causes a comet-shaped cavity in the solar wind, which is called the *magnetosphere*.

Progress towards the solution of the three-dimensional magnetosphere boundary problem was made using the approximation that the magnetic field at the boundary is proportional to the tangential component of the centred dipole field.

$$H = -\frac{a^3 H_0}{r^3}(\hat{\Theta}\sin\theta + \hat{r}\,2\cos\theta)$$

Where $(r,\theta,\lambda)$ are the coordinates of a point on the magnetospheric surface current sheet, H is the terrestrial magnetic field at the point, a is the radius of the Earth, and $H_0$ at the surface of the Earth has its usual meaning, and $\hat{r}$ and $\hat{\theta}$ are unit vectors in the direction of increasing r and $\theta$ respectively. The latitude $\lambda$ is used later in the calculation.

Ferraro (1952) used this relationship to trace the equatorial boundary and Beard (1960) used it to determine the whole boundary. Unfortunately, this approximation is only applicable to the equatorial plane and the meridional plane, including the magnetic dipole axis and the Sun.

Davis and Beard (1962) and Mead and Beard (1964) obtained differential equations for the solution of the magnetosphere boundary. They equated the equivalent magnetic pressure of the solar wind on the surface of the magnetosphere and the magnetic pressure due to the boundary, with the magnetie pressure due to the axial dipole field.

The theoretical shape of the magnetosphere was solved to a first order approximation by Briggs and Spreiter (1963) and to a higher order by Midgley and Davis (1963) and Mead and Beard (1964). The shape of the magnetosphere boundary is illustrated in Figure 102.

A model of the Earth's magnetic field within the magnetosphere in terms of a spherical harmonic expansion was also developed (*Mead 1964*). The field obtained is illustrated for the simple case (Gilbert) of a dipole co-incident with the Earth's spin axis and compared with the pure dipole field (Figure 103). This method produces neutral points on the solar meridional plane through the axis of the dipole.

Examine the conditions in the solar wind. If one treats the solar wind as a gas of proton particles, then the solar wind is supersonic. If one treats the solar wind as a plasma, then waves of several types can propagate through the plasma. Corresponding to the sound waves in a gas, there are Alfvén waves in a plasma; corresponding to sonic velocity there is an Alfvénic velocity. The solar wind in the first sense is supersonic, and in the second sense super-Alfvénic.

When an aircraft flies at supersonic speed a shock wave forms ahead of the nose and wings of the aircraft. The same effect is achieved experimentally by positioning a model of an aircraft fuselage in a wind tunnel and causing a supersonic wind to flow past the model. This is, in effect, what happens with the magnetosphere.

A mathematical solution for the flow of the solar wind around the magnetosphere, which produces a shock front, was initially developed by Inouye and Lomax (1962); they used the *method of characteristics*. The method, which treats the problem as one in gas dynamics, requires an axi-symmetric solution for the magnetosphere boundary. Near the nose of the magnetosphere, the gas flow is subsonic, so in this region an inverse iteration method was used. The shape of the bow shock-wave and the free-stream conditions were taken as known, and the shape of the magnetosphere was found.

The surface given by rotating the trace of the equatorial boundary found by Spreiter and Briggs (1962) was used by Spreiter *et al.* (1968) as the axi-symmetric shape of the magnetosphere. They found the pattern of stream-lines as indicated in Figure 104, where $M_\infty$ is the free-stream Mach number and $\gamma$ is the ratio of specific heats.

The shape of the magnetosphere and the shape of the bow wave were confirmed by experiments carried by satellite IMP 1 and analysed by Ness *et al.* (1964). In Figure 105 the experimental results are compared with the calculated locations of the shock wave and the boundary of the magnetosphere, or magnetopause, the latter based on the Spreiter and Jones (1963) model.

One of the best examples of the fit of experimental data is that given by Spreiter *et al.* (1968) to the data from IMP 1 Orbit 17 reported by Wolfe *et al.* (1966) (Figure 106).

The theory and experiment briefly outlined above give a reasonable picture of the nose of the magnetosphere for an axial dipole model of the Earth's magnetic field.

An early concept of the magnetic field in the tail of the magnetosphere was presented by Dungey (1961), with the alternative concepts of an open or closed magnetosphere, depending on whether the magnetic field of the solar wind has a South-pointing (open) or North-pointing (closed) component. Schematic diagrams are presented in Figure 107.

A mechanism by which a long magnetic tail would be formed was proposed by Piddington (1960). He suggested that the solar plasma that passes around the Earth would become embedded in the outer strands of the Earth's magnetic field on the night side. The plasma would have the tailwards momentum to carry with it part of the Earth's magnetic field. The resultant situation is shown in Figure 108.

In the equatorial plane the lines of force $L_1$ in the region A are carried away from the Earth to form the lines $L_1'$. This results in a reduction of magnetic pressure on the inner field, with the result that lines $L_2$ and $L_3$ move to positions $L_2'$ and $L_3'$.

In the region B, the magnetic field lines connecting to the North Polar Cap have a magnetic field directed towards the Earth. In the region C, the field lines connecting to the South Polar Cap have a magnetic field directed away from the Earth.

An alternative approach was taken by Taylor and Hones (1965). They examined the concept of an image dipole, following Chapman and Ferraro (1932), and also an infinite current sheet of finite thickness to simulate the tail. They produced the model shown in Figure 109.

In this model the image dipole $\mu_I$ was assigned a value 28 times as strong as the Earth's axial dipole $\mu_E$ and was placed at a distance 40 $R_E$ towards the Sun. The field of the current sheet was taken to be 30$\gamma$. Using this model and the laws of adiabatic motion of charged particles in this magnetic field, Taylor and Hones showed that solar wind particles of energy less than 1 KeV would reach energies of 1-40 KeV within the magnetosphere. These higher-energy particles, which are still low-energy particles in the overall particle spectrum, would be precipitated in a narrow latitudinal belt, with electrons closer to the geographic pole than protons.

Satellite data was used to construct a diagram of the magnetosphere (Figure 110) (*Ness 1969*). The best fit ellipse and hyperbola for the magnetopause and the bow shock respectively were determined from several hundred positions observed by six IMP spacecraft (Fairfield 1971). The results are illustrated in Figure 111. The ellipse representing the best fit to the points terminates at $X = -15\ R_E$ (Earth radius). The circles representing the tail boundary crossings reported by Mihalov *et al.* (1970) were rotated through 4° and plotted in the diagram, but were not used to determine the ellipse. The magnetopause tail boundaries from the point $X = -15\ R_E$ through the Mihalov points are straight lines. The dashed line in the diagram refers to Olson (1969), in which he considered the case of the tilted dipole. It can be seen from Figure 111 that the experimental results of Mihalov *et al.* (1970) indicate a greater flaring of the tail than had been found closer to the Earth.

An early theoretical attempt to model the magnetosphere with a representation of the tail magnetic field was that by Williams and Mead (1965). This simple, two-dimensional model, is useful for obtaining rough estimates quickly; it is shown in Figure 112. The Williams and Mead model was obtained by adding a tail field to the Mead (1964) model. This tail field consists of a semi-infinite current sheet in the equatorial plane, with the current flowing counter to the Earth's orbital velocity vector. The near-Earth commencement of the sheet is at 10 $R_E$; the sheet ends at 40 $R_E$. The current sheet perpendicular to the Sun–Earth axis is infinite in extent. It has a current that gives a magnetic field of 40 $\gamma$ adjacent to the sheet.

Magnetic variations observed by satellite magnetometers near the Earth's equator can be explained by the concept of an equatorial ring current in a belt girding the Earth above the ionosphere. The ring current was usually represented by a line or by a current of toroidal form, until Sugiura and Poros (1973) published a three-dimensional model incorporating the equatorial ring current and tail current.

The basic concept behind this model was proposed by Sugiura *et al.* (1971). They had found the difference $\Delta\mathbf{B}$ between the magnetic field determined from magnetometers on board satellites OGQ 3 and OGO 5 and the time-related International Geomagnetic Reference Field

(IGRF). Their data was presented in the form of contours of $\Delta\mathbf{B}$ for magnetic disturbance conditions Kp = 0–1 and Kp = 2–3. The Kp = 0–1 data are reproduced in Figures 113 and 114.

In their 1973 paper, Sugiura and Poros represented the ring current evident in the two figures by an equatorial current sheet, rather than the more usual linear or toroidal current. In addition, the current in the neutral sheet is shown flowing along circular arcs concentric with the Earth, so that the circular sheet current representing the ring current continues into the tail current without any geometric discontinuity. The return current from the neutral sheet flows around the magnetopause surface. Pictorial views of the tail current for the model are given in Figure 118.

In the Sugiura–Poros model, the dipole and magnetopause currents for the nose are represented by the Mead (1964) model. Consequently the Sugiura–Poros model is self-consistent only insofar as the dipole field is concerned; it is not self-consistent with the combined field of the dipole, tail current and ring current. Nevertheless, as indicated in Figures 116 and 117, the model reproduces many of the features of the $\Delta\mathbf{B}$ contours previously observed. For comparison with other models, the field lines for this model are presented in Figure 121.

A tail field model was presented by Halderson *et al.* (1975) as a correction to the work of Choe and Beard (1974a,b) and Choe *et al.* (1973). It is illustrated in Figure 119. The resultant meridian plane magnetic field model for zero tilt is shown in Figure 120.

The theoretical models at present available give reasonable comparisons with magnetometer data collected by satellites. Four IMP satellites provided data from which Mead and Fairfield (1975) derived a quantitative model of the magnetospheric field by a least-squares fit method. The data were divided into four sets, based on the range of Kp values. They were then fitted to a power series expansion in terms of solar magnetic co-ordinates and solar wind–dipole tilt angle. In this model the average northwards component of the external magnetic field is smaller than that predicted by theoretical models. An example of the magnetic field obtained is presented in Figure 121. For further details of the model, the reader is referred to the original paper.

Having examined the magnetic field of the magnetosphere, the stage is set to turn in the next chapter to the subject of plasma in the magnetosphere.

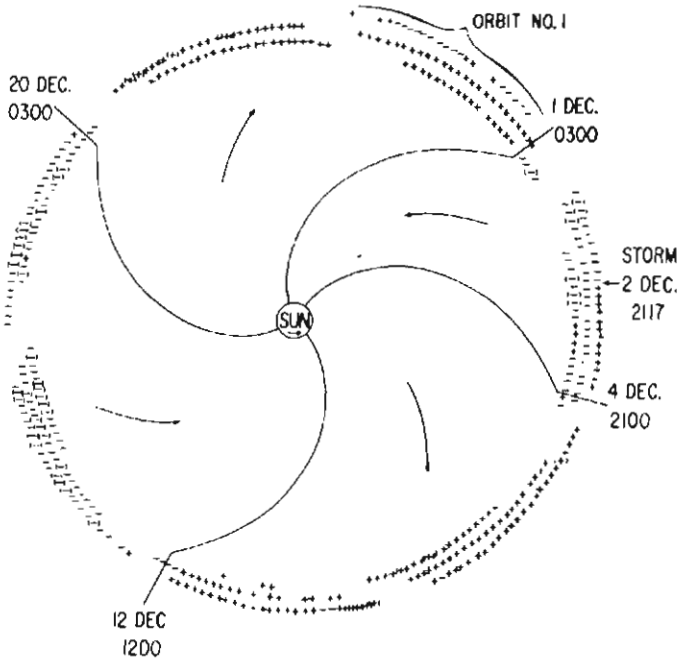


Figure 100. The signs, forming the circumference of the figure, plus (away from the Sun) and minus (towards the Sun), show the direction of the measured interplanetary field during successive 3-hourly intervals. The inner portion of the figure indicates the sector structure. (*Wilcox and Ness 1965*)

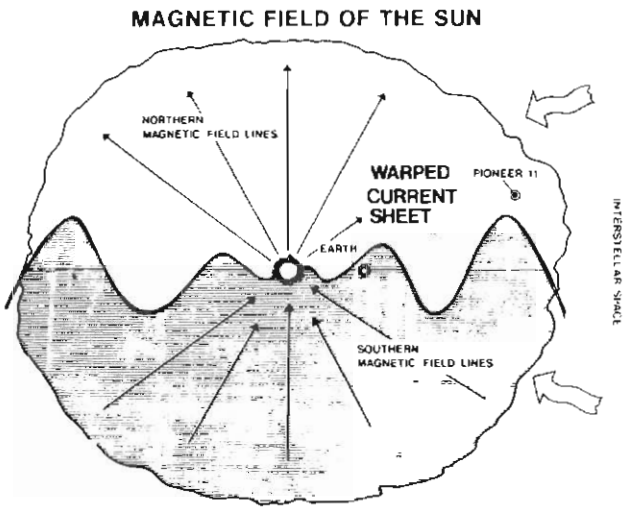


Figure 101. Current sheath in the equatorial plane derived from space measurements. When the current sheath waves up and down like the skirt of a ballerina, the interplanetary magnetic field changes sign. (*Smith et al. 1976*)

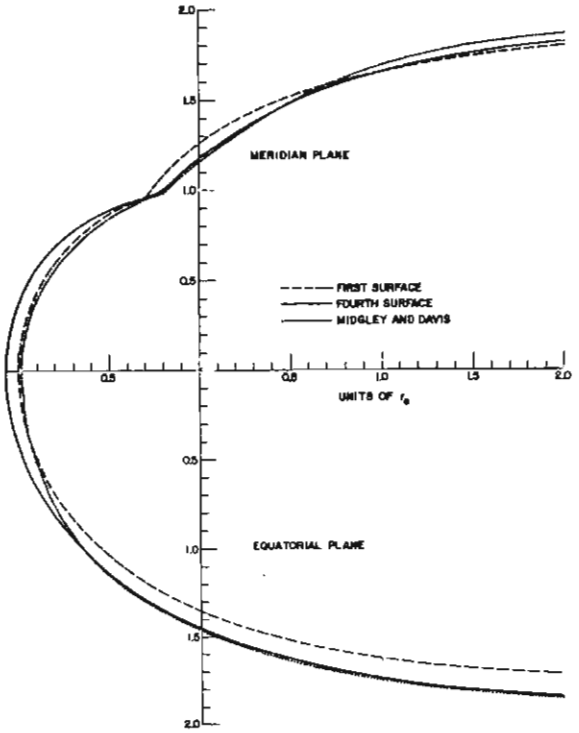


Figure 102. Comparison of the Mead and Beard (1964) first-approximation surface, the fourth-approximation surface, and the surface obtained by Midgley and Davis (1963), in the meridian and equatorial planes.

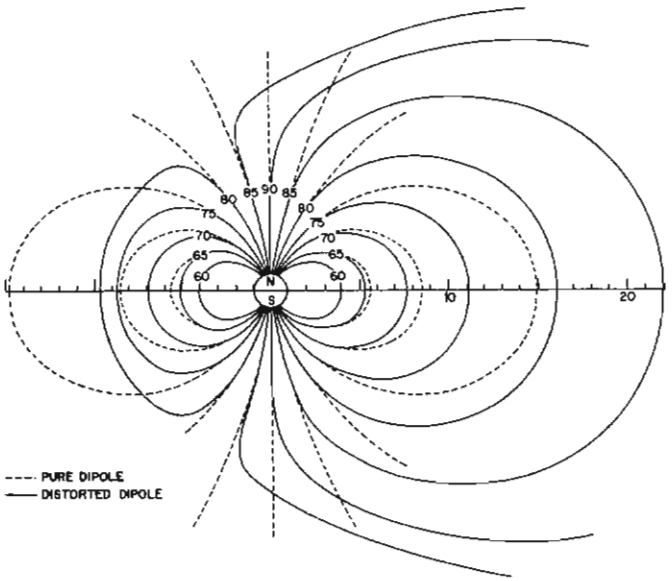


Figure 103. Field-line configuration in the noon-midnight meridian plane due to Mead (1964). With $r_b = 10$ Earth radii, the critical latitude is about 83°. The dipole lines are compressed on both the daytime and night-time sides.

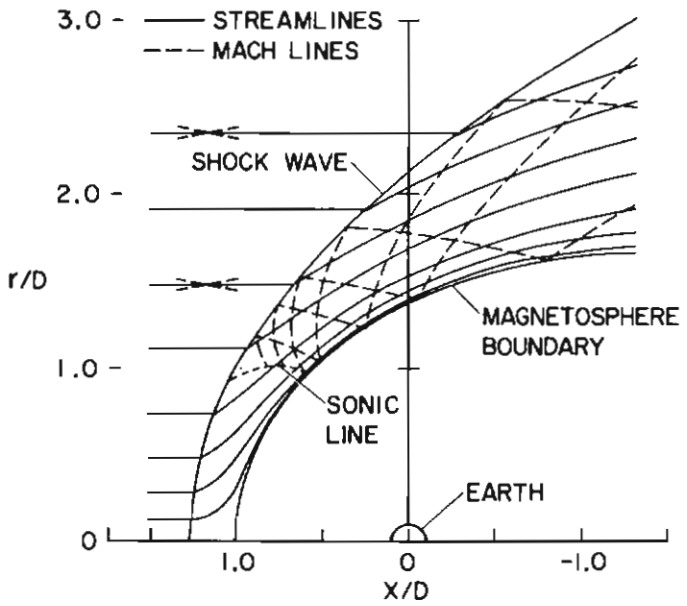


Figure 104. Stream lines and wave patterns for supersonic flow past the magnetosphere when $M_\infty = 8$ and $\gamma = \frac{5}{3}$. *(Spreiter et al. 1968)*

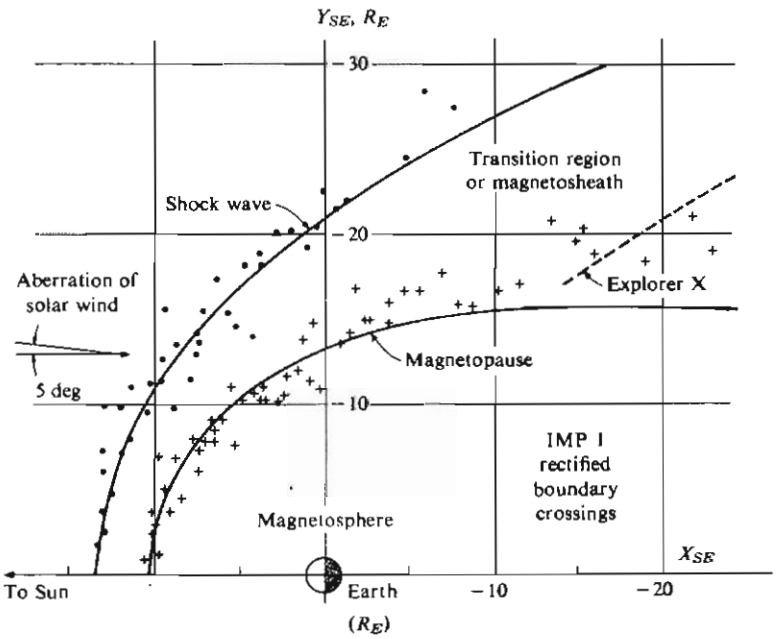


Figure 105. Location of the shock wave and magnetopause boundary crossings measured on IMP 1. A dotted line is earlier data on the magnetopause location from Explorer 10. The solid curves are the calculated locations of the shock wave and magnetopause, after Spreiter and Jones (1963), with the stand-off ratio adjusted to match the observed measurements. *(Ness et al. 1964)*

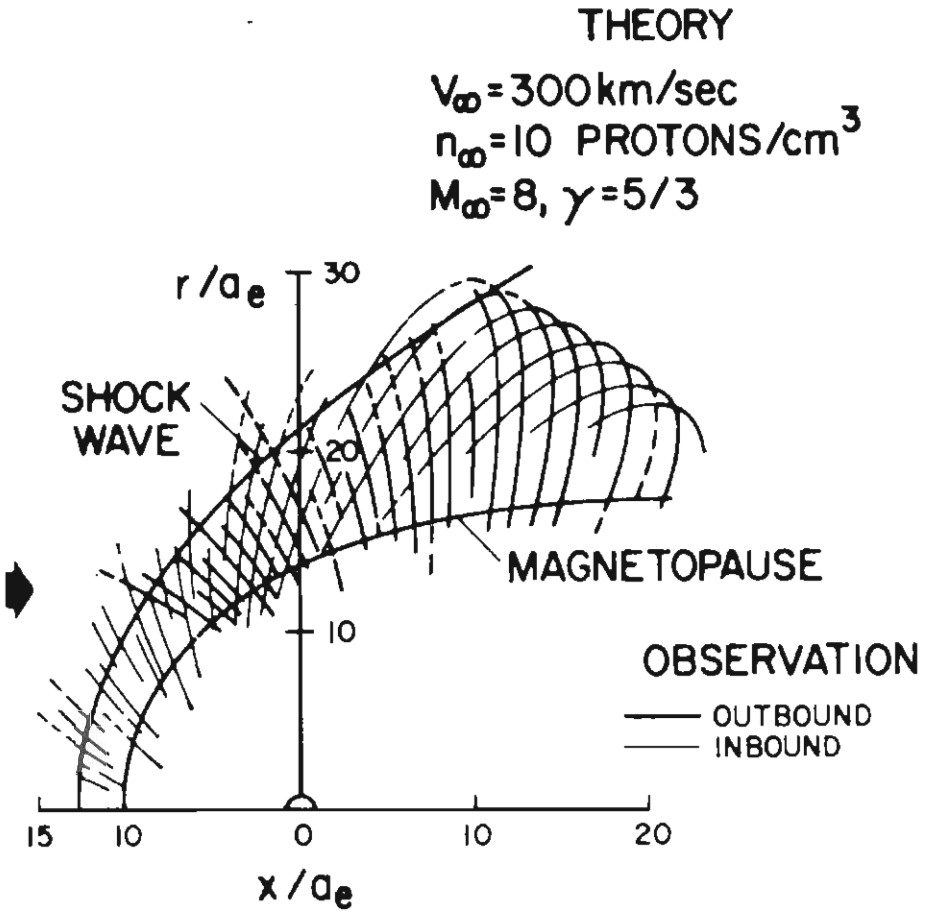


Figure 106. IMP 1 plasma probe measurements of the shock wave and magnetosphere boundary-crossing positions. The theoretical shock wave and magnetopause were calculated from the values of the solar wind velocity $(V_\infty)$ and proton density $(n_\infty)$, which are shown. (*Spreiter et al. 1968*)

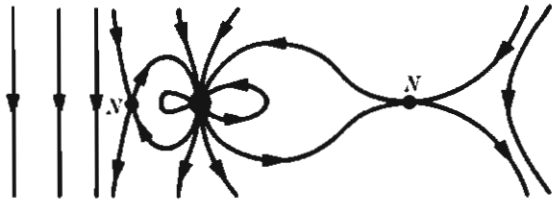


(a) 'Open' configuration

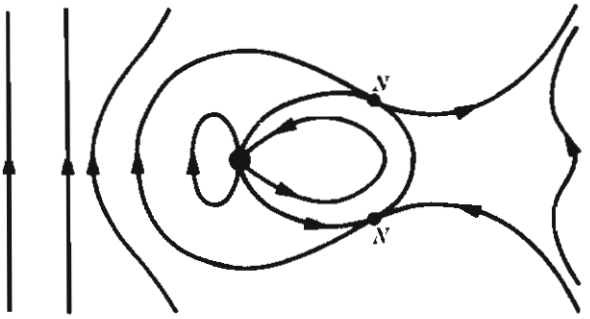


(b) 'Closed' configuration

Figure 107. Dungey's "open" (a) and "closed" (b) model magnetospheres. The neutral points are denoted by the letter N. *(Dungey 1963)*

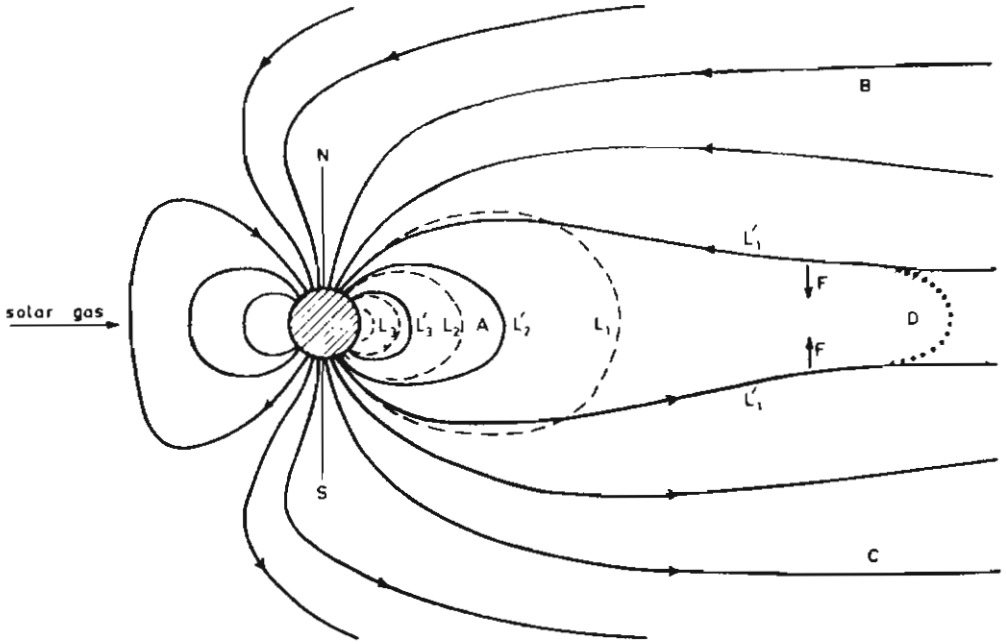


Figure 108. Piddington's (1960) diagram of a magnetosphere with a magnetic tail extended in the anti-solar direction.

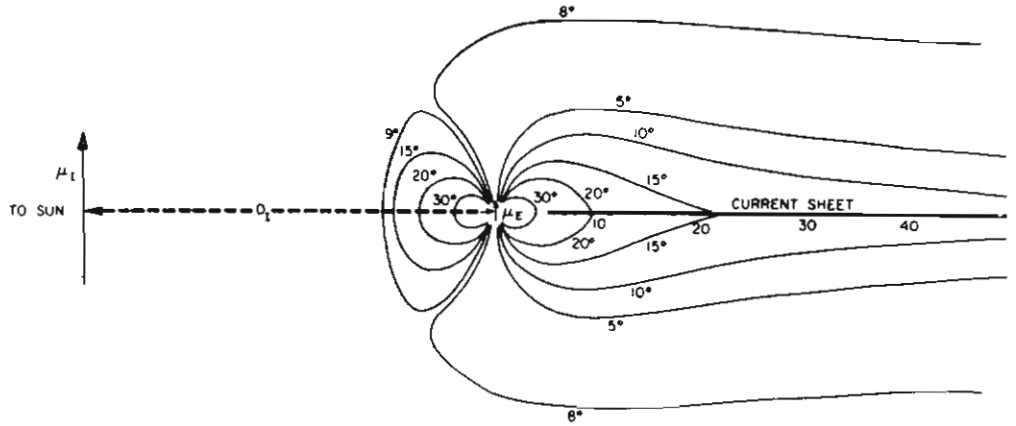


Figure 109. The cross–section of the model used for the magnetic field in the noon–midnight plane. The strength of the image dipole moment $\mu_I$, its distance $(D_I)$ from the dipole of the Earth $(\mu_E)$, and the strength of the magnetic field caused by the current sheet were the parameters varied to fit magnetometer measurements of the real field. Numbers along the anti-solar axis are radial distances in Earth radii. (*Taylor and Hones 1965*)

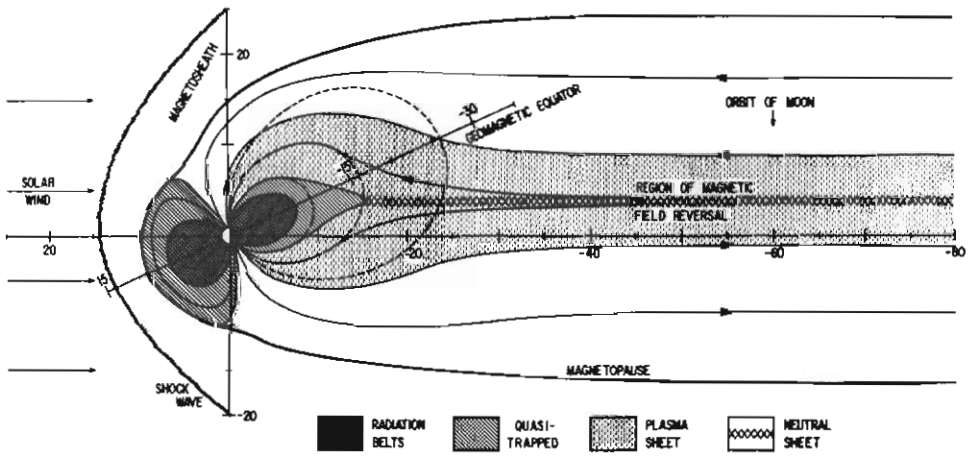


Figure 110. A summary view of the magnetosphere and the geomagnetic tail, as deduced from spacecraft measurements. (*Ness 1969*)

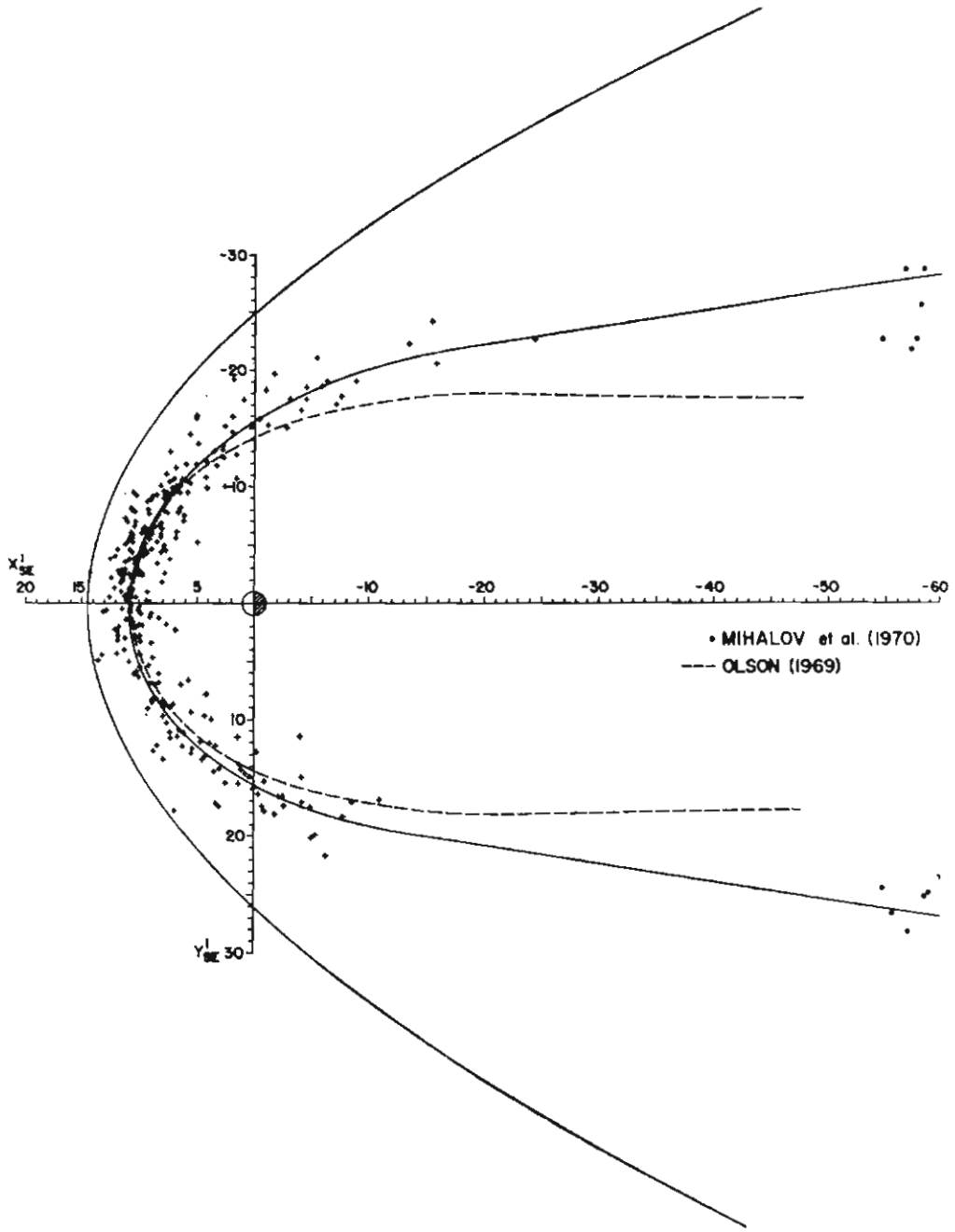


Figure 111. Position of the magnetopause in the solar ecliptic plane, as determined by measurements on six IMP spacecraft, 1963–68. Crosses represent the average location on individual passes, and the solid-line ellipse represents the best-fit curve to the points $|Z_{SE}| < 7R_E$. Points have been rotated by 4° to remove the effects of aberration due to the Earth's motion about the Sun. A solid line has been joined to the ellipse at X = −15 to represent the boundary of the tail. (*Fairfield 1971*)

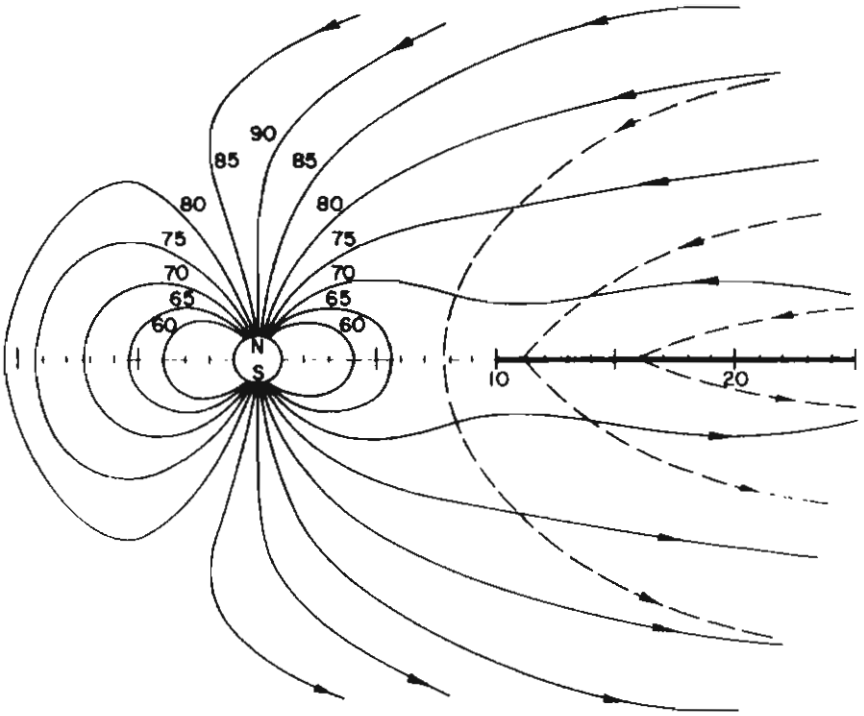


Figure 112. Solid lines show the field lines in the noon–midnight meridian plane obtained by adding a current sheet in the tail of Mead's (1964) model. Dashed lines show the field-line configuration of the field due to the current sheet alone. The latitudes shown are those at which field lines intersect the surface of the Earth. This configuration fits the experimental observations of trapped electron latitude shifts. (*Williams and Mead* 1965)

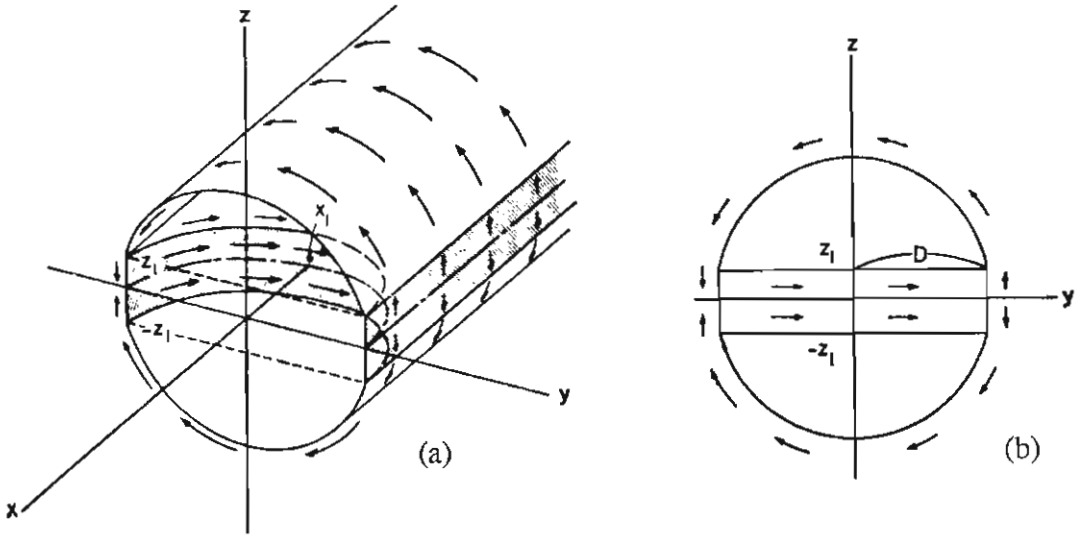


Figure 115. The tail current system. (a) Schematic view of the tail current; (b) view toward the -x axis. (*Sugiura and Poros 1973*)

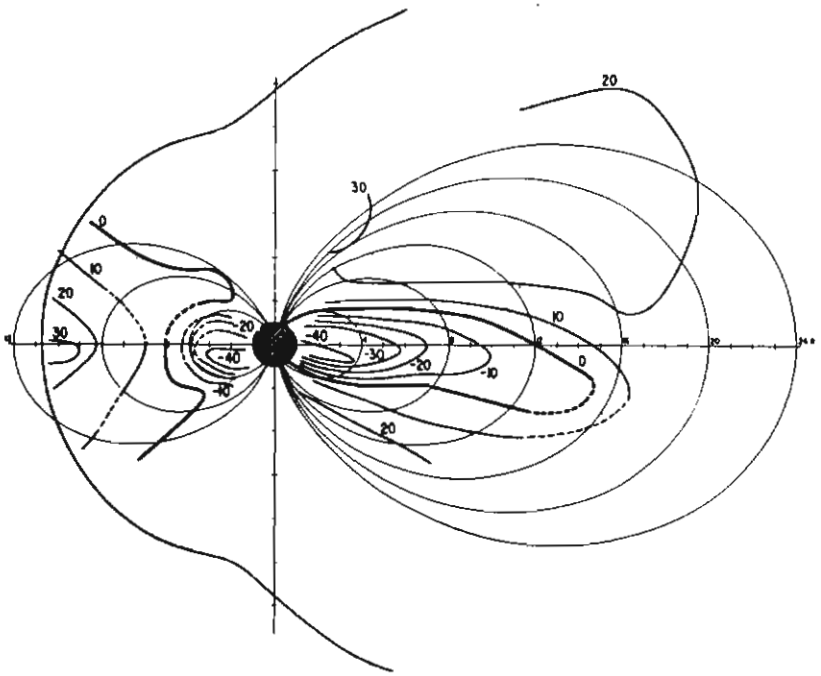


Figure 113. Contours of equal **ΔB** in the geomagnetic noon–midnight meridian plane for a quiet condition, Kp = 0–1; units: gammas. (*Sugiura et al. 1971*)

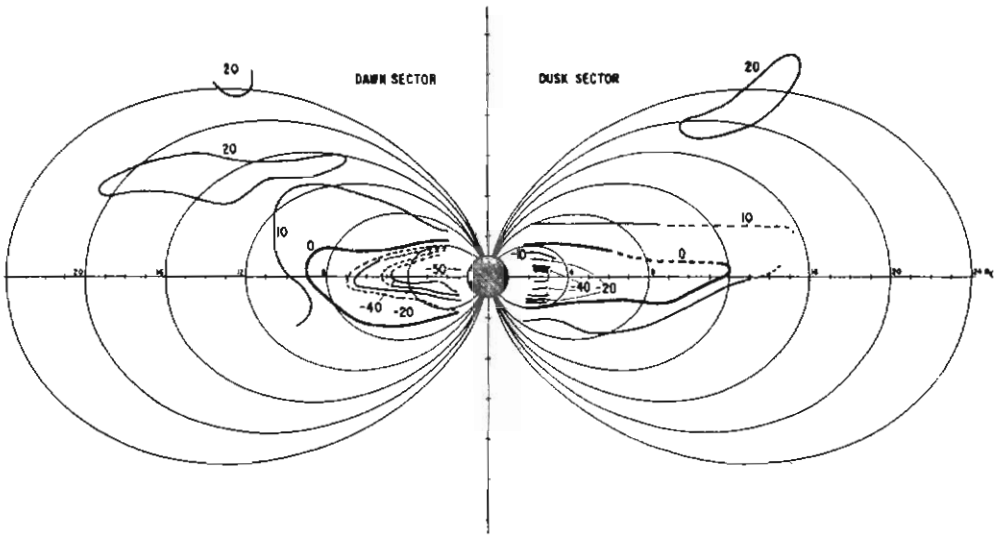


Figure 114. Contours of equal **ΔB** in the geomagnetic dawn—dusk meridian plane for a quiet condition, Kp = 0–1. (*Sugiura et al. 1971*)

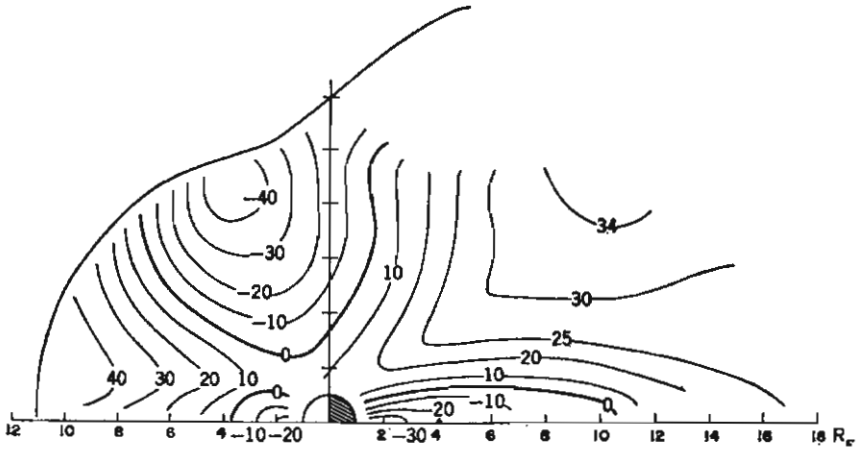


Figure 116. **ΔB** contours in the noon–midnight meridian derived from the Sugiura–Poros (1973) model. (*Sugiura and Poros 1973*)

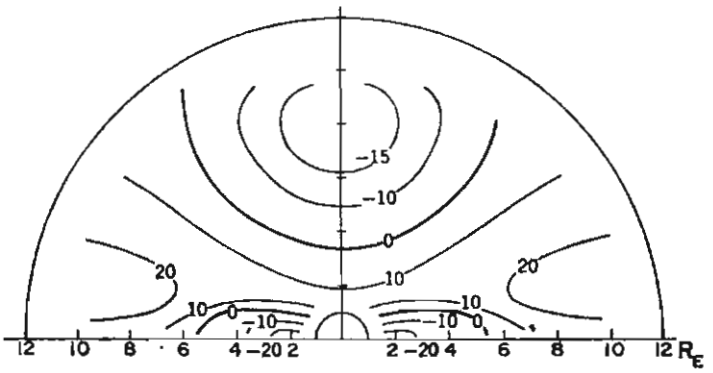


Figure 117. **ΔB** contours in the dawn-dusk meridian derived from the Sugiura–Poros (1973) model. (*Sugiura and Poros 1973*)

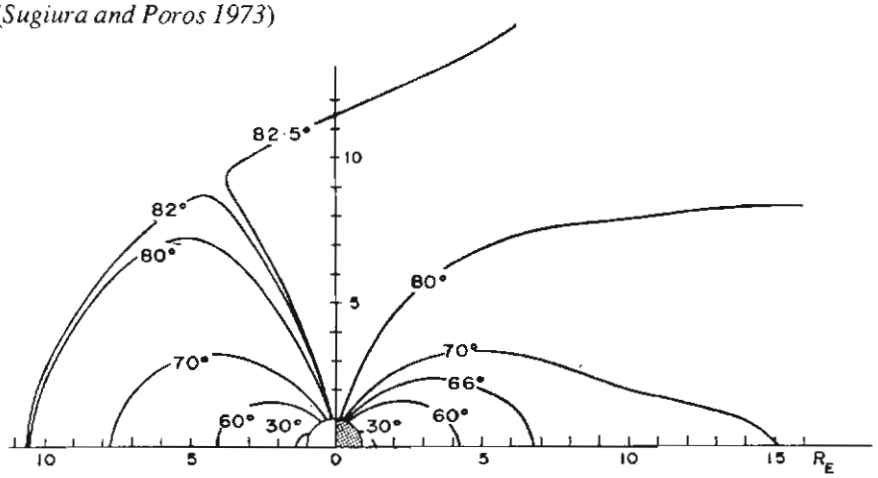


Figure 118. Field lines for the Sugiura–Poros (1973) model in the noon-midnight meridian plane. Field lines are labelled by the dipole latitudes at which they leave the Earth's surface. (*Sugiura and Poros 1973*)

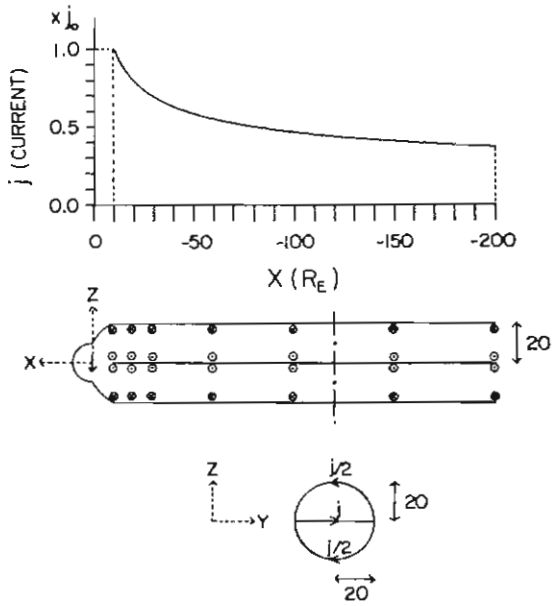


Figure 119. An illustration of the coordinates and tail current system used in the calculation of Halderson *et al.*'s (1975) tail field model.

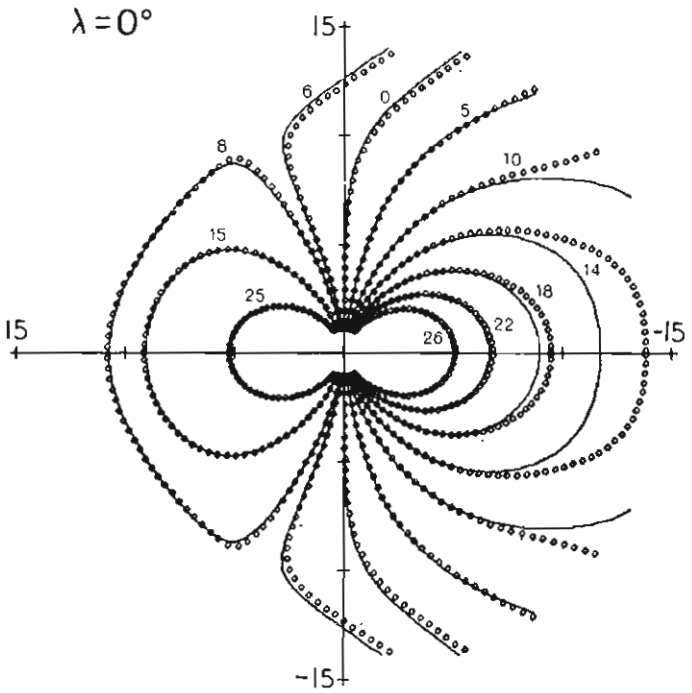


Figure 120. Meridian plane magnetic field configuration at $\gamma = 0°$ contrasting the magnetic contributions of the surface plus dipole field (solid line) with those of the surface current plus dipole field plus tail current (circles). (*Halderson et al. 1975*)

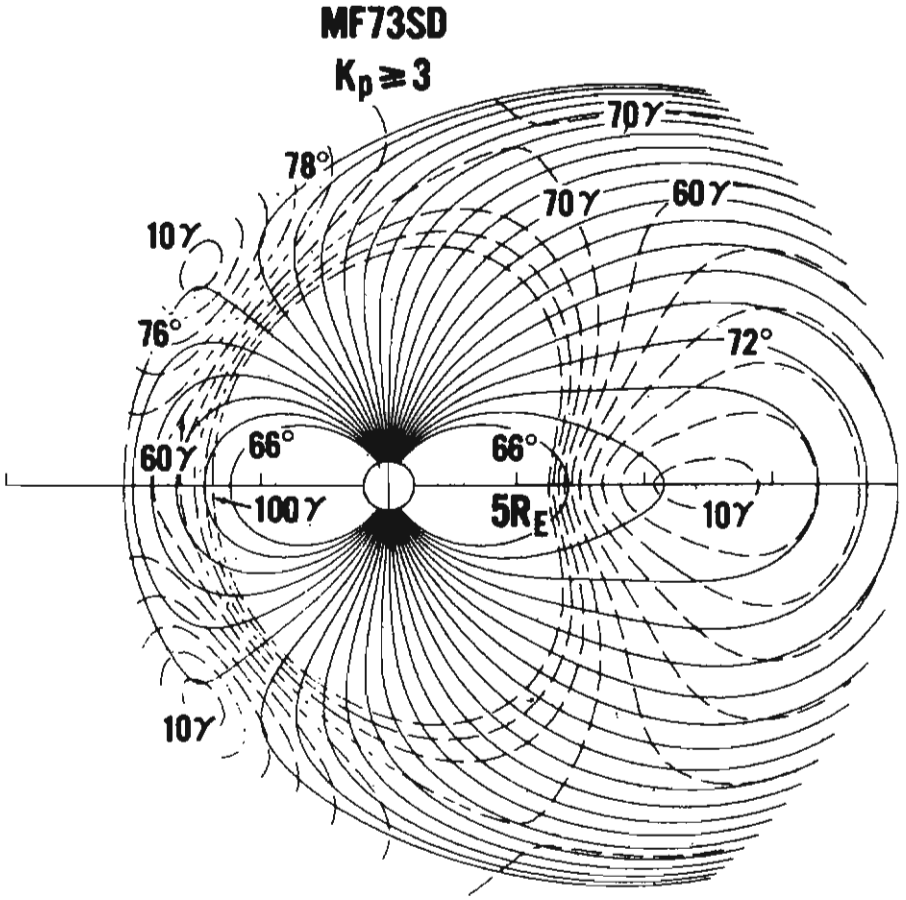


Figure 121. Field lines (solid lines) and contours of total field magnitude (dashed lines) in the noon–midnight meridian for tilt angle T = 0. Field lines are plotted every 2° in latitude, beginning with 66°. Contours are given every 10 γ from 10 to 100 γ. North–south symmetry is built into the model. Field lines are terminated beyond 20 $R_E$. (*Mead and Fairfield 1975*)

# 15. Plasma in the magnetosphere

In the spring of 1958 the Geiger counters on board artificial satellite Explorer 1 at first gave counts of the order of magnitude expected, but as the satellite ventured further into space the unexpectedly high density of particles jammed the counting mechanism. This discovery of the radiation belts by James A. Van Allen of the USA and, simultaneously, by S.N. Vernov of the USSR, mark the modern era of the understanding of particle populations within the Earth's magnetic field.

As later exploration satellites extended this knowledge, the first pictures of an inner and an outer radiation belt were built up, as illustrated in Figure 122.

The present picture is rather of one large radiation belt with considerable variation in the location of protons and electrons of different energy within the belt. A set of schematic representations (Figure 123) Van Allen gave in a tutorial lecture (*Van Allen 1968*) perhaps presents the information most succinctly.

Besides the radiation belts, particles that comprise a plasma sheet in the region of the magnetic neutral sheet have also been found. The electrons and protons in the plasma sheet have energies up to several hundred keV (kilo-electron-Volts). Vasyliunas' (1968) description of the near-Earth plasma is depicted diagrammatically in Figures 124 and 125. His interpretation of the behaviour of the near-Earth plasma sheet during magnetic bays is illustrated in Figure 126.

Edward W. Hones Jnr and his associates at the University of California used the information obtained from the set of Vela satellites at about 18 $R_E$ and satellites orbiting the moon at about 60 $R_E$ to show that there is a sheet of plasma both north and south of the magnetic neutral sheet. They also described the behaviour of the plasma, which is associated with the substorm behaviour of the aurora, but this we shall discuss in the next chapter.

From the data gathered by IMP 5 Frank (1971) concluded that there is a plasma polar cusp on the noon meridian from the region above the day-side aurora to the region of the high-latitude magnetic neutral point found in several models of the magnetosphere boundary. This information is shown pictorially in Figure 127, with a "road map" of the various plasma regions encountered in Figure 128.

A band of magnetosheath plasma ~50 km, or a few tenths of a degree wide, was identified as the low-altitude indication of the magnetic neutral point. Since this band, or signature of the neutral point, was observed at a large range of local times, or longitudes, above the sunlit auroral oval, Frank suggested that the "neutral point" was in fact a "neutral line" as Piddington (1965) had proposed.

However, evidence against the concept of a neutral line is to be found in more recent analyses of the magnetic field in high latitudes. Away from the noon meridian plane there appears to be no sharp distinction between field lines that close on the day side and those that go back over the polar cap. Data from two Heos satellites supported this proposition (Fairfield 1977) as shown in Figures 129 and 130.

Recent experiments indicate that the magnetopause comprises a layer of denser plasma with a low density tail plasma between the magnetopause and the plasma sheet in the tail.

After this brief description of plasma in the magnetosphere, the next chapter turns to the behaviour in the solar wind and the magnetosphere which lead to the production of the aurora and the auroral substorm.

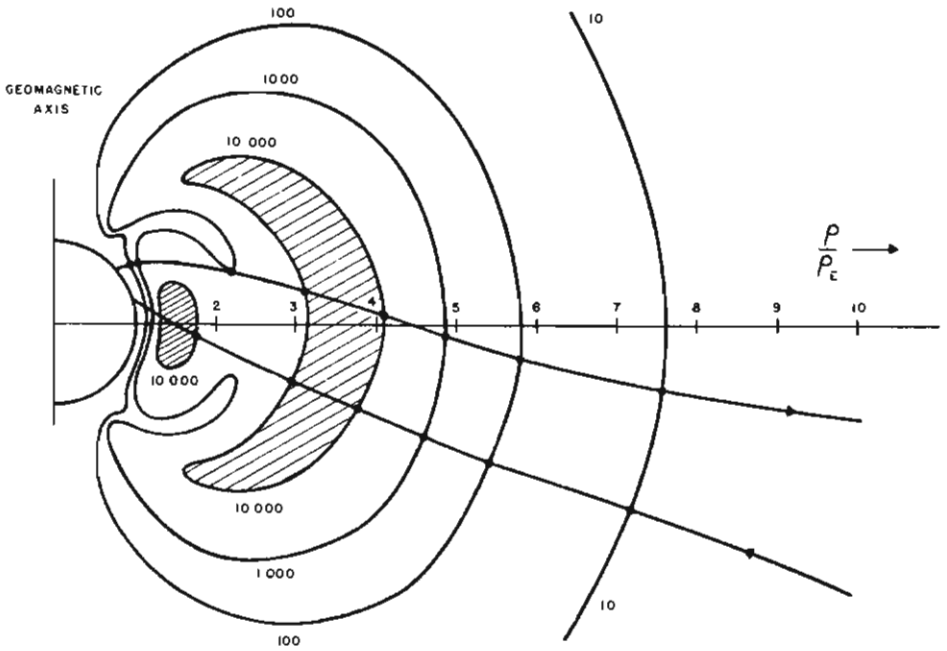


Figure 122. Early representation of the natural particle distributions. The trajectory shown is that of Pioneer 3, and data from it and Explorer 4 were used to construct the intensity contours. (*Van Allen 1968*)

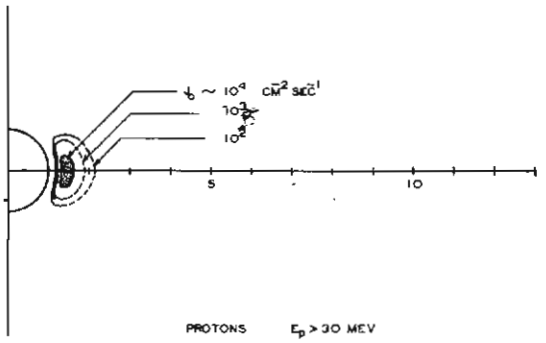


Figure 123a. Schematic representation of the high-energy proton component in the radiation belts.

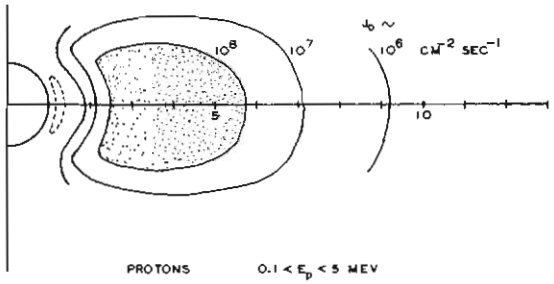


Figure 123b. Schematic representation of the proton component in the energy range 0.1–5.0 MeV.

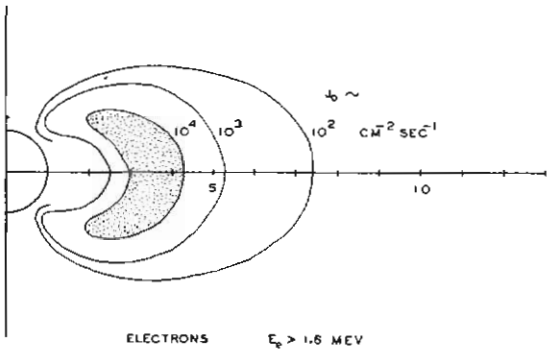


Figure 123c. Schematic representation of the high-energy electron component in the radiation belts.

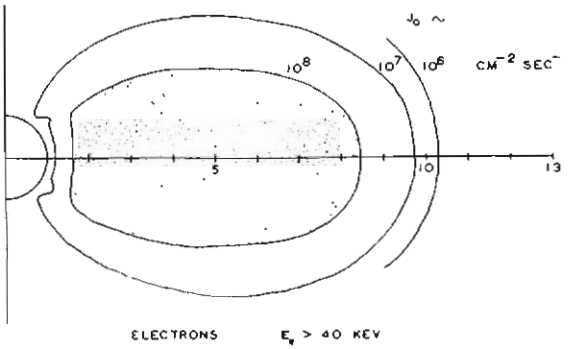


Figure 123d. Schematic representation of the electron distribution in the radiation belts. (*Van Allen 1968*)

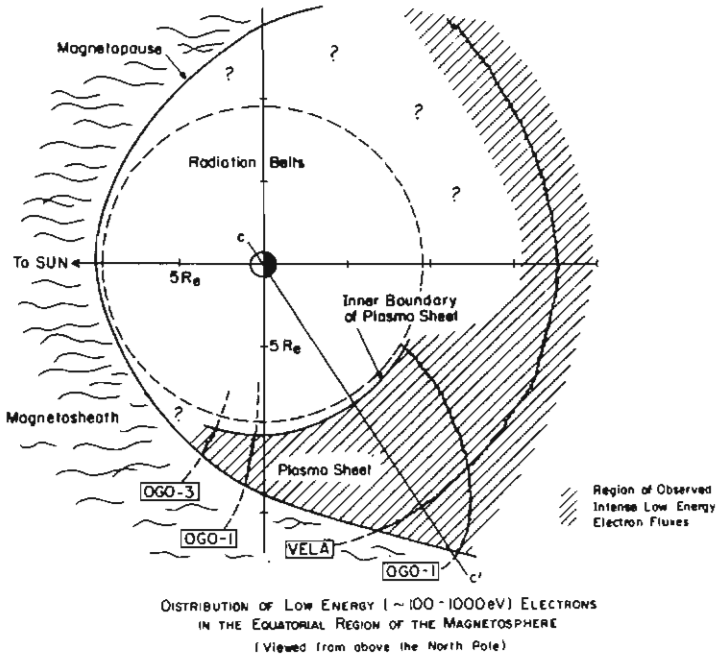


Figure 124. Equatorial cut of the magnetosphere, showing the principal features of the low-energy electron population as established by various satellites. (*Vasyliunas 1968*)

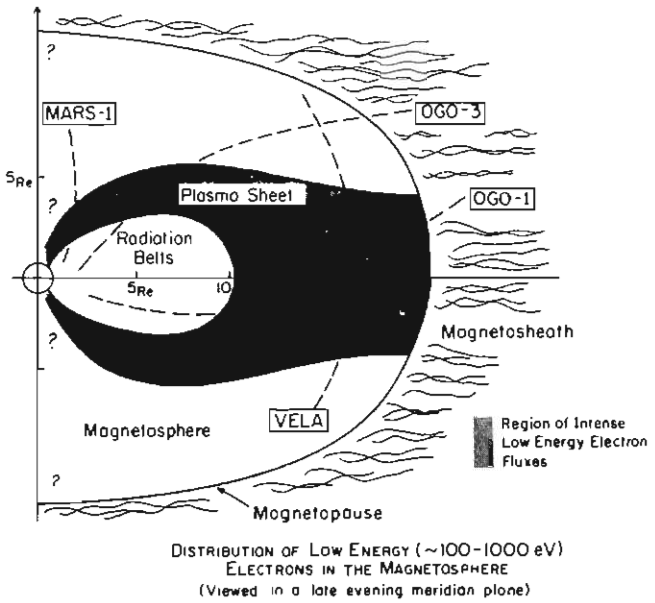


Figure 125. Meridian cut of the magnetosphere, along the line CC' of Figure 124. (*Vasyliunas 1968*)

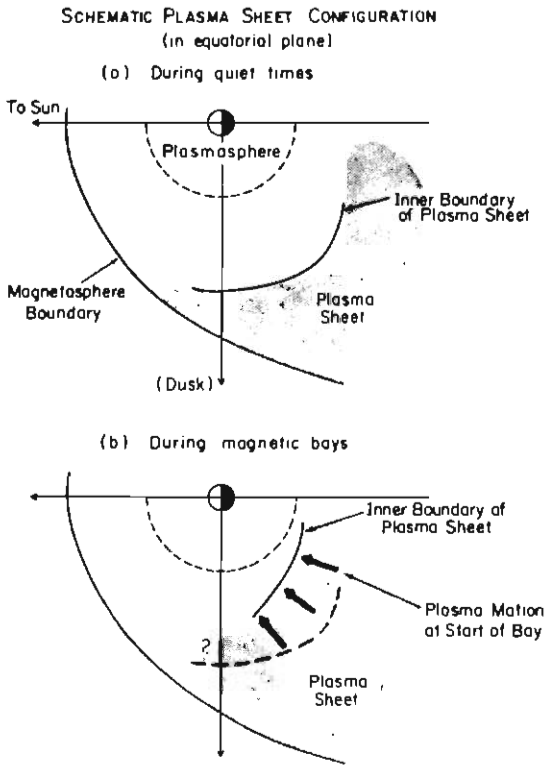


Figure 126. Sketch of changes in the spatial distribution of low-energy electrons during magnetic bays. (*Vasyliunas 1968*)

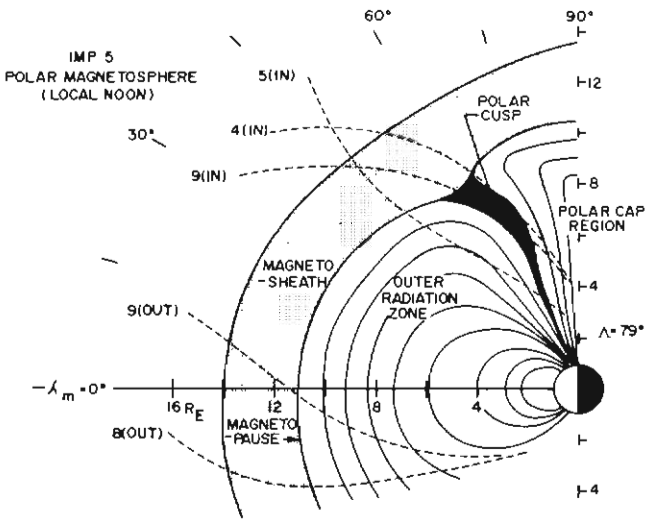


Figure 127. A diagram showing the magnetospheric polar cusp in the noon meridional plane during quiet magnetic conditions. The cusp intersects the auroral oval at $\Lambda \simeq 79°$. The satellite trajectories are indicated. (*Frank 1971*)

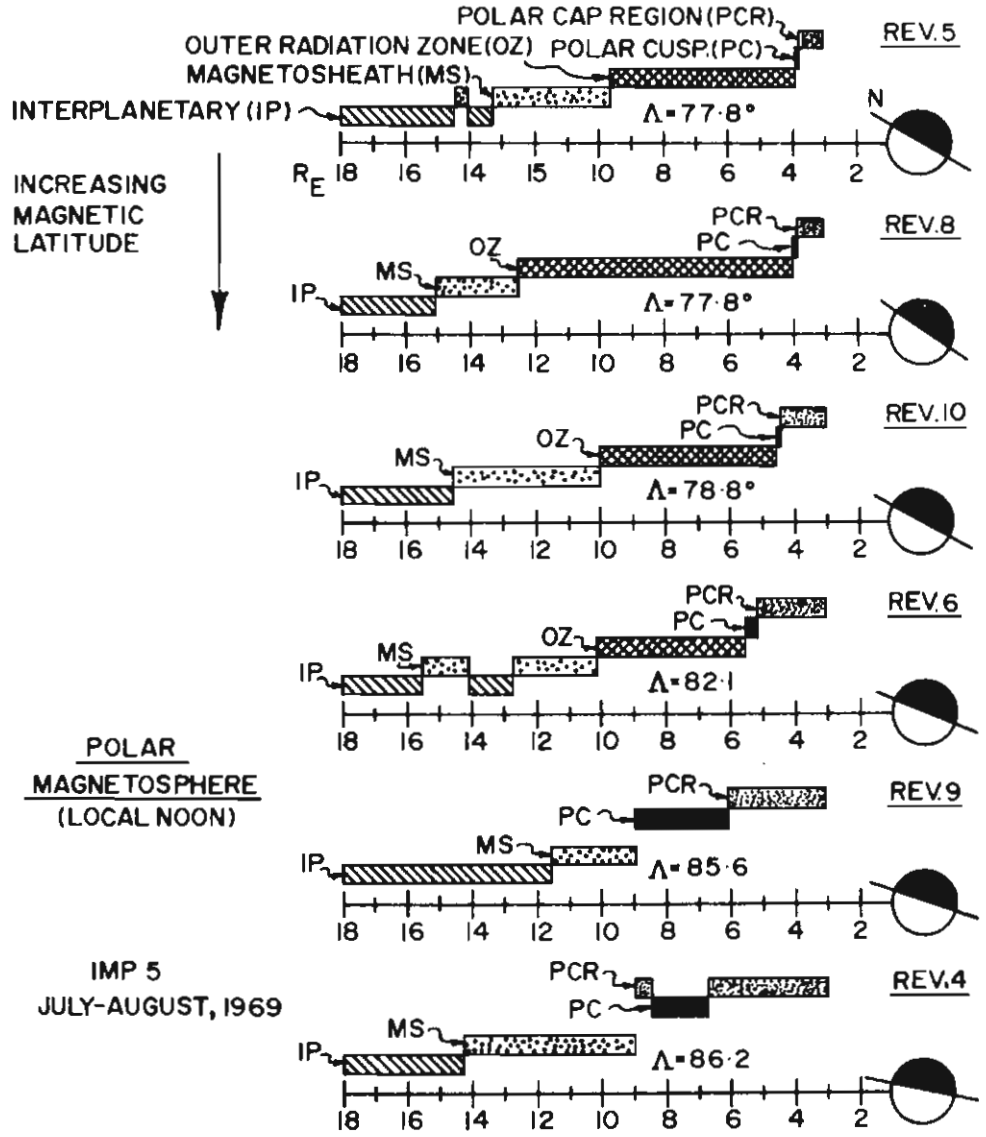


Figure 128. "Road maps" along the trajectory of IMP 5 for specified revolutions (see Figure 127). (*Frank 1971*)

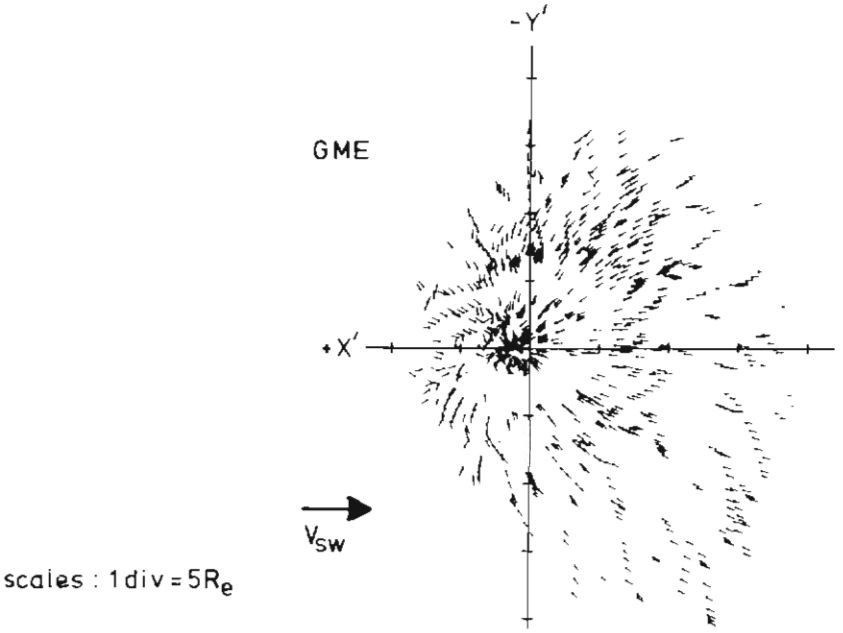


Figure 129. Geomagnetic field configuration in the noon–midnight meridian plane as defined by Heos spacecraft. Solid lines are computed from a Mead-Fairfield-like model using modified coefficients. (*Fairfield 1977*)

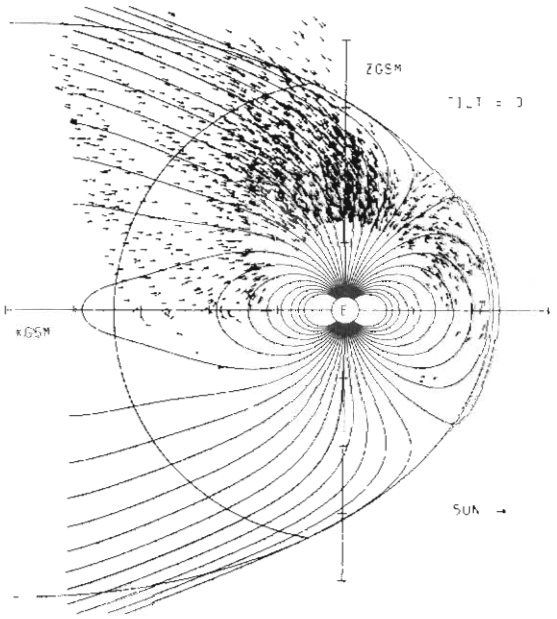


Figure 130. View from above the north pole of high-latitude Heos magnetospheric field vectors. Field lines appear to radiate from a point near the noon meridian and thus indicate a funnel type geometry near the dayside cusp. (*Fairfield 1977*)

# 16. The magnetospheric substorm

The relationship between the magnetic field in the solar wind and magnetic storms was summarised by Hirshberg and Colburn (1969). When the magnetic field in the solar wind has a south-pointing component, a magnetic substorm occurs. A change to a southward-oriented magnetic field in the solar wind results in magnetic merging at the solar side of the magnetosphere and an increase in flux in the magnetospheric tail.

The changes that take place in the magnetic field during substorms are shown in Figures 131 and 132 from Fairfield and Ness (1970). They pointed out that the mere adding of flux to the tail does not of itself increase the tail field strength, but the greater flaring of the tail subjects the magnetospheric boundary to a greater pressure from the solar plasma flowing past the magnetosphere, and it is this greater pressure that increases the magnetic strength.

Auroral electrojet activity – the strong ionospheric current associated with the aurora – can be measured by the A E index, which was introduced by Davis and Sugiura (1966). A comparison of the A E index against the south-pointing component $B_z$ of the magnetic field in the solar wind, summed over the previous hour, gave a correlation coefficient of 0.8 (Arnoldy 1971). Arnoldy concluded that a period of up to about one hour elapses after the change to $B_z$ south. During this time energy is transferred from the solar wind and built up in the magnetospheric tail, before the onset of an auroral substorm.

In the same year Mozer (1971) analysed balloon-measured electric-field data for 5-hour periods during each of 19 substorms near local midnight between L = 6.6 and 8.3 ($\Lambda_4$ = 67° to 70°) in the auroral region. He found that the ionospheric electric field is made up of approximately equal contributions from a large-scale field and small-scale turbulence. The large-scale field initially developed a westward component during the pre-substorm stage, and an equatorwards component about one hour later at the explosive stage of the substorm. He related the westward electric field to a westward field in the magnetic tail plasma sheet, and the associated $\mathbf{E} \times \mathbf{B}$ drift of plasma towards the Earth. After an hour, this drift would have carried the night-side magnetosphere into an unstable configuration; therefore the polewards surge of the aurora and subsequent thickening of the plasma sheet might be due to the tailwards propagation of the instability.

Hones *et al.* (1970) found that when the E > 40 keV electron count at a Vela satellite increased, the thickness of the plasma sheet increased; and when the electron count decreased, the sheet became thinner. Akasofu *et al.* (1971) related the occurrence of an increased count of electrons E > 46 keV to the start of the recovery stage of the auroral substorm.

With this information and data from satellite Vela 4A, together with auroral, magnetic and cosmic noise absorption data, Bond *et al.* (1973) made two estimates of the average rate of movement towards the Earth of plasma in the neutral sheet. The average velocity of about 45 km $s^{-1}$ was related to a high electron count associated with the brightening of an auroral arc that developed into a westwards and polewards auroral surge. During the early recovery stage, the average velocity in the plasma sheet was about 35 km $s^{-1}$. These values were of the same order as the 50 km $s^{-1}$ (0.5 $R_E$ $min^{-1}$) found at 6.6 $R_E$ by Lezniack and Winkler (1970).

The effect, if any, of the formation of a magnetic neutral point (or line) within the plasma sheet has not yet been discussed. As we have seen, the formation of a magnetic neutral point in the tail of the magnetosphere was first postulated theoretically by Dungey (1961). Experimental evidence of a neutral point was provided by Mihalov *et al.* (1968) from magnetometer data recorded on the Explorer 33 satellite. These authors presented two diagrams shown at Figures 133

and 134. Examples of magnetic reversals and values of $B_z = 0$ indicating the presence of neutral points can readily be seen.

Based on data from the OGO–5 satellite during a substorm that occurred on 15 August 1968, Russell and Dyer (1972) proposed a model for substorm behaviour in the neutral sheet. Their model is presented diagramatically in Figure 135.

A description of the general behaviour of the solar wind–magnetosphere–aurora system covering the period of an auroral substorm (Hones 1973) is shown in Figure 136.

From data at present available it would appear that a single (X type) neutral point may be formed between about $-8\ R_E$ and $-25\ R_E$ and then move tailwards. If we consider the situation in the magnetosphere at the end of a substorm, then the plasma sheet appears to be full, the magnetic field is dipole-like and the action of an electric field across the tail causes a plasma drift towards the Earth. At this stage the aurora is of the quiet arc type, but the fact that rayed arcs appear from time to time seems to indicate that electric fields form in the region of the aurora, or along the magnetic field lines associated with auroral particle precipitation.

If the auroral shell is defined as that magnetic shell down which the particles precipitate, then at least two alternative mechanisms exist. Either there is a mechanism that selects particles of the energy that causes the aurora, E = 1–10 keV, or there is a mechanism that selects particles of lower energy, which are accelerated by an electric field to auroral energies. With the change to a south-pointing magnetic field in the solar wind, magnetic merging takes place at the nose of the magnetosphere, field lines are carried back into the tail, the skirt of the tail flares, and the solar wind pressure results in magnetic compression on the plasma sheet. The Earth's magnetic field becomes less dipole-like. In time, a neutral point forms.

The passage of the change from a north-pointing solarwind magnetic vector to a south-pointing vector may initiate rarefaction wave around the equatorial regions of the magnetosphere, which results in a shock wave developing in the tail plasma sheet (Lyatskiy and Mal'tsev 1971). These authors presented a greatly simplified geometrical model of the plasma sheet (Figure 137) and by approximations simplified the equations governing the plasma sheet. Using data from satellite observations, they solved the equations by the methods of finite increments, giving a set of diagrams (Figure 138) that show the build up of a rarefaction shock wave and the formation of a neutral point at X = –17 to $-8\ R_E$ about 135–180 seconds after the initiating wave has reached X = $-9\ R_E$.

After the formation of the magnetic neutral point, the magnetic field between the neutral point and the Earth changes slowly compared with the rapid change that takes place in the aurora. It would, therefore, seem that the auroral precipitation moves progressively to magnetic shells that are successively more distant from the Earth, while the magnetic field collapses at a slower rate to a more dipole-like configuration. After an interval of about 30 minutes, presumably to maintain a magnetic and plasma pressure balance on each side of the neutral point (line), the neutral point would appear to move tailwards, and the auroral quiet arc regime resumes.

The dependence of substorm occurrence probability on the interplanetary field and on the size of the auroral oval was investigated by Kamide *et al.* (1977). They found a number of cases where a substorm was associated with a northwards component of the magnetic field in the solar wind, however, the majority of substorms were associated with a southward component (Figure 139).

This raises the problem of how the magnetospheric neutral sheet behaves when the interplanetary magnetic field is northwards. This problem is still unresolved, so we must turn from considering the electron aurora to considering the proton aurora.

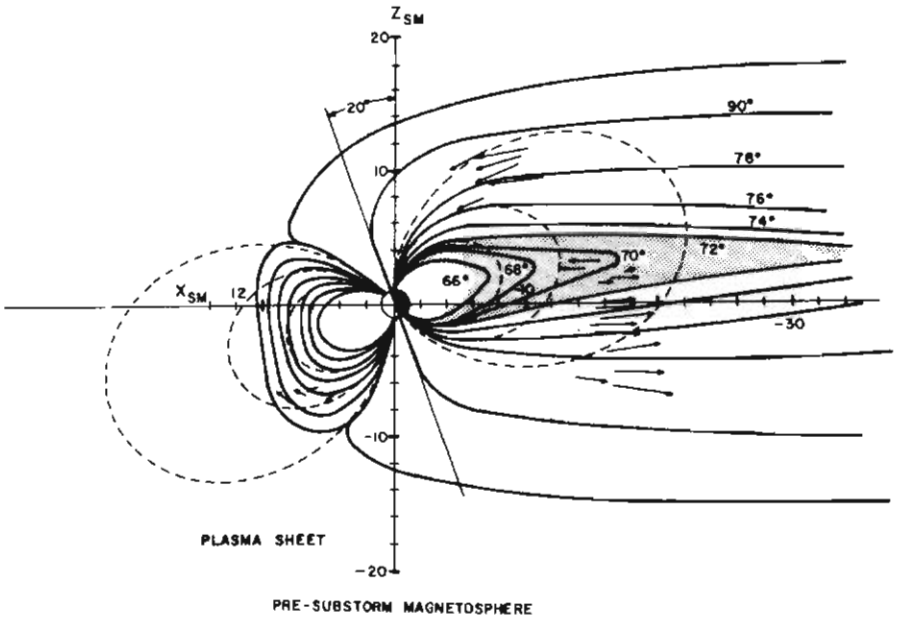


Figure 131. Field configuration in the noon–midnight meridian plane drawn to illustrate the thin plasma sheet and small $Z_{sm}$ component associated with the early phases of a geomagnetic substorm. (*Fairfield and Ness 1970*)

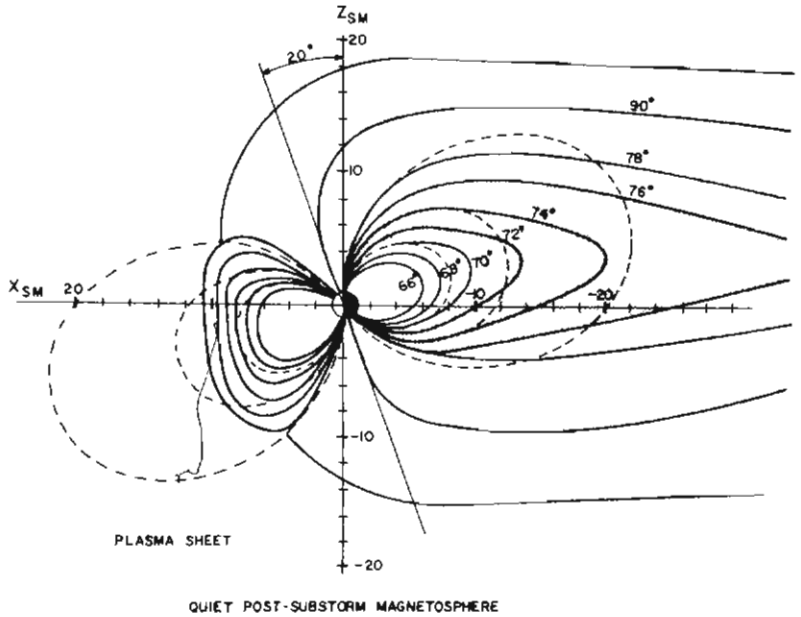


Figure 132. Field configuration in the near–midnight meridian plane drawn to illustrate an expanded plasma sheet with enhanced flux crossing the equatorial plane. This configuration exists during quiet conditions or after a substorm. (*Fairfield and Ness 1970*)

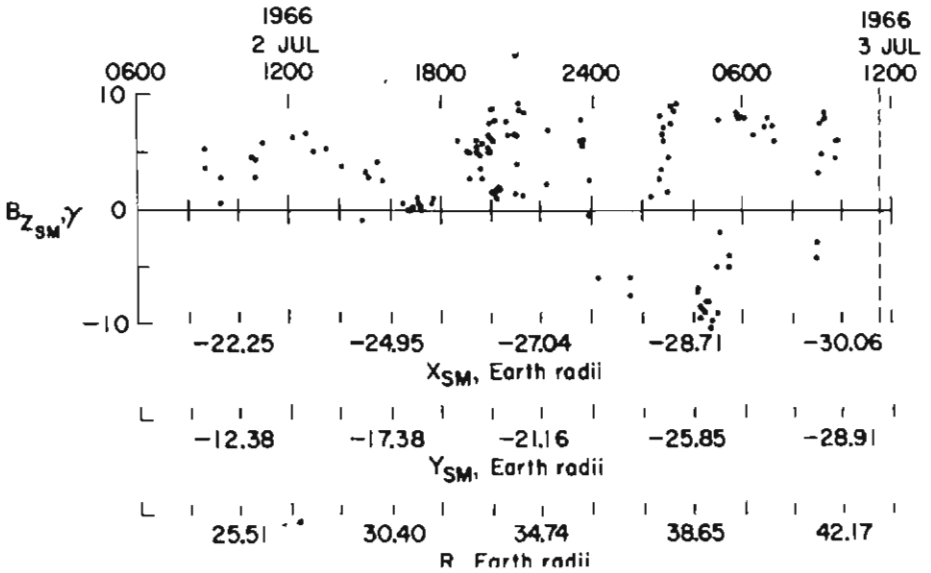


Figure 133. **Z** component of magnetic field at field reversals (when **X** component reverses sign) during orbit 1 of Explorer 33. A tentative location of the magnetopause is indicated by a dashed line. The segment is approximately 36 hours long. The location of the spacecraft in solar magnetospheric coordinates is given at the bottom of the graph. (*Mihalov et al. 1968*)

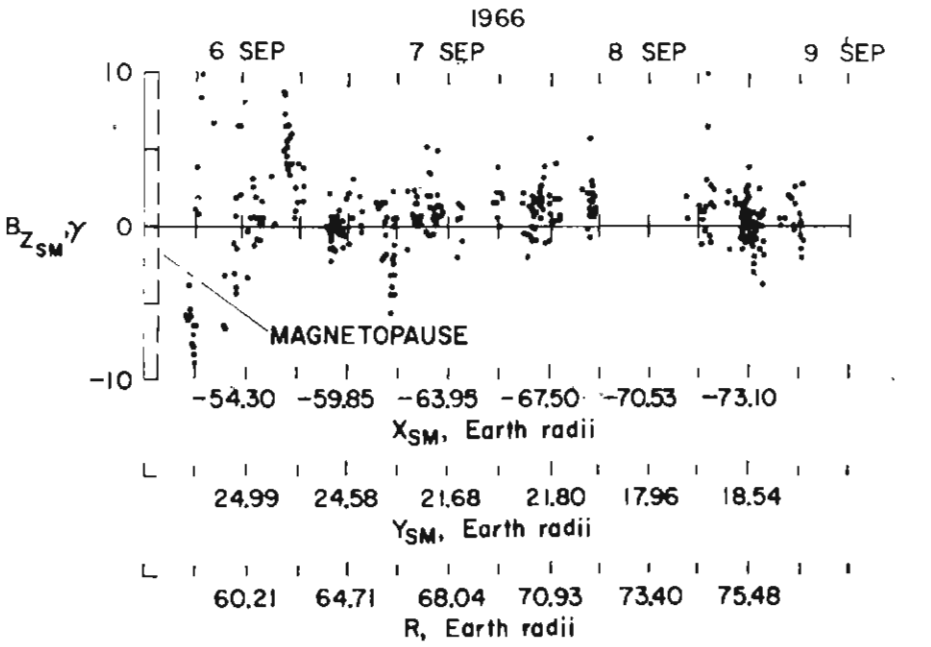


Figure 134. **Z** component of magnetic field in the field reversal region (when **X** component reverses sign) during orbit 5 of Explorer 33. The location of the magnetopause is indicated. (*Mihalov et al. 1968*)

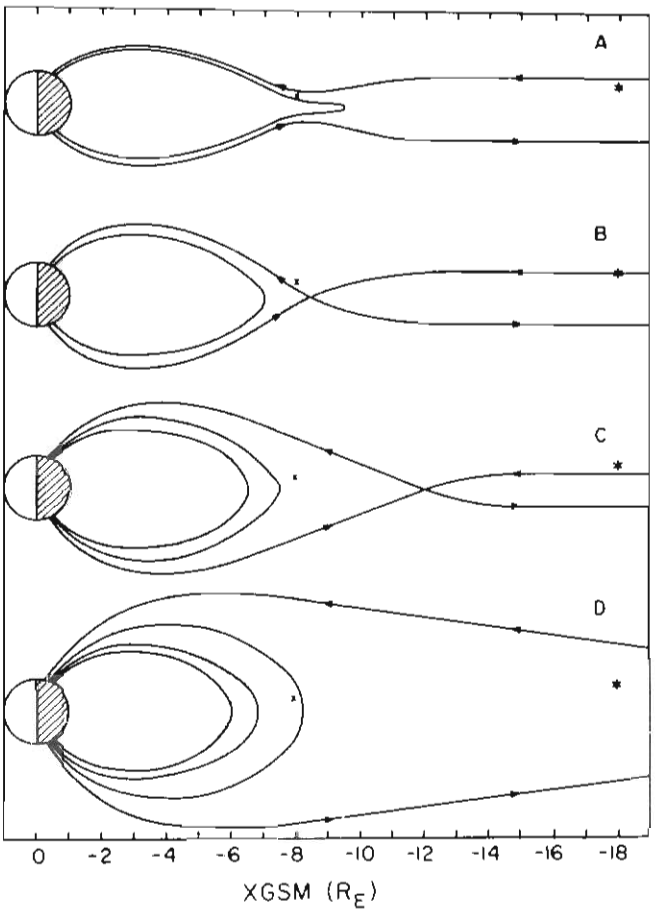


Figure 135. A model for the onset of the expansion phase of a magnetospheric substorm. The x marks the position of the OGO–5 satellite during a well-documented substorm on 15 August 1968. The asterisk marks a typical location of a Vela satellite during a substorm. At time A, the plasma sheet is thinning but thins faster near the Earth. At time B, an X type neutral point has formed near OGO–5, and OGO leaves the plasma sheet. The neutral point moves away from the Earth and OGO is enveloped in the expanding plasma sheet. Finally, at D, the neutral point has moved far down the tail enveloping Vela in the plasma sheet also. (*Russell and Dyer 1972*)

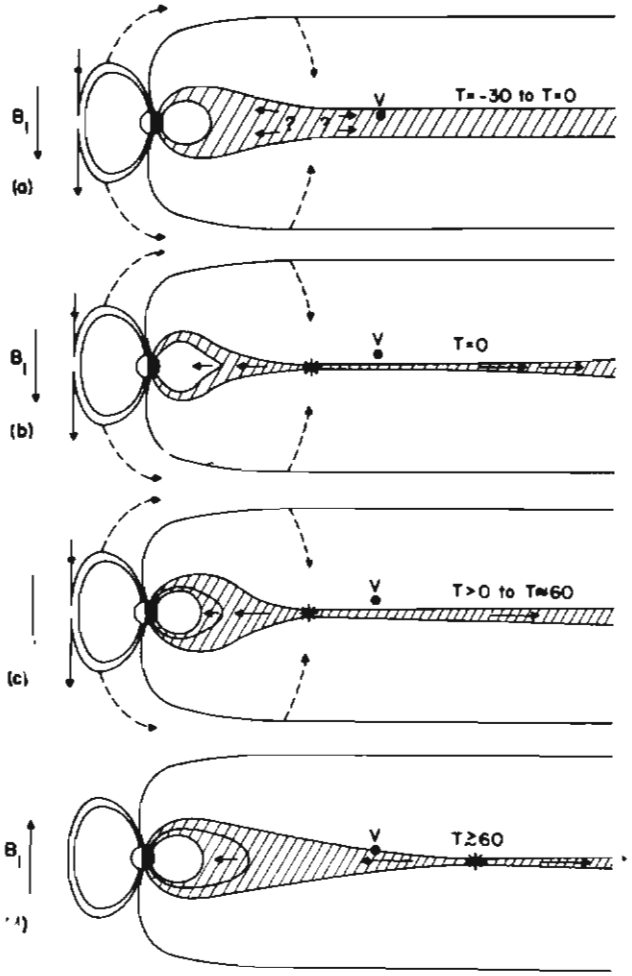


Figure 136. Schematic representation of plasma sheet behaviour during a substorm: (a) The plasma sheet may thin gradually for some tens of minutes before breakup (signified by T = 0). The question marks indicate that Vela measurements have as yet not identified any characteristic pattern of flow during such periods of gradual plasma loss. The solid arrow $\mathbf{B}_I$ and the dashed arrows suggest the possible role that the interplanetary magnetic field may play in this (and the subsequent two) epoch(s). (b) The field line reconnection (star) starts somewhere Earthward of the Vela satellite (V) at T = 0. Very rapid flow of plasma Earthward and tailward from the neutral lines begins. A Vela satellite more than ~1 $R_E$ from the neutral sheet (i.e., $|dZ_{SM}| \geq 1R_E$) encounters a rapid further reduction of plasma intensity to background levels at this time. A rapid tailward flow of the disappearing plasma is quite typically encountered. (c) Reconnection continues near the site of its initial onset throughout the expansive phase of the substorm. (d) The reconnection region suddenly moves much farther tailward as substorm recovery begins. Earthward of the reconnection region the plasma sheet rapidly becomes much thicker, and the reappearing plasma flows very rapidly Earthward. (*Hones 1973*)

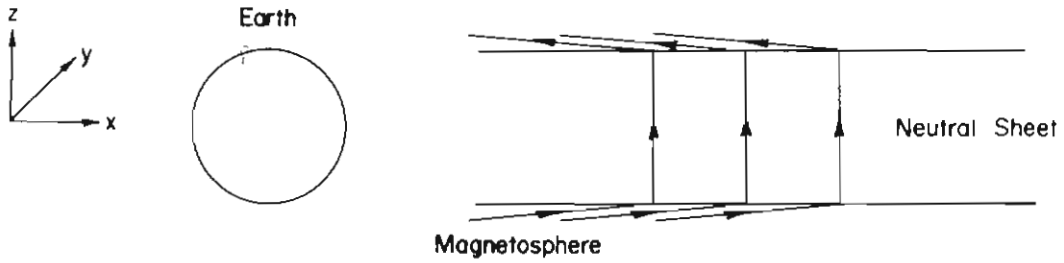


Figure 137. Simplified model of the plasma sheet as described by Lyatskiy and Mal'tsev (1971).

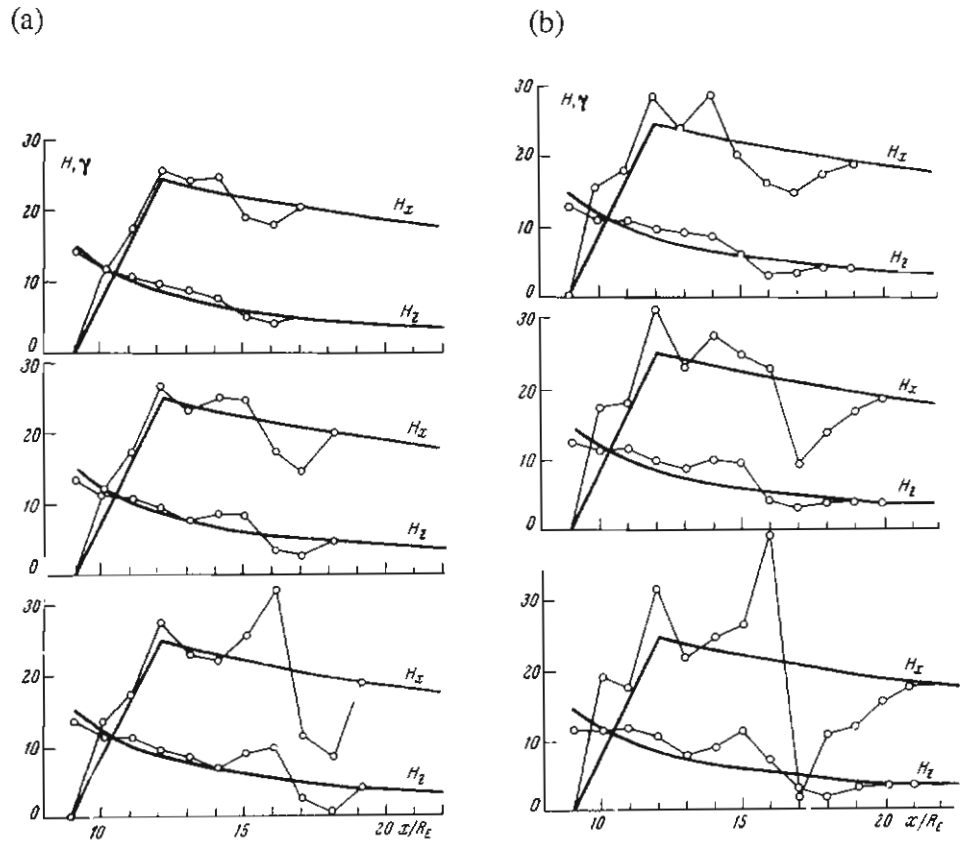


Figure 138. The heavy line shows the quiet condition prior to the shock wave. The lighter line with circles shows: (a) a solar wind discontinuity moving at 420 km $s^{-1}$ and an Alfvén velocity of 420 km $s^{-1}$; (b) a solar wind discontinuity moving at 420 km $s^{-1}$ and an Alfvén velocity of 210 km $s^{-1}$. (*Lyatskiy and Mal'tsev 1971*)

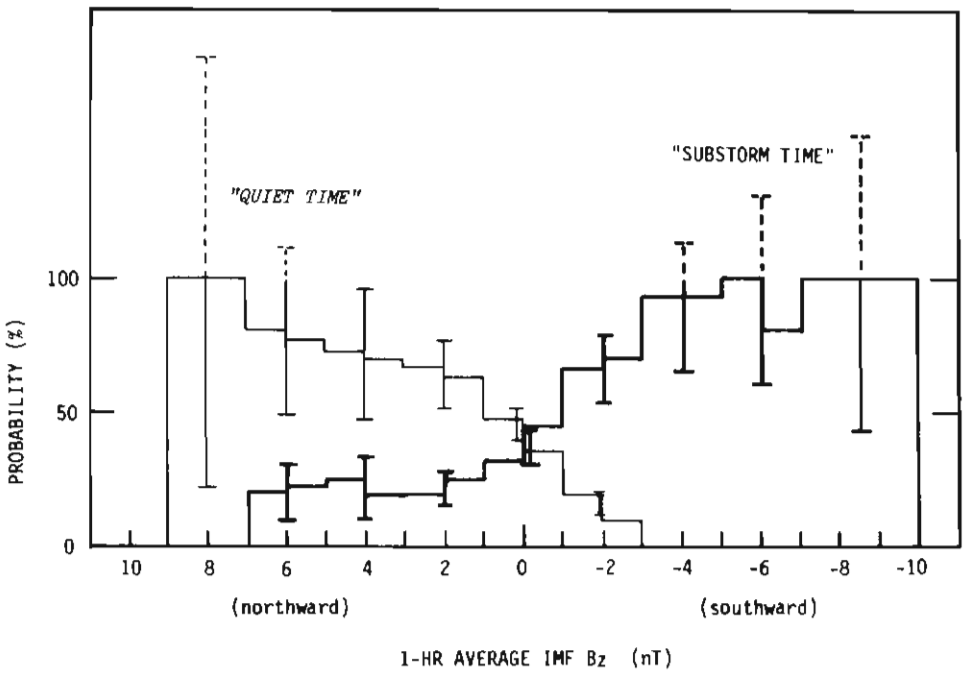


Figure 139. Probability of substorm time (represented by the heavy line) and quiet time (represented by the light line) as a function of the Bz value of the interplanetary magnetic field. (*Kamide et al. 1977*)

# 17. The proton aurora

The first indication of the precipitation of protons in auroral regions was the discovery of the Balmer lines of hydrogen in auroral spectra by Vegard (1939).

The auroral zone corresponding to the hydrogen aurora was determined by Eather and Sandford (1966) from measurements with an Hβ scanning photometer at Mawson and patrol spectrographs at Scott and Hallett. The pattern of the Southern Hemisphere proton auroral oval found by these authors is shown in Figure 140.

Using the same Hβ data from Mawson, Eather and Jacka (1966) found that the region of maximum hydrogen emission always appeared equatorwards of visual forms. An equatorwards movement of the zone of emission was observed before midnight. The zone moved polewards after the breakup of the visible electron aurora and later returned equatorwards. A return of the zone polewards was sometimes observed in the morning hours.

The special relationship of the proton aurora to the electron aurora was demonstrated in Montbriand's (1971) analysis of the electron auroral substorm. The quiet time pattern shows proton aurora on the equatorwards side of the discrete aurora in the dusk–midnight sector and overlapping with the more diffuse region of patchy and pulsating aurora in the midnight–dawn sector. Montbriand's findings with regard to the westerly surge were confirmed by Oguti (1973). There is enhanced proton precipitation equatorwards and eastwards of the electron aurora.

Oguti also found that at the beginning of a substorm, at least on some occasions, a portion of the arc that brightens breaks away and moves equatorwards until it lies very close to the boundary of the hydrogen aurora (Figure 141).

The existence of both proton and electron precipitation gives rise to three dimensional current systems. This variant of Birkeland currents forms the subject of the next chapter.

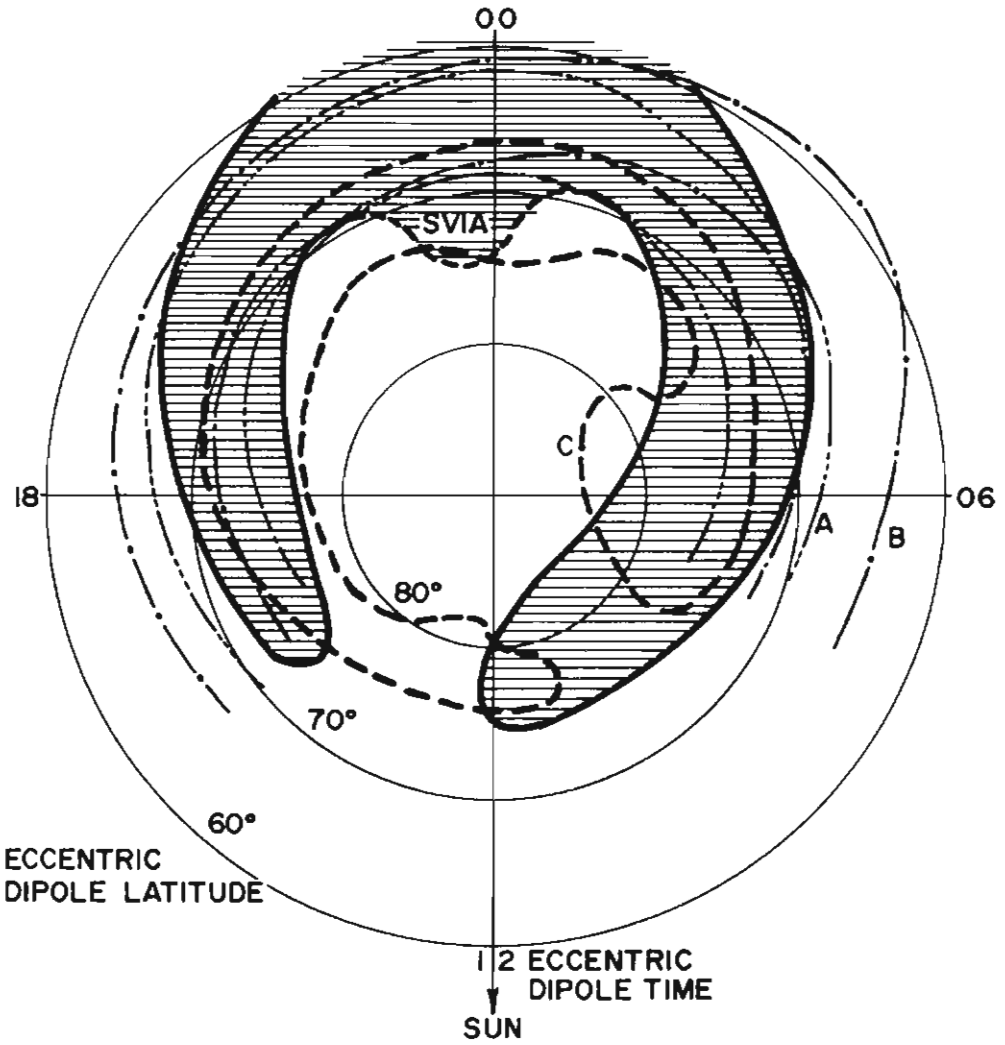


Figure 140. The zone of hydrogen emission in the Southern Hemisphere as a function of eccentric dipole latitude and eccentric dipole time. For comparison, Curve A shows the conjugates of the Northern Hemisphere hydrogen emission zones of Montalbetti and McEwen (1962), Curve B of Yevlashin (1963) and Curve C shows the Southern Hemisphere zone of maximum visual aurora of Sandford (1964). (*Eather and Sandford 1966*)

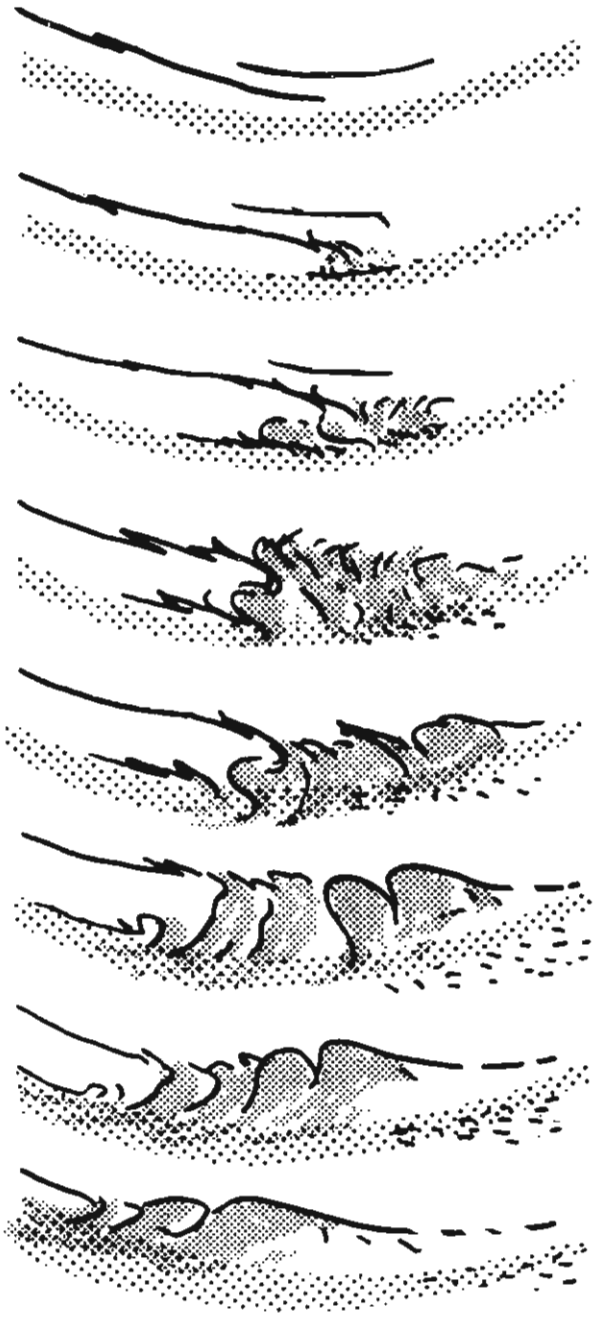

Figure 141. A schematic illustration of the "contact breakup". The breakup starts when an electron sheet aurora, which has split from the high-latitude arc, comes into contact with the hydrogen emission (indicated by sparse dots). Then a new electron aurora appears along the poleward boundary of the hydrogen emission, and the rotating expansion of the new aurora occurs in association with the enhancement of the hydrogen emission on its southeastward side. (*Oguti 1973*)

# 18. Birkeland currents

From a study of the generation of ionospheric currents by mapping magnetospheric electric fields onto the ionosphere, Boström (1964) deduced that two types of Birkeland current would be necessary to satisfy the two cases he considered. These two cases are illustrated in Figures 142 and 143.

Verification of the presence of Birkeland currents by rocket flights through an aurora is not a simple matter. However, several such experiments have been undertaken and analysed. The results of one carried out in the Northern Hemisphere by Casserly and Cloutier (1975) are presented in Figure 144.

The cause of Birkeland currents can probably be best explained by adapting Hones's (1979) presentation of the interaction of the solar wind with the magnetosphere. Hones considers the effect of a Lorentz force on protons and electrons moving as a plasma perpendicular to a magnetic field. The effect is shown in Figure 145a.

The result of collecting the deflected protons and electrons on separate electrodes connected through an external load is shown at Figure 145b. Incidentally, although this is the system that operates in the aurora, since 1971 Dr Sergei Pischikov of the USSR (Anon. 1981) has used this process on the ground to produce direct current (DC) electricity, which is then converted to alternating current (AC) electricity and fed into the Moscow power grid system. The plasma used is pre-heated natural gas combusted with oxygen, or oxygenated air, to a temperature of 3000°C, which is released through a nozzle into a magnetic field.

In the auroral situation, Hones indicates (Figure 145c) that the solar wind penetrates the boundary of the magnetosphere to depths of several hundred to several thousands of kilometres. In this boundary layer, the density of the plasma decreases with increasing depth of penetration. Within the boundary the solar wind flows both eastwards and westwards being perpendicular to the Earth's magnetic field. Since the field lines connected to the boundary layer at low latitudes are rooted in the Earth, there will exist a polarisation electric field that permits the plasma to flow across the field as indicated on the diagram. In consequence, on the morning side, a current flows upwards from the ionosphere to the boundary (the conventional current being in the opposite direction to the electron flow) then Earthwards through the plasma layer, completing the circuit by a downward current followed by a current through the auroral ionosphere. On the evening side the current flow is reversed.

However, Iijima and Potemra (1976a, 1976b and 1978) used the Triad satellite data, which measured magnetic fields at 800 km that were presumed to correspond with the movement of electrons with energies between 150 eV and several keV recorded by the Isis 2 satellite (McDiarmid and Burrows 1964; McDiarmid *et al.* 1975, 1976), presented a diagram (Figure 146) showing the directions of large-scale field-aligned currents into and out of the ionosphere.

Returning to the work by Hones, two items may be pertinent. Firstly, when electrons and protons are of equal velocity at the point of penetration of the magnetospheric boundary layer, the protons will penetrate deeper than electrons. Secondly, although Earthwards of the shock front the protons and electrons in the solar wind have low energies (typically below ~1.5 eV); by the time they have reached 1400 km from the Earth they have been accelerated to energies in the range measured by McDiarmid *et al.* (1975), of 150 eV to 200 keV, with the prospect of further acceleration down to auroral heights of about 105 km, where only those electrons then having energies between about 1–12 keV produce auroral light.

It would therefore seem that only those dense electrons close to the boundary on the morning side precipitate into the auroral oval, producing an upwards conventional current from the

ionosphere. The diffuse return current, equatorwards of the auroral oval, consists of precipitating protons and the upwards movement of electrons from the ionosphere. There will of course be diffuse precipitation from the loss cone of spiralling electrons, which will reduce the effect of downwards spiralling protons and upwards spiralling electrons to produce the conventional current downwards into the ionosphere indicated by Hones. This is seen as diffuse aurora in which the hydrogen line can be detected. Depletion of the ionosphere of electrons equatorwards of the auroral oval is therefore to be expected. This depletion in the form of the mid-latitude ionospheric trough, examined by Thomas and Andrews (1968, 1969) and Rycroft and Thomas (1970), is indicated as the region between the outer "boundary of density enhancement" and the plasma pause in Figure 147.

Neither the night side nor the plasma in the frontal tail lobes north and south of the polar cusps are followed up by Hones. The presence of plasma in these lobes is indicated in Figure 148 (Rosenbauer *et al.* 1975). However, a similar discussion relating to these latter regions would explain the inner ring of current into and out of the magnetosphere found by Iijima and Potemra, as far as the Sun-wards side of the magnetosphere is concerned.

Concerning the night-side, a discussion of the relationship of types of aurora to their origin in the magnetosphere by Swift (1981) is relevant. Swift, using a slightly different nomenclature from this book, distinguished four basic types of aurora: *diffuse aurora*, which is restricted to the veil aurora that is often seen equatorwards of all other forms around the entire night-side discrete auroral oval from dusk to dawn (see Figures 151a and 153); *patchy aurora* which is the same as 'auroral patches'; *discrete aurora*, which in Swift's usage is restricted to, 'thin arcs and bands' (a somewhat different usage from the *International Auroral Atlas* which includes broad arcs and bands); *inverted-V aurora* derived from Frank and Ackerson's (1971) interpretation of observations of electron precipitation recorded by the Injun 5 satellite. They noted that when the satellite passed through certain regions of electron precipitation some tens of kilometres across, the characteristic energy increased, passed through a maximum, and then decreased. When energy is plotted against distance the graph shows a Λ or inverted-V shape. This type of precipitation region was referred to as inverted-V electron precipitation. Swift's inverted-V aurora is a type of discrete aurora of thickness compatible with the thickness of the region of the energy changes in inverted-V electron precipitation, being arcs or bands some tens of kilometres in thickness.

In relation to *diffuse aurora*, Swift notes that Eather *et al.* (1976) compared parallel particle fluxes recorded by the ATS 5 satellite in equatorial orbit at 6.6 $R_E$ with the readings of meridian scanning photometers, and found evidence of an unbroken band of luminosity that endured throughout the period of darkness. The intensities of spectral line emissions were reported to be consistent with the observed fluxes of precipitating particles with energies ranging from a few hundred electron volts to 1 keV, as measured by instruments on the Isis 2 satellite (Winningham *et al.* 1978). Data from the ATS 6 satellite and the low-altitude DMSP satellite when both were above the evening diffuse aurora showed nearly identical electron spectra, with the upper bounds of the relevant portions of the spectra at 1 keV and 5 keV respectively (Meng 1979).

From these and other results, Swift tentatively concluded that diffuse aurora is caused by electrons with energies of the order of 1 keV that precipitated directly from the region of the inner Earthwards edge of the tail plasma sheet.

In considering the published work on *auroral patches and pulsations*, Swift suggests that from the observed conjugacy of pulsations, there is strong evidence that the cause of the pulsations lies near the equatorial plane, although the cause is not yet understood.

Studies of simultaneous low-energy electron and auroral data from DMSP weather satellites showed that inside bright, discrete, thin arcs there is a distinct spectral peak near 3.2 keV (Meng 1976). Spectral peaks in electron spectra had previously been observed by rockets launched

through aurora (Evans 1969, Arnoldy 1974, Hultqvist 1974). They had been interpreted as evidence of electron acceleration due to electric fields that are parallel to the Earth's magnetic field lines. Meng argued that most of the potential drop would have to be above the height of the DMSP satellite at 850 km. By injecting barium, using a shaped explosive charge, along magnetic flux tubes above discrete aurora to altitudes greater than 10 000 km, Westcott *et al.* (1976) found that portions of the barium streak above 4000 km show very rapid drift, which they interpreted as due to an **E** x **B** drift.

Swift explains the *discrete aurora* as due to electric double layers or current-driven shocks in which an upwards electric field forms V-shaped equipotentials above the auroral ionosphere. These shocks were first recognised from satellite electric field measurements as pairs of oppositely directed electric field structures. It was later recognised that most events have a single, unpaired field spike (Figure 149).

Swift considered that the broad *inverted-V* structures reported by Frank and Ackerson (1971) are associated with the broad discrete (inverted-V) aurora, largely on the basis of dimensional compatibility.

The behaviour of the aurora on the night side in relation to neutral points or neutral lines has previously been discussed in Chapter 16.

With this brief look at Birkeland currents, we turn in the next chapter to a form of the aurora that is located nearer the Equator than the hydrogen or proton aurora, the subvisual red arc.

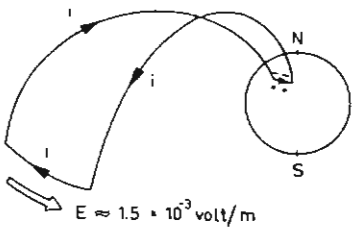


Figure 142. Simplified picture of the magnetospheric current system in case 1. A current flows into the ionosphere at one end of the arc and out at the other. (*Boström 1964*)

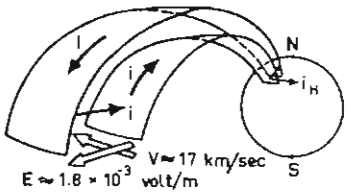


Figure 143. Simplified picture of a part of the magnetospheric current system in case 2. A current flows into the ionosphere on the equatorward side of the arc all the way along the arc and flows out of the ionosphere on the poleward side. (*Boström 1964*)

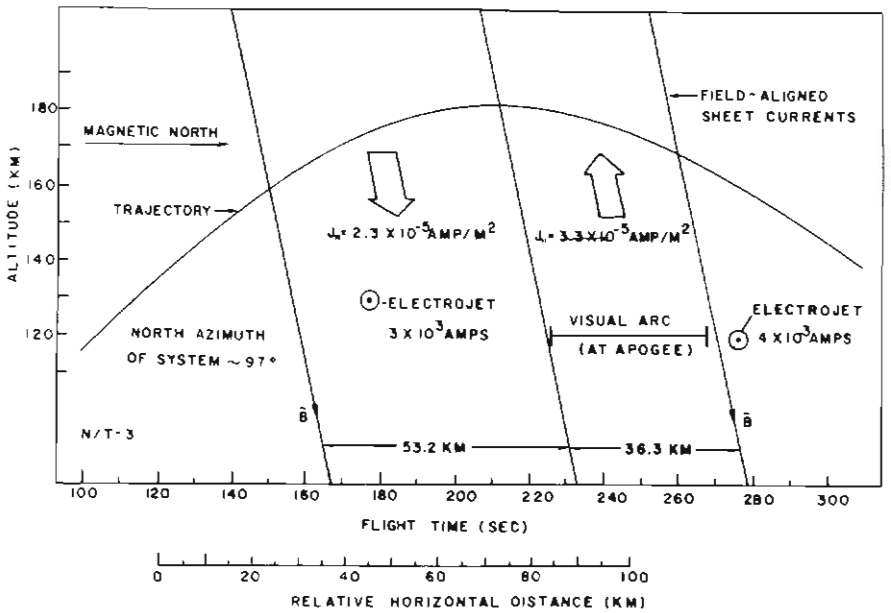


Figure 144. The model current system showing the two eastward electrojets and the two Birkeland current sheets drawn in the stationary positions that they are assumed to hold for the major portion of the flight. This is a view in the plane perpendicular to the arc system. The location of the visual arc inferred from the Fort Yukon all-sky camera photographs and photometer data is shown to be under the region of the upward Birkeland current. (*Casserly and Cloutier 1975*)

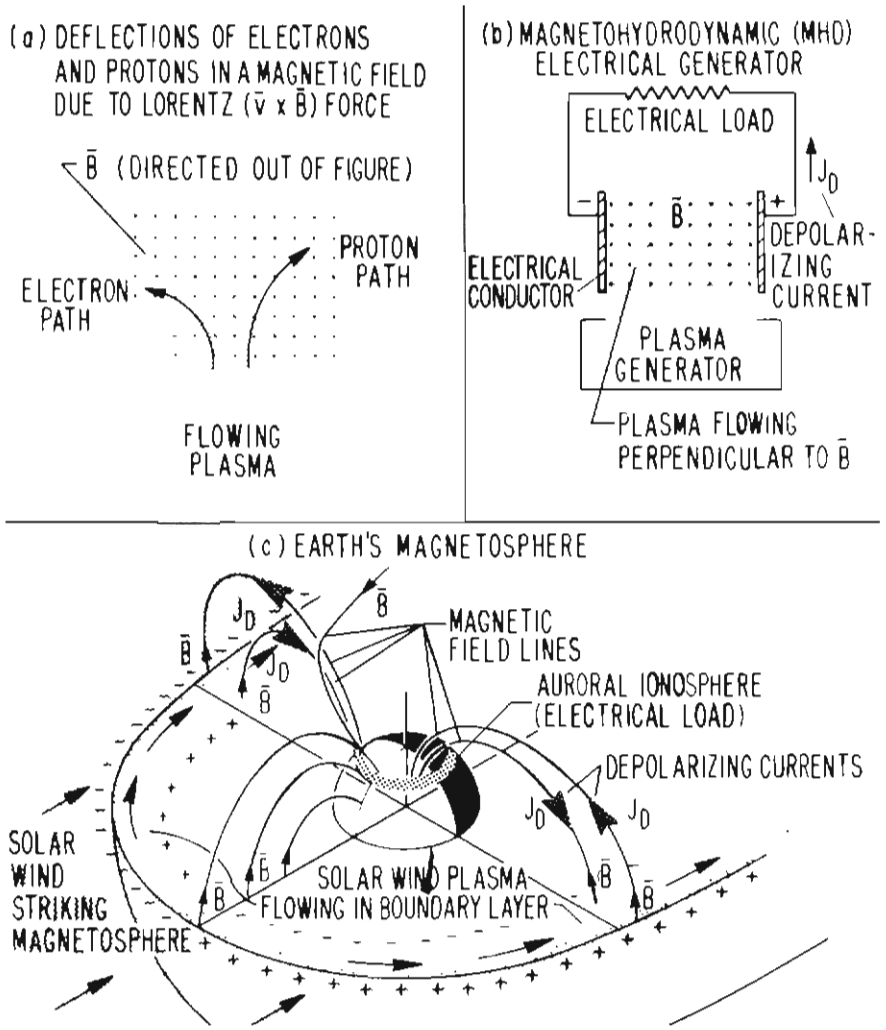


Figure 145. (a) curved paths of electrons and protons in a magnetic field; (b) electrostatic polarisation of, and depolarising current from, plasma forced to flow across a magnetic field; (c) polarisation of plasma in magnetospheric boundary layer resulting in depolarising currents to the Earth's ionosphere. (*Hones 1979*)

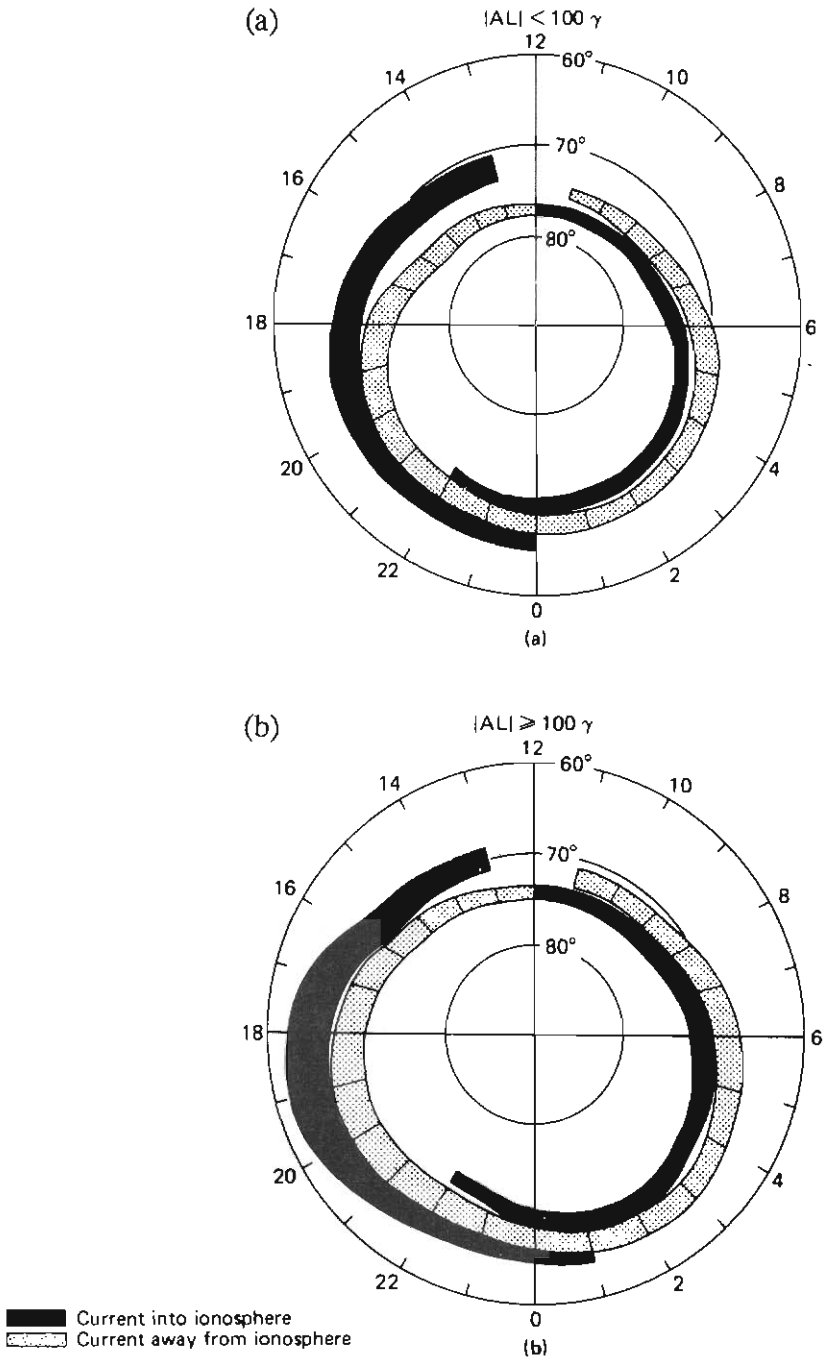


Figure 146. A summary of the distribution and flow directions of large-scale field-aligned currents determined from (a) data obtained from 439 passes of Triad during weakly disturbed conditions ($|AL| < 100\ \gamma$) and (b) data obtained from 366 Triad passes during active periods ($|AL| \geq 100\ \gamma$). (*Iijma and Potemra 1978*)

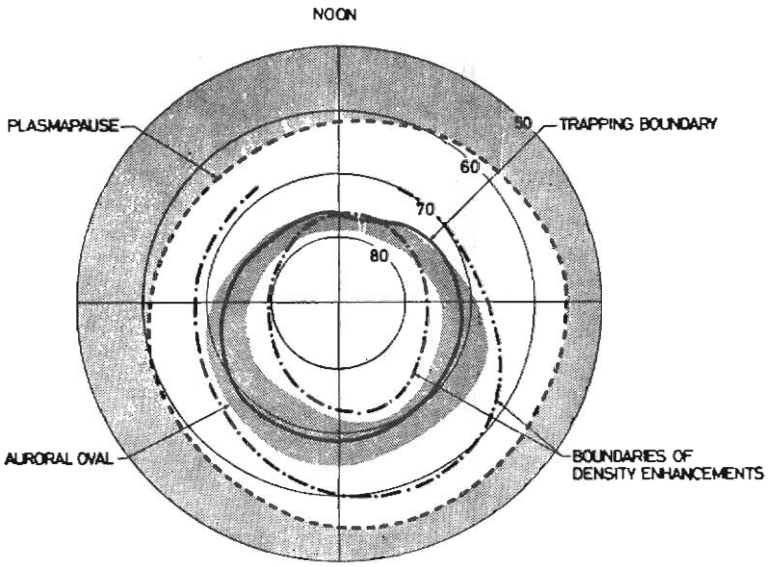


Figure 147. The relative locations of various high-latitude phenomena discussed in the text in terms of invariant latitude and local time for a Kp of 3. The plasmasphere termination is clearly seen. The smoothed upper and lower boundaries of the high-latitude ring of enhanced plasma density are also plotted. (*Rycroft and Thomas 1970*)

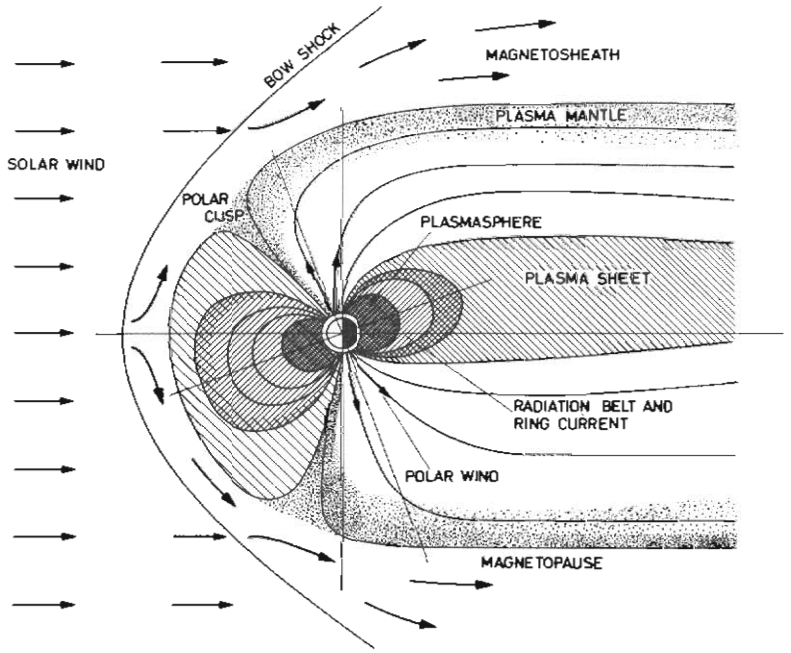


Figure 148. Noon—midnight cross-section of the magnetospheric plasma distribution. (*Rosenbauer et al. 1975*)

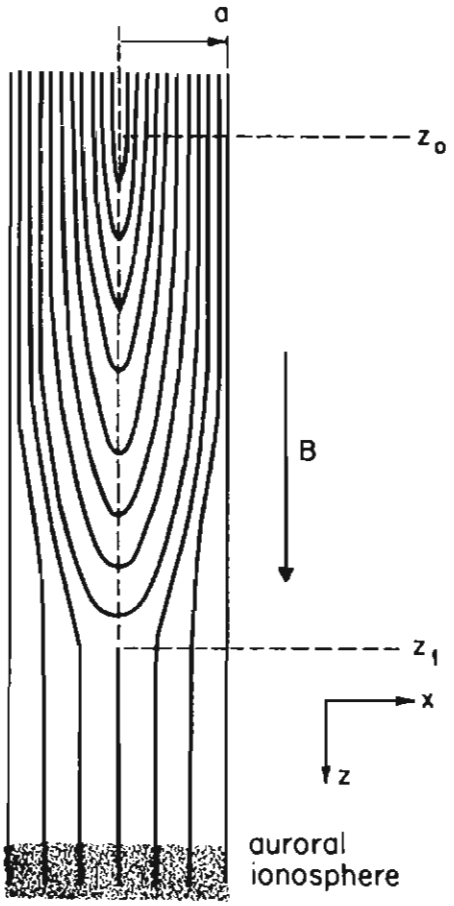


Figure 149. Equipotentials of the V–shock model. Solid lines represent equipotential surfaces. The electric field is directed upward and toward the central axis of the figure.

# 19. The subvisual red arc

Subvisual red (SAR) arcs were discovered by Barbier (1958) during photometric observations in Haute Provence. Perhaps in modern terminology they should be called cis-auroral red arcs, but the term SAR arcs is in general use.

The properties of SAR arcs were described by Cole (1965), based on earlier observations. The arcs are stable for up to 10 hours, and probably form complete rings around the Earth. They are located as broad diffuse bands of emission of the red oxygen line at 630.0 nm (about 400 km wide), at an altitude of about 370–400 km in the F region, equatorwards of the auroral zones.

Cole suggested they are activated by thermal energy conducted down magnetic field lines and define the sink region for the energy that forms the main storm disturbance (Dst) phase of magnetic storms.

Although thermal energy is probably the source of the red colour, there is some evidence of particle precipitation. O'Brien *et al.* (1960) reported peaks of fluxes of energetic electrons $E > 30$ keV on successive passes by a satellite at 1000 km altitude over SAR arc, when the Planetary Geomagnetic Index had a high value $Kp = 8$. Barbier had reported in 1958 that SAR arcs also contained traces of the oxygen emission at 557.7 nm, but it was not until this was confirmed by Shaeffer and Jacka (1971) that the presence of this emission became generally accepted. Hock *et al.* (1971) also found the 557.7 nm oxygen line, but more importantly found the nitrogen $N_2^+$ band emission at 427.8 nm. They triangulated the 630.3 nm emission and found that it lies at a height of 400–500 km, while the 557.7 nm emission lies at the normal height of about 100 km, which is presumably due to particle precipitation.

When hydrogen aurora and SAR arcs were measured simultaneously, the SAR arcs were found about 1.6 L-units equatorwards of hydrogen precipitation and correlated with the plasmapause determined by satellite observation (Figure 150).

A great aurora took place on the nights 1- and 2 September 1859. On the morning of 1 September, Richard Christopher Carrington, the astronomer, made the first recorded observation of a solar flare, which must have been very intense to have been seen in full sunlight. It was followed by a major magnetic storm. In association with this storm the aurora was seen overhead at Valparaiso, Chile, 22°S of the Geomagnetic Equator.

A similar aurora seen from Singapore on 25 September 1909 was included in a synoptic study by D.S. Kimball and shown on a map by Sydney Chapman in *Annals of the International Geophysical Year* (Stoffregen 1962). Singapore is shown as about 10° south of the Geomagnetic (centre dipole) Equator. One may guess that, as in the Valparaiso case, an intense flare occurred and the compression of the magnetosphere and the associated great heating caused a wide visible SAR arc close to the Geomagnetic Equator, so that it was seen from Singapore.

It is perhaps to a similar earlier event that Coleridge, who died in 1814, referred in his "Rhyme of the Ancient Mariner": 'All the sea and sky one red'.

This brief review of SAR arcs leads into the final chapter – a relatively recent development in auroral morphology.

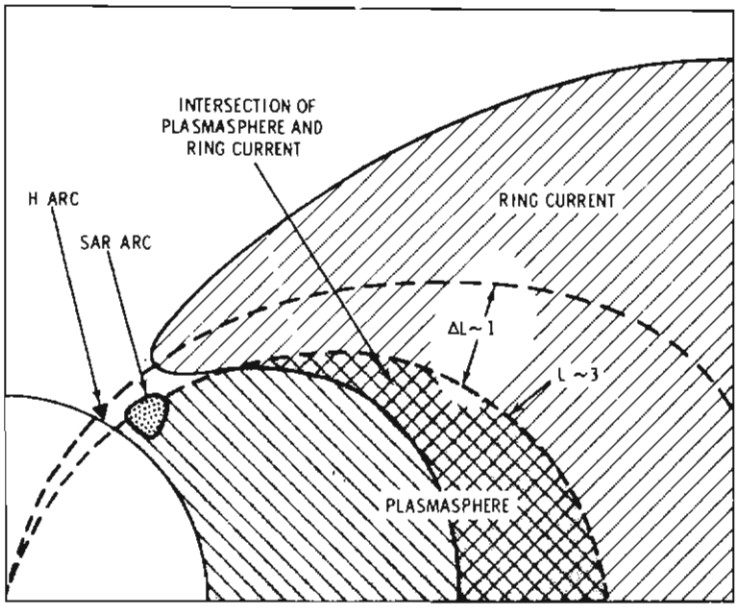


Figure 150. Suggested locations of the simultaneously occurring SAR arc and H arc. (*Hock et al. 1971*)

# 20. Satellite pictures of the aurora

The first, somewhat distorted "pictures" of large sections of the aurora were presented by Lui and Anger (1973). The satellite ISIS2 carried an imaging and scanning photoelectric photometer. The data were reproduced to form pictures in much the same way as pictures are produced on a television screen. One such picture is reproduced in Figure 151 and the corresponding polar geographic plot is presented in Figure 152.

These authors found that the most striking and persistent feature of the pictures is a fairly uniform belt of diffuse auroral emission extending along the auroral oval. They suggest that this region follows, contributes to, and may in a sense actually define, the auroral oval during quiet times, and that the mantle aurora and proton aurora both contribute emissions to the region. This diffuse aurora or veil can be clearly seen on all-sky camera photographs published by Bond *et al.* (1973) in Figure 153. In the same year, the concept of the auroral substorm and the presence of polar cap aurora was confirmed by Anger and Lui (1973).

Actual satellite auroral photographs covering a small area, though larger than that obtainable by all-sky camera, were published in 1974. Two years later satellite photographs coverging a large area appeared in the literature. Akasofu (1976) presented several montage photographs, and other photographs covering large portions of the auroral oval. One example has already been shown at Figure 3 (Chapter 2). For comparison, Figure 4 showns a Bond and Paine (1971) montage of the geographic auroral ovals for Kp = 1 at 1041 UT and Kp = 1 at 1727 UT determined from all-sky camera data.

Figure 154 illustrates a quiet aurora during the first orbit with several arcs in the forenoon sector and a bright polar-cap arc approximately along the midnight meridian bending towards the evening sector. During the second orbit the typical substorm feature of the polewards expanding bulge can be seen. Note also the truncation of the very bright arc near the noon meridian. The third orbit shows the completion of the arc.

In Figure 155 the particular new feature to note is the annular belt of auroral arcs in the morning sector, and the horn-like luminosity extending towards the midday sector from the afternoon sector.

These features are presented in diagrammatic form as they would be seen in the Northern Hemisphere in Figure 156 (*Akasofu 1976*).

Akasofu also reported that from an examination of satellite auroral photographs he was able to confirm that substorms also occur when the interplanetary magnetic field $B_z$ has a northwards or positive component. He suggested that there is sufficient energy accumulated in the magnetosphere from magnetic merging and plasma injection during periods when $B_z$ again points northwards. The concept is presented diagrammatically in Figure 157.

These findings seem to require a mechanism within the magnetosphere or even within the ionosphere by which the auroral substorm is initiated.

Frank *et al.* (1982), using a vacuum ultraviolet imaging photometer on board satellite Dynamics Explorer DE1, and instruments (Frank *et al.* 1981) for presenting the ultraviolet images at visible wavelengths, found that frequently the northern auroral oval has a sun-aligned arc extending from the midday sector to the night time sector of the oval. This type of display they denoted as a $\theta$-aurora.

Plate 5 shows the way the $\theta$-aurora was formed on 8 November 1981. In true perspective, with local evening on the left side of each image, the three images on the left side, top to bottom at 1507, 1531 and 1543 UT show the movement of the sun oriented or polar arc from the evening sector toward the noon-midnight line. The enlarged centre image at 1607 UT) with map

superimposed shows the midnight magnetic meredian drawn from the north magnetic pole making an angle of $\simeq 10°$ with the 'sun oriented' aurora. The images on the right at 1619, 1631 and 1644 UT show the movement of the sun oriented trans polar arc towards the morning auroral oval.

Simultaneous *in situ* data from DE2 confirm that the evening, trans polar and morning aurora have similar electron spectra.

The DE1 plasma instrument shows that the polar arc is associated with magnetic field aligned currents as is the case with the auroral oval.

Plate 6 shows a DE1 image of the southern aurora. It was taken from a height of 21 000 km at geographic latitude 54°S and longitude 161°E (almost over Macquarie Island) at 1515 UT on 31 July 1986. It shows the zone of diffuse aurora and on the night side, opposite to the sunlit crescent showing the day side, the westerly surge and, to the east, the movement of the discrete aurora toward the auroral pole (L.A. Frank, J.D. Craven and J. Sigworth, personal communication, 1989).

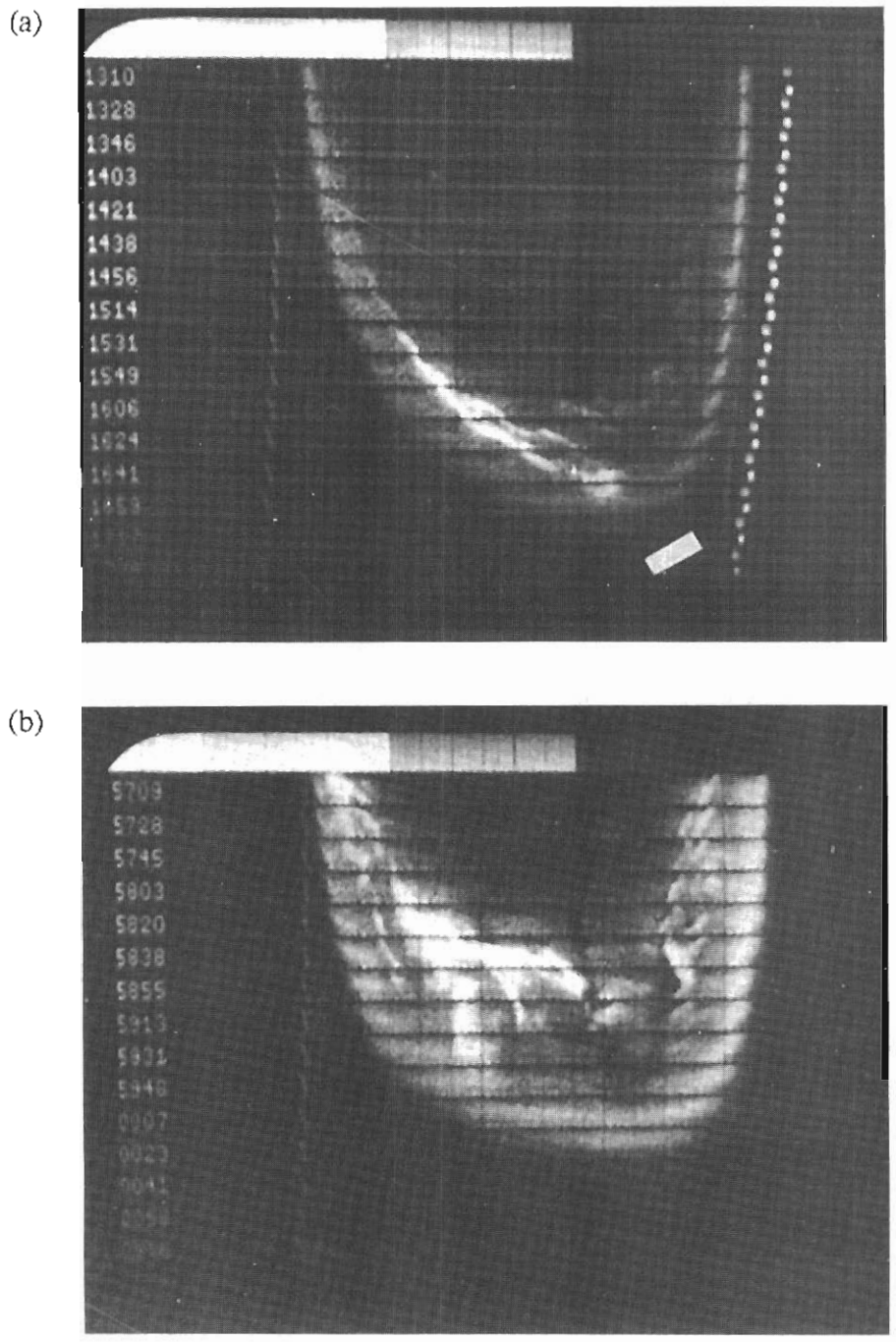


Figure 151. The composite pictures of data from four selected passes over Ottawa during the period in December 1971 when the satellite ISIS2 was in orbit-aligned configuration: (a) 12 December pass at 0413 UT; (b) 13 December pass at 0257 UT. (*Lui and Anger 1973*)

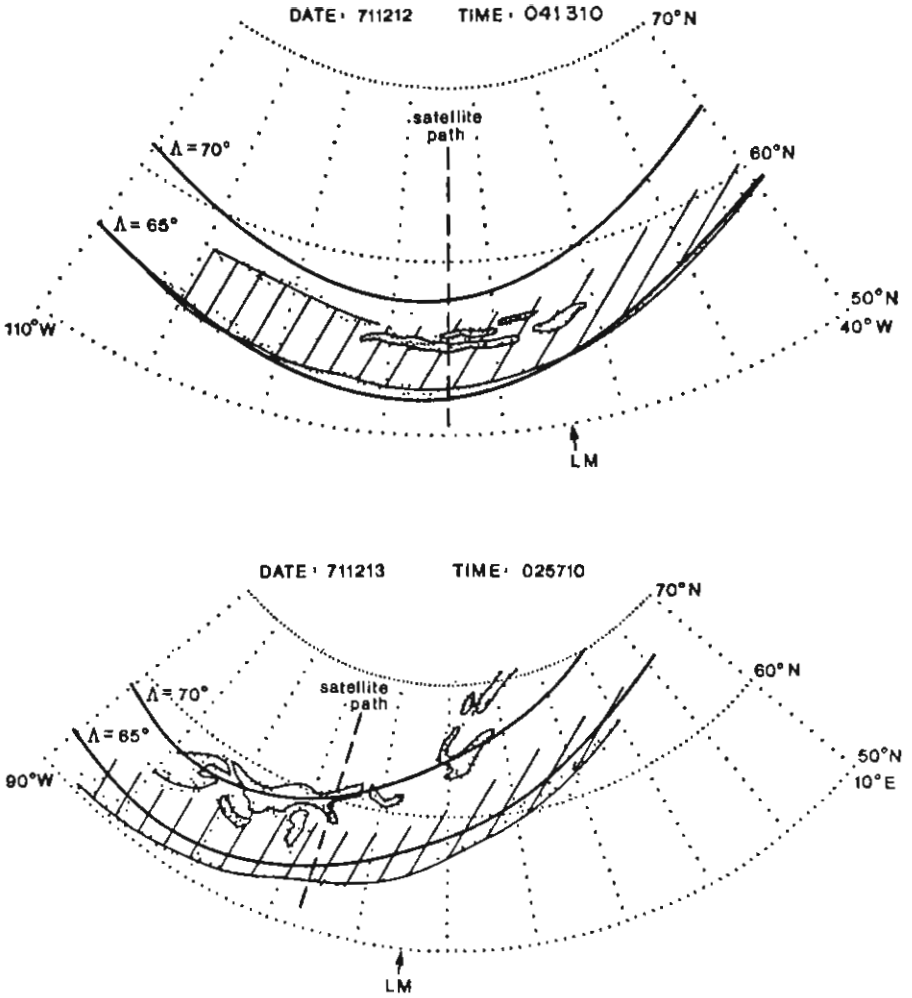


Figure 152. A corresponding set of transformations into Polar Geographic coordinates for the composite pictures shown in Figure 151. Local midnight is indicated by an arrow marked LM. Invariant latitudes 65° and 70° at the 100 km level are also shown. The diffuse auroral belt is indicated by shading. The poleward boundary of the diffuse belt is sometimes not drawn when it is not clearly indicated by the corresponding composite pictures. (*Lui and Anger 1973*)

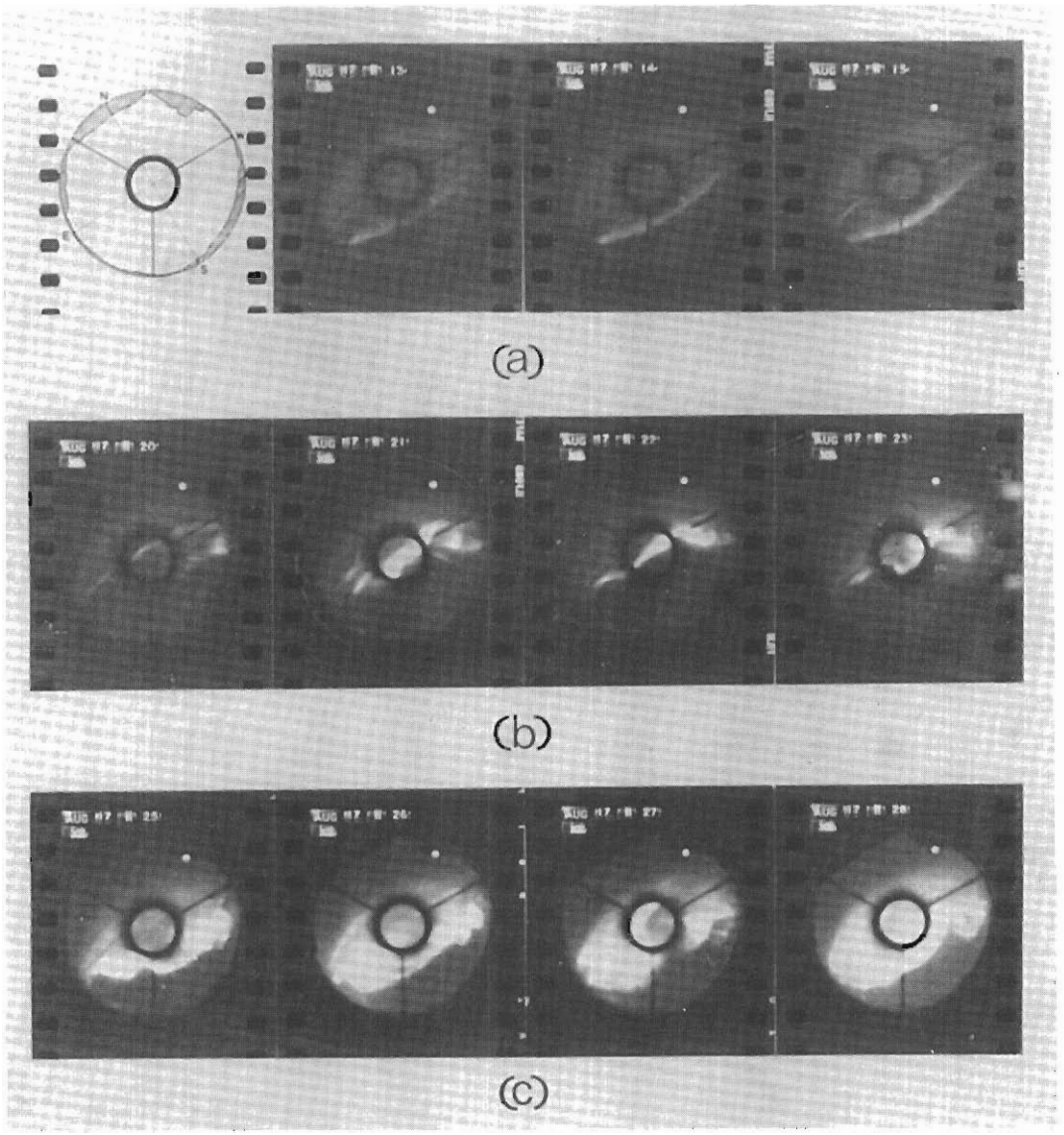


Figure 153. (a) A diagram of the all-sky camera field of view at Macquarie Island. The centre circle separates the (zenith filler) lens field from the larger field of the concave mirror of the SCAR 35 mm all-sky camera. The photographs show the quiet arc situation from 1113 to 1115 UT; (b) The equatorwards movement and the auroral break-up surge at 1123 UT; (c) Continuation of the auroral break–up surge and polewards movement 1125 to 1128 UT. On all pictures diffuse aurora can be seen equatorwards of the distinct auroral forms. *(Bond et al. 1973)*

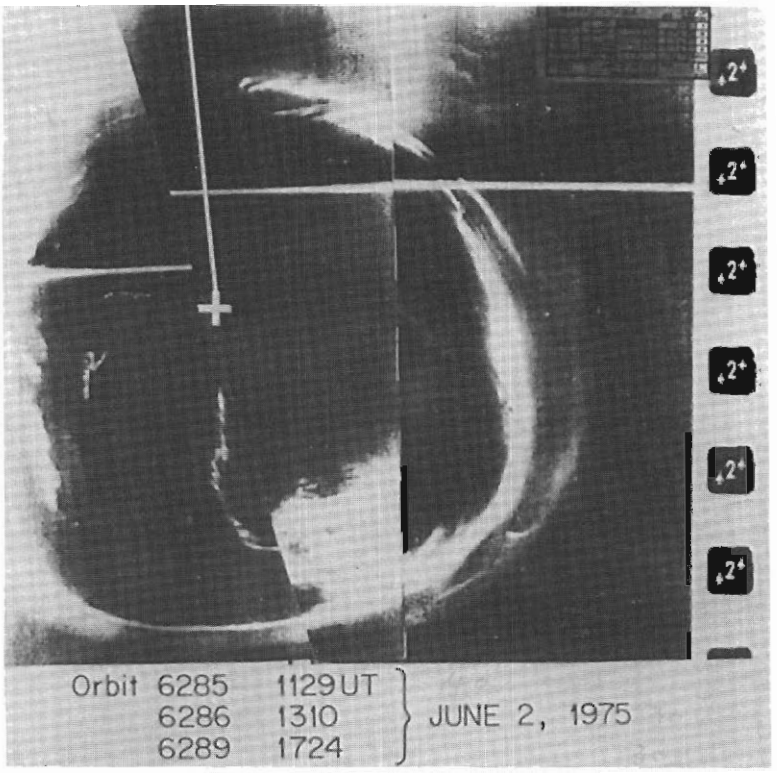


Figure 154. A montage photograph taken from three orbits of a DMSP satellite on 2 June 1975. (*Akasofu 1976*)

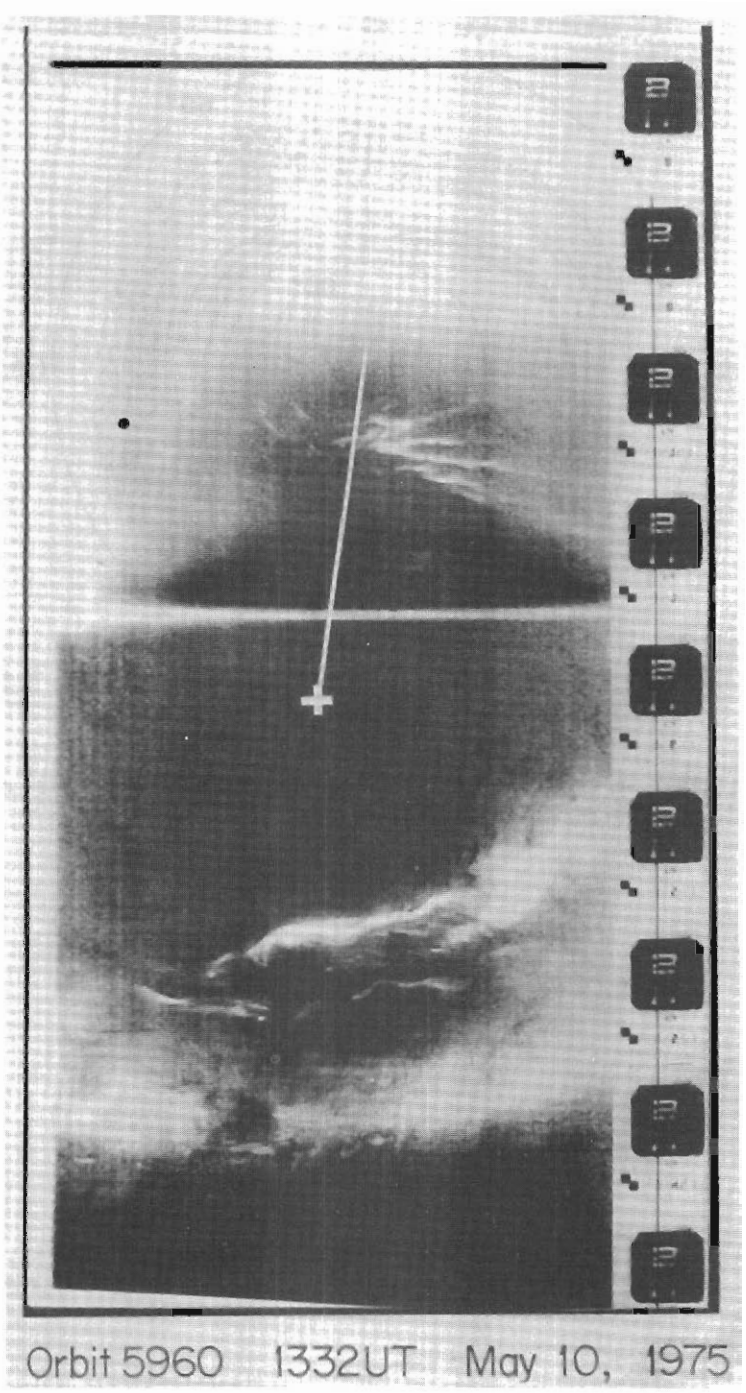


Figure 155. A single orbit photograph taken on 10 May 1975. (*Akasofu 1976*)

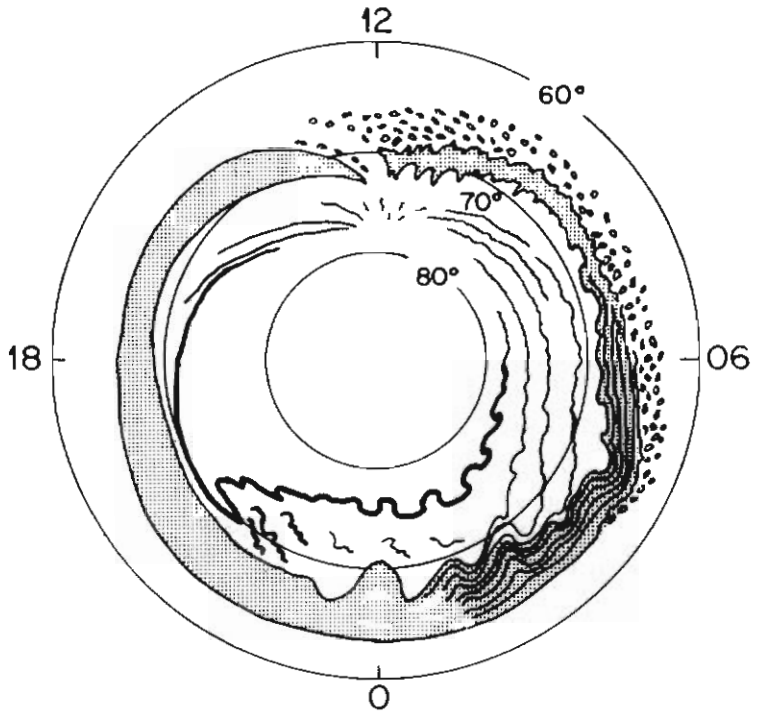


Figure 156. Diagram of the main characteristics of auroral displays. Discrete arcs are indicated by lines and the diffuse auroral regions are shaded. (*Akasofu 1976*)

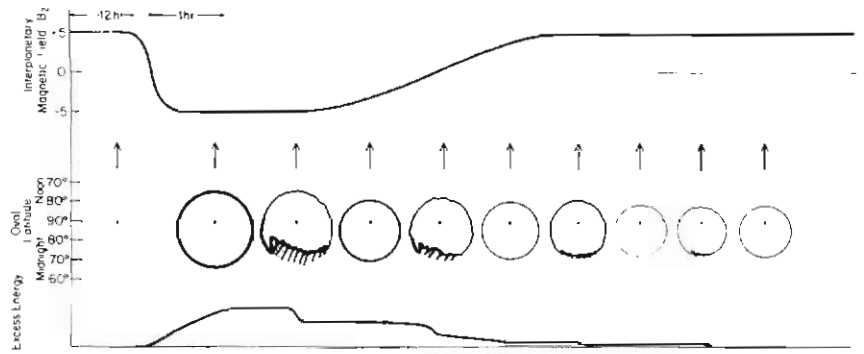


Figure 157. Hypothetical change of the $B_z$ component of the IMF and the resulting changes of the auroral oval, substorm activity and the amount of energy available for substorms, which is accumulated in the magnetotail. (*Akasofu 1976*)

Plate 1. Homogeneous arc; rayed arc at left. (*Photograph by D.D. Parer, Antarctic Division, taken at Mawson in 1970.*)

Plate 2. Rayed bands. (*Photograph by D.D. Parer, Antarctic Division, taken at Mawson in 1970.*)

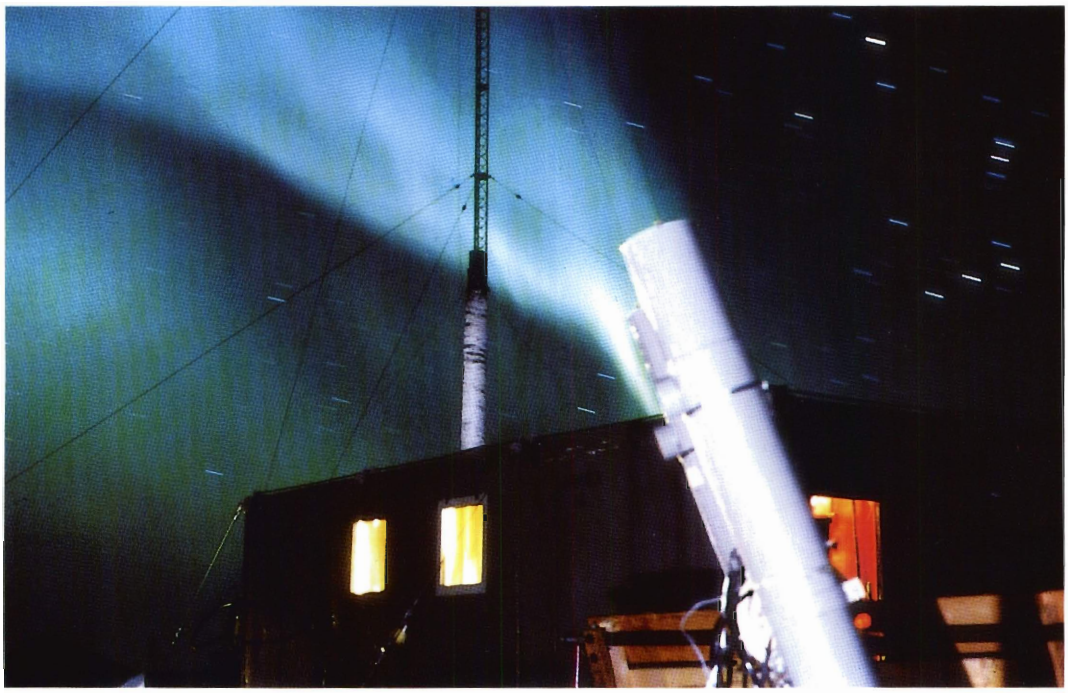

Plate 3. Rayed band with twin photomultiplier photometer in foreground. (*Photograph by I.L. Thomas, Antarctic Division, taken at Mawson in 1967.*)

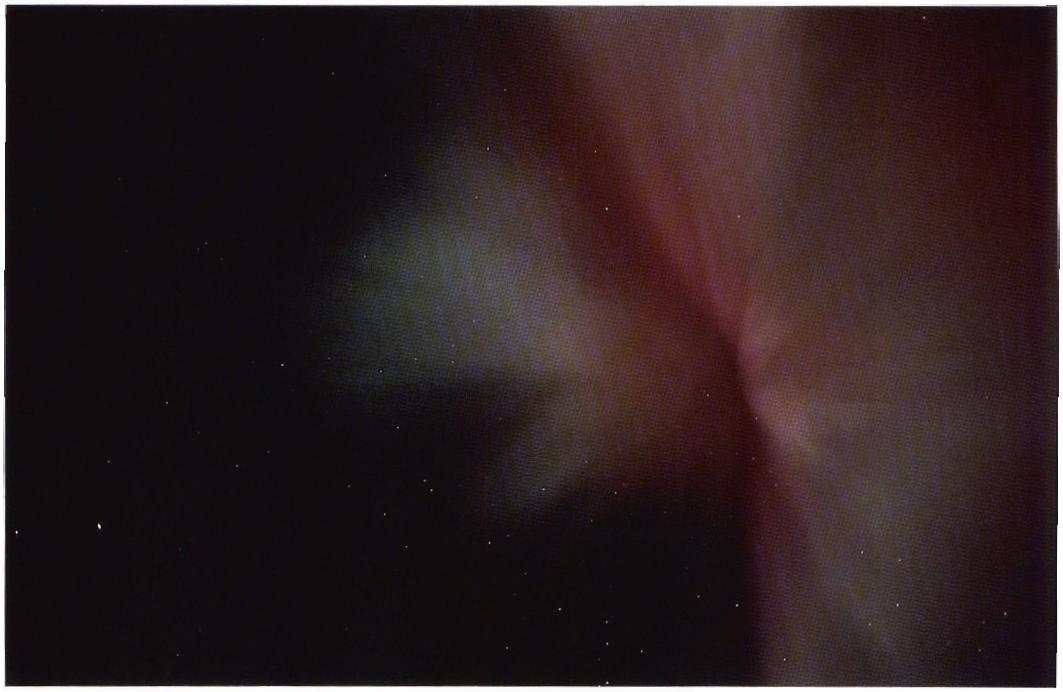

Plate 4. An auroral corona or crown.

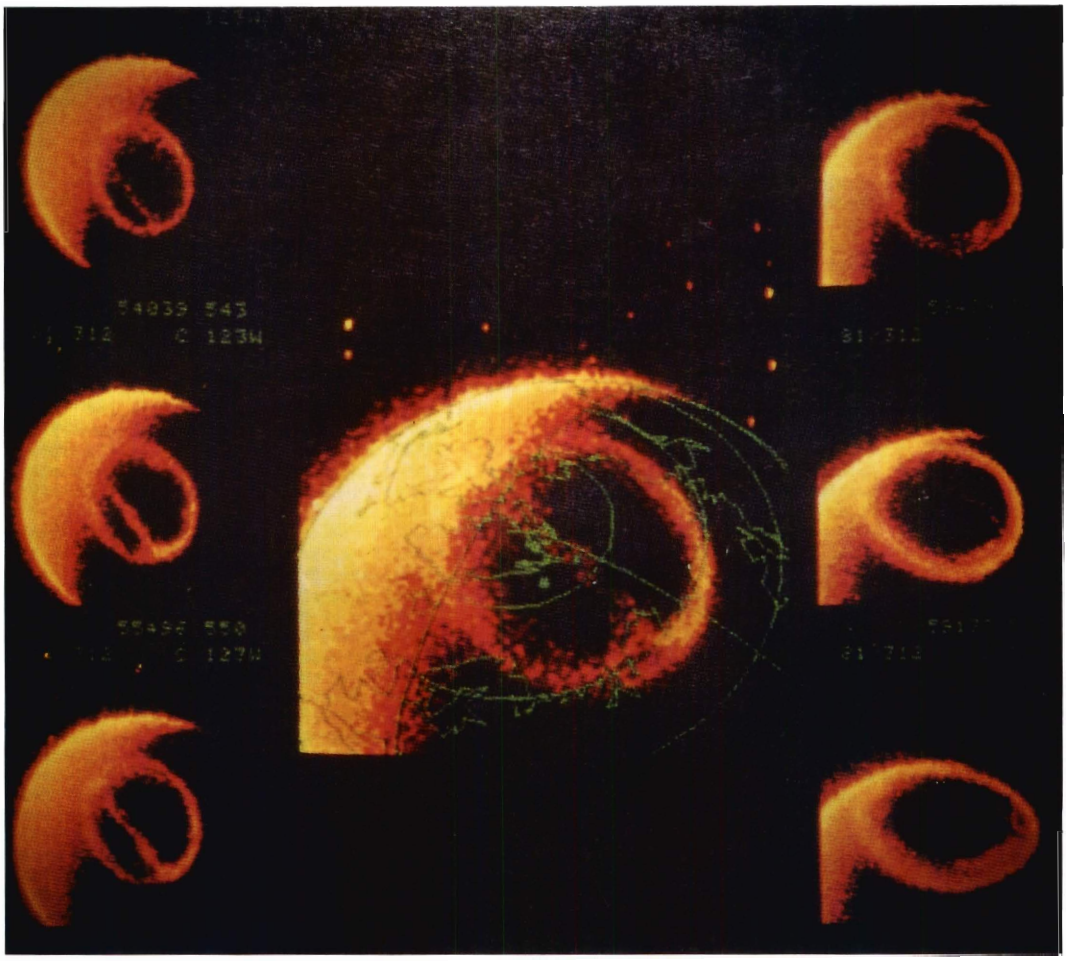

Plate 5. Sequence of images of Northern Hemisphere aurora for 8 November 1981 showing θ aurora due to OI emissions.

Plate 6. Southern Hemisphere aurora on 31 July 1986 taken from Dynamics Explorer DE1. The bright crescent on the right side of the image is the sunlit atmosphere. The aurora was photographed by a camera sensitive to ultraviolet light from oxygen atoms. The image is presented in false colour from an altitude of 21 000 km above a point near Macquarie Island. Note the distortion due to perspective.

# Post scriptum

This book has dealt mainly with the first stage of scientific enquiry, the problem of describing the phenomenon accurately. The next stage is the postulation of an hypothesis. In auroral physics many seemingly plausible hypotheses can apparently be justified by verbal argument. However, the crucial stage is the formulation of equations that describe the physical process and then "to put the numbers in". But the equations are often difficult to solve, and not all the numbers are known to the degree of accuracy required, so that a numerical solution may be unreliable.

Even while this book was being written, much progress has been made in our understanding of the aurora and the magnetosphere. It is hoped that this book has provided a background for further study.

By studying the behaviour of charged particles, electric fields and magnetic fields in the aurora and the magnetosphere, under conditions that are nearer to a vacuum than any vacuum that can yet be produced on Earth, scientists are slowly finding and confirming the basic physical processes that govern the interactions which take place in that vast vacuum. This information may prove to be of some importance in the search for a controlled hydrogen–helium–fusion reaction. As noted earlier, the physics of auroral processes has already been used in the USSR for generationg direct current electricity, which after conversion to alternating current has been fed into the Moscow electricity grid system.

The aurora is mankind's only visible marker of the interactions taking place in the vast and complicated region of the Earth's magnetosphere.

# Acknowledgments

I acknowledge with thanks the permission of Mr Rex Moncur, Director, Antarctic Division, to publish this work.

I am very grateful to all members of the Antarctic Division, past and present, who have made this work possible including Mr H. Burton (computing), Mr R. Reeves and Mrs J. Hosel (photography), Mrs A. Winslow (word processing) and Mr G.C. Moulton (drafting).

Drawings and photographs included in this book were reprinted by permission of: The Editor, Antarctic Journal of the United States, Division of Polar Programs, National Science Foundation, USA; Kluwer Academic Publishers, The Netherlands; American Institute of Physics, USA (for *Journal of Applied Physics 28,* 1388-1397); National Institute of Polar Research, Japan; CSIRO, Australia (*Australian Journal of Physics*); Bureau of Mineral Resources, Geology and Geophysics, Australia; The Editor, Munksgaard International Publishers Ltd (*Tellus 16*, 252-267; *10*, 104-116; *7*, 65-85); General Manager, Australian Surveying and Land Information Group, Department of Administrative Services, Canberra, ACT, Australia; Dr K. Lassen, Danish Meteorological Institute, Denmark; Macmillan Magazines Ltd, UK (*Nature 184*, 1375-1377 c 1959 Macmillan Magazines Ltd; University of Calgary, Canada (*Solar Terrestrial Relations*); Pergamon Press PLC, UK (*Journal of Atmospheric and Terrestrial Physics 25*, 163-163 c 1963; *27*, 1275-1305 c 1965; *Planetary and Space Science 15*, 209-229 c 1967; *12*, 273-282 c 1964; *21*, 1763-1773 c 1973; *23*, 887-890 c 1975; *21*, 799-809; American Geophysical Union, USA (*EOS. Transactions of AGU 57*, 997; *Reviews of Geophysics and Space Physics 15*, 285-298; *Geomagnetism and Aeronomy 3*, 183-192; *11*, 872-876; *Journal of Geophysical Research 72*, 3518-3521; *70*, 5793-5805; *69*, 3531-3569; *65*, 93-106; *70*, 3605-3628; *76*, 6700-6716: *76*, 7552-7565; *80*, 523-534; *76*, 5202-5219; *75*, 7032-7047; *73*,943-959; *82*, 5521-5528; *78*, 7543-7547) and L.A. Frank and J.D. Craven, The University of Iowa, USA.

# Appendix I. Papers by F.R. Bond


Bond, F.R. (1959). Motion of the aurora and magnetic bays. Part I: Observations. *Antarctic Symposium, Buenos Aires.*

Bond, F.R. (1960). Motion of the aurora and magnetic bays. *Australian Journal of Physics 13*(3), 477.

Bond, F.R. (1960). A preliminary account of the auroral display of 15 July 1959 as recorded in Australia and at ANARE stations. Symposium on the July 1959 events and associated phenomena. *IUGGI Monograph Number 7.* Pp. 115-126.

Bond, F.R. (1964). Auroral rays. *Nature 203*(4951), 1275-1276.

Bond, F.R. (1967). Auroral poles. *Australian Journal of Physics 20*, 743-746.

Bond, F.R. (1968). Magnetic and auroral conjugacy. *Annales de Geophysique 24*(2), 1-7.

Bond, F.R. (1969). Auroral morphological similarities at two magnetically conjugate stations: Buckles Bay and Kotzebue. *Australian Journal of Physics 22*, 421-433.

Bond, F.R. (1973). A possible explanation of the auroral substorm process. In: L.R. Alldvedge (Ed.). *Program and abstracts for the Second General Scientific Assembly-Kyoto 1973. IAGA Bulletin 34*, 442.

Bond, F.R. (1980). Auroral precipitation and atmosphere vorticity at the 500 mb level. *Journal of Planetary and Space Science 28*, 419.

Bond, F.R. (1980). Physicists in society. *The Australian Physicist 17*, 95.

Bond, F.R. and Akasofu, S.-I. (1979). Comparison of auroral ovals from all-sky camera studies and from satellite photographs. *Planetary and Space Science 27*, 541-549.

Bond, F.R. and Jacka, F. (1959). Location of the southern auroral zone. *Antarctic Symposium, Buenos Aires.*

Bond, F.R. and Jacka, F. (1960). Distribution of auroras in the southern hemisphere. *Australian Journal of Physics 13*(3), 610.

Bond, F.R. and Jacka, F. (1962). Distribution of auroras in the southern hemisphere. II. Nightly probability of overhead aurora. *Australian Journal of Physics 15*(2), 261-272.

Bond, F.R. and Jacka, F. (1963). Distribution of auroras in the southern hemisphere. III. Comparison with northern hemisphere. *Australian Journal of Physics 16*(4), 514-519.

Bond, F.R. and Paine, R.L. (1971). Geographical maps of the auroral ovals for different levels of geomagnetic disturbance. *Antarctic Division Technical Note Number 7.* Antarctic Division, Melbourne. 56 pp.

Bond, F.R. and Thomas, I.L. (1971). The southern auroral oval. *Australian Journal of Physics 24*, 97-102.

Bond, F.R., Stracey, M.R. and Retallack, D.S. (1976). Auroral surges in Southern Hemisphere. *Planetary and Space Science 24*, 611-612.

Bond, F.R., Sulzberger, P.H. and Thelander, H.A. (1973). Electron counts in the neutral sheet and magnetic variations at a geomagnetic longitude associated ground station. *Planetary and Space Science 21*, 2013-2025.

Burns, G.B., Bond, F.R. and Cole, K.D. (1980). An investigation of the southern hemisphere vorticity response to solar sector boundary crossings. *Journal of Atmospheric and Terrestrial Physics 42*, 765-769.

Cole, K.D. and Bond, F.R. (1961). Criticism of the theory of magnetic bays of Bless, Gartlein, Kimball, and Sprague. *Journal of Geophysical Research 66*(1), 327.

Cole, K.D., Bond, F.R., Raspopov, O.M., Sverdlov, Yu.L. and Voloshinov, N.N. (1979). Radar exploration of the ionosphere in the dayside cusp. *Antarctic Division Technical Memorandum Number 90*. Antarctic Division, Melbourne. 9 pp.

Denholm, J.V. and Bond, F.R. (1961). Orientation of polar auroras. *Australian Journal of Physics 14*(1), 193-195.

Jacka, F. and Bond, F.R. (1967). Optical auroral morphology. *Symposium Birkeland, September 1967*. 7 pp.

McGregor, P.M., Bond, F.R. and Parkinson, W.D. (1985). Rossbank revisited. *Search 16*(5-6), 152-156.

Paine, R.L. and Bond, F.R. (1972). Relationship of wideband VLF hiss to the auroral oval. *Antarctic Division Technical Note Number 8*. Antarctic Division, Melbourne.

Schmidt-Harms C.A. and Bond F.R. (1982). Dip-pole movements and magnetic reversals. *Antarctic Division Technical Memorandum Number 101*. Antarctic Division, Kingston. 19 pp.

Stubbs, L.C., Boyd, J.S. and Bond, F.R. (1983). Measurement of the OH rotational temperature at Mawson, East Antarctica. *Planetary and Space Science 31*(8),923-932.

Thomas, I.L. and Bond, F.R. (1977). An empirical equation for the austral auroral oval. *Geophysical Research Letters 4*(10),411-412.

Thomas, I.L. and Bond, F.R. (1978). A spherical harmonic analysis of the austral auroral oval. *Planetary and Space Science 26*,691-695.

# References


Abbott, F. (1863). On atmospheric electricity: its effects on various kinds of matter, with especial reference to the condition of auroras and thunder storms. *Proceedings of the Royal Society of Tasmania.* Supplement to Vol. III.

Akasofu, S.-I. (1961). Thickness of an active auroral curtain. *Journal of Atmospheric and Terrestrial Physics 21,* 287–288.

Akasofu, S.-I. (1963). The auroral rays. *Journal of Atmospheric and Terrestrial Physics 25,* 163–165.

Akasofu, S.-I. (1964). The development of the auroral substorm. *Planetary Space Science 12,* 273–282.

Akasofu, S.-I. (1965). Dynamic morphology of auroras. *Space Science Review 4,* 498–540.

Akasofu, S.-I. (1976). Recent progress in studies of DMSP auroral photographs. *Space Science Review 19,* 169–215.

Akasofu, S.-I. (1968). *Polar and magnetospheric substorms.* D. Reidel, Dordrecht, Holland.

Akasofu, S.-I. and Chapman, S. (1961). The ring current, geomagnetic disturbance, and the Van Allen Radiation Belts. *Journal of Geophysical Research 66,* 1321–1350.

Akasofu, S.-I., Chapman, S. and Meng, C.-I. (1965). The polar electrojet. *Journal of Atmospheric and Terrestrial Physics 27,* 1275–1305.

Akasofu, S.-I., Hones, E.W., Jnr., Montgomery, M.D., Bame, S.T. and Singer, S. (1971). Association of magnetotail phenomena with visible auroral features. *Journal of Geophysical Research 76,* 5985.

Alfven, H. (1955). On the electric field theory of magnetic storms and aurorae. *Tellus 7,* 50.

Alfven, H. (1958). On the theory of magnetic storms and aurorae. *Tellus 10,* 104–116.

Alfven, H. and Fälthammar, C.-G. (1963). *Cosmical electrodynamics.* Oxford University Press. 228 pp.

Anger, C.D. and Lui, A.T.Y. (1973). A global view at the polar region on 18 Dec. 1971. *Planetary and Space Science 21,* 873–878.

Anon. (1981). MHD* – cheaper, cleaner power for the Soviet Union. *New Scientist, 90*(1256), 622.

Arnoldy, R.L. (1971). Signature in the interplanetary medium for substorms. *Journal of Geophysical Research 76,* 5189–5201.

Arnoldy, R.L. (1974). Auroral particle precipitation and Birkeland currents. *Review of Geophysics and Space Physics 12,* 217–231.

Barbier, D. (1958). L'activité aurorale aux basses latitudes. *Annales Geophysicae 14,* 334–355.

Bartels, J. (1938). Potsdamer erdmagnetische Kennziffern. 1. Mitteilung. *Zeitschrift für Geophysik 14,* 68–78.

Bartels, J. (1949). The standardized index, Ks, and the planetary index, Kp. *IATME Bulletin No. 126 Geomagnetic Indices, K and C, 1948.* pp. 97-120.

Beard, D.B. (1960). The interaction of the terrestrial magnetic field with the solar corpuscular radiation. *Journal of Geophysical Research 65,* 3559.

Belon, A.E., Mather, K.B. and Glass, N.W. (1967). The conjugacy of visual aurorae. *Antarctic Journal of the United States 2,* 124–127.

Biermann, L. (1951). Comets' tails and solar corpuscular radiation. *Zeitschrift für Astrophysik 29,* 274.

Biermann, L. (1952). The tail of Halley's comet in 1910. *Zeitschrift für Naturforschung 7a,* 127.

Biermann, L. (1957). Solar corpuscular radiation and the interplanetary gas. *Observatory 77*, 109–110.

Birkeland, K. (1901). Expédition Norvégienne de 1899-1900. Résultats magnétiques. *Vidensk. Skrifter, I. Mat. naturv. Kl.* pp. 1-80.

Birkeland, K. (1908). On the cause of magnetic storms and the origin of terrestrial magnetism. *Norwegian Aurora Polaris Expedition 1902-3 1*(1-2)1-801. Christiania, H. Aschenboug and Co, 1908 and 1913.

Block, L. (1955). Model experiments on aurorae and magnetic storms. *Tellus 1*, 65–85.

Boller, W. (1898). Das Sudlicht. *Gerlands Beiträge zur Geophysik 3*, 550–557.

Bond, F.R. (1960a). Motion of the auroral and magnetic bays. *Australian Journal of Physics 13*, 477–483.

Bond, F.R. (1960b). A preliminary acount of the auroral display of 15 July 1959 as recorded in Australia and at ANARE stations. *IUGG Monograph Number 7*, Helsinki, July 1960. pp. 115–126.

Bond, F.R. (1968). Magnetic and auroral conjugacy. *Annales de Géophysique 24*, 459–465.

Bond, F.R. (1969). Auroral morphological similarities at two magnetically conjugate stations, Buckles Bay and Kotzebue. *Australian Journal of Physics 22*, 421–433. Paper read at the Inter-Union Symposium on Solar Terrestrial Physics, Belgrade, 1966.

Bond, F.R. and Cole, K.D. (1959). *Motion of the aurora and magnetic bays.* Paper presented at the Antarctic Symposium, Buenos Aires, November 1959.

Bond, F.R. and Jacka, F. (1960). Distribution of auroras in the Southern Hemisphere. *Australian Journal of Physics 13*, 610–612.

Bond, F.R. and Jacka, F. (1962). Distribution of auroras in the Southern Hemisphere. *Australian Journal of Physics 15*, 261–272.

Bond, F.R. and Jacka, F. (1963). Distribution of auroras in the Southern Hemisphere. III. Comparison with Northern Hemisphere. *Australian Journal of Physics 16*, 514–519.

Bond, F.R. and Paine, R.L. (1971). Geographical maps of the auroral ovals for different levels of geomagnetic disturbance. *Antarctic Division Technical Note Number 7.* Melbourne.

Bond, F.R. and Thomas, I.L. (1971). The southern auroral oval. *Australian Journal of Physics 24*, 97–102.

Bond, F.R., Sulzberger, P.H. and Thelander, H.A. (1973). Electron counts in the neutral sheet and magnetic variations at a geomagnetic longitude associated ground station. *Planetary and Space Science 21*, 2013–2025.

Boström, R. (1964). A model of the auroral electrojets. *Journal of Geophysical Research 69*, 4983–4999.

Boyd, J.S. (1977). Invariant geomagnetic coordinates for Epoch 1977.25. *Planetary and Space Science 25*, 411–414.

Briggs, B.R. and Spreiter, J.R. (1963). Theoretical determination of the boundary and distortion of the geomagnetic field in a steady state solar wind. *NASA TR R–178.*

Bruche, E. (1931). Some new theoretical and experimental results on the Aurora Polaris. *Terrestrial Magnetics 36*, 41–52.

Burns, G.B. Bond, F.R. *and* Cole, K.D. (1980). An investigation of the southern hemisphere vorticity response to solar sector boundary crossings. *Journal of Atmospheric and Terrestrial Physics 42*,756.

Campbell, W.H. and Matsushita, S. (1967). World maps of conjugate coordinates and L contours. *Journal of Geophysical Research 72*, 3518–3521.

Casserly Jr., R.T. and Cloutier, P.A. (1975). Rocket-based magnetic observations of auroral Birkeland currents in association with a structured auroral arc. *Journal of Geophysical Research 80*, 2165–2171.

Chapman, S. (1935). The electric current-system of magnetic storms. *Terrestrial Magnetics 40*, 349–370.

Chapman, S. (1953). Polar and tropical aurora and the isoauroral diagram. *Proceedings of the Indian Academy of Science 37*(2) Second A.

Chapman, S. (1954). *Ap. J. 120*:151.

Chapman, S. and Bartels, J. (1940). *Geomagnetism* Vol. II. Clarendon Press, Oxford.

Chapman, S. and Ferraro, V.C.A. (1932). A new theory of magnetic storms. *Nature* 126, 129, 130; *Terrestrial Magnetics* (1931), *36*, 77–97; *Terrestrial Magnetics* (1932), 37, 269.

Choe, J.Y. and Beard, D.B. (1974a). The compressed geomagnetic field as a function of dipole tilt. *Planetary and Space Science 22*, 595–608.

Choe, J.Y. and Beard, D.B. (1974b). The near Earth magnetic field of the magnetotail current. *Planetary and Space Science 22*, 609–615.

Choe, J.Y., Beard, D.B. and Sullivan, E.C. (1973). Precise calculation of the magnetosphere surface for a tilted dipole. *Planetary and Space Science 21*, 485–498.

Cole, K.D. (1963). Eccentric dipole coordinates. *Australian Journal of Physics 16*. 423–429.

Cole, K.D. (1965). Stable auroral red arcs, sinks for energy of the Dst main phase. *Journal of Geophysical Research 70*, 1689–1706.

Davies, F.T. (1930). Observations of the Aurora Australis, Byrd Antarctic Expedition 1929. *Terrestrial Magnetics 36*, 199–230.

Davis, Jnr. L.D. and Beard, D.B. (1962). A correction to the approximate condition for locating the boundary between a magnetic field and a plasma. *Journal of Geophysical Research 67*, 4505–4507.

Davis, T.N. (1962a). Auroral displays of 1957–1958, detailed analyses of Alaska data and analyses of high latitude data. *Journal of Geophysical Research 67*(1), 75-110.

Davis, T.N. (1962b). The morphology of the auroral displays of 1957–1958. *Journal of Geophysical Research 67*, 59–74.

Davis, T.N. and Sugiura, M. (1966). The auroral electrojet activity index AE and its universal time variations. *Journal of Geophysical Research 71*, 785–801.

De Witt, R.D. (1962). The occurrence of aurora in geomagnetically conjugate areas. *Journal of Geophysical Research 67*, 1347.

Denholm, J.V. (1961). Some observations inside the southern auroral zone. *Journal of Geophysical Research 66*, 2105–2111.

Denholm, J.V. and Bond, F.R. (1961). Orientation of polar auroras. *Australian Journal of Physics 14*, 193–195.

Dungey, J.W. (1961). Interplanetary magnetic field and the auroral zones. *Physical Review Letters 6*, 47–48.

Dungey, J.W. (1963). *Solar Terrestrial Physics*. p. 444.

Eather, R.H. (1964). The Antarctic aurora. *Australian Photography* (December).

Eather, R.H. and Jacka, F. (1966). Auroral hydrogen emission. *Australian Journal of Physics 19*, 241–274.

Eather, R.H. and Sandford, B.P. (1966). The zone of hydrogen emission in the night sky. *Australian Journal of Physics 19*, 25–33.

Eather, R.H., Mende, S.B. and Judge, R.J.R. (1976). Plasma injection at synchronous orbit and spatial and temporal auroral morphology. *Journal of Geophysical Research 81*, 2805–2824.

Elvey, C.T. (1957). Problems of auroral morphology. *Proceedings of the National Academy for Science, Washington 43*, 63–75.

Evans, D.S. (1969). Fine structure in the energy spectrum of low energy auroral electrons. In: B.M. McCormac and A. Omholt (Eds). *Atmospheric emissions*. Van Nostrand Reinhold, New York. pp. 107–118.

Evans, J.E., Newkirk, L.L. and McCormac, B.M. (1969). *North polar, south polar, world maps and tables of invariant magnetic coordinates for six altitudes: 0, 100, 300, 600, 1000 and 3000 km.* Lockheed Palo Alto Research Laboratory. DASA 2347 October.

Fairfield, D.H. (1971). Average and unusual locations of the Earth's magnetopause and bow shock. *Journal of Geophysical Research 76*, 6700–6716.

Fairfield, D.H. (1977). Electric and magnetic fields in the high-latitude magnetosphere. *Reviews of Geophysics and Space Physics 15*, 285–298.

Fairfield, D.H. and Ness, N.F. (1970). Configurations of the geomagnetic tail during substorms. *Journal of Geophysical Research 75*, 7032–7047.

Fel'dstein, Ya.I. (1960). Geographical distribution of auroras and azimuth of arcs. *Investigations of the aurora 4*, 61–77. Academy Science USSR, Moscow (in Russian).

Fel'dstein, Ya.I. (1963). Some problems concerning the morphology of auroras and magnetic disturbances at high latitudes. *Geomagnetism and Aeronomy 3*, 183–192 (English translation).

Fel'dstein, Ya. I. (1964). Auroral morphology. I. The location of the auroral zone. *Tellus 16*, 252–267.

Fel'dstein, Ya.I. and Starkov, G.V. (1967). Dynamics of auroral belt and polar geomagnetic disturbances. *Planetary and Space Science 15*, 209–229.

Fel'dstein, Ya.I., Starkov, G.V. and Zverov, V.A. (1974). Conjugacy of the auroral ovals. *Memoirs of National Institute of Polar Research Special Issue Number 3.*

Ferraro, V.C.A. (1952). On the theory of the first phase of the geomagnetic storm: a new illustrative calculation based on an idealised (plane not cylindrical) model field distribution. *Journal of Geophysical Research 57*, 15–49.

Finch, H.F. and Leaton, R.B. (1957). The Earth's main magnetic field – epoch 1955.0. *Monthly Notices of the Royal Astronomical Society Geophysical Supplement 7*(6),314-317

Frank, L.A. (1971). Plasma in the Earth's polar magnetosphere. *Journal of Geophysical Research 76*, 5202–5219.

Frank, L.A. and Ackerson, K.L. (1971). Observations of charged particle precipitation into the auroral zone. *Journal of Geophysical Research 76*, 3612–3643.

Frank, L.A., Craven, J.D., Ackerson, K.L., English, M.R., Eather, R.H. and Carovillano, R.L. (1981). Global auroral imaging instrumentation for the Dynamics Explore Mission. *Space Science Instrumentation 5*:369.

Frank, L.A., Craven, J.D., Burch, J.L. and Winningham, J.D. (1982). Polar views of the Earth's aurora with Dynamics Explorer. *Geophysical Research Letters 9*(9), 1001-1004.

Fritz, H. (1881). *Das Polarlicht.* Leipzig.

Fukushima, N. (1953). Polar magnetic storms and geomagnetic bays. *Journal of the Faculty of Science, Tokyo University 8*, 293.

Gadsden, D.M. (1959). Studies of the upper atmosphere from Invercargill, New Zealand. Part II. Correlation of the radar echoes and magnetic activity. *Annales de Géophysique 15*, 395–402.

Gartlein, C.W. and Sprague, G. (1959). Auroral occurrence. In: WDC-A report on IGY visual auroral observations. *IGY General Report 12*, 68–72.

Gauss, C.F. (1838). Allgemeine Theorie des Erdmagnetismus. In: *Resultate magn. Verein.* Reprinted in *Werke* 5, 121–193.

Gellibrand, H. (1635). *A discourse mathematical on the variation of the magneticall needle*, London. (Republished in facsimile by G. Hellmann, Neudrucke von Schriften und Karten über Meteorologie und Erdmagnetismus. No. 9).

Gilbert, W. (1600). *De Magnete* (Gilbert Club revised English translation) Chiswick Press, London, 1900.

Hakura, Y. (1965). Tables and maps of geomagnetic coordinates corrected by the higher order spherical harmonic terms. *Report of Ionosphere and Space Research in Japan 19*, 121–157.

Halderson, D.W., Beard, D.B. and Choe, J.Y. (1975). Corrections to 'The compressed geomagnetic field as a function of dipole tilt.' *Planetary and Space Science 23*, 887–890.

Hendricks, S.J. and Cain, J.C. (1966). Magnetic field data for trapped–particle evaluation. *Journal of Geophysical Research 71*, 346–347.

Hirshberg, J. and Colburn, D.S. (1969). Interplanetary field and geomagnetic variations: a unified view. *Planetary and Space Science 17*, 1183–1206.

Hock, R.J., Smith, L.L. and Clarke, K.C. (1971). 5577 (OI) and 4278($N_2$+) emissions in a SAR arc. *Journal of Geophysical Research 76*, 7663.

Hones, Jnr, E.W. (1973). Substorm phenomena in the distant magnetosphere. In: D. Venkateson (Ed.). *Solar terrestrial relations.* University of Calgary, Alberta, Canada.

Hones, Jnr, E.W., Asbridge, J.R. and Bame, S.J. (1970). Time-variations of the magnetotail plasma sheet at 18 $R_E$ determined from concurrent observations by a pair of Vela satellites. Los Alamos Scientific Laboratory, University of California, Los Alamos LA-DC-12176 (Reprint).

Hones, Jnr, E.J. (1979). Solar-wind–magnetosphere–ionosphere coupling. In: B.M. McCormac and T.A. Seliga. (Eds). *Solar-terrestrial influences on weather and climate.* D. Reidel, Dordrecht-Holland. pp. 83–99.

Hultqvist, B. (1958). The geomagnetic field lines in higher approximation. *Arkiv för Geofysik 3*, 63–77.

Hultqvist, B. (1959). Auroral isochasms. *Nature 184*, 1478–1479.

Hultqvist, B. (1974). Rocket and satellite observations of energetic particle precipitation in relation to optical aurora. *Annales Geophysicae 30*, 223–258.

Hunten, D.M., Roach, F.E. and Chamberlain, J.W. (1956). A photometric unit for the airglow and aurora. *Journal of Atmospheric and Terrestrial Physics 8*, 345–346.

Iijima, T. and Potemra, T.A. (1976a). The amplitude distribution of field-aligned currents at northern high latitudes observed by Triad. *Journal of Geophysical Research 81*, 2165–2174.

Iijima, T. and Potemra, T.A. (1976b). Field-aligned currents in the day-side cusp observed by Triad. *Journal of Geophysical Research 81*, 5971–5979.

Iijima, T. and Potemra, T.A. (1978). Large scale characteristics of field-aligned currents associated with substorms. *Journal of Geophysical Research 83*, 599–615.

Inouye, M. and Lomax, H. (1962). *Comparison of experimental and numerical results for the flow of a perfect gas about blunt-nosed bodies.* NASA TN D–1426.

Jacka, F. (1953). The southern auroral zone as defined by the position of homogenous arcs. *Australian Journal of Physics 6*, 219–228.

Jacka, F. and Bond, F.R. (1968). Optical auroral morphology. *Annales de Géophysique 24*, 547–553.

Jackson, J.D. (1962). *Classical electrodynamics.* John Wiley & Sons, Inc., New York.

Kamide, Y., Perreault, P.D., Akasofu, S.-I. and Winningham, J.D. (1977). Dependence of substorm occurrence probability on the interplanetary magnetic field and on the size of the auroral oval. *Journal of Geophysical Research 82*, 5521–5528.

Khorosheva, O.V. (1961). The space and time-distribution of auroras and their relationship with high-latitude geomagnetic disturbance. *Geomagnetism and Aeronomy 1*, 615–621 (English translation).

Kilfoyle, B.P. and Jacka, F. (1968). Geomagnetic L coordinates. *Nature 220*, 773–775.

Larsen, M.F. *and* Kelley, M.C. (1977). A study of an observed and forecasted meteorogical index and its relation to the interplanetary magnetic field. *Geophysical Research Letters 4*:337.

Lassen, K. (1959). Existence of an inner auroral zone. *Nature 184*, 1375–1377.
Lezniack, T.W. and Winkler, J.R. (1970). Experimental study of magnetospheric motions and acceleration of energetic particles during substorms. *Journal of Geophysical Research 75*, 7075–7098.
Lindemann, F.A. (1919). Note on the theory of magnetic storms. *Philosphical Magazine 38*, 669–684.
Lui, A.T.Y. and Anger, C.D. (1973). A uniform belt of diffuse auroral emission seen by the ISIS–2 scanning photometer. *Planetary and Space Science 21*, 799–809.
Lyatskiy, V.B. and Mal'tsev, Yu P. (1971). Shock wave in the tail of the magnetosphere as the reason for the active phase of a magnetospheric substorm. *Geomagnetism and Aeronomy 11*, 872–876.
Malfors, K.G. (1946). Experiments on the aurorae. *Archives for Mathematical Astronomy and Physics 34B*(1).
Mawson, D. and Chree, C. (1925). Records of the Aurora Polaris Australasian Antarctic Expedition 1911–1914, Science Report B Vol. 2, Magnetism and aurora. Sydney, A.J. Kent, Government Printer.
Mayaud, P.N. (1960). Un nouveau systeme de coordonnees magnétiques pour l'étude de la haute atmosphére: les coordonnees de l'anneau equatorial. *Annales de Géophysique 16*, 278–288.
McDiarmid, I.B. and Burrows, J.R. (1964). Diurnal intensity variations in the outer radiation zone at 1000 km. *Canadian Journal of Physics 42*, 1135–1148.
McDiarmid, I.B., Burrows, J.R. and Budzinski, E.E. (1975). Average characteristics of magnetospheric electrons (150 ev to 200 keV) at 1400 km. *Journal of Geophysical Research 80*, 73–79.
McDiarmid, I.B., Burrows, J.R. and Budzinski, E.E. (1976). Particle properties in the day side cleft. *Journal of Geophysical Research 81*, 221–226.
McIlwain, C.E. (1961). Coordinates for mapping the distribution of magnetically trapped particles. *Journal of Geophysical Research 66*, 3681–3691.
Mead, G.D. (1964). Deformation of the geomagnetic field by the solar wind. *Journal of Geophysical Research 69*, 1181–1195.
Mead, G.D. and Beard, D.B. (1964). Shape of the geomagnetic field solar wind boundary. *Journal of Geophysical Research 69*, 1169–1180.
Mead, G.D. and Fairfield, D.H. (1975). A quantitative magnetospheric model derived from space craft magnetometer data. *Journal of Geophysical Research 80*, 523–534.
Meng, C.-I. (1976). Simultaneous observations of low-energy electron precipitation and optical auroral arcs in the evening sector by DMSP 32 satellite. *Journal of Geophysical Research 81*, 2771–2785.
Mihalov, J.D., Colburn, D.S. and Sonnett, C.P. (1970). Observations of magnetopause geometry and waves at the lunar distance. *Planetary and Space Science 18*, 239–258.
Mihalov, J.D., Colburn, D.S., Currie, R.G. and Sonett, C.P. (1968). Configuration and reconnection in the geomagnetic tail. *Journal of Geophysical Research 73*, 943–959.
Montbriand, L.E. (1971). The proton aurora and auroral substorm. In: B.M. McCormac (Ed.). *The radiating atmosphere*. D. Reidel, Dordrecht, Holland. pp. 366–373.
Mozer, F.S. (1971). Origin and effects of electric fields during isolated magnetospheric substorms. *Journal of Geophysical Research 76*, 7595–7608.
Needham, J. (1962). *Science and civilization in China*, Vol. 4, Part 1, Sec. 26(c). Cambridge University Press, London. 230 pp.
Ness, N.F. (1969). The geomagnetic tail. *Reviews of Geophysics 7*(1,2), 97–127.

Ness, N.F., Searce, C.S. and Seek, J.B. (1964). Initial results of the IMP I magnetic field experiment. *Journal of Geophysical Research 69*, 3531–3569.
Northrop, T.G. and Teller, E. (1960). Stability of the adiabatic motion of charged particles in the Earth's field. *Physics Review 117*, 215–225.
O'Brien, B.J. (1961). Coordinates for mapping the distribution of magnetically trapped particles. *Journal of Geophysical Research 66*, 3681–3706.
O'Brien, B.J. (1962). Lifetimes of outer-zone electrons and their precipitation into the atmosphere. *Journal of Geophysical Research 67*, 3687–3706.
O'Brien, B.J., Van Allen, J.A., Roach, F.E. and Garlein, C.W. (1960). Correlation of an auroral arc and a sub-visible monochromatic 6300 A arc with outer-zone radiation on November 28, 1959. *Journal of Geophysical Research 65*, 2759–2766.
Oguti, T. (1973). Hydrogen emission and electron aurora at the onset of the auroral breakup. *Journal of Geophysical Research 78*, 7543–7547.
Olson, W.P. (1969). The shape of the tilted magnetopause. *Journal of Geophysical Research 74*, 5642–5651.
Parker, E.N. (1958). Dynamics of the interplanetary gas and magnetic fields. *Astrophysics Journal* 128, 664–676.
Parkinson, W.D. and Cleary, J. (1958). The eccentric geomagnetic dipole. *Geophysical Journal R.A.S. 1*, 346.
Piddington, J.H. (1960). Geomagnetic storm theory. *Journal of Geophysical Research 65*, 93–106.
Piddington, J.H. (1965). The magnetosphere and its environs. *Planetary and Space Science 13*, 363–376.
Rosenbauer, H., Grünwaldt, H., Montgomery, M.D., Pashmann, G. and Sckopke, N. (1975). Heos-2 plasma observations in the distant polar magnetosphere: the plasma mantle. *Journal of Geophysical Research 80*, 2723–2737.
Russell, C.T. and Dyer, E.R. (Eds) (1972). *Critical problems of magnetospheric physics.* IVCSTP Secretariat. National Academy of Sciences, Washington.
Rycroft, M.J. and Thomas, J.O. (1970). The magnetospheric plasma pause and the electron density trough at Alouette I orbit. *Planetary and Space Science 18*, 65–80.
Sabine, E. (1837). Contributions to terrestrial magnetism, No. 7: Containing a magnetic survey between 0° and 125°E and -20° and -70°S. *Philosophical Transactions, London 136*, 336–432.
Schaeffer, R.C. and Jacka, F. (1971). Stable auroral red arcs observed from Adelaide during 1967–69. *Journal of Atmospheric and Terrestrial Physics 33*, 237–250.
Schmidt, A. (1898). Der magnetische Zustand der Erde zur Epoche 1885.0. *Aus dem Afchiv der Deutschen Seewarte und des Marine Observatoriums 21*, No. 2 Hamburg.
Schmidt, A. (1918). Geomagnetische koordinaten. *Archiv des Erdmagnetismus Heft 3*, 14. Potsdam.
Schmidt, A. (1934). Der magnetische Mittelpunkt der Erde und seine Bedeutung. *Gerlands Beiträge z. Geophysik 41*, 346–358.
Schmidt, A. (1935). *Tafeln der normierten Kugelfunktionen, sowie Formeln zur Entwicklung.* Gotha, Engelhard-Reyer.
Schuster, A. (1911). On the origin of magnetic storms. *Proceedings of the Royal Society London 85*, 44–50.
Seaton, M.J. (1954). Excitation processed in the auroral and airglow. 2. Excitation of forbidden atomic lines in high latitude aurorae. *Journal of Atmospheric and Terrestrial Physics 4*, 295–313.

Silsbee, H.C. and Vestine, E.H. (1942). Geomagnetic bays, their frequency and current systems. *Terrestrial Magnetism and Electricity 47*, 195-208.

Smith, E.J., Tsurutani, B.T. and Rosenberg, R.L. (1976). Pioneer II observations of the interplanetary sector structure up to 16° heliographic latitude. (Abstract). *EOS Transactions, American Geophysical Union 57*, 997.

Snyder, Jnr, A.L. and Akasofu, S.-I. (1976). Auroral oval photographs from the DMSP 8531 and 10533 satellites. *Journal of Geophysical Research 81*, 1799–1806.

Spreiter, J.R. and Briggs, B.R. (1962). Theoretical determination of the form of the boundary of the solar corpuscular stream produced by interaction with the magnetic dipole field of the earth. *Journal of Geophysical Research 67*, 37-51.

Spreiter, J.R. and Jones, W.P. (1963). On the effect of a weak interplanetary magnetic field on the interaction between the solar wind and the geomagnetic field. *Journal of Geophysical Research 68*, 3555-3565.

Spreiter, J.R., Alksne, A.Y. and Summers, A.L. (1968). External aero-dynamics of the magnetosphere. In: R.L. Carovillano, J.F. McClay, H.R. Radoski (Eds). *Physics of the magnetosphere*. D. Reidel, Dordrecht–Holland. pp. 301–375.

Stoffregen, W. (Ed) (1962). IGY Ascaplots. *Annals of the International Geophysical Year 20*(1-2),1-307.

Størmer, C. (1913). On an auroral expedition to Bossekop in the spring of 1913. *Terrestrial Magnetism 18*, 133.

Størmer, C. (1913). Rapport sur une expédition d'aurores boréales á Bossekop et store korsnes pendant le printemps de l'année 1913. *Geofysiske Publikasjoner 1(5)*, Figure 17.

Størmer, C. (1942). Remarkable aurora forms from Southern Norway. III-IX. *Geofysiske Publikasjoner* Oslo *13(7)*. Plate 32, lowest two figures.

Størmer, C. (1955). *The polar aurora*. Oxford University Press. 403 pp.

Sugiura, M. and Heppner, J.P. (1965). The Earth's magnetic field. In: W.N. Hess (Ed.). *Introduction to space science*. Gordon and Breach, New York. p. 45.

Sugiura, M. and Poros, D.J. (1973). A magnetospheric field model incorporating the OGO 3 and 5 magnetic field observations. *Planetary and Space Science 21*, 1763–1773.

Sugiura, M., Ledley, B.G., Skilkman, T.L. and Heppner, J.P. (1971). Magnetospheric field distortions observed by OGO 3 and 5. *Journal of Geophysical Research 76*, 7552–7565.

Swift, D.W. (1981). Mechanisms for auroral precipitation: a review. *Review of Geophysics and Space Physics 19*, 185–211.

Taylor, H.E. and Hones, Jnr, E.W. (1965). Adiabatic motion of auroral particles in a model of the electric and magnetic fields surrounding the earth. *Journal of Geophysical Research 70*(15), 3605–3628.

Thomas, J.O. and Andrews, M.K. (1968). The transpolar exospheric plasma. 1. The plasmasphere termination. *Journal of Geophysical Research 73*, 7407–7417.

Thomas, J.O. and Andrews, M.K. (1969). The trans-polar exospheric plasma. 3: A unified picture. *Planetary and Space Science 17*, 433–446.

Van Allen, J.A. (1968). Particle description of the magnetosphere. In: R.L. Carovillano, J.F. McClay and H.R. Radoski (Eds). *Physics of the magnetosphere*. D. Reidel, Dordrecht Holland. pp. 147–217.

Vasyliunas, V.M. (1968). Low energy electrons in the magnetosphere as observed by OGO-a and OGO-3. In: R.L. Carovillano, J.F. McClay and H.R. Radoski (Eds). *Physics of the magnetosphere*. D. Reidel, Dordrecht Holland. pp. 622–640.

Vegard, L. (1939). *Nature 144*, 1089–1090.

Vegard, L. and Krogness, O. (1920). The position in space of the Aurora Polaris from observations made at the Haldde Observatory, 1913–14. *Geofysiske Publication* (1) Kristiania.

Vestine, E.H. (1938). Asymmetrical characteristics of the Earth's magnetic disturbance-field. *Terrestrial Magnetics 43*, 261–282.

Vestine, E.H. (1944). The geographic incidence of aurora and magnetic disturbance, North Hemisphere. *Terrestrial Magnetism and Atmospheric Electricity 49*, 77–102.

Vestine, E.H. and Sibley, W.L. (1960). The geomagnetic field in space, ring currents and auroral isochasms. *Journal of Geophysical Research 65*(7),1967–1979.

Vestine, E.H. and Snyder, E.J. (1945). The geographic incidence of aurora and magnetic disturbance, Southern Hemisphere. *Terrestrial Magnetism and Atmospheric Electricity 50*(2), 105–124.

Vestine, E.H., Lange, I., Laporte, L. and Scott, W.E. (1947). The geomagnetic field; its description and analysis. *Carnegie Institution of Washington Publication 580*. Washington DC.

Webster, H.F. (1957). Structure in magnetically confined electron beams. *Journal of Applied Physics 28*, 1388–1397.

Weill, G. (1958). Aspects de l'aurore observée à la base Dumont d'Urville en Terre Adélie. *Comptes rendus des Séances de l'Académie des Sciences (Paris) 246*, 2925–2927.

Wescott, E.M., Stenbaeck-Nielsen, H.C., Davis, T.N. and Peek, H.M. (1976). The Skylab barium plasma injection experiments. 1. Convection observations. *Journal of Geophysical Research 81*, 4487–4494.

Wescott, E.M., Stenbaeck-Nielsen, H.C., Davis, T.N., Murcray, W.B., Peek, H.M. and Bottoms, P.J. (1975). The L=6.6 Oosik barium plasma injection experiment and magnetic storm of March 7, 1972. *Journal of Geophysical Research 80*, 951–967.

White, F.W.G. and Geddes, M. (1939). The antarctic zone of maximum auroral frequency. *Terrestrial Magnetics and Atmospheric Electricity 43*, 261–377.

Wilcke, J.C. (1768). Försök til en Magnetisk Inclinations –Charta. *Kongl. Vetenskaps Akademiens Handlinger (Stockholm) 29*, 193–225.

Wilcox, J.M. and Ness, N.F. (1965). Quasi-stationary co-rotating structure in the interplanetary medium. *Journal of Geophysical Research 70*, 5793–5805.

Williams, D.J. and Mead, G.D. (1965). Nightside magnetosphere configuration as obtained from trapped electrons at 1100 km. *Journal of Geophysical Research 70*, 3017–3029.

Winningham, J.D., Anger, C.D., Shepherd, G.G., Weber, E.J. and Wagner, R.A. (1978). A case study of the aurora, high-latitude ionosphere, and particle precipitation during near-steady state conditions. *Journal of Geophysical Research 85*, 5717–5731.

Wolfe, J.H., Silva, R.W. and Myers, M.A. (1966). Observations of the solar wind during the flight of IMP I. *Journal of Geophysical Research 71*, 1319–1340.

# Glossary

*auroral curtains* - An old term for a rayed band, usually when the rays are relatively high above the lower border, giving a curtain-like appearance.

*auroral electroject activity* - Following solar activity, part of the hot plasma which enters the magnetosphere is injected into the ionosphere above the Earth's polar regions. Here it may be identified as an intense concentrated electric current along part of the auroral oval. This auroral electrojet causes polar magnetic substorms.

*auroral oval* - Under quiet conditions, the general shape of the auroral arc(s) as seen from above, e.g. as seen by a satellite high enough to record the Earth's polar cap and beyond, down to middle latitudes.

*auroral regions* - The auroral region is defined by a belt of light 7.5° of latitude on each side of the auroral zone, the line marking the maximum occurrence of overhead aurora. The *cis*-auroral region lies equatorwards (*cis* - on this side of.) The *trans*-auroral region lies polewards (*trans* - to the other side of.)

*auroral substorm* - A term introduced by S.-I. Akasofu to denote the break-up of the simple arc or rayed arc aurora. It occurs at (magnetic) midnight and is characterised by a surge of bands from midnight to the west and the equatorwards movement of bands in the east.

*border* - In the sense used, the upper or lower edge of an auroral form.

*Centred Dipole North (Boral) Pole* - The point on the sphere representing the Earth at which the axis of the centred dipole cuts the surface in the Northern Hemisphere.

*Centred Dipole South (Austral) Pole* - The point on the sphere representing the Earth at which the axis of the centred dipole cuts the surface.

*centred dipole co-latitude* - For any type of latitude (geographic, geomagnetic etc.) of value $\phi$, measured from the relevant equators, there is a co-latitude propagated upwards to the ionosphere. They then travel along the magnetic field line to $\theta°$ measured from the pole such that $\theta = 90° - \phi°$. Centred dipole co-latitude is the co-latitudes measured in the centred dipole latitude-longitude system.

*centred dipole coordinates* - A latitude and longitude system based on the centred dipole poles.

*centred dipole field* - A simple mathematical approximation to the actual Earth's magnetic field which is equivalent to the field of a sphere of the same mass as the Earth with a dipole at the centre. In old texts it is called the geomagnetic field.

*di-pole (for small magnet)* - A mathematical conception derived by considering the geomagnetic field as due to a small bar magnet at the centre of the Earth, and then treating the magnet as a point.

*dip pole* - A point on the Earth where a declinometer needle will point vertically. Usually refers to the North Magnetic Pole or the South Magnetic Pole, when the horizontal component of the Earth's magnetic field at ground level is zero. Due to ionospheric and Earth currents, the instantaneous dip pole moves over distances of tens or even hundreds of kilometres during a day. It is usually located by an analysis of the elements of the magnetic field for the whole Earth.

*discrete aurora* - Arcs, bands and rays.

*disturbance daily variation* - The disturbance daily variation $S_D$ is derived by subtracting the hourly value of $S_q$ from the hourly values on the magnetometer traces of the three magnetic elements recorded.

*disturbance polar field* - The perturbations from the mean of the magnetic elements in polar regions due to changes in direction and intensity of electric currents in the ionosphere.

*eccentic dipole field* - The eccentric dipole field is a better mathematical approximation to the Earth's true field If the dipole is not constrained to lie at the centre of the sphere, then the best fit to the worldwide magnetic data is given by a dipole moved parallel to the centred dipole axis.

*equatorial ring coordinates* - Starting from a point on a circle centred on the Earth's centre, in the equatorial plane of the dipole, a field line can be traced down to the Earth's surface using the higher order Gaussian coefficients. This point is then labelled with centred dipole latitude and longitude corresponding to the point of origin.

*flaming* - Successive belts of intense light moving upwards through active rayed bands, giving the impression of rising flames.

*Geomagnetic time* - This is time which is based on geomagnetic longitude (or one of its specified approximations) rather than on geographic longitude.

*geomagnetic co-latitude* - An older terminology for centred dipole co-latitude.

*geomagnetic field* - The true magnetic field of the Earth.

*geomagnetic poles* - Correctly, the true poles of the Earth's magnetic field. In early work the term was used for those points which are now called the Centred Dipole Poles. In some contemporary work the term is used for the "invariant" or "auroral" poles.

*homogeneous arc* - A thin ribbon of light of uniform intensity with the lower border usually about 105 km above the surface of the Earth. When seen from the ground it forms an arc or arch in the night sky.

*homogeneous band* - A thin ribbon of light of uniform intensity with the lower border showing curves and bends.

*International Geomagnetic Reference Field* - At intervals, usually 10 years, a committee set up by the International Union of Geology and Geophysics analyses worldwide geomagnetic data and issues the values of the Gauss coefficients and their rate of eclipse. These data comprise the International Geomagnetic Reference Field.

*isoaurore* - An isoaurore is the locus of points for which the nightly frequency of occurrence of overhead aurora is constant (*iso* - the same).

*isochasm* - The locus of points for which the nightly frequency of observing the aurora in any direction is constant.

*loss cone* - Although charged particles spiral around a magnetic field line and are reflected at a magnetic mirror point when the magnetic field becomes sufficiently strong, if the particle spirals at a quite small angle to the magnetic field the angle never reaches the value required for reflection and hence particles of this type continue on beyond the reflection point. Particles which are reflected form circles around the field line and with the point of capture by the field line form a cone. The unreflected particles are lost from this cone and hence are called particles from the loss cone.

*magnetic conjugate* - From a point A the external magnetic field line is traced until it reaches a point B in the opposite hemisphere. The points A and B are then said to be magnetically conjugate.

*magnetic declination* - The angle, east or west of True Geographic North made by the horizontal components of the Earth's magnetic field at a particular location (mariners use the term magnetic deviation).

*magnetic inclination* - The angle measured in the plane of the horizontal component, between the horizontal and the direction of the Total Magnetic Field at a particular location. Also known as dip or dip angle.

*magnetic meridian* - The locus of a point moving from the South Magnetic Pole to the North Magnetic Pole such that the tangent to the line always points in the direction of the horizontal component of the Earth's magnetic field.

*magnetosphere* - The magnetosphere is that region of space in which the Earth's magnetic field dominates the motion of charged particles.

*overhead aurora* - Those auroral forms appearing within a circle within a circle of zenith distance 60° which corresponds to a circle on the Earth's surface with radius 1.5° of great-circle distance.

*patch* - Increased light intensity covering an area with diffuse light.

*patchy aurora* - Auroral patches.

*plasma* - A rarefied state of matter. A typical example of a hot plasma is a flame. Technically, an assembly of ions (mainly protons), electrons, neutral atoms and molecules in which the motion of the particles is dominated by electric and magnetic fields. There is greater separation of particles than in a rarefied un-ionised gas.

*polar elementary storm* - Birkeland (1908) described changes from the mean of the magnetic elements at a station in polar regions as "polar positive" and "polar negative" perturbations. The general term for either of these perturbations is a "polar elementary storm".

*ray* - A vertical column of light. Tall rays are similar to vertical search-light beams.

*rayed band* - A series of vertical columns of light, close together, and joined at the base. See also auroral curtains. The lower border shows curves and smooth bends.

*solar corona/wind* - The solar corona is that region of hot plasma which can be photographed during a total eclipse of the Sun. It consists of hot particles ejected from the Sun. As these particles move further from the Sun they cool and form the solar wind.

*solar daily variation* - The solar daily variation $S_q$ is the difference for each hour from the mean value as determined for the five quiet days of each month for each of the three magnetic elements recorded by a station magnetometer.

*striations* - Narrow strips of light separated by narrow strips of low intensity or darkness that form in some auroral bands.

*subvisual red arc* - An arc caused by photons of the oxygen doublet 630.0 nm and 634.4 nm which can be seen through a spectroscope but not with the naked eye. Occasionally when there is a very intense magnetic storm Kp>9o the emanation of the red doublet becomes visible, usually as a broad band to the naked eye.

*sunspot* - A relatively dark patch on the Sun. Sunspots vary greatly in size but when the diamater is 40 000 km they are visble to the naked eye. (Never look at the bright Sun, use a point hole in a card, and focus the image of the Sun on a screen in a dark room.)

*terella* - Literally – a little Earth. A uniformly magnetised ? sphere, or a hollow non-magnetic sphere with a small magnet at its centre, or a small solenoid at the centre of a non-magnetic sphere, all produce the same pattern of field as the main component of the Earth's magnetic field and those types of terella can be used in model experiments.

*vector* - A quantity having both magnitude and direction. It is usually represented by a point of action and an arrow (to scale) representing the magnitude of the quantity.

*veil* - A large area of weak diffuse light.

*whistlers* - When a lightning strike occurs, a series of radio waves of different frequencies is propagated upwards to the ionosphere. They then travel along the magnetic field line to the opposite hemisphere where the higher frequencies arrive first and others arrive in descending order. Being in the aural range of frequencies, a whistle of descending pitch is heard in the radio receiver.